

SCALE-DOWN PRINCIPLES FOR THE ACCELERATED DESIGN OF PROTEIN PURIFICATION PROCESSES

A thesis submitted to the University of London
for the degree of DOCTOR OF PHILOSOPHY

By

R. Michael Boychyn, B. Eng., M. Sc.

The Advanced Centre for Biochemical Engineering
Department of Biochemical Engineering
University College London
Torrington Place
London WC1E 7JE

March, 2000

ProQuest Number: 10608895

All rights reserved

INFORMATION TO ALL USERS

The quality of this reproduction is dependent upon the quality of the copy submitted.

In the unlikely event that the author did not send a complete manuscript and there are missing pages, these will be noted. Also, if material had to be removed, a note will indicate the deletion.



ProQuest 10608895

Published by ProQuest LLC (2017). Copyright of the Dissertation is held by the Author.

All rights reserved.

This work is protected against unauthorized copying under Title 17, United States Code
Microform Edition © ProQuest LLC.

ProQuest LLC.
789 East Eisenhower Parkway
P.O. Box 1346
Ann Arbor, MI 48106 – 1346

ABSTRACT

With speed to market as a critical factor determining the economic success of a therapeutic product, bioprocess development must be carried out as efficiently as possible. This relies heavily on the ability to predict industrial-scale operation with only small (< 0.5 L) quantities of available feed; laboratory scale-down is superior to pilot-plant work in terms of speed, ease, and cost. Application of such a strategy is particularly relevant to early solid-liquid separation stages, where the performance of a centrifuge or filter may largely determine process yield and the quality of material to be delivered to subsequent guard filtration and chromatographic stages.

Previous work focused on the modification of a disc stack centrifuge and laboratory prediction of clarification for shear-insensitive species such as cell debris. This thesis extends this work by developing laboratory-scale methods to mimic sediment dewatering and recovery of shear-sensitive protein precipitates in continuous-flow centrifuges. Initial experiments conducted with a multichamber-bowl, resulted in a great difference between predicted and pilot clarifications (50% lower) due to particle break-up occurring in the high-velocity entrance zone of the pilot centrifuge. The hydrodynamic forces in this region were analysed by computational fluid dynamics and reproduced in a small high-speed rotating disc device. Exposing suspension to the device prior to laboratory centrifugation permitted accurate prediction of pilot clarification. This technique was translated to other continuous centrifuges (disc stack, CARR, production multichamber-bowl). Importantly, the performance of the production centrifuge was more accurately predicted by the scale-down process than the pilot one. A simpler scaling tactic of constant tip velocity of the distributor in the centrifuge feed zone was also examined and found to be a good predictor of large-scale clarification.

Conventional filtration (with precoat and body feed) was investigated as an alternative primary separation step. A production rotating vertical leaf filter was scaled down by transformation of a laboratory-batch, Nutsche pressure-filter; the continuous filter resulted in cakes of more uniform composition with lower specific resistances. Filtration gave significantly better clarification and sediment dryness than centrifugation.

Finally, chromatographic performance was shown to depend moderately on the extent but principally on the type of solid-liquid separation, with centrifugation samples resulting in significantly greater column dynamic capacities than filtrates, which was not predicted by the response of a guard (cartridge) filter.

ACKNOWLEDGEMENTS

Personal

I first want to thank Professor Mike Hoare who has provided me with invaluable advice and support throughout this project, as well as words of encouragement when needed. I would also like to thank Dr. Mark Bulmer for his guidance, creative yet pragmatic advice, and uplifting humour. And thank you to Dr. John More who gave me the opportunity to work in an industrial environment, the experience proving extremely worthwhile.

Special recognition is owed to Billy Doyle for assisting with centrifugation work in the pilot plant, particularly regarding operation of the temperamental AS-26. I am also grateful to members of the departmental workshop and other technical staff for all their work, especially John Graham and Martin Town. Tobi Sanderson was also a great help in getting me settled at BPL and tacking filtration.

I also thank Lars Pampel and Shane Storey for intellectually stimulating conversations on bioprocess synthesis, design and scale-down, and for their friendship. Thank you to Dr. John Maybury for helping tame the Elzone particle sizer, Shane for chromatography, and Dr. Samson Yim for the CFD work. I deeply appreciated the advice, encouragement and consideration of my advisor, Dr. Nigel Titchener-Hooker.

And finally, I owe an immense debt of gratitude to my family, my wife Karin, Mom, Dad and Steven, for having shown constant love, support and understanding during some unsettled periods and the good times.

Financial support

University College London is the Biotechnology and Biological Sciences Research Council's sponsored Advanced Centre for Biochemical Engineering and the Council's support is gratefully acknowledged, as is that of Bio Products Laboratory, Elstree, UK.

Financial support from the Natural Sciences and Engineering Research Council of Canada and the ORS Council, University of London, is also appreciated.

Thank you once again to everyone who has contributed in some way to me seeing this Ph. D. to fruition.

TABLE OF CONTENTS

TABLE OF CONTENTS.....	1
LIST OF FIGURES.....	8
LIST OF TABLES.....	11
NOTATION.....	12
1. CHAPTER 1	17
1.1. INTRODUCTION.....	17
1.2. PROCESS DEVELOPMENT	18
1.2.1. Definition	18
1.2.2. Sources of competitive advantage.....	18
1.2.3. Justification.....	19
1.3. RESEARCH AND DEVELOPMENT CYCLE.....	21
1.3.1. Discovery	21
1.3.2. Host selection and cloning	21
1.3.3. Bioprocess research and development	22
1.3.4. Clinical trials	23
1.3.5. Window for bioprocess development.....	23
1.4. REASONS FOR SCALE-DOWN.....	24
1.4.1. Scale-down versus design of better large-scale equipment	24
1.4.2. Scale-down versus modelling	25
1.4.3. Scale-down versus pilot plant studies	25
1.5. THE ROLES OF SCALE-DOWN	26
1.5.1. Scale-down of a production-scale bioprocess	26
1.5.2. Scale-down for more efficient scale-up	27
1.5.3. Scale-down's integration with other process development tools	28
1.5.3.1. Purification process synthesis	29
1.5.3.2. Total process synthesis	29
1.5.3.3. Interdependence of process synthesis, modelling and scale-down.....	30
1.5.3.4. Process design	31
1.6. METHODS OF SCALING	32

1.7. SCALING OF UNIT OPERATIONS	33
1.7.1. Degree of scale-down	33
1.7.2. Scale-up problems	34
1.7.3. Impact of computational fluid dynamics (CFD)	35
1.7.4. Fermentation	35
1.7.5. Homogenisation	36
1.7.6. Precipitation	36
1.7.7. Centrifugation.....	37
1.7.8. Conventional filtration using precoat and body feed	38
1.7.9. Tangential-flow membrane filtration	38
1.7.10. Chromatography	39
1.8. SYNOPSIS OF CHAPTERS	40
2. CHAPTER 2	42
ABSTRACT	42
2.1. INTRODUCTION.....	43
2.1.1. Scale-down	43
2.1.2. Precipitation	44
2.1.3. Centrifugation.....	45
2.2. THEORETICAL CONSIDERATIONS	49
2.2.1. Precipitation	49
2.2.2. Centrifugation.....	50
2.2.2.1. Clarification.....	50
2.2.2.2. Dewatering.....	52
2.2.3. Separation process	54
2.3. MATERIALS AND METHODS	57
2.3.1. Chemicals	57
2.3.2. Description of equipment	57
2.3.3. Preparation of particle suspension	58
2.3.4. Preparation of precipitate suspension	59
2.3.5. Separation of precipitate suspension	59

2.3.5.1. <i>Scale-down process</i>	59
2.3.5.2. <i>Pilot-scale process</i>	61
2.3.5.3. <i>Reference</i>	61
2.3.6. Analyses	61
2.3.6.1. <i>Physical properties</i>	61
2.3.6.2. <i>Protein assay</i>	62
2.3.6.3. <i>Alcohol dehydrogenase (ADH) activity assay</i>	62
2.3.6.4. <i>Solids fraction</i>	63
2.3.6.5. <i>Moisture content of sediment</i>	63
2.4. RESULTS AND DISCUSSION	64
2.4.1. Correction factor for multichamber-bowl centrifuge	64
2.4.2. Mass balance	65
2.4.3. Centrifugation performance	67
2.5. CONCLUSIONS	74
3. CHAPTER 3	75
ABSTRACT	75
3.1. INTRODUCTION	76
3.1.1. Centrifugation of shear-sensitive species	76
3.1.2. Computational fluid dynamics (CFD)	77
3.1.3. Selection of a “shear” device	77
3.1.4. Selection of test material	78
3.2. THEORETICAL CONSIDERATIONS	81
3.2.1. Mapping the flow field	81
3.2.1.1. <i>Pilot centrifuge</i>	81
3.2.1.2. <i>Laboratory-scale high-speed rotating disc</i>	81
3.2.2. Centrifugation	83
3.3. MATERIALS AND METHODS	84
3.3.1. Chemicals	84
3.3.2. Preparation of precipitate suspension	84
3.3.3. Separation of suspension	84
3.3.4. High-speed laboratory rotational device	85

3.3.5. Analysis	86
3.3.5.1. <i>Physical properties of the suspension</i>	86
3.3.5.2. <i>Assay for particle damage</i>	86
3.3.5.3. <i>Particle size measurements</i>	86
3.3.5.4. <i>Clarification</i>	88
3.3.6. Experimental design	88
3.4. RESULTS AND DISCUSSION	90
3.4.1. Particle size	90
3.4.2. Dependence of clarification on time of centrifugation	90
3.4.3. Dependence of clarification on tip speed and residence time	93
3.4.4. Laboratory compared to pilot-scale centrifugation	93
3.4.5. Process intensification	96
3.4.6. CFD of pilot-continuous centrifuge	97
3.4.7. CFD of rotating disc device	99
3.4.8. Experimental verification of CFD prediction	99
3.5. CONCLUSIONS	106
4. CHAPTER 4	107
ABSTRACT	107
4.1. INTRODUCTION	108
4.1.1. Previous work	108
4.1.2. Modelling using computational fluid dynamics (CFD)	108
4.1.3. Modelling using tip velocity	108
4.1.4. Description of centrifuges	109
4.2. THEORETICAL CONSIDERATIONS	112
4.2.1. Scaling on tip velocity	112
4.2.2. Maximum energy dissipation rate	112
4.2.3. Recovery curves	112
4.2.4. Centrifugation	113
4.3. MATERIALS AND METHODS	114
4.3.1. Chemicals	114

4.3.2. Description of equipment	114
4.3.3. Analyses	116
4.3.3.1. <i>Physical properties</i>	116
4.3.3.2. <i>Assay for particle damage</i>	116
4.3.3.3. <i>Clarification</i>	116
4.4. RESULTS AND DISCUSSION	117
4.4.1. Estimating maximum energy dissipation rates using tip velocity	117
4.4.2. Dependence of relative of clarification on maximum energy dissipation rate	117
4.4.3. Recovery curves.....	118
4.4.4. Scaling on tip velocity	123
4.4.5. Scale-down versus pilot plant trials	124
4.4.6. CFD versus tip velocity.....	127
4.4.7. Maximum centrifugation performance	130
4.4.8. Procedure to predict clarification in a continuous centrifuge	131
4.5. CONCLUSIONS.....	134
5. CHAPTER 5	135
ABSTRACT	135
5.1. INTRODUCTION.....	136
5.1.1. General	136
5.1.2. Scale-Up and Down	136
5.1.3. Filtration performance	137
5.1.4. Types of filters.....	138
5.1.5. Filtration in plasma fractionation	140
5.2. THEORETICAL CONSIDERATIONS	142
5.2.1. Permeability	142
5.2.2. Constant-pressure filtration.....	143
5.2.3. Constant-rate filtration.....	145
5.3. MATERIAL AND METHODS.....	147
5.3.1. Chemicals	147

5.3.2. Description of equipment	147
5.3.3. Preparation of feed suspension	147
5.3.4. Filtration	148
5.3.4.1. <i>Laboratory batch</i>	148
5.3.4.2. <i>Scale-down (continuous) RVLf</i>	148
5.3.5. Centrifugation.....	149
5.3.5.1. <i>Laboratory</i>	149
5.3.5.2. <i>Production</i>	150
5.3.6. Analyses	152
5.3.6.1. <i>Turbidity</i>	152
5.3.6.2. <i>Moisture content</i>	152
5.3.6.3. <i>Physical properties</i>	152
5.4. RESULTS AND DISCUSSION	153
5.4.1. Vacuum filtration.....	153
5.4.2. Effect of precoat	153
5.4.3. Effect of body feed.....	154
5.4.4. Constant pressure batch filtration	156
5.4.5. Compressibility	156
5.4.6. Predicted performance of scale-down RVLf	161
5.4.7. Actual performance of scale-down RVLf	163
5.4.8. Comparison of filtration and centrifugation performance	166
5.5. CONCLUSIONS.....	168
6. CHAPTER 6	169
ABSTRACT	169
6.1. INTRODUCTION.....	169
6.2. MATERIAL AND METHODS.....	172
6.2.1. Chemicals	172
6.2.2. Description of equipment	172
6.2.3. Preparation of feed suspension	172
6.2.4. Centrifugation.....	173
6.2.5. Filtration	173

6.2.5.1. <i>Primary</i>	173
6.2.5.2. <i>Guard</i>	173
6.2.5.3. <i>Membrane</i>	174
6.2.6. Chromatography	174
6.2.7. Analyses	175
6.2.7.1. <i>General</i>	175
6.2.7.2. <i>Guard filter fouling</i>	175
6.2.7.3. <i>Chromatographic breakthrough time</i>	176
6.2.7.4. <i>Dynamic capacity and process yields</i>	176
6.2.8. Experimental design	177
6.3. RESULTS AND DISCUSSION	178
6.3.1. Selection of starting material	178
6.3.2. Filter fouling	178
6.3.3. Quality of filtrate	183
6.3.4. Chromatographic performance	185
6.4. CONCLUSIONS	191
7. CONCLUSIONS	192
8. FUTURE WORK	194
8.1. HIGH-VELOCITY FLOW FIELDS	194
8.1.1. Scaling on tip velocity	194
8.1.2. Incorporation of shear into scale-down	196
8.1.3. Incorporation of shear into bioprocess synthesis	197
8.2. FILTRATION	198
8.3. IMPACT OF PRIMARY SEPARATION ON CHROMATOGRAPHY	199
8.4. SCALE DOWN OF THE ENTIRE UNIT OPERATION	200
8.5. SCALE-DOWN FOR ACCELERATED BIOPROCESS DEVELOPMENT	201
REFERENCES	203
APPENDIX A	216
APPENDIX B	218

LIST OF FIGURES

Page	Figure legend
22	Figure 1.1. Summary of the research and development process for the manufacture of a biopharmaceutical (Pisano, 1997).
48	Figure 2.1. Cross-section of a generic multichamber bowl centrifuge displaying the main liquid flow path.
54	Figure 2.2. A general solid-liquid separation with all relevant streams.
60	Figure 2.3. Procedural overview of the laboratory scale-down and pilot processes involving the formation of protein precipitates and their centrifugal recovery.
64	Figure 2.4. Probability-log relationship of % clarification* and equivalent flow rate per centrifuge separation area for polyvinyl acetate particles.
67	Figure 2.5. An error analysis of all mass balances for the range of flow rates investigated in the laboratory and the pilot centrifuge.
68	Figure 2.6. The dependence of purification factor of ADH in the supernatant on the logarithm of equivalent flow rate per centrifuge separation area.
69	Figure 2.7. The linear-log relation of yield of soluble ADH in the supernatant to the equivalent flow rate per centrifuge separation area for the precipitate suspension.
71	Figure 2.8. The probability-log dependence of % solids sedimented on equivalent flow rate per centrifuge separation area for the precipitate suspension.
72	Figure 2.9. The linear-log relationship of the degree of dewatering on equivalent flow rate per centrifuge separation area for the precipitate suspension.
78	Figure 3.1. Schematic of the laboratory, high-speed rotating-disc device.
89	Figure 3.2. Laboratory scale-down of large-scale precipitation and centrifugal recovery achieved with the novel utilization of a shear device.
91	Figure 3.3. Particle size distributions of precipitate suspension exposed to the rotating-element device.
92	Figure 3.4. Relationship between clarification on ratio of equivalent flow rate to centrifuge separation area plotted on probability-logarithmic axes.

- 95 **Figure 3.5.** Dependence of the relative clarification on tip velocity for times of shearing in the laboratory, rotational device.
- 98 **Figure 3.6.** Influence of process integration on shear-sensitivity of particles.
- 102 **Figure 3.7.** Computational fluid dynamic (CFD) simulation of the pilot multichamber-bowl centrifuge operated under flooded conditions.
- 103 **Figure 3.8.** CFD simulation of the pilot multichamber-bowl centrifuge operated under non-flooded conditions.
- 104 **Figure 3.9.** CFD simulation of the laboratory disc device.
- 105 **Figure 3.10.** Dependence of the relative clarification on maximum energy dissipation rate.
- 110 **Figure 4.1.** Schematics of continuous-flow centrifuges.
- 119 **Figure 4.2.** Dependence of the relative clarification on maximum energy dissipation rate for precipitates processed through the laboratory rotating disc device and centrifuge.
- 120 **Figure 4.3.** Recovery curve (dependence of clarification on ratio of equivalent flow rate to centrifuge separation area plotted on probability-logarithmic axes) for yeast-protein and plasma precipitate suspensions.
- 122 **Figure 4.4.** Dependence of the ordinate intercept of the recovery curve (Figure 4.3) on maximum power dissipation of the rotating-disc device.
- 125 **Figure 4.5.** Dependence of the relative clarification on maximum energy dissipation rate.
- 128 **Figure 4.6.** CFD analysis of the feed zone of a pilot disc stack, multichamber-bowl and CARR centrifuge.
- 132 **Figure 4.7.** Effect of particle break-up and operating conditions on the centrifuge recovery curve.
- 133 **Figure 4.8.** The predicted maximum clarification of yeast-protein precipitates achievable in the continuous centrifuges.
- 139 **Figure 5.1.** A standard laboratory, batch Nutsche filter driven by pressure.
- 141 **Figure 5.2.** Photograph of an LFC Rotojet rotating vertical leaf filter.
- 150 **Figure 5.3.** Schematic of the scaled-down rotating vertical leaf filter.
- 151 **Figure 5.4.** Illustration of the experimental apparatus.

- 155 **Figure 5.5.** The dependence of average flux on pressure in the batch filter.
- 157 **Figure 5.6.** Filtration curve: dependence of the mass of filtrate on time.
- 158 **Figure 5.7.** The dependence of the ratio of time to mass of filtrate on mass of filtrate for a constant pressure.
- 159 **Figure 5.8.** The dependence of the ratio of time to mass of filtrate on mass of filtrate for step-pressure increases.
- 160 **Figure 5.9.** The average specific cake resistance plotted against pressure on logarithmic axes.
- 162 **Figure 5.10.** Theoretical pressure-ramping profiles required for constant-flux rate filtration.
- 164 **Figure 5.11.** Linear relationship between mass of filtrate collected and square root of time for the scale-down rotating vertical leaf filter operating at constant pressure.
- 165 **Figure 5.12.** Dependence of the ratio of time to mass of filtrate to mass for the scale-down rotating vertical leaf filter operating at a constant pump rate.
- 180 **Figure 6.1.** Filtration curve: dependence of the mass of filtrate on time at a constant pressure of 0.5 bar in the guard filter.
- 181 **Figure 6.2.** Dependence of the ratio of time to mass of filtrate on mass of filtrate.
- 182 **Figure 6.3.** Dependence of the filtration index (normalised slope of the linearised filtration curve) on clarification.
- 184 **Figure 6.4.** Dependence of the clarity of the guard filtrate on the clarification of the original suspension.
- 186 **Figure 6.5.** Solute breakthrough curves: dependence of the breakthrough (%) of ADH on the number of column volumes.
- 187 **Figure 6.6.** Elution peaks for HIC purification of ADH: dependence of activity on volume.
- 188 **Figure 6.7.** Dependence of the normalised dynamic capacity on clarification of the suspension.
- 190 **Figure 6.8.** Process yields and purity results for HIC purification of ADH.
- 195 **Figure 8.1** Variation in fluid dynamic parameters with disc size.

LIST OF TABLES

Page	Table legend
23	Table 1.1. Phases of clinical trials as specified by the FDA.
58	Table 2.1. Dimensions and characteristics of the precipitation vessels.
65	Table 2.2. Example of mass balance of a scale-down, laboratory process.
73	Table 2.3. Percentage dryness of sediment for samples in the centrifuges.
94	Table 3.1. Dependence of clarification achieved in the laboratory and pilot centrifuges.
97	Table 3.2. Dependence of shear-sensitivity of precipitates on cell debris concentration.
115	Table 4.1. Name, type and operating conditions of the studied centrifuges.
118	Table 4.2. Comparison of predicted and experimental clarifications.
131	Table 4.3. Predicted maximum clarification, for yeast-protein precipitates, obtainable in the continuous-flow centrifuges based on their minimum throughput.
167	Table 5.1. The average sediment dryness and clarification as a function of centrifugation and batch filtration operating conditions.
173	Table 6.1. Operating conditions of the laboratory centrifuge.
177	Table 6.2. Description of process streams.
179	Table 6.3. The degree to which the suspension was clarified, the fouling index of the stream loaded on to the guard filter and the clarification effected by this filter, are provided for each stream listed in Table 6.2.
185	Table 6.4. The clarification of the suspension, normalised breakthrough times and dynamic capacities.
216	Table A.1. Experimental mass balance data for protein and ADH.

NOTATION

Symbol	Description
A	area, m^2
A	ordinate intercept of recovery curve
ΔA	change in OD
a, b, c, d	correction factors for mass balance
B	slope of the recovery curve
B_L	caulk width, m
C	centrifugation correction factor
c	dry solids per unit volume of filtrate, kg m^{-3}
c_1, c_2, c_μ	constants in $k-\varepsilon$ turbulence model
Ca	Camp number
$Clar$	clarification, %
D	impeller diameter, m
d	particle diameter, m
E	ADH activity, U mL^{-1}
e	error in mass balance
F	fouling index
F	fractional recovery of solids
F_L	correction factor for caulks on discs in centrifuge
G	turbulent kinetic energy, J
\bar{G}	mean velocity gradient, s^{-1}
g	gravitational constant, m s^{-2}

H	liquid depth, m
K	Kozeny constant, m^{-1}
k	turbulent kinetic energy, $J\ kg^{-1}$
k	permeability, m^2
L	length, m
M	mass of filtrate, kg
m	ratio of mass of wet cake to dry cake
N	rotational speed, $r\ s^{-1}$
n	cake compressibility coefficient
n	number of discs
OD	optical density
P	power dissipation, W
P	amount of protein, mg
$[P]$	concentration of protein, $mg\ mL^{-1}$
ΔP	pressure differential, Pa
p	pressure, Pa
Q	flow rate, $m^3\ s^{-1}$
R	radius, m
r	radius, m
r	radial coordinate, m
RCF	relative centrifugal force
Re	Reynolds number
R_m	filter medium resistance, m^{-1}
s	mass fraction of solids in feed suspension
T	torque, $kg\ m^2\ s^{-2}$

t	time, s
u	radial velocity, m s^{-1}
v	axial velocity, m s^{-1}
v_g	settling velocity of a particle under gravity, m s^{-1}
v_s	settling velocity of a particle under centrifugal force or pressure, m s^{-1}
v_ω	tip velocity, m s^{-1}
V	volume, m^3
w	azimuthal velocity, m s^{-1}
w_c	mass of cake deposited per unit area, kg m^{-2}
X	distance from edge of disc, m
x	fractional acceleration time
y	fractional deceleration time
Z_L	number of caulks on a disc in the centrifuge
z	axial coordinate, m
<i>Greek letters</i>	
α	specific cake resistance, m kg^{-1}
Γ	dynamic capacity
δ	boundary layer thickness, m
ε	energy dissipation rate, W kg^{-1}
ε	porosity
θ	half disc angle, rad
μ	viscosity, Pa s
μ_t	coefficient of turbulent viscosity coefficient, Pa s
π	Pi

ρ	density, kg m^{-3}
Σ	equivalent settling area, m^2
$\sigma_k, \sigma_\epsilon$	constants in k - ϵ turbulence model
τ	shear stress, Pa
τ	breakthrough time, s
ϕ_V	volume fraction of solids in feed suspension
ω	angular velocity, rad s^{-1}

Subscripts

av	average
C	continuous centrifuge
c	compaction (i.e. dewatering)
c	filter cake
cr	critical
ds	disc stack centrifuge
i	inner
L	liquid
lab	laboratory
max	maximum
mc	multichamber-bowl centrifuge
min	minimum
N	normalised
n	number of chambers
o	original suspension
o	outer

<i>r</i>	radial direction
<i>rd</i>	rotating disc
<i>ref</i>	reference
<i>S</i>	solids
<i>sed</i>	sediment
<i>sup</i>	supernatant
<i>T</i>	precipitation tank
<i>t</i>	turbulent
<i>tb</i>	tubular-bowl centrifuge
<i>z</i>	axial direction
θ	azimuthal direction

1. CHAPTER 1: SCALE-UP AND SCALE-DOWN IN RELATION TO BIOPROCESSING

1.1. INTRODUCTION

In the last twenty years there have been significant advances in molecular biology, biochemistry, protein chemistry, physiology, pharmacology, genetics and genetic engineering. This explosion of knowledge has had two major effects on the research and development (R&D) of pharmaceutical products. One is the creation of rational drug design: molecular sites of potential drug action are identified and chemicals (mainly chiral organic molecules) with suitable structures synthesised and screened, increasingly with the aid of combinatorial chemistry and biocatalysis. The other impact of the molecular biology revolution is complex biological products (therapeutic proteins, DNA vaccines, viruses and DNA-liposome--antibody fragments complexes for gene therapy) synthesised through genetic engineering (Pisano, 1997).

This increased capacity to discover and create new drug candidates has a knock-on effect on the biotechnology industry where the key challenge is the cost-effective production of biopharmaceuticals in sufficient quantities to meet market demand while ensuring that product quality is maintained (Anicetti and Hancock, 1994). This will only be accomplished if *efficient* full-scale production systems are designed and implemented and this requires deeper understanding and more rapid process development. The latter may be facilitated by an approach termed scale-down in which small-scale equipment is operated in such a way that it mimics the conditions and hence generally poorer performance of its larger scale counter-parts. Laboratory scale-down is superior to pilot-plant development work in terms of speed, ease, operating and capital costs.

This work focuses on the application of scale-down technologies because of the benefits they can deliver, despite the *initial* demand for more company resources (finite and extremely sought after) to be focused on process development. Next, the traditional research and development cycle along with the numerous factors transforming it are summarised to provide a basis for the resulting discussion on scale-down. Reasons for and types of scale-down are detailed, particularly its integration with process synthesis and modelling. Scaling methodologies and the scaling of unit operations are then discussed. Finally, a synopsis of all subsequent chapters in this thesis is provided.

1.2. PROCESS DEVELOPMENT

1.2.1. Definition

Process development can be defined as the design, implementation and optimisation of a specific process. The goal of process development according to Pisano (1997) is:

“to find the process parameters (sequence, timing, and specification of process steps, equipment design and setting; and materials handling procedures) that either optimise performance or achieve a satisfactory target level when operated under actual production conditions...”

Furthermore, in a *“competitive environment, development goals should include finding this process as quickly and efficiently as possible.”* The critical challenge of process development is to maximise yields and throughput rapidly by moving from a complex, inefficient and sensitive initial process to one that is practical, efficient and robust.

1.2.2. Sources of competitive advantage

Wheelwright (1991) identified three main sources of competitive advantage in the manufacture and sale of high value protein products: first to market, high quality (in terms

of purity, activity), and low cost. Each of these advantages at present can only be maximised at the expense of the others; a company must identify the over-riding criterion. Thus, the optimal process is one that delivers superior performance with respect to the desired advantage.

For new therapeutics, speed-to-market is considered paramount by biotechnology companies; lead-time virtually always takes precedence over other considerations such that substantial resources will be dedicated/re-directed to a project in order to offset potential delays. The cost penalties of not doing so may be significant. For example, each day of delay for a drug with peak annual sales of \$500 million costs the company approximately \$1 million in lost sales revenue. Furthermore, being first to market generally results in a dominant position (Pisano, 1997).

Firms are now forced to operate within harsher pricing environments due to increased government regulation and intensifying competition. At the same time they have to deal with increased R&D and manufacturing costs due to stricter regulatory standards and more active supervision by the FDA (Food and Drug Administration) and EPA (Environmental Protection Agency), greater product complexity and a burgeoning number of drug candidates. Between 1980 and 1990, manufacturing expenses as a percentage of sales doubled from 10% to 20% (Pisano, 1997). Such costs erode profits and make it more difficult to recoup research and development expenditures. Therefore, new methods are needed to reduce product time-to-market and costs.

1.2.3. Justification

Thorough and efficient process development can achieve both of the above and permit rapid increase in productivity. The latter is valuable because it allows a firm to: expand production capacity without adding new capital; generate revenue; and begin to

accumulate high-volume production experience that may lead to lower future production costs. An example of the enormous impact of diligent process development is a drug firm that managed to increase yields so dramatically that it was able to meet 1994 market demand with only twelve fermenters instead of the originally planned 118 vessels (based on data compiled in 1980); a savings of approximately \$600 million (Pisano, 1997).

Bobrowicz (1999) provides costly examples of hasty process development, usually carried out to save money or time in the rush to get a product to market. Several companies have failed to investigate sufficient formulation options and invested in expensive lyophilisers, which are difficult to maintain and scale up, but several of their bulk pharmaceutical ingredients can withstand the much simpler and economical operation of spray-drying. One biotechnology manufacturer was experiencing a 10% failure rate in cell cultures. This could be eliminated by a simple modification to the medium but this would affect patents and filings. Another biopharmaceutical firm resisted altering a process for similar reasons; a five-column purification scheme was established but data generated for submission demonstrated that only three of the columns had any effect. Aviron, developer of a nasal-spray flu vaccine, had to delay the product's launch by at least one year due to issues encountered "in the process of scaling up production" (Bloomberg, 1999). Many biotechnology companies only have sufficient cash to survive a couple of years, and such a delay to their first major revenue could be destructive. Clearly, inadequate process development can result not only in a less efficient process, but also an unreliable one, spelling potentially much higher costs.

1.3. RESEARCH AND DEVELOPMENT CYCLE

1.3.1. Discovery

Figure 1.1 is a schematic representation of the research and development cycle for a biopharmaceutical product. The first step is the discovery of a biological substance, usually a protein, critical to controlling a disease or condition. The advent of genomics and proteomics has highlighted our still limited knowledge of the molecular basis of life as only a fraction of the proteins and genes implicated in most diseases have been identified (Ashton, 1999). The automation of genomics and proteomics is serving to increase dramatically the number of proteins which must be screened ever more swiftly in high-throughput devices.

1.3.2. Host selection and cloning

Great effort is put into the search for a suitable cell line. The host should facilitate a high level of protein expression, reproduce quickly (i.e. a low doubling time), grow to high concentrations and yields, require inexpensive nutrients and if possible, be robust enough to render negligible any shear effects associated with proper mixing. Initial shake flask experiments are then performed to collect growth data on the organisms and then the most promising candidates are scaled up to bench-top fermenters ranging from 1 to 10 L. The cell line resides at the top of the process design hierarchy because a change in the type of cell used may have ramifications for virtually every other step in the development process. It also should be noted that the initial research and development focuses on the biological process. Consequently, there is a tendency to delay shifting attention to scale-up and this often results in the delivery of a sub-optimal process.

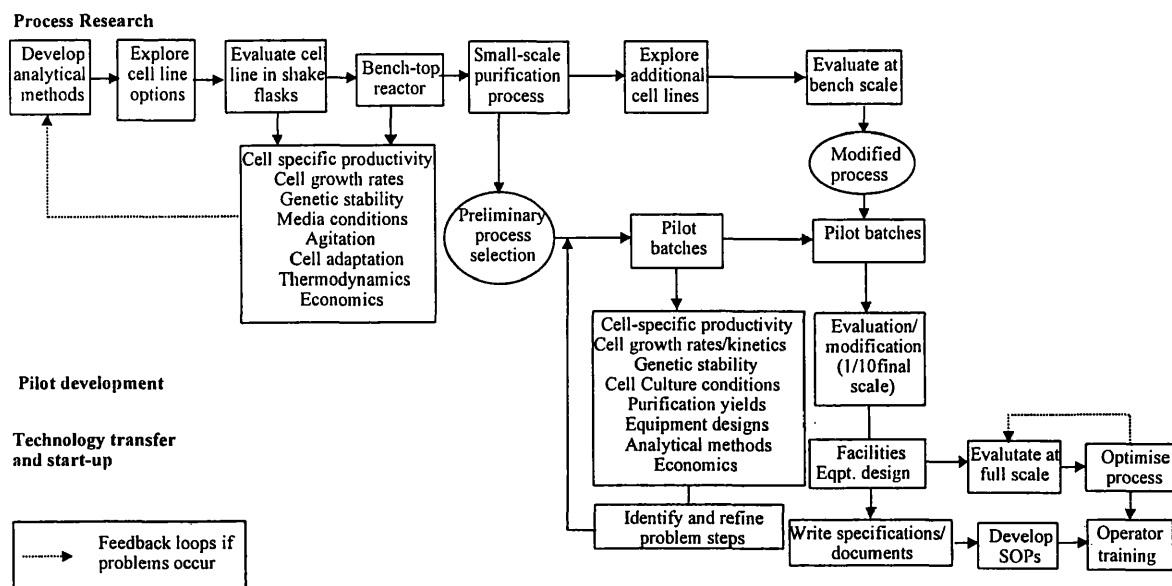


Figure 1.1. Summary of the research and development process for the manufacture of a biopharmaceutical (Pisano, 1997).

1.3.3. Bioprocess research and development

Once sufficient material is available data should be acquired on the product and major contaminants: solubility data in regard to salt solutions, organic solvents, pH, size, shape, net charge and distribution of charge; density; hydrophobicity; and adsorption isotherms (Wheelwright, 1987). FDA assessment of a process and its validation studies requires demonstration of adequate control of various factors such as the product's sensitivity to temperature, freezing and thawing, solvents, pH, oxygen, metals, etc. Protein chemists exploit differences in the properties of the product to those of contaminants to devise a sequence of, usually chromatographic, steps that will sufficiently purify the desired product. This process, called chromatographic scouting, involves a large number of experiments wherein various resins (e.g. ion exchange, hydrophobic interaction, reverse phase and/or affinity) and loading and elution conditions (mainly pH, ionic strength and protein concentration) are screened. Recently scouting has become

highly automated permitting a great variety of conditions to be analysed over a shorter time frame.

1.3.4. Clinical trials

Taking place in parallel with larger laboratory studies is the pre-clinical development of the therapeutic compound, which is conducted by observing its effects on animals before proceeding on to the much more expensive and potentially risky step of testing in humans. Human clinical trials consume the majority of the time and resources in the development of a drug, the phases of which are summarised in Table 1.1.

Table 1.1. Phases of clinical trials as specified by the FDA. Market approval is usually granted within one year of successful completion of phase III and the overall probability of a therapeutic candidate making it to market is 0.40 (Mackler *et al.*, 1996).

	Preclinical	Phase I	Phase II	Phase III
Purpose	Gather sufficient data to warrant human trials	Safety	Dosage and efficacy	Definitive safety and efficacy
Number of subjects	---	20-80	50-200	100-500
Product required (kg)	0.01-0.10	0.1-0.5	0.2-1	0.5-5
Probability of phase success	0.57	0.88	0.86	0.93
Timing (years after cloning)	0.5-1	1-2	2-3	3-6

1.3.5. Window for bioprocess development

The above set of trials may last anywhere from two to six years. Process development tends to focus on sorting out the details of the process (equipment type and operating parameters), scaling up of the process to the commercial manufacturing site, commissioning and validation and then meeting market demand. Despite the mean period

of a biopharmaceutical to attain commercial launch is 7.5 years (starting with the cloning of the genes for a specific protein), the window for process development is quite small (Foo *et al.*, 2000). It should commence very soon after clinical promise is established (i.e. after preclinical studies) and be completed before the start of phase III trials; a total of only about three to four years. This window has recently been shrinking as much effort has been expended to designing more efficient clinical trials (through pharmaco-genetics and computer simulations; Carr, 1998), scheduling, and streamlining of regulatory guidelines, data review and approval. If the duration of clinical trials continues to be reduced, process development, in its current state, could become the rate-determining step in a drug reaching the market. To avoid delays in product launches, companies must accelerate process development. Scale-down is a powerful strategy that can substantially shorten development times in several ways.

1.4. REASONS FOR SCALE-DOWN

1.4.1. Scale-down versus design of better large-scale equipment

Why focus on scaling down manufacturing equipment and not improving it? The latter is possible only to a certain degree. Large-scale equipment will probably never perform as well as its ideal laboratory counterpart due to changes in time constants, mode of operation and shear, despite innovative design improvements made by manufacturers. Moreover, once a biopharmaceutical firm has decided to purchase production items, these significant capital expenditures must be justified economically through extensive use.

1.4.2. Scale-down versus modelling

Why scale down if one can model? Unlike purely chemical systems, biological feed stocks have many uncharacterised components in terms of their size, structure, charge, hydrophobicity, etc. Even a great percentage of the defined constituents have unknown responses to various environmental conditions and stresses. This leads to considerable uncertainty (usually $\pm 30\%$) in generic models. Nevertheless, these models can be very helpful in designing scale-down experiments, the outputs from which can be used to improve the simulation. Varga *et al.* (1998) utilised this approach to refine the accuracy of natural yeast homogenisation models to a recombinant strain from $\pm 30\%$ down to $\pm 10\%$.

1.4.3. Scale-down versus pilot plant studies

If good scale-down mimics of manufacturing equipment can be developed these constitute a more advantageous strategy than pilot-plant studies given the extreme importance of time-to-market. Scale-down laboratory devices enable the more rapid integration of unit operations into a process resulting in an earlier and more accurate indication of the true overall process performance. Furthermore, this concept allows the very economical exploration of a greater number of process options than can be achieved at pilot-scale in the same amount of time. Scale-down runs save money and time due to their intrinsically smaller volume requirements of process materials, easier handling, operation and cleaning, fewer personnel and reduced energy consumption. Scale-down can also be used for validation, trouble shooting, and further optimisation based on large-scale experience. For example, most companies generate a “process capability specification” wherein the known variability of data is determined for a certain number of runs (almost always fewer than ten, usually less than five; Bobrowicz, 1999). This

validation effort is flawed in that more runs are required to establish process variability and specifications tend to be made before scale-up and optimisation changes to the process; accurate scale-down models can resolve both of these issues. The above factors minimise the extent of piloting needed and maximise the benefits gained from the small number of pilot plant trials required.

1.5. THE ROLES OF SCALE-DOWN

Bylund *et al.* (1999) correctly pointed out two independent circumstances in bioproduction when a scaling methodology is required: during scale-up of a new process and modification of an existing one. However, scale-down may also be utilised *with* process synthesis and modelling to accelerate development and corroborate performance of the predicted manufacturing process with respect to some difficult-to-measure variable.

1.5.1. Scale-down of a production-scale bioprocess

Scale-down can also be used to facilitate validation of a manufacturing process and/or implementation of changes to it. Kennedy *et al.* (1995) accentuated the need for well-managed change control in any validation program to minimise expensive delays and unforeseen circumstances. If a process can be scaled down sufficiently accurately, a company would be able to demonstrate and validate equivalence to the production one. This is very powerful because it permits studies such as virus-spiking which could never be done on actual processing equipment due to the inability to validate their complete removal from the facility. Trouble-shooting, assessing process sensitivity to changes in feed stocks or performance of a unit operation, and process improvement and optimisation (by implementation of new equipment, operating conditions, chemistry,

streamlining, etc.) could all be done using laboratory mimics. With increasingly sensitive and robust analytical tools and control instruments, it may be possible to conduct only the minimum of three full-scale verification batches. Obviously when implementing major process changes such as replacing one unit operation with another, significant validation is required; however, the burden can once again be minimised with a validated scale-down process and careful consideration of the manufacturing environment.

1.5.2. Scale-down for more efficient scale-up

Of course the level of manufacturing detail one chooses to inject into a scale-down process is a function of the context in which scale-down is being used. Generally in product development, the ultimate scale of manufacture can only be estimated roughly thus limiting equipment design information and the useful accuracy of the small-scale process. Despite faced with this uncertainty, scale-down is still an extremely powerful tool to accelerate development. Since the performance of much manufacturing equipment differs fairly slightly with change of scale (i.e. the difference in process performance between the laboratory and pilot plant is generally more than that between pilot and production scale) as scaling technologies have improved, it is beneficial to run a small-scale process which incorporates exposure of product streams to conditions found commonly in all large-scale equipment of a particular type. In other words, it is better to include scale-down aspects (however approximate) in the laboratory process because it permits one to assess rapidly the feasibility of the proposed full-scale process.

In fact, when a good understanding of the fluid dynamic conditions within larger scale equipment is obtained, the challenge remains to see if laboratory scale-down models can be developed that are more accurate predictors of production performance than pilot-plant trials.

1.5.3. Scale-down's integration with other process development tools

Accurate scale-down mimics would expedite the transition of a product from laboratory to production; however, some *rational* framework is required in order to conceptualise potential processes and select the best one. (As previously mentioned, development should be as efficient and rapid as possible, and result in the most economical process.) The coherent development strategy will be referred to as total process synthesis and design. A rational methodology is one in which a process is formulated by selecting unit operations compatible with some defined properties of a feed stream (explained in sections 1.5.3.1 and 1.5.3.2); executing random screening experiments, attributed to an unawareness of relevant mechanisms, may be practical and sensible but is not considered *truly* rational (according to this author).

A lack of fundamental understanding of biological systems precludes application of a rational synthesis methodology for a fermentation process. The main upstream challenges are selection of optimal strain, media components and their concentrations, feeding regime, reactor design and scale-up parameters. Selection of strain and media components is accomplished through factorial design screening experiments, guided only loosely by the elemental composition of an organism and perhaps some knowledge of its metabolism. The baffled stirred-tank reactor has gained near universal acceptance for microbial, yeast and animal cell culture, and been scaled on oxygen transfer rate (Humphrey, 1998). There is some scope for rational determination of the optimal feeding regime by metabolic pathway engineering, yet much of the underlying biochemistry has still to be discovered. At present, considerably more opportunity exists to develop a rigorous strategy that specifies the best sequence and conditions of downstream operations.

1.5.3.1. Purification process synthesis

Work has been done to develop expert systems that can specify the most efficient sequence of chromatographic steps for the purification of a certain product based on its properties and those of the contaminants (Lien *et al.*, 1987; Leser and Asenjo, 1992; Lienqueo *et al.*, 1996; Leser *et al.*, 1997). This method should complement chromatographic scouting and render it more focused. Expert systems are being made ever more powerful with the mapping of genomes of the most popular cell lines such as *E. coli*, *S. cerevisiae* and Chinese Hamster Ovary (CHO), and the application of proteomics. These serve to elucidate the full range of proteins found in cells and their relative concentrations in different parts of the cell when it is exposed to various environmental conditions (Ashton, 1999). A more defined process stream permits intelligent software to exploit property differences more effectively. These simulation packages address the synthesis of high-resolution operations, but do not include a global perspective required for *total* or *whole* process synthesis because they ignore primary recovery and isolation stages of downstream processing.

1.5.3.2. Total process synthesis

This is currently being addressed (Storey and Dunnill, 2000). First, feed stream characteristics (density, viscosity, volume, solids concentration, clarification by laboratory spin test, shear sensitivity of product, cells and precipitates/flocculates, and fouling of chromatographic matrices) are measured and converted into *synthesis indices*. For example, homogenates would be assigned a much lower separation rating on an arbitrary scale (say 1 to 10) than their whole cell suspensions because the former are much more difficult to clarify due to their smaller and relatively broader size distributions. Next, indices for equipment are estimated using historical data; e.g. a

typical filter gives a better clarification but perhaps a lower throughput or solids capacity than a disc stack centrifuge.

Indices of the starting material are then compared to indices of various pieces of equipment and the most similar one(s) selected. The composition of the exit streams from the applied unit operation(s) are then estimated. One of the exit streams becomes the feed for the next unit operation and the process repeats itself, thus generating several process flow-sheets. Quantification of the degree of similitude between a stream and piece of equipment is rather complicated because the importance of an index is a function of position within the overall bioprocess, e.g. clarification is important in earlier stages but fouling becomes a more prevalent concern closer to ultrafiltration and chromatography. Despite this complexity, the above synthesis method is rational because it involves the creation of process based on the properties of the feed stream.

1.5.3.3. Interdependence of process synthesis, modelling and scale-down

As one progresses downstream, the number of flow-sheets increases steadily but not dramatically because many stages are predetermined such as cell disruption, cell or debris separation and chromatography. However, the ability to predict stream composition and quality may decrease markedly after only a few steps. This loss in prognostic capability is alleviated by linking mathematical models of the relevant unit operations through a windows approach (Woodley and Titchener-Hooker, 1995; Zhou and Titchener-Hooker, 1999) to discriminate better options to within an accuracy of $\pm 30\%$. Should greater accuracy be needed, experiments should be conducted with laboratory mimics of the large-scale unit operations. Starting with the same upstream material, processes should be scaled down to a critical juncture in the downstream, beyond which, effort would be wasted. For example, it would be useless to carry through a process in which sufficient

solid-liquid separation had not been achieved to prepare for chromatography. At the critical point, synthesis indices would be re-measured and the information used to select more promising processes. In this way, process synthesis is inextricably linked to scale-down because for the indices to be evaluated accurately, the process must be scaled-down and run. The converse is also true, as the synthesis methodology directs which flow-sheets should be experimentally verified and to what point. Obviously it would be too time-consuming to explore all options experimentally. Through a somewhat overlapping integration of synthesis indices, modelling and scale-down mimics, a final process is defined.

1.5.3.4. *Process design*

The above process becomes the basis for design, which includes equipment specification and operating conditions. From the information gathered on process streams by synthesis and scale-down tests, equipment options are proposed and then tested on scale-down systems. For example, it may have been determined that ultrafiltration is most suitable for a concentration step but at least a few membranes types should be considered. They may differ in composition (determines strength and maximum operating pressure, resistance to cleaning agents, hydrophobicity, charge, protein adsorption, etc.), mean pore size and distribution (retention and transmission of various species), and structure (flat sheet, spiral wound, hollow fibre, etc.), all of which affect flux rates and hence the final size. Another example would be selection of the *most* appropriate type of centrifuge (e.g. disc stack, tubular-bowl, multichamber-bowl or CARR) for separation of a certain suspension. Equipment selection requires an in-depth knowledge of the bioprocess, equipment and its availability, facility and economics. Once a sequence of operations have been specified, the impact of changes in the operating

conditions can be determined, thus permitting a preliminary optimisation of the process at the smallest scale feasible.

Total process synthesis and design form a complex procedure where the design evolves from an initial stage to the final stage using the available tools such as synthesis, modelling and scale-down, and repeatedly revising and refining the initial assumptions and restrictions (Leser and Asenjo, 1992). Or as Siirola (1996) notes:

“Process design is a complex activity involving a combinatorially large number of considerations, decisions, alternatives, and actions, involving different disciplines and points of view, and taken with different focus and at different levels of detail. Process design is but a part of the overall chemical innovation process which leads from the identification of a need to the construction and operation of a facility to produce material believed to satisfy that need.”

1.6. METHODS OF SCALING

The following section is a summary of general scaling methodologies, but it must be noted that each unit operation has its own specific scaling criteria.

Tactical methods for scaling include (Atkinson and Mavituna, 1991): fundamental methods; semi-fundamental methods; dimensional analysis, regime analysis; heuristics; trial and error; and combinations of the above. In dimensional analysis, the values of dimensionless groups of parameters are kept constant on scale-up so that the relative importance of the mechanisms influencing the process remains. In practice, it is impossible to maintain all dimensionless groups constant and, therefore, the most influential groups must be identified and the rest neglected. To deal with a lack of fundamental knowledge of all mechanisms involved in the behaviour of large-scale, transient bioprocesses, regime analysis bases on scaling constant characteristic times and

not dimensionless numbers. Oosterhuis *et al.* (1985) employed the following technique to optimise a gluconic acid fermentation: régime analysis of the process at production scale; simulation of the rate-limiting mechanisms at laboratory scale; modelling and optimisation of the process at laboratory scale; and optimisation of the process at production scale by translation of the optimised laboratory conditions.

Kossen (1992) stated that “empathy” must be shown for the product by considering the following when scaling equipment: phenomena experienced by the product in terms of gradients (chemical potential, temperature, velocity, pressure); values of the time constants of these events and the response of the organism to them; scales (i.e. size) of these events compared to those of the product; and cumulative effects.

Regardless of the scaling methodology utilised, it is well worth following some practical considerations when scaling up: performing careful material balances; paying attention to the biochemistry involved; initially examining a wide ranges of variables and their limits; and performing proper engineering analysis (Harrison, 1994).

1.7. SCALING OF UNIT OPERATIONS

1.7.1. Degree of scale-down

The goal of scale-down is to simulate the conditions and performance of manufacturing equipment at a smaller scale. This could be accomplished in some cases by fabricating a geometrically similar, small-scale replica of the industrial machine, which is the case for stirred tank reactors and membranes. However, this approach would prove cost-prohibitive and unfeasible when applied to a continuous centrifuge. A better strategy is to modify the existing piece of industrial equipment in such a way that it

requires only a fraction of the process material to give similar performance (Maybury, 1998); however this still requires several (>5) litres of material. The following section examines the progress made in the scaling of various unit operations, particularly from manufacturing to laboratory.

1.7.2. Scale-up problems

Reisman (1993) asserts that *“because it is impossible to keep all chemical/physical parameters constant on changing scale, it is important to know what boundaries exist for successful implementation.”* Several problems can be encountered when scaling up a process, giving rise to issues of asepsis (volume of inputs and sterilisation), containment, time (heating/cooling cycles, holding time, transfer time), volume of equipment (turnover time, heat transfer, fill/emptying time, internal fittings, finish, material of construction), cleaning (fouling, scale formation, equipment reuse, equipment inspection, agents to use and their disposal), and regulation (Installation, Operational and Performance Qualification, current Good Manufacturing Practices, waste disposal, environmental, local codes). One reason for a failed commercial run may be that the process technology itself was not fully communicated and/or properly transferred to the manufacturing setting. Even a minor change may result in poor performance. Young *et al.* (1984) described the physical simulation of a complex automated manufacturing and material handling system by constructing scaled-down fully functional components for purposes of analysis and design in a laboratory to experience all the intricacies in the full-scale production environment.

1.7.3. Impact of computational fluid dynamics (CFD)

One of the major reasons for advances in the scale-down of unit operations is progress in understanding fluid dynamics and particle-fluid interactions by CFD. These simulation packages are now less expensive, easier to use and more powerful due to improvements in mesh design (highly flexible, unstructured), the ability to modify dynamically selected regions, numerical solvers, physics modelling, user interfaces and computer hardware (Gosman, 1998; Harris *et al.*, 1996).

1.7.4. Fermentation

Obviously efficient product formation lies at the top of the hierarchy. Traditionally, the scaling of fermentation is based on maintaining physical parameters such as volumetric oxygen transfer coefficient, power input, aeration rate, mixing time, etc., constant (Enfors *et al.*, 1998). Despite the great advances in mixing technology through meticulous attention to geometric design and computational fluid dynamics (Harris *et al.*, 1996; Gosman, 1998), poorer yields and productivities are often observed upon scale-up. This may be due to several reasons: limited heat transfer capability especially in fermenters larger than 10^5 L; flooding of the impeller at lower superficial air velocities; increased culture age (25-50 generations) which limits stability; hidden auxotrophy upon exposure to poorer mixing and media quality; and locally high substrate concentrations around the feed point resulting in a reversible increase in the substrate metabolism, which at high cell densities causes the local oxygen consumption rate to exceed the transfer rate (Humphrey, 1998; Enfors *et al.*, 1998; Bylund *et al.*, 1999). Future models should concentrate on integrating fluid dynamics and microbial kinetics.

Efforts have also been made to minimise the performance gap between the shake flask and the fermenter, with growth rates substantially lower in the former type of vessel

due to pH shifts, oxygen limitation and depleted nutrient concentrations. While giving more representative data of industrial fermenters, bench-top ones are still awkward, complicated and expensive items of equipment. A fed-batch, shake flask system (fed-batch-pro and PROFORS; DASGIP GmbH, Germany) with pH, oxygen, temperature and nutrient control has been developed to achieve more efficient screening and scale-up of cell lines.

In the past, it was generally accepted that fermentations costs accounted for 50% or more of the overall unit product cost; however with newer products and the demand for greater purity by regulatory authorities processes leading to increasing use of affinity resins, downstream processing now can incur up to 90% of costs (Reisman, 1993). Most work has been done on the scale-up of fermentations, but greater attention is being paid to isolation and purification steps.

1.7.5. Homogenisation

Homogenisation is used to release intracellular products by rupturing cells. Cell breakage is a function of the pressure and number of passes (Hetherington *et al.*, 1971). Siddiqi *et al.* (1997) demonstrated equivalent protein release and particle size distribution of cell debris for homogenisers of different sizes (40 mL batch, 2 L at 80 L h⁻¹, and 30 L at 300 L h⁻¹); performance was independent of valve geometry and flow rate which was due to similar velocities being achieved in the valve gap and was consistent with elongational stresses acting as the mechanism for disruption.

1.7.6. Precipitation

Baffled stirred tanks are the standard precipitation vessels and are readily scaleable in terms of fluid dynamics if geometric similarity is maintained for all components (Nagy

et al., 1993). Differences can arise when insufficient detail is paid to impeller design such as failure to keep blade width to diameter constant upon change of scale (Oldshue, 1983). Precipitation has been scaled quite successfully on constant mean velocity gradient, Camp number and rate of reagent addition to volume of reactor (Bell and Dunnill, 1982; Bell *et al.*, 1983; Fisher and Glatz, 1988). In practice, it may be difficult to maintain design similarity between vessels due to limited desired effort to design and construct an *exact* small-scale replica. This results in different contacting conditions, which could influence precipitate properties and composition. It is generally accepted that poorer mixing upon addition of reagent produces more nuclei and thus more and smaller particles, sometimes resulting in over-precipitation due to solubility being a function of mixing (Foster *et al.*, 1976; Rothstein, 1994; Richardson *et al.*, 1990). Mixing effects seem to be very dependent on the biological system as some authors have reported no influence of contacting conditions on precipitate characteristics, and others have actually observed the formation of larger particles (Fisher *et al.*, 1986; Iyer and Przybycien, 1994; Iyer and Przybycien, 1995). Suffice to say that optimisation of a precipitation would be facilitated by elucidation of the complex mechanisms *relevant* to each specific system of study. This unit operation is covered in more detail in Chapter 2.

1.7.7. Centrifugation

Centrifugation has traditionally been scaled by maintaining the ratio of flow rate over centrifuge separation area (Sigma) constant and the introduction of correction factors accounting for non-ideal flow (Ambler, 1959). A disc stack centrifuge was scaled down with inserts which reduced the available separation area and solids capacity (Mannweiler and Hoare, 1992; Maybury *et al.*, 1998). Maybury *et al.* (2000) manipulated Sigma theory to account for acceleration and deceleration periods, which become significant

during short spin times in laboratory batch centrifugation. Good agreement was shown for shear-insensitive species such as polyvinyl acetate particles or cell debris, but gross differences were observed with precipitates. The main focus of this thesis is the development of a laboratory process (high-speed rotating disc device linked to centrifugation; Chapter 3) to mimic the performance of a larger-scale, continuous centrifuge. An overview of the results may be found in the abstract as well in section 1.9, which provides a summary of the chapters. A review of centrifugation is provided in Chapter 2.

1.7.8. Conventional filtration using precoat and body feed

Filtration scale-up has been developed from practical experience with limited attention paid to theory due to its limitations. These include: the unique nature of most slurries meaning that filtering characteristics must be determined on the actual slurry in question and for the specific operating conditions; the evolving nature of the filter cake; and the effect of complex interactions between the different process parameters (Wolthuis and Dichiarra, 1997). CFD should help to elucidate the mechanisms involved in formation of the cake structure, flow through it and particle entrapment. Chapter 5 describes the scale-down of an industrial rotating vertical leaf filter by converting a Nutsche pressure filter to allow continuous, constant-rate operation when connected to a miniature diaphragm pump.

1.7.9. Tangential-flow membrane filtration

Traditional scale-up procedures for cross-flow or tangential-flow filtration (TFF) include keeping the same membrane material, filtrate volume to surface area ratio, pore size, channel height, flow path, geometry and retentate and filtrate pressure constant,

while increasing channel width and number of channels to enlarge the membrane area (Brose *et al.*, 1996). However, many other variables have not been controlled, leading to differences in product quality, yield and process time. Van Reis *et al.* (1997) demonstrated that “*predictable scale-up can only be achieved by maintaining fluid dynamic parameters which are independent of scale.*” This is accomplished by controlling operating parameters (feed flow rate, retentate pressure, feed batch ratio and temperature, geometry (channel length, height, turbulence promoter and entrance/exit design), materials (membrane, turbulence promoter and encapsulant compression), system geometry (flow distribution) and cassette manufacturing procedures and tolerances.

1.7.10. Chromatography

For chromatography, most work has focused on scaling up elution methods using relationships of similitude. Several variables such as flow rate, sample load, gradient conditions, production rates and column utilisation have been derived for large-scale columns (Kennedy *et al.*, 1988). Many parameters should remain constant when scaling a chromatographic process. Generally, the column bed-height and linear flow velocity are kept constant and the diameter increased (Freitag and Horvath, 1995). The following variables should also remain constant: stationary phase (particle size, base matrix, functional groups and degree of substitution), mobile phase (buffers, protein concentration, etc.), inlet and outlet pressures, type of ancillary equipment (e.g. pump), and the ratios of sample load and gradient volumes to resin volume (Sofer and Hagel, 1997; International Conference on Harmonization, 1995). Adherence to the above principles should result in resolution and peak shape being independent of the column size. In practice, however, a decrease in efficiency is noted on scale-up primarily due to the existence of unstable, non-uniformly packed regions (Versele and Dewaela, 1985), so

that bed height must also be increased slightly to maintain the number of theoretical plates (Sofer and Hagel, 1997). Kaltenbrunner *et al.* (1997) noted that the use of very small columns leads to extra (i.e. pre- and post-) column effects that may overwhelm all broadening effects.

1.8. SYNOPSIS OF CHAPTERS

Chapter 1 has provided a review of scaling technologies and their role within bioprocess development. It was mentioned that very little effort has gone into the scale-down of centrifugation and extending this to the laboratory. Two primary biological systems of study were chosen for scale-down work. The first is a suspension of yeast precipitates derived from the salting-out of clarified homogenate with ammonium sulphate; the second is Fraction IV, a cold-ethanol precipitation stage in the Cohn fractionation process for the purification of albumin from human plasma. Both suspensions have small mean particle sizes, posing serious difficulty in attaining a high degree of clarification.

Work focused on mimicking the performance of a pilot multichamber-bowl centrifuge because of its widespread use in plasma fractionation. Chapter 2 outlines the development of a scale-down methodology for centrifugation and how a careful mass balance of total protein and product permits the calculation of several performance parameters, especially the fraction of solids sedimented and the degree of sediment dewatering. Good agreement was obtained in terms of dewatering but a much poorer recovery was observed in the continuous centrifuge, this attributed to particle break-up in the feed zone as process material is rapidly accelerated to the speed of the bowl. Chapter 3 discusses how a rotating-disc device can generate fluid forces of similar magnitude to

those in the entrance region of a pilot centrifuge. Shearing of the precipitate suspension under specific conditions prior to laboratory scale-down centrifugation permitted accurate prediction of pilot-scale clarification. This concept was then translated to predict the performance of other large-scale centrifuges (disc stack, CARR, production-scale multichamber-bowl), as detailed in Chapter 4. Chapter 5 describes the scale-down of a rotating vertical leaf filter by modification of a laboratory-batch, Nutsche pressure-filter and compares its performance to that of centrifugation, the former yielding superior clarification and dewatering for the plasma precipitate suspension. The influence of the extent and type of primary solid-liquid separation on guard filtration and chromatography was investigated in Chapter 6. General conclusions are formulated in Chapter 7 and proposals for future work presented in Chapter 8, followed by references and appendices. Appendix A gives the tabulated values of the protein mass balance performed on the laboratory and pilot processes described in Chapter 2. Theoretical considerations central to the computational fluid dynamics (CFD) analysis utilised in Chapters 3 and 4, are explained in Appendix B.

2. CHAPTER 2: THE LABORATORY SCALE-DOWN OF PROTEIN PURIFICATION PROCESSES INVOLVING FRACTIONAL PRECIPITATION AND CENTRIFUGAL RECOVERY

ABSTRACT

The ability to predict the performance of large-scale processes is central to the rapid development of successful operations at the pilot and industrial scale. In this chapter, the operation at laboratory scale of precipitation reactors and centrifuges is examined for protein precipitate recovery and dewatering and how they might best mimic large-scale reactors and centrifuges, in this case a pilot-scale batch stirred-tank reactor and a multichamber-bowl centrifuge. Novel approaches to bench-top centrifuge operation are provided, in particular with a view to delivery of material for subsequent high resolution purification which would be obtained at full pilot scale. Results are presented in terms of properties of the protein precipitates, the fraction of solids recovered and the extent of dewatering achieved. Good agreement was obtained at bench-scale (a 1000-fold scale-down factor) for all of these parameters for pilot-scale, batch-feed operation. In addition, the methodology developed allows identification of the extent of break-up that occurs in continuous-feed centrifuges when processing shear-sensitive materials such as the protein precipitates studied here.

Note: A modified version of this chapter has been accepted for publication as a paper in *Biotech. Bioeng.* (Boychn *et al.*, 2000a).

2.1. INTRODUCTION

2.1.1. Scale-down

The scale-down of industrial processes provides a powerful tool to minimise the time required for bioprocess development because it allows the study of more process options at small scale and hence rapid identification of unacceptable ones, and of the operating window to be studied. Small-scale experimentation is more advantageous than pilot-plant work because the former offers ease of use, minimal process run times, the opportunity to study a wider range of process options and delayed risk of capital investment. This study reports the translation of scale-down to the laboratory level by developing techniques to mimic the performance of a pilot-scale process using laboratory bench-top equipment. The specific sequence of unit operations, precipitation, feed, centrifugation and recovery, is central to many industries including blood fractionation where good separation (clarification and dewatering) is critical to achieving high yields (Bell *et al.*, 1983; Foster, 1994). This process also addresses one of the most challenging aspects of scale-down studies; that is the key link between the material generated in a reactor and the subsequent high-resolution chromatography columns. The successful scale-down of the latter also depends crucially on the relevant material being available for study, i.e. as generated by a good scale-down mimic rather than an ideal, laboratory-scale process.

The formation and recovery of protein precipitates are important operations widely used in industrial-scale purifications (Englard and Seifter, 1990). Applications range from primary isolation procedures, in which the amounts of contaminating proteins are decreased and/or sizeable reduction of process volume is achieved, to finishing operations (Paul and Rosas, 1990). Precipitation is generally a low-cost, high-yield stage suitable for

use with biological streams containing highly concentrated soluble and insoluble contaminants (Stavriniades *et al.*, 1993).

2.1.2. Precipitation

Successful scale-down requires a detailed understanding of the mechanisms involved in order to identify the key parameters for scaling purposes. Precipitation occurs in four distinct stages (Bell *et al.*, 1983): nucleation upon achievement of supersaturation by addition of a reagent to the protein solution or through adjustment of pH to the isoelectric point and by temperature regulation; perikinetic growth of nuclei by the incorporation of insoluble colloidal protein through Brownian diffusion until a maximum particle size is attained; orthokinetic growth by random collision and adhesion of primary particles to form aggregates promoted by turbulent mixing; and conditioning of the precipitate suspension under low shear rates to promote further growth and also increase in density and strength of the aggregate by shear-induced rearrangement.

Protein solubility affects the purification performance and the aggregate characteristics impact on the performance of the subsequent centrifugal separation step. Protein solubility is affected primarily by the type and concentration of precipitant, pH and ionic strength (Foster *et al.*, 1976; Fisher and Glatz, 1988; Iyer and Przybycien, 1994, 1995). The physical properties of the aggregates depend on several factors: the type of precipitation reactor (Foster *et al.*, 1976); choice, concentration and rate of addition of precipitating agent (Fisher *et al.*, 1986); initial protein concentration; nature and extent of mixing and residence time in the reactor (Glatz *et al.*, 1986; Fisher and Glatz, 1988; Rothstein, 1994). Many precipitator designs have been studied including the batch stirred-tank reactor (BSTR), the continuous stirred-tank reactor (CSTR) and the continuous-flow tubular reactor (Bell and Dunnill, 1982). In the last case, a short

conditioning time results in large, irregularly shaped particles of low density which are more prone to shear damage than precipitates formed in a STR. This is due to the high flow stresses in the impeller region which cause precipitate break-up leading to smaller, denser and consequently less shear-sensitive particles. This work focuses on the batch tank due to its widespread industrial use (Foster, 1994). It consists of a baffled tank agitated by an impeller, usually a Rushton turbine. These reactors have been scaled successfully for protein precipitate formation by maintaining constant the mean power dissipation per unit volume constant for tanks ranging from 0.27 to 200 L. Reasonable agreement was obtained for the d_{90} values, which largely determines subsequent centrifugal recovery (Hoare *et al.*, 1982) with the lowest mean velocity gradients giving the largest final aggregates. Scaling using constant mean velocity gradient, Maybury (1999) observed good agreement for d_{50} values of yeast protein-ammonium sulphate precipitates using vessels of 0.9 to 50 L.

2.1.3. Centrifugation :

Once a protein has been precipitated in a vessel it must then be recovered from the mother liquor by some separation operation, usually centrifugation or filtration. To design properly an entire precipitation process, knowledge of protein chemistry, phase equilibration, particle behaviour, solid-liquid separation and reactor design is essential. To date, no theoretical model exists that successfully consolidates all of these various factors and consequently process design is mainly an empirical exercise consisting of laboratory- and pilot-scale experiments through to full-scale operation (England and Seifter, 1990).

The multichamber-bowl centrifuge used in this study is representative of the centrifuges used in the biotechnology industry; namely continuous-feed, high-speed

machines designed for the recovery of fine, low-density-difference biological particles (Foster, 1994). Characteristics of the multichamber-bowl centrifuge are a large solids-holding space with good clarification efficiency and dewatering. The machine consists of two to six concentric sections that serve to extend the axial flow path and increase the area available for separation (Figure 2.1). Heavier solids are deposited in the inner chamber (closest to the centre of rotation) while lighter particles are able to reach the outer chamber before the greater centrifugal force causes them to collide with the bowl wall. The liquid is fed through the top of the centrifuge, progresses radially outwards through the series of chambers and is expelled at the top of the machine; this leads to long residence times, often resulting in temperature increases which are overcome by direct cooling of the bowl, centripetal pump and frame. Multichamber bowls operate with a flooded or hydro-hermetic feed zone, allowing feed material to be accelerated more slowly than the standard entrance region in which feed simply impacts on the metal surface. Disadvantages of multichamber-bowl centrifuges include those of tubular-bowl centrifuges, notably no solids discharge and batch recovery of solids and difficult cleaning (Bell *et al.*, 1983).

Several methods have been suggested for comparing the performance of centrifuges. One popular method is the Sigma concept, that is the equivalent settling area of the centrifuge (Ambler, 1959). It is based on Stokes' law, which describes the sedimentation of a particle in a centrifugal field. Theoretically, maintaining the ratio of flow rate to separation area constant should result in the same clarification for all centrifuges. The settling area is evaluated based on idealised flow patterns and correction factors must be introduced to account for non-ideal flow (i.e. regions of local turbulence), which often occurs in industrial equipment.

If product loss due to over-precipitation can be minimised, then the yield is crucially dependent on the extent of centrifugal dewatering of the sediment (Bulmer, 1992). This is particularly important when processing suspension of high solids content and when there is a need to avoid excess dilution of the soluble phase, for example in a wash step (Ward and Hoare, 1990).

Previous scale-down studies have been by modification of pilot-scale centrifuges. The throughput of a disc stack centrifuge has been reduced ten-fold by decreasing the number of active discs through a series interlocking of inserts (Mannweiler and Hoare, 1992). The volume of process material required for centrifuge characterisation has been reduced four-fold using inserts in the solids-holding space (Maybury *et al.*, 1998). Similar recoveries of a dilute suspension of polyvinyl acetate particle in the full-stack and scaled-down centrifuges confirmed validity of the mimic.

Disc-stack centrifuges have not found considerable use in the plasma industry because the loss of liquid on solids discharge severely affects yields over a multistage fractionation process. Hence, for the multichamber-bowl centrifuge studied here, there is a need to consider carefully both clarification and dewatering issues to reflect performance of scale-down achieved (More and Harvey, 1991).

The aim of this study is to examine how an integrated precipitate preparation and recovery sequence can be operated at a laboratory scale (e.g. 10 to 100 mL process material) to mimic pilot-scale or industrial-scale operation. The initial target is a scale-down factor of approximately 1000-fold for the precipitation stage and the translation from continuous-flow pilot to laboratory-batch centrifuges with a similar scale-down ratio.

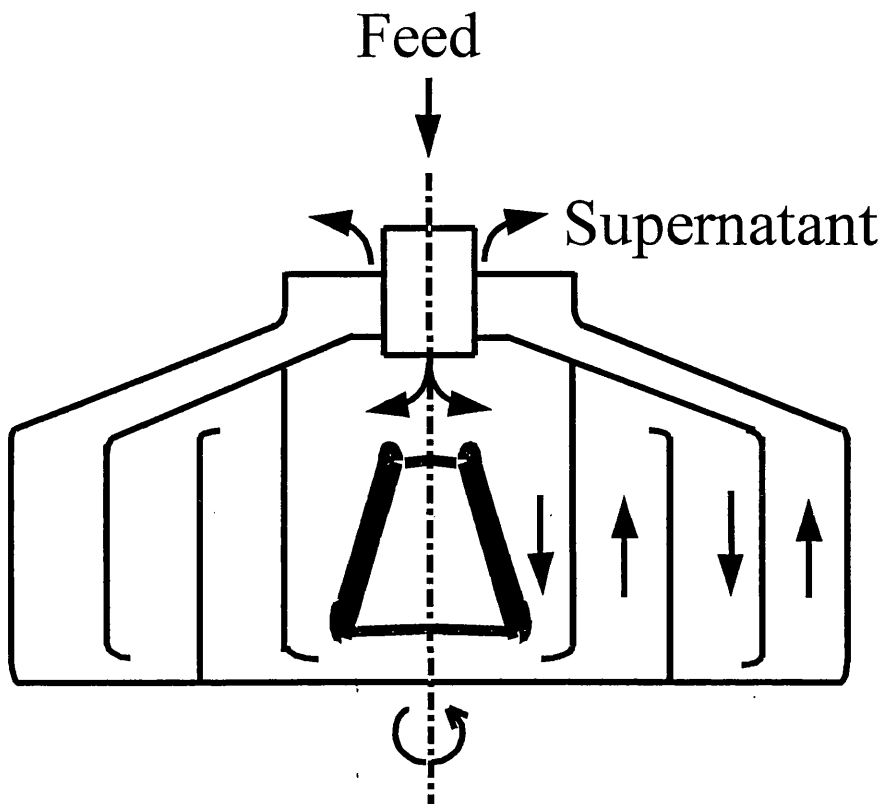


Figure 2.1. Cross-section of a generic multichamber-bowl centrifuge displaying the main liquid flow path. Dimensions of the Westphalia KDD 605 pilot multichamber-bowl are the following:

Chamber	r_i (m)	r_o (m)	L (m)
1 (inner)	0.024	0.047	0.094
2	0.053	0.060	0.100
3	0.063	0.070	0.100
4 (outer)	0.074	0.079	0.100

where r_o is the radius of the chamber and r_i is the inner radius determined by the weir and L is the length of the chamber. The rotational speed of the bowl N , is 167 r s^{-1} . Characteristics of the laboratory centrifuge are as follows: $R_1 = 0.049\text{m}$, $R_2 = 0.130 \text{ m}$.

2.2. THEORETICAL CONSIDERATIONS

2.2.1. Precipitation

When scaling-down a precipitation process, the goal is to be able to mimic a larger reactor operating under feasible conditions and to provide the basis whereby the eventual larger-scale process can be operated under identical conditions. Several parameters should be kept constant including tank geometry (height to diameter ratio), impeller type, diameter of the impeller relative to that of the tank, placement of the impeller, baffle geometry, mean velocity gradient, ageing parameter (Camp number) and residence time. However, fluid flow patterns will change somewhat when increasing the scale of a reactor even if the above factors are similar for the two scales, thus affecting mixing.

There is a wide range of velocity gradients in the vessel but an average value, \bar{G} can be assumed based on power dissipated, P per unit volume, V (Bell *et al.*, 1983):

$$\bar{G} = \left(\frac{P}{V\mu} \right)^{1/2} \quad (2.1)$$

where μ is the dynamic viscosity.

The power input, P , is calculated by:

$$P = P_o \rho N^3 D^5 \quad (2.2)$$

where P_o is the power number ($P_o = 6$ for a four-baffled stirred tank with Rushton impeller and $Re > 5 \times 10^3$, where Re is Reynolds number, $Re = \rho ND^2 / \mu$), ρ is the density of the bulk suspension, N is the impeller speed and D is the impeller diameter (Rushton *et al.*, 1950).

In addition to particle size it is also important to maximise strength because precipitate particles are sensitive to shear forces which may result in breakage in high

flow devices such as pumps and centrifuge feed zones (Bell and Brunner, 1983; Mannweiler *et al.*, 1989). It has been shown that particle strength is maximised when precipitate suspensions are aged to a Camp number, $Ca = \bar{G} t$ of 10^5 for a range of shear rates and times (Bell and Dunnill, 1982).

2.2.2. Centrifugation

2.2.2.1. Clarification

The Sigma or equivalent “settling area” is commonly used to describe the recovery process in a centrifuge and is an index of its size, i.e. the area equivalent to that of a settling tank capable of the sample separation performance whilst acting under gravity. The concept based on Stokes’ definition of settling velocity v_g , of a particle due to gravity (Ambler, 1959):

$$v_g = \frac{d^2 \Delta \rho}{18 \mu} g \quad (2.3)$$

where d is the particle diameter, $\Delta \rho$ is the density difference between the solid and suspension, μ is the dynamic viscosity of the suspension and g is the gravitational constant. Extending the above to a centrifugal field results in:

$$v_s = \frac{d^2 \Delta \rho \omega^2 r_e}{18 \mu} \quad (2.4)$$

where ω is the angular bowl velocity and r_e is the settling radius. The above equations assume a low particle concentration (no hindered settling) and laminar settling of the particle, i.e. $Re = v_s \rho d / \mu < 0.5$ where ρ is the suspension density.

Different centrifuge designs result in different expressions for the settling area. Sigma derivations assume an ideal system in which particles starting at half the settling distance will just be removed from the suspension.

For a continuous-flow tubular-type centrifuge, a particle at radius r and distance z from the bottom inlet has two velocity components due to: radial motion,

$$\frac{dr}{dt} = \frac{v_g \omega^2 r}{g} \quad (2.5)$$

and due to flow through the centrifuge (assuming a uniform flow field),

$$\frac{dz}{dt} = \frac{Q}{\pi(r_2^2 - r_1^2)} = \frac{QL}{V} \quad (2.6)$$

where V is the volume of suspension in the bowl. Rearrangement, combination and integration leads to the following expressions for the equivalent (to a gravity settling pond) area, Σ , of the centrifuge:

$$\Sigma = \frac{\pi L \omega^2}{g} \frac{(r_o^2 - r_i^2)}{\ln\left(\frac{2r_o^2}{(r_o^2 + r_i^2)}\right)} \quad (2.7)$$

where L is the length of a chamber, and r_i and r_o are the inner and outer radii of the chamber bowl.

The equivalent settling area for a multichamber-bowl centrifuge (see Figure 2.1) is calculated by considering the machine to be a series of tubular bowls:

$$\Sigma_{mc} = \Sigma_1 + \Sigma_2 + \dots + \Sigma_n \quad (2.8)$$

where n is the number of chambers.

For a laboratory centrifuge with a swing-out rotor, only radial motion occurs. Rearranging and integrating Equations 2.5 yields:

$$\Sigma_{lab} = \frac{V_{lab} \omega^2}{2g \ln\left(\frac{2R_2}{R_2 + R_1}\right)} \quad (2.9)$$

where V_{lab} is the volume of material in the tube, and R_1 and R_2 are respectively the inner and outer radii (i.e. the respective distances between the centre of rotation and the top of the liquid and the bottom of the tube).

For short spin times, acceleration and deceleration phases also contribute significantly to the process (Maybury *et al.*, 2000). Assuming linearity for changes in rotational speed, a modified expression is obtained:

$$\Sigma_{lab} = \frac{V_{lab} \omega^2 (3 - 2x - 2y)}{6g \ln\left(\frac{2R_2}{R_2 + R_1}\right)} \quad (2.10)$$

where x and y are the fractional times required for acceleration and deceleration, respectively.

It is possible to compare centrifuges of different designs and sizes as follows:

$$\frac{Q_{mc}}{C_{mc} \Sigma_{mc}} = \frac{V_{lab}}{t_{lab} C_{lab} \Sigma_{lab}} \quad (2.11)$$

where Q_{mc} is the flow rate through the multichamber-bowl machine, t_{lab} is the residence time in the laboratory centrifuge, and C_{mc} and C_{lab} are correction factors to account for non-idealities in fluid flow. If the laboratory centrifuge is considered as the baseline (i.e. $C_{lab} = 1.0$), then the multichamber-bowl has been shown to have a correction factor, C_{mc} , of approximately 0.9 (Svarovsky, 1990).

2.2.2.2. Dewatering

A centrifuge is often characterised by the maximum or the mean relative centrifugal force (RCF), which is defined for the laboratory centrifuge as:

$$RCF_{max} = \frac{v_s}{v_g} = \frac{\omega^2 R_2}{g}; \quad RCF_{mean} = \frac{\omega^2}{g} \left(\frac{R_2 - R_1}{\ln(R_2/R_1)} \right) \quad (2.12)$$

and similarly for the multichamber-bowl centrifuge.

In a continuous-feed centrifuge such as the multichamber-bowl, recovery occurs in a short time (the liquid/suspension residence time in the bowl), followed immediately by compaction until the bowl is filled (solids residence time, which is generally 10-fold the liquid residence time). Laboratory spin times required to mimic this recovery (conducted at the same RCF_{mean}) are considerably longer than the mean liquid residence time in industrial centrifuges, approximately 3 fold greater. However, the initial spin time accounts only for sedimentation, which is the trajectory of a particle up to its point of impact with a solid surface. To mimic the compaction in a pilot centrifuge, laboratory tubes must be re-spun at a rotor speed corresponding to the RCF_{max} experienced in the large-scale machine (determined using the outer radius of the outer chamber). The time for which the sediment is to be compacted, t_c , is calculated by determining the *average* residence time of solids in the holding area of the centrifuge (i.e. the first solids sedimented see the full compaction time, but the last ones to settle experience virtually no compression), which is dependent on the fractional recovery of solids, F , and Q_{mc} :

$$t_c = \frac{V_s}{2F\phi_v Q_{mc}} \quad (2.13)$$

where V_s is the solids holding capacity of the pilot centrifuge and ϕ_v is the volume fraction of solids in the feed stream. The laboratory time of compaction is merely an estimate of the much more complex process occurring in the multichamber-bowl centrifuge. Larger particles will sediment in the inner chamber and experience a greater compaction time; smaller particles will tend to settle in the outer chamber, undergo a lower compaction time and yet a much higher RCF . Hence, not only may particles of varying sizes exhibit different dewatering potentials, they will also be exposed to distinct

compaction processes, which may or may not lead to significant differences in dewatering values.

2.2.3. Separation process

The study of separation processes requires as a first basis a mass balance for the various components. In order to compare these it is necessary to arrive at a balance in full agreement for the protein phase, P :

$$P_F = P_L + P_S = P_{sup} + P_{sed} \quad (2.14)$$

where the subscripts F , L , S , sup and sed denote feed, liquid, solid, supernatant and sediment, respectively (see Figure 2.2 for an explanation of these terms). There are also errors, e , in the measured mass balance:

$$\begin{aligned} e_1 &= P_F - (P_L + P_S) \\ e_2 &= P_F - (P_{sup} + P_{sed}) \end{aligned} \quad (2.15)$$

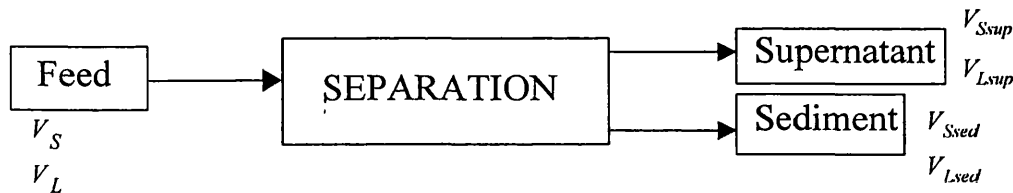


Figure 2.2. A general solid-liquid separation with all relevant streams. Subscript S denotes solid, L liquid, sup supernatant and sed sediment.

Consistent correction of the mass balance is achieved by using pre-determined weightings for each of the process streams analysed:

$$\begin{aligned} P_S &= P_S + ae_1 \\ P_L &= P_L + be_1 \\ P_{sup} &= P_{sup} + ce_2 \\ P_{sed} &= P_{sed} + de_2 \end{aligned} \quad (2.16)$$

where a , b , c and d are weighting factors such that $a + b = 1$ and $c + d = 1$. In this study, since the measured errors are distributed approximately equally between the liquid and solid phases, $a = b = c = d = 0.5$.

From a complete protein mass balance on all process streams displayed in the above diagram, the following augmented matrix can be obtained:

Inputs Outputs	V_{Ssed}	V_{Lsed}	V_{Ssup}	V_{Lsup}
P_{sed}	$[P_S]$	$[P_L]$	0	0
P_{sup}	0	0	$[P_S]$	$[P_L]$
V_{sed}	1	1	0	0
V_{sup}	0	0	1	1

where V is the volume of material in the respective phase and $[]$ indicate concentration.

The solution of the above matrix is the following set of equations:

$$V_{Ssed} = \frac{[P_L]V_{sed} - P_{sed}}{[P_L] - [P_S]} \quad (2.17)$$

$$V_{Lsed} = \frac{[P_S]V_{sed} - P_{sed}}{[P_S] - [P_L]} \quad (2.18)$$

$$V_{Ssup} = \frac{[P_L]V_{sup} - P_{sup}}{[P_L] - [P_S]} \quad (2.19)$$

$$V_{Lsup} = \frac{[P_S]V_{sup} - P_{sup}}{[P_S] - [P_L]} \quad (2.20)$$

From the outputs of the matrix, two key process parameters can be calculated:

$$\% \text{ Solids Sedimented} = \frac{V_{Ssed}}{V_S} \times 100 = \frac{V_{Ssed}}{V_{Ssed} + V_{Ssup}} \times 100 \quad (2.21)$$

$$\% \text{ Sediment Dewatered} = \frac{V_{Ssed}}{V_{sed}} \times 100 = \frac{V_{Ssed}}{V_{Ssed} + V_{Lsed}} \times 100 \quad (2.22)$$

It is these parameters which are used to compare laboratory and large-scale centrifuges. It is noted that the latter parameter is measured against dewatering in a high

g centrifuge and as such is not an absolute value. Absolute values are often not possible to obtain due to an inability to discriminate between free and bound water in precipitate suspensions.

2.3. MATERIALS AND METHODS

2.3.1. Chemicals

All chemicals, unless specified otherwise, were obtained from Sigma Chemical Co. Ltd. (Dorset, UK) and were of analytical grade. A concentrated suspension of polyvinylacetate particles, DM 130, was kindly donated by Hoechst AG, Frankfurt, Germany. The particles were chosen for their small size (0.5 to 3 μm) and low density difference to water ($< +2\%$) as well as various mechanical and electrical properties to aid their analysis.

2.3.2. Description of equipment

Equipment used in laboratory runs and pilot plant verification trials, respectively, is listed below. Homogenisation was carried out at laboratory-scale using an APV Manton Gaulin High-Pressure Homogeniser Lab 40 and at pilot-scale using a K3 machine (APV Baker Ltd., Derby, UK). Debris clarification was achieved in a Beckman J2-M1 laboratory centrifuge with JS-13.1 swing-out rotor (Beckman Instruments Ltd., High Wycombe, UK; $R_1 = 0.049$ m, $R_2 = 0.130$ m, $V_{lab} = 70$ mL, $N_{lab} = 217$ r s⁻¹, $t_{lab} = 1.5$ h, $\Sigma_{lab} = 17.5$ m², $C_{lab} = 1.0$, $V_{lab}/t_{lab}C_{lab}\Sigma_{lab} = 0.74 \times 10^{-9}$ m s⁻¹) and Alfa Laval AS-26 Tubular Bowl Centrifuge (Alfa Laval Separations Ltd., Camberley, U.K.; $r_i = 0.00265$ m, $r_o = 0.062$ m, $L = 0.75$ m, $Q_{tb} = 30$ L h⁻¹, $N = 287$ r s⁻¹, $\Sigma_{tb} = 4660$ m², $C_{tb} = 0.9$, $Q_{tb}/C_{tb}\Sigma_{tb} = 2.0 \times 10^{-9}$ m s⁻¹). Table 2.1 gives the dimensions of the precipitation reactors used in this study. Precipitates were recovered in the Beckman J2-M1 and Westfalia KDD 605 multichamber-bowl centrifuge shown in Figure 2.1 (Westfalia Separator AG, Oelde, Germany). This machine was operated under a back-pressure of approximately 1.5 barg (tightening of valve on the supernatant line until liquid began to over-flow the bowl of the

centrifuge) to flood the feed zone, thus preventing air entrainment which causes foaming of the supernatant. The flow rate was determined by calibration of a Watson Marlow 605 Di Peristaltic Pump (Watson Marlow Ltd., Falmouth, UK) with water and direct measurement. Analytical samples were centrifuged in a Beckman Microfuge 11 (reference centrifuge) prior to assays performed using a Beckman DU 650 spectrophotometer.

Table 2.1. Dimensions and characteristics of the precipitation vessels. Minor differences do exist between the two precipitators, but all *major* scaling parameters (D_I/D_T , number of baffles, D_B/D_T , mean velocity gradient and ageing time) have been maintained constant.

	Laboratory scale	Pilot scale
Maximum volume (L)	0.10	100
Operating volume (L)	0.07	50
Tank Height (m)	0.06	0.60
Liquid depth, H (m)	0.040	0.25
Tank diameter, D_T (m)	0.047	0.50
Impeller Diameter, D_I (m)	0.0191	0.15
D_I/D_T	0.41	0.40
N (r s ⁻¹) for $\bar{G} = 200$ s ⁻¹	8.33	2.30
Impeller type	6-bladed Rushton	12-bladed Rushton
Number of baffles	4	4
Baffle diameter, D_B (m)	0.0047	0.05
D_B/D_T	0.10	0.10
Blade to Bottom (m)	0.07	0.06
Liquid Depth Ratio	2.11	1.70
Off Bottom Ratio	0.37	0.39
Bottom Shape	flat	curved
Material	glass	stainless steel

2.3.3. Preparation of particle suspension

To determine the efficiency factor of the multichamber centrifuge, grade efficiency curves were derived for both this machine and the laboratory centrifuge using a suspension of latex particles. 0.10 kg of concentrated polyvinylacetate emulsion was

diluted in 2 L of distilled water and homogenised at 500 bar for 5 passes in a Lab 60 high-pressure homogeniser. Exposure to homogenisation conditions should ensure that the latex particles are broken down to their minimum size such that they will not be further degraded when feeding to or during passage through a centrifuge. The conditioned particle suspension was diluted into 100 L of reverse osmosis water in a 100 L tank to give a final particle concentration of approximately 0.1% (w/v). The suspension was stirred at 3.33 r s^{-1} and held for 0.5 h prior to use.

2.3.4. Preparation of precipitate suspension

High Activity Bakers Yeast (*Saccharomyces cerevisiae*), provided by DCL (London, UK), was suspended to 28% packed wet weight per volume in phosphate buffer (0.1 M KH_2PO_4 , adjusted to pH 6.5 using 4 M NaOH). This was then disrupted by five discrete passes at 500 bar pressure through a high-pressure homogeniser and centrifuged to remove the debris. The clarified homogenate was placed into an agitated precipitation vessel, to which a saturated solution of $(\text{NH}_4)_2\text{SO}_4$ (519 g L^{-1} or 3.93 M, buffered with 0.1 M KH_2PO_4 , pH 6.5) was added resulting in a 40% saturated (1.57 M) suspension. At the laboratory scale, the salt solution was rapidly decanted ($< 2 \text{ s}$) from a beaker in a single dose at the surface and near the impeller. In the pilot plant, the addition was carried out in a similar fashion within approximately 5 s. All precipitations were aged at $\bar{G} = 200 \text{ s}^{-1}$ for $t = 0.63 \text{ h}$ (Camp number, $\bar{G}t = 10^5$).

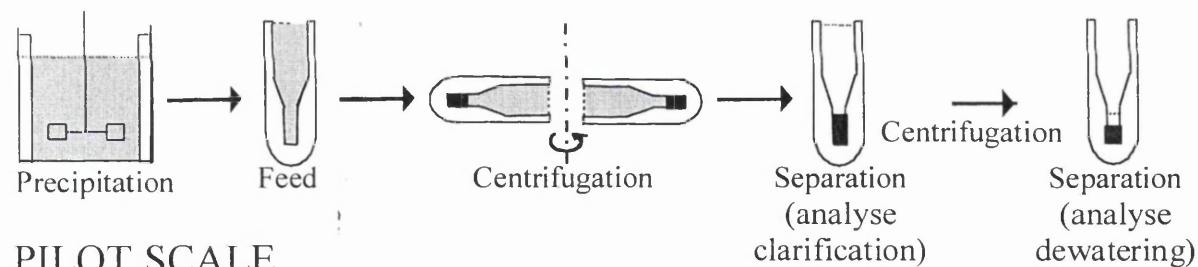
2.3.5. Separation of precipitate suspension

2.3.5.1. Scale-down process

For the scale-down process (see Figure 2.3), the precipitate suspension, 30 mL, was placed in a centrifugation tube made of clear polyvinyl chloride graduated (bottom 20 mm of tube) in 1 mm (0.2 mL) increments for accurate solids volume measurements ($\pm 0.3\%$

as a fraction of total volume). The tubes were centrifuged for purposes of clarification in Beckman J2-MI ($N = 140 \text{ r s}^{-1}$, $RCF_{mean} = 6550$, $t_{lab} = 0.072 \text{ to } 0.738 \text{ h}$, $\Sigma_{lab} = 6.1 \text{ m}^2$), after which the supernatant was removed slowly using a 5 mL pipette down to the sediment-liquid boundary; this boundary became blurred at shorter spin times. The tubes were then re-spun for compaction ($N = 130 \text{ r s}^{-1}$, $RCF_{max} = 8830$, $t = 0.208 \text{ to } 1.33 \text{ h}$) and the minimal resultant liquid added to that obtained from the clarification spin. The volume of sediment was recorded after the compaction run. The sediment was re-suspended to 30 mL with buffer (0.1 M, KH_2PO_4 , pH 6.5) to re-dissolve the precipitates prior to analysis.

LABORATORY SCALE-DOWN



PILOT SCALE

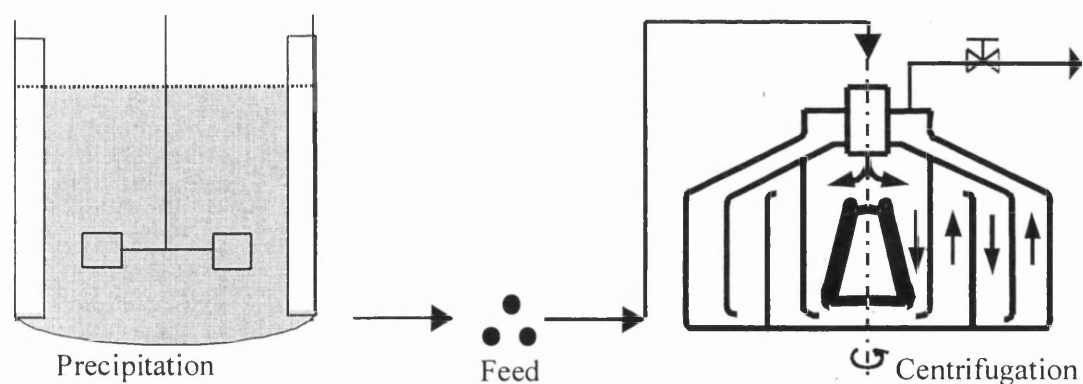


Figure 2.3. Procedural overview of the laboratory scale-down and pilot processes involving the formation of protein precipitates and their centrifugal recovery, as described in sections 2.3.4, 2.3.5.1 and 2.3.5.2. The critical dimensions and operating conditions of the precipitation reactors and centrifuges are provided in Table 2.1 and Figure 2.1, respectively. The precipitate suspension was derived from clarified yeast homogenate (prepared with $280 \text{ g packed cells L}^{-1}$) taken to $1.57 \text{ M } (\text{NH}_4)_2\text{SO}_4$ at pH 6.5, 4°C .

2.3.5.2. Pilot-scale process

In the pilot plant, suspension (30 L) was fed continuously to the multichamber-bowl centrifuge ($Q_{mc} = 20 \text{ L h}^{-1}$, $N = 167 \text{ r s}^{-1}$, $\Sigma_{mc} = 1110 \text{ m}^2$) via a peristaltic pump. The supernatant was collected in a vessel for analysis. Excess liquid in the centrifuge bowl was siphoned out to enable recovery of sediment; sediment from all chambers was pooled, weighed ($\rho \cong 1200 \text{ kg m}^{-3}$; Maybury, 1999) and then suspended in buffer for analysis. The multichamber-bowl was also run in the batch mode in which the bowl was filled and spun for a set time ($V_{mc} = 1.4 \text{ L}$, $\Sigma_{mc} = 187 \text{ m}^2$ calculated by the volumetrically weighted sum of Σ values for each chamber and accounting for acceleration and deceleration, $t_{mc} = 0.38 \text{ h}$, $V_{mc}/t_{mc}C_{mc}\Sigma_{mc} = 6.3 \times 10^{-9} \text{ m s}^{-1}$).

2.3.5.3. Reference

For the purposes of this study, 100% separation (100% clarification and dewatering) of the precipitate suspension into its solid and liquid components is achieved by spinning down a 1 mL (V_{ref}) Eppendorf sample in the reference centrifuge, i.e. Microfuge ($R_1 = 0.048 \text{ m}$, $R_2 = 0.061 \text{ m}$, $N_{ref} = 221 \text{ r s}^{-1}$, $t_{ref} = 0.5 \text{ h}$, $\Sigma_{ref} = 0.85 \text{ m}^2$, $C_{ref} = 1.0$, $V_{ref}/t_{ref}C_{ref}\Sigma_{ref} = 0.65 \times 10^{-9} \text{ m s}^{-1}$, no cooling).

2.3.6. Analyses

2.3.6.1. Physical properties

The density of the protein precipitate suspension was 1115 kg m^{-3} , measured with a specific gravity bottle. The viscosity of the suspension was determined to be 0.0035 Pa s at a shear rate of 200 s^{-1} using a Contraves Rheomat 115 viscometer with concentric cylinders (Contraves Industrial Products, Ruislip, UK).

2.3.6.2. Protein assay

The protein concentration of all streams was measured using the Bio-Rad assay (Bio-Rad Labs Ltd., Herts, UK) which is based on the Bradford assay (Bradford, 1976). Process samples were diluted 50- to 200-fold in buffer (0.1 M, KH_2PO_4 , pH 6.5) depending on the protein concentration, and thereafter diluted 30-fold with assay mix (this is Biorad reagent diluted 5 fold). The shift in optical density (OD) was monitored with a spectrophotometer at 595 nm. Analysis of solid products was performed by spinning down 1 mL samples in Eppendorfs in the reference centrifuge. After decanting the supernatant, the pellet was re-suspended to 10 mL with buffer (0.1 M, KH_2PO_4 , pH 6.5) followed by analysis procedure as described above.

All samples were stored in Eppendorfs on ice and all assays were performed within 12 h. A calibration curve was generated from standards of bovine serum albumin (BSA). Samples were analysed in triplicate with a reproducibility of $\pm 3\%$.

2.3.6.3. Alcohol Dehydrogenase (ADH) activity assay

The total concentration of ADH in each stream was determined using a modified Bergmeyer (1979) method. The enzymatic activity, E , is expressed in terms of units of activity per mL of solution and is defined by:

$$E = \frac{1}{\epsilon_{340}} \frac{\Delta A}{\Delta t} \frac{V_{cuvette}}{V_{sample}} D_N \quad (2.23)$$

where $\epsilon_{340} = 6.22 \text{ cm}^2 \mu\text{mol}^{-1}$, $\Delta A/\Delta t$ is the rate of change of OD at 340 nm with respect to time, V_{sample} is the sample volume added to the cuvette, $V_{cuvette}$ is the total volume in the cuvette and D_N is the dilution factor). The spectrophotometer was used to monitor the change in absorption of the solution at 340 nm over 60 s at 25°C, from which the reaction

rate was calculated by linear regression. Samples were analysed in triplicate with a reproducibility of $\pm 3\%$.

2.3.6.4. Solids fraction

In independent laboratory experiments, the solids fraction of the precipitate suspension (scale-down and pilot) was measured using the 30 mL tubes (transparent and graduated; spin conditions were $N_{lab} = 217 \text{ r s}^{-1}$, $RCF_{max} = 24500$, $t_{lab} = 1.5 \text{ h}$, $\Sigma_{lab} = 7.5 \text{ m}^2$, $V_{lab}/t_{lab}C_{lab}\Sigma_{lab} = 0.74 \times 10^{-9} \text{ m s}^{-1}$). A mean solids volume fraction of 0.062 ± 0.003 was obtained.

2.3.6.5. Moisture content of sediment

To determine the absolute moisture content of a sediment, the material was weighed before and after drying in an oven at 106°C for 24 h.

2.4. RESULTS AND DISCUSSION

2.4.1. Correction factor for multichamber-bowl centrifuge

Figure 2.4 displays the clarification of polyvinyl acetate suspension for both the laboratory and multichamber bowl centrifuges, from which its correction factor, C_{mc} was determined to be 0.88 ± 0.05 for $C_{lab} = 1.0$.

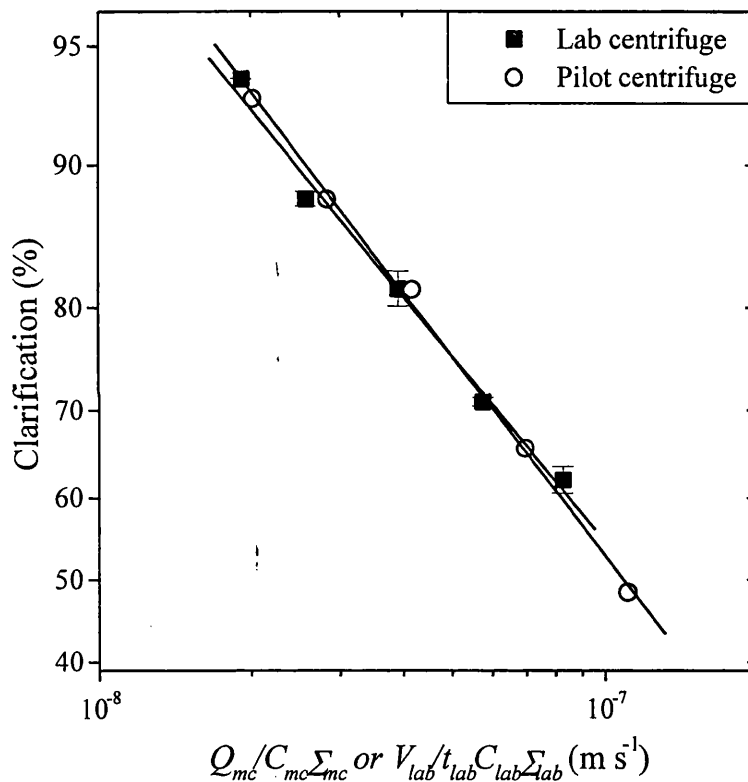


Figure 2.4. Probability-log relationship of % clarification* and equivalent flow rate per centrifuge separation area for polyvinyl acetate particles. An average correction factor for the multichamber-bowl centrifuge, $C_{mc} = 0.88 \pm 0.05$, was derived to give the best fit of separation characteristics of laboratory ($C_{mc} = 1.0$) and multichamber-bowl centrifuges for equivalent extents of clarification. Symbols: (■) laboratory centrifuge and (○) pilot-flow centrifuge.

$$*\%Clarification = \left(\frac{OD_{feed} - OD_{sup}}{OD_{feed} - OD_{reference}} \right) \times 100$$

where OD is the optical density at 670 nm (using a Beckman spectrophotometer). Some samples were diluted 10-fold in RO water to ensure readings were in the linear range of the spectrophotometer (0.05 to 1.0). The OD of samples spun in the reference centrifuge was 0.

2.4.2. Mass balance

Table 2.2 shows a typical mass balance carried out in triplicate for the characterisation of its centrifugal recovery (see Appendix 1 for all data). All process streams are detailed in terms of volumes and normalised amounts of protein and ADH and good reproducibility was achieved with all balances within $\pm 5\%$. The one notable feature is that the amount of total protein in the supernatant tends to be greater than the soluble amount in the reactor as measured by the laboratory centrifuge ($V_{ref}/t_{ref}C_{ref}\Sigma_{ref} = 0.65 \times 10^{-9} \text{ m s}^{-1}$), indicating the presence of concentrated precipitates due to non-ideal separation in the case of the former ($V_{lab}/t_{lab}C_{lab}\Sigma_{lab} = 7.2 \times 10^{-9} \text{ m s}^{-1}$, approximately 11-fold greater than the reference centrifuge).

Table 2.2. Example of mass balance of a scale-down, laboratory process (scale-down precipitator and centrifuge) at an equivalent flow rate of 20 L h^{-1} ($V_{lab}/t_{lab}C_{lab}\Sigma_{lab} = 7.2 \times 10^{-9} \text{ m s}^{-1}$). Amounts of feed protein ($1270 \pm 50 \text{ mg mL}^{-1}$) and ADH ($17300 \pm 1000 \text{ U mL}^{-1}$) are normalised to 100.

	Volume (mL)			Protein			ADH		
FEED	42.0	42.0	42.0	100.0	100.0	100.0	100.0	100.0	100.0
PRECIPITANT	28.0	28.0	28.0	0.0	0.0	0.0	0.0	0.0	0.0
PRECIPITATION									
Soluble	66.0	65.7	65.8	68.5	66.7	68.7	92.1	92.7	97.7
Insoluble	4.0	4.3	4.2	28.9	29.8	29.4	5.2	5.3	6.9
Sum	70.0	70.0	70.0	97.4	96.5	98.1	97.3	98.0	104.6
Error (%)	0.0	0.0	0.0	-2.6	-3.5	-1.9	-2.7	-2	+4.6
CENTRIFUGATION									
Supernatant	64.1	64.0	63.8	75.6	69.1	74.2	91.7	95.6	95.1
Sediment	5.9	6.0	6.2	27.0	26.8	28.8	7.6	7.2	8.3
Sum	70.0	70.0	70.0	102.6	95.9	103.0	99.3	102.8	103.4
Error (%)	0.0	0.0	0.0	+2.6	-4.1	+3.0	-0.7	+2.8	+3.4

As seen in Figure 2.5, the mean error of the protein balances was +0.1% and that of ADH was +1.6%, i.e. there was no significant activation or denaturation of ADH during laboratory trials. 97% of all protein points fell within a range of $\pm 6\%$ and ADH data exhibiting a tolerance of $\pm 8\%$. Furthermore, there is no significant relationship between

the error in the mass balance and the time of centrifugation. Approximately the same amount of protein was precipitated in the laboratory and pilot vessels, 30% compared to 32% respectively, and similar amounts of ADH remaining soluble, 93% compared to 90%. The mass balance approach adopted in this study allows process characterisation and comparison independent of these small differences. The greater extent of homogenate clarification at laboratory scale (97% versus 75%) leads to differences in debris carry-over to the precipitate stage. This results in about a 5% increase in solids concentration after precipitation, again the difference being accounted for within the mass balance. Over-precipitation of product may be attributed to:

- poorer mixing resulting from the size of the vessel and the rapid batch addition of ammonium sulphate;
- greater concentration of yeast debris at the pilot which tends to reduce the sharpness of the cut in fractionation curve for ADH and protein (Alsaffar *et al.*, 1993).

Usually undesired co-precipitation of product could be minimised by slower incorporation of precipitating agent and slightly smaller addition so as not to exceed the theoretical solubility limit. However, for batch precipitation, Foster *et al.* (1976) observed no effect of contacting conditions, i.e. rate of precipitant addition and degree of mixing, or scale of operation on solubility of ADH (but the maximum vessel size investigated was 1.87 L).

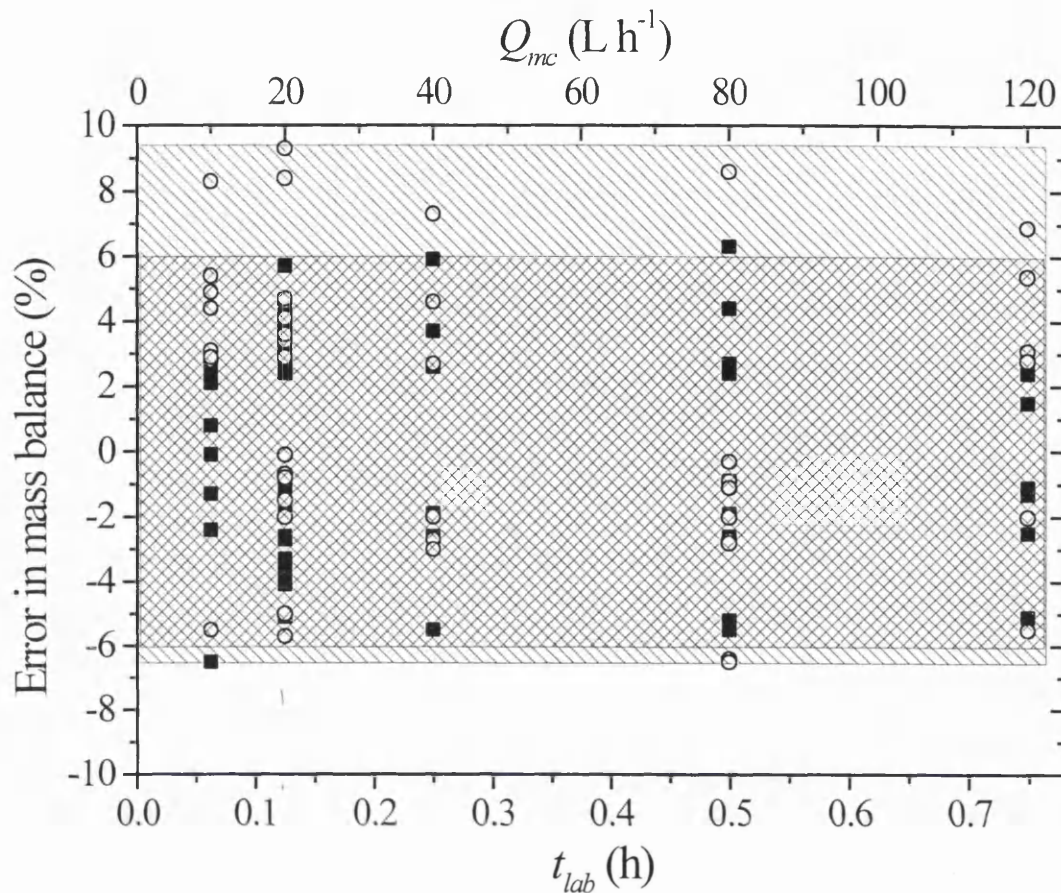


Figure 2.5. An error analysis of all mass balances for the range of flow rates investigated in the laboratory and the pilot centrifuge. Solid points indicate protein data with a mean of 0.1 % error and open symbols pertain to ADH data having a mean value of + 1.6%. The shaded area gives a range to 97% tolerance of $\pm 6\%$ for protein and $\pm 8\%$ for ADH.

2.4.3. Centrifugation performance

Figures 2.6 displays the purification factor of ADH in the supernatant for a range of Q/Σ values which decreases with an increase in flow rate. Good agreement was obtained for lab scale-down and pilot-prepared precipitates put through the laboratory scale-down centrifuge, the lower purification of the pilot-prepared suspension attributable to an increase in the amount of ADH precipitated at pilot scale. The large decrease in purification factor when using the multichamber-bowl centrifuge may be due to several factors. The mass balance for ADH indicated an overall 16% loss of activity which may

be attributed to denaturation (the supernatant temperature was 20°C and that of the bowl was 35°C; the feed temperature was 4°C). Additionally there is the possibility that the clarification and dewatering performance of the multichamber-bowl centrifuge is different to the laboratory centrifuge. This will be assessed later.

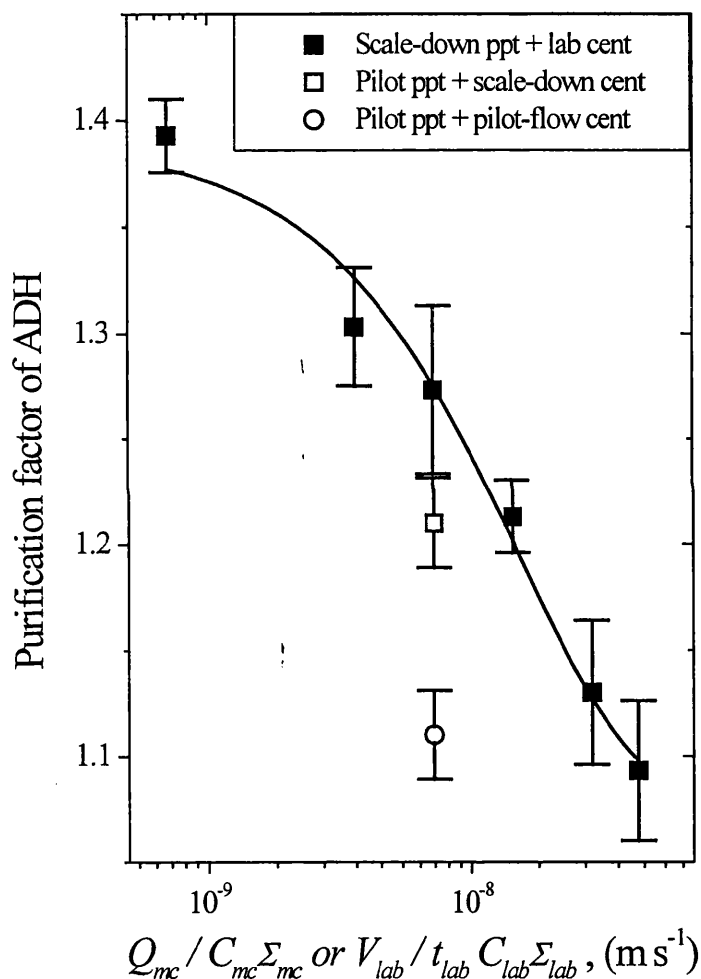


Figure 2.6. The dependence of purification factor of ADH in the supernatant on the logarithm of equivalent flow rate per centrifuge separation area. The curve is a trend first order exponential decay fit. Clarification was performed at $N = 140 \text{ r s}^{-1}$, $RCF_{mean} = 6550$, $t_{lab} = 0.072$ to 0.738 h , $V_{lab}/t_{lab}C_{lab}\Sigma_{lab} = 3.6$ to $43 \times 10^{-9} \text{ m s}^{-1}$; compaction was carried out at $N = 130 \text{ r s}^{-1}$, $RCF_{max} = 8830$, $t = 0.208$ to 1.33 h . Reference: the maximum purification was 1.39 measured at $V_{ref}/t_{ref}C_{ref}\Sigma_{ref} = 0.65 \times 10^{-9} \text{ m s}^{-1}$. Solid points indicate precipitate (ppt) prepared in the laboratory and open points pertain to the pilot vessel; squares and circles represent the laboratory and pilot-continuous centrifuge. Data points indicate mean values and error bars show the 95% confidence interval for (at least) duplicate runs. Data is not presented for the pilot-batch centrifuge ($V_{mc}/t_{mc}C_{mc}\Sigma_{mc}$) due to considerable error associated with the calculation.

Figure 2.7 shows the centrifugation yield of soluble ADH in the supernatant for various equivalent flow rates. The yield calculation only considers the recovery of soluble ADH. The yield curve, initially at a high value, decreases markedly with increasing Q/Σ as a result of poorer dewatering of the sediment. The yield exhibits a possible minimum at approximately $2.5 \times 10^{-8} \text{ m s}^{-1}$. Yield increase at lower Q/Σ could be due to fewer solids being settled, thus decreasing the volume of sediment.

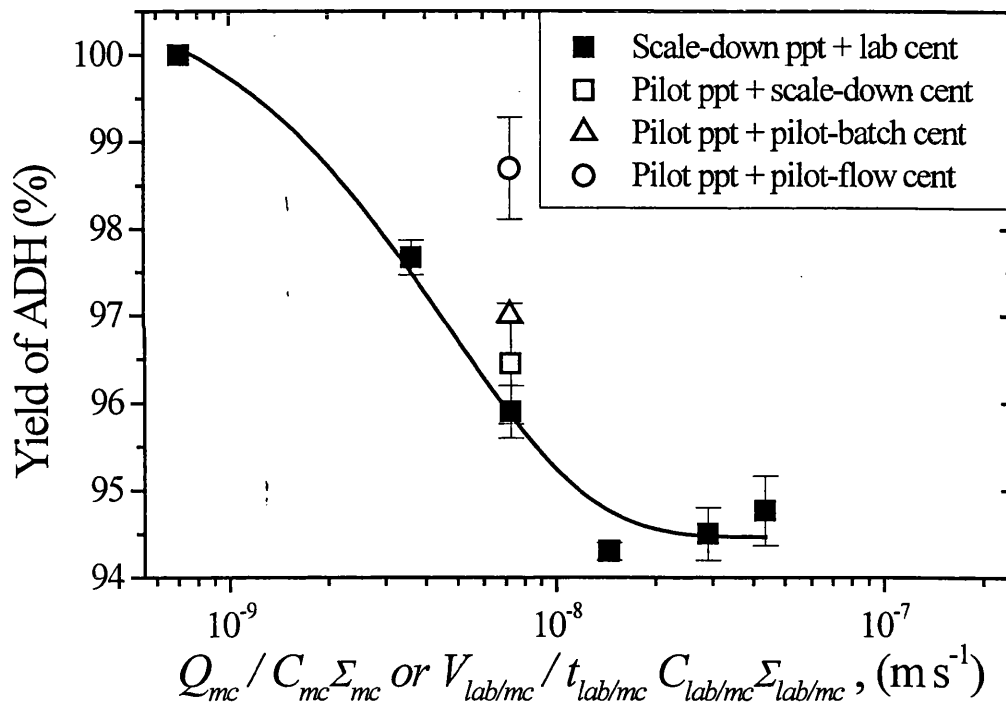


Figure 2.7. The linear-log relation of yield of soluble ADH in the supernatant to the equivalent flow rate per centrifuge separation area for the precipitate suspension. Centrifugation conditions and symbols are as per Figure 2.6; triangle represents pilot-batch centrifuge. *Reference:* the maximum yield was 100%.

Figure 2.8 is a plot of the solids sedimented against equivalent flow rate for various processes. First, the relationship between these two parameters is obtained for the laboratory centrifuge; a linear and relatively sensitive dependence is observed, e.g. a 10-fold decrease in $V/t\Sigma$ results in the solids remaining in the supernatant decreasing from about 30% to 1%. A mid-range clarification performance at lab scale was used to test the prediction at pilot scale in a continuous-flow centrifuge. However, a large difference was observed between the laboratory prediction (79% clarification) and the observed pilot value (30%). Possible reasons for this discrepancy were then investigated. Similar recoveries obtained for both scale-down and pilot-prepared precipitate suspensions (79% and 74%, respectively) rule out major differences in the settling properties of the precipitates. Operation of the multichamber-bowl centrifuge in batch mode (i.e. pre-filled with precipitate suspension) gave comparable but slightly lower performance (67% as compared with 74% clarification), the lower value at pilot scale being explained by some re-entrainment of solids during siphoning of supernatant out of the bowl. Hence the most probable explanation for the much lower recovery in the pilot-flow centrifuge than the scale-down one is the break-up of precipitate aggregates in the feed region of the continuous machine. High flow stresses generated by the extremely rapid acceleration of material upon entrance into the pilot machine leads to aggregate breakage and hence lower recoveries. Use of a peristaltic pump excluded the possibility of precipitate damage due to pumping as Hoare *et al.* (1982) demonstrated that this device showed no disruptive effect on precipitates.

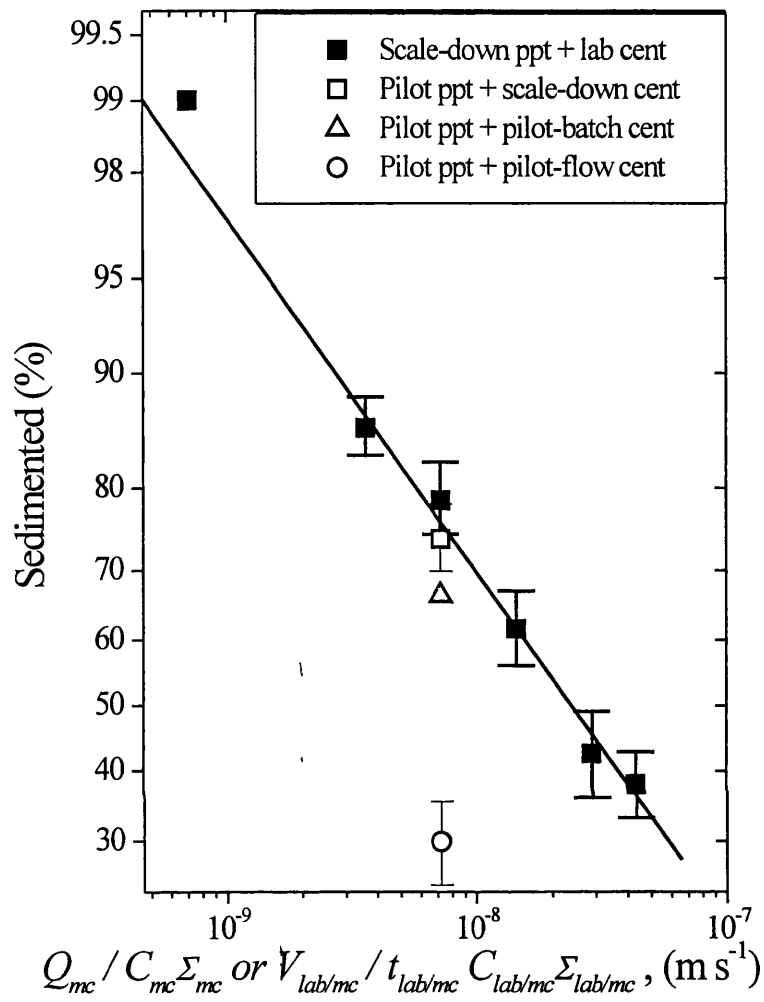


Figure 2.8. The probability-log dependence of % solids sedimented on equivalent flow rate per centrifuge separation area for the precipitate suspension. The line is a trend linear fit. Centrifugation conditions and symbols are as per Figure 2.6. *Reference:* the maximum recovery was >99%.

As observed in Figure 2.9, good agreement in terms of dewatering exists for laboratory- and pilot-scale prepared precipitates processed in the lab scale-down centrifuge (55% versus 58%), with a marginally drier sediment being obtained in the multichamber-bowl (63% versus 58%). Dewatering results in Figure 2.9 are presented not in terms of dry weights but values relative to the maximum compaction possible in the microfuge ($RCF_{max} = 20\ 000$).

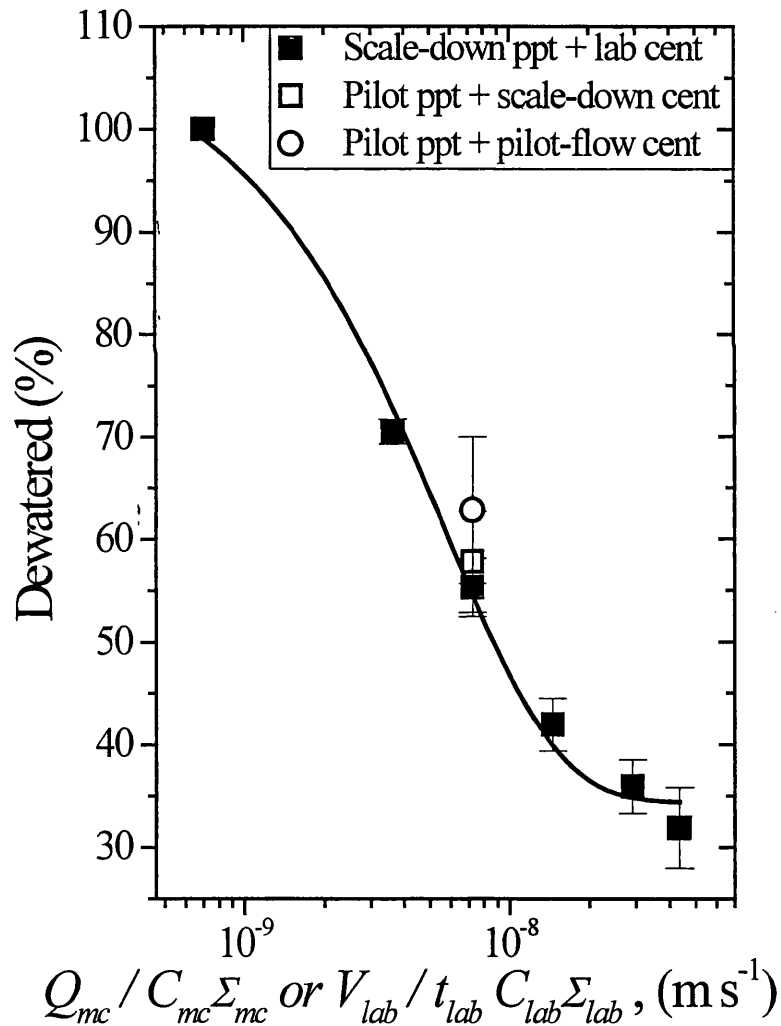


Figure 2.9. The linear-log relationship of the degree of dewatering on equivalent flow rate per centrifuge separation area for the precipitate suspension. The line is a trend first order exponential decay fit. Centrifugation conditions and symbols are as per Figure 2.6. *Reference:* maximum dewatering is considered to be 100%. Data is not presented for the pilot-batch centrifuge ($V_{mc}/t_{mc}C_{mc}\Sigma_{mc}$) due to considerable uncertainty associated with the calculation.

To validate the above analysis, the moisture content of the centrifuge sediments was measured using material prepared at the pilot scale (Table 2.3). The sediment in the reference centrifuge was the driest (37%), followed by that obtained in the pilot (32.4%) and scale-down centrifuges (30%). This confirms that longer spin times are needed for the scale-down centrifuge to mimic the dewatering of the sediment of the multichamber-bowl. The sediment in the outer chamber was only slightly drier than the sediment in the other chambers, despite the former being exposed to the greatest *RCF*. This may be attributed to the sediments having different particle size distributions and hence, dewatering potentials.

Table 2.3. Percentage dryness of sediment for samples in the reference (Microfuge), scale-down (Beckman J2-MI) and pilot (multichamber-bowl) centrifuges. Pilot-prepared precipitate was used for this experiment.

Centrifuge	t_c (h)	<i>RCF</i>		% Dewatered
Reference ($V_{ref}/t_{ref}C_{ref}\Sigma_{ref} = 0.65 \times 10^{-9} \text{ m s}^{-1}$)	0.5	12 000		37 ± 1
Scale-down ($V_{lab}/t_{lab}C_{lab}\Sigma_{lab} = 7.2 \times 10^{-9} \text{ m s}^{-1}$)	0.38	10 000		30 ± 4
Pilot ($Q_{mc}/C_{mc}\Sigma_{mc} = 6.0 \times 10^{-9} \text{ m s}^{-1}$)	0.75	Chamber 1	5 250	32.4 ± 0.5
		Chamber 2	6 700	31.8 ± 0.6
		Chamber 3	7 800	32.2 ± 0.3
		Chamber 4	8 830	33.2 ± 0.4
		Average	6 890	32.4 ± 0.3

2.5. CONCLUSIONS

Scaling precipitation based on a constant mean velocity gradient and ageing resulted in particles with similar characteristics as evidenced by similar clarification in the laboratory scale-down centrifuge for material prepared at the laboratory and pilot scales. Good agreement was achieved between the scale-down and multichamber-bowl centrifuges in terms of solids dewatering and also for precipitate recovery in the batch-operated, pilot machine. The techniques developed in this study allowed identification of the extent of precipitate break-up occurring in the continuous-flow centrifuge, in this case leading to approximately 50% reduction in clarification.

3. **CHAPTER 3: CHARACTERISATION OF FLOW INTENSITY IN CONTINUOUS CENTRIFUGES FOR THE DEVELOPMENT OF LABORATORY MIMICS**

ABSTRACT

Predicting the recovery of “delicate” biological materials by centrifugation using laboratory centrifuge has been a major challenge to biochemical engineers partly because of the difficulty in accurately quantifying the hydrodynamic shear stresses in continuous-flow industrial centrifuges and partly because the clarification and dewatering conditions in the laboratory units do not represent those occurring in industrial centrifuges. In this study, the flow field in the feed zone of an industrial centrifuge is mapped and its profile of energy dissipation rate established using computational fluid dynamics (CFD). A laboratory-scale high-speed rotating-disc device is designed with the capacity to reproduce the CFD-predicted energy dissipation rates in the feed zone. Millilitre quantities of the process material are shear-treated in the device operating at a speed that mimics the local critical flow conditions in the industrial centrifuge. Such a technique was used to assess the impact of flow conditions in the feed zone of a continuous pilot multichamber-bowl centrifuge on the physical properties of protein precipitates and on their predicted recovery, using a laboratory centrifuge. A quantitative prediction was established using the laboratory-scale mimic of the centrifuge feed zone for the observed reduction in pilot-scale centrifuge performance from the predicted 88% clarification to the observed 39% clarification of the precipitate particles.

Note: A modified version of this chapter has been submitted as a paper to *Chem. Eng. Sci.* (Boychyn *et al.*, 2000b).

3.1. INTRODUCTION

3.1.1. Centrifugation of shear-sensitive species

Centrifugation is a key process step in the recovery of most biological materials. Despite its widespread application, prediction of the performance of centrifugation is currently not possible because most biological materials are physically “fragile” and it has proven exceptionally difficult to quantify the impact of flow stresses occurring in centrifuges on their performance. Mannweiler and Hoare (1992) performed a grade efficiency analysis of a precipitate suspension processed through a disc stack centrifuge and concluded that breakage of aggregates occurred primarily in the feed zone. This has also been demonstrated recently for a multichamber-bowl centrifuge (Boychyn *et al.*, 2000a). The breakage of the feed material in a centrifuge increases the proportion of fines causing a reduction in the clarification of the material. The difficulty in predicting the consequences of the impact of flow stresses on the performance of centrifugation is that in the past the complex flow fields of industrial centrifuges have not been amenable to rigorous mathematical analysis. The prediction of the effect of flow-induced breakage on centrifuge performance is possible by direct experimentation, but this requires large quantities of test material and requires an analysis to distinguish between precipitate breakage and particle separation effects where often a unique solution is not possible (Mannweiler and Hoare, 1992). Additionally, with the new generation of low-volume, high-value biopharmaceutical products, large quantities of test material are rarely available for process development. In such cases, scale-down techniques requiring milliliter quantities of test materials offer major advantages. However, currently the prediction of the performance of industrial centrifuges is made difficult because, unlike a continuous machine, shear damage in a laboratory centrifuge is practically negligible

since the fluid is at rest relative to the centrifuge tube. These issues provided the motivation for the present investigation, the aim of which was to establish an engineering framework for predicting the performance of an industrial centrifuge using small laboratory centrifugation data.

3.1.2. Computational fluid dynamics (CFD)

Successful prediction for the processing of new materials requires models based on mechanical properties of particles and hydrodynamic data, to predict breakage during exposure to stress (Thomas and Zhang, 1998). However, in most operations, the flow field is often turbulent and the flow geometry sufficiently complex to frustrate identification of the type and magnitude of these stresses through normal analytical calculations. Hence, the increasing use of numerical techniques based on computational fluid dynamics (CFD) to simulate flow and particle-fluid interactions. Modelling of the latter still has considerable mathematical and computational challenges compared with simulating only fluid flow. Recent advances in CFD coupled with the availability of modern computers with the capacity to solve the necessary equations routinely provide a means by which the complex flow field in an industrial equipment, such as a centrifuge, may be quantified (Gosman, 1998; Harris *et al.*, 1996). The remaining challenge is how to utilise the data obtained from a CFD analysis of flow in an industrial centrifuge in order to assess its performance in the recovery of shear sensitive materials.

3.1.3. Selection of a “shear” device

Once the flow field has been characterised, the higher energy dissipation rate regions causing damage to the process material, will be reproduced in an appropriate small-scale device. Capillary devices are often used in shear studies, nevertheless these are large, require strict safety measures (due to the great pressures generated by the

driving pistons) and yet permit a maximum sample volume of only 2 mL which is generally insufficient for further processing. It was hypothesised that flow in the region of a rotating disc (Figure 3.1) could be regulated to mimic the local flow in the entrance zone of a continuous centrifuge (Levy *et al.*, 1998). A CFD analysis of the flow and energy dissipation patterns for this high-speed rotating-disc device was recently reported (Levy *et al.*, 1999). Such a device will be used to mimic the local flow conditions in the critical region (entrance zone) of a continuous, pilot multichamber-bowl centrifuge. CFD analysis will be used to predict the speed of disc rotation required to mimic the feed zone and a combination of laboratory-scale shear and centrifugation used to test the prediction for the pilot-scale, continuous-flow centrifuge.

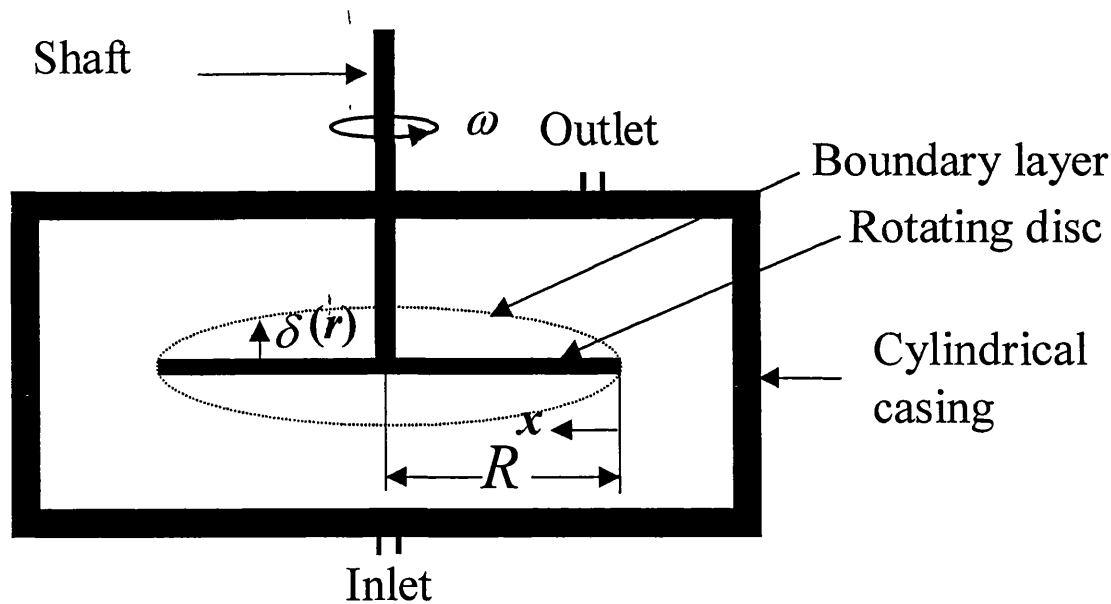


Figure 3.1. Schematic of the laboratory, high-speed rotating-disc device.

3.1.4. Selection of test material

Design of the experimental verification of the CFD model requires careful consideration. Deleterious effects to a soluble species such as a protein or nucleic acid could be used as a test system for the magnitude of flow stresses within the processing

equipment. Advantages of this approach include relatively easy assays for damage (e.g. gels to detect uncoiling of plasmids and spectrophotometric-based activity assays) and the avoidance of extremely complex nature of particle-fluid interactions and particle settling. Despite this method being able to determine the suitability of processing a soluble product with a certain piece of equipment, its *operational performance*, i.e. efficiency of solid-liquid separation cannot be predicted.

A more appropriate system for scaling operational performance is by default one with an insoluble component that is structurally sensitive to its flow environment. Perhaps the best examples of this are protein precipitates and mammalian cells. The latter are arduous to grow in a reproducible manner and require special containment facilities. Cell strength is a function of many things (media components, growth rate and stage, etc.) and is difficult to assay. For example, shearing may *not* break-up cells, such that particle recovery remains unchanged but may cause small ruptures in the cells leading to “leakage” of intracellular proteins which is exacerbated during compaction of the sediment. In the case of precipitates, damage assumes the form of a downward shift in particle size distribution, which can be measured directly with a particle sizer or evidenced by an increase in supernatant turbidity. Many protein precipitates are relatively easily and reproducibly formed and may be found in many industrial bioprocesses from primary isolation to finishing operations (Rothstein, 1994; Foster, 1994; Englard and Seifter, 1990; Paul and Rosas, 1990).

Another criterion for the test material is that it must exhibit a *gradual and measurable response* when exposed to the *range of fluid stresses experienced in the industrial equipment*. Murrell (1999) noted the application of shear forces above 10^5 W kg^{-1} to a suspension of PEG (polyethylene glycol)-protein precipitates in a rotating-disc

device, resulted in their rapid disintegration (< 3 s) to a specific particle size regardless of the applied stresses. In other words, exposure to even greater flow forces did not result in finer particles. A gradual degradation in the particle size of PEG precipitates, as for casein precipitates, may only occur at much lower flow forces ($< 10^4$ W kg⁻¹) such as those experienced in pumps, microfiltration units or rapidly agitated tanks. However, the aim of this study is to mimic the high flow occurring in the feed zone of a continuous centrifuge and therefore, a different precipitate system, one which is less shear-sensitive, must be chosen.

In the present investigation, precipitates derived from the salting-out of yeast proteins and prepared under a fixed set of conditions, were used as the target material. Considerable work has already been done with such precipitates (Dunnill and Lilly, 1962; Richardson *et al.*, 1990; Clarkson *et al.*, 1993; Maybury *et al.*, 1998; Boychyn *et al.*, 2000a). This precipitate suspension is a challenging one to separate because its particles are small (approximately 1 μ m) and readily damaged in high-flow environments.

3.2. THEORETICAL CONSIDERATIONS

3.2.1. Mapping the flow field

3.2.1.1. Pilot centrifuge

In the present investigation CFD was used to establish the flow-induced parameters by numerically solving the governing flow equations in a multichamber-bowl centrifuge. While CFD can be used to map the flow field in the entire centrifuge, the area of interest is the entrance zone of the centrifuge where the highest flow stresses are expected to prevail (Mannweiler *et al.*, 1989). The work presented below is the first reported attempt on the simulation of the transient flow patterns in a pilot centrifuge. All theoretical considerations pertaining to CFD are contained in Appendix B. All CFD figures were generated by Dr. Samson Yim (Dept. of Biochemical Engineering, University College, London, UK), based on the dimensions and operation conditions specified by the author of this thesis.

3.2.1.2. Laboratory-scale high-speed rotating disc

The construction of an in-house rotating disc device, capable of generating high local shear rates comparable to those expected in an industrial centrifuge, was previously described (Levy *et al.*, 1998). Standard analytical solutions of the equations of motion for flow over the rotating disc showed that the maximum shear stresses occurred in the laminar boundary layer δ , given by:

$$\delta = 5 \sqrt{\frac{\mu X}{\rho v_{\infty}}} \quad (3.1)$$

where X is the distance from the edge of the disc, ρ is the density of the suspension and v_∞ is the tangential tip velocity (Schlichting, 1979). The corresponding maximum shear stress τ_{max} , at position X is determined by:

$$\tau_{max} = 0.322 \mu v_\infty \left(\frac{\rho v_\infty}{\mu X} \right)^{1/2} \quad (3.2)$$

Integration of Equation 3.2 over the diameter of the disc gives the applied torque T , thus:

$$T = 0.664 \pi \mu v_\infty \left(\frac{\rho v_\infty}{\mu} \right)^{1/2} \left(\frac{16R^{5/2}}{15} \right) \quad (3.3)$$

where R is the disc radius.

Equation 3.3 is then used to obtain the power input, P :

$$P = 2\pi N T \quad (3.4)$$

where N is the rotational speed. The maximum energy dissipation rate ε_{max} , is given by:

$$\varepsilon_{max} = \frac{P}{\rho V_{bl}} \quad (3.5)$$

where V_{bl} is the volume of the boundary layer. This is obtained by integrating the expression for boundary layer thickness over the entire disc:

$$V_{bl} = 2\pi \int_0^{\delta_{max}} r^2 d\delta = 2\pi \left[5R^2 \left(\frac{\mu R}{\rho v_\infty} \right)^{1/2} - \left(\frac{10R\rho v_\infty}{\mu} \right) \left(\frac{\mu R}{\rho v_\infty} \right)^{3/2} + \left(\frac{\mu R}{\rho v_\infty} \right)^{5/2} \left(\frac{\rho v_\infty}{\mu} \right)^2 \right] \quad (3.6)$$

Equations 3.1 to 3.6 provide a good estimate of the shear related parameters in the boundary layer of the rotating disc as a function of the rotational speed and these were subsequently confirmed by CFD solutions of the flow equations (based on Eqs. B.1-B.4) in the rotating disc device (Levy *et al.*, 1999). The shear stresses in the boundary layer were found to be sufficiently high to cause the breakage of the particles falling within it.

Considering that in the experiments to be presented later in this chapter, particle size was of the order of $1\ \mu\text{m}$ and that the boundary layer thickness was of the order of $200\ \mu\text{m}$, it is assumed that the breakage of particles occurs by fluid stresses prevailing in the boundary layer. In the case of the multichamber-bowl centrifuge, the CFD solutions were used to identify the local regions in the entrance to the centrifuge where the fluid stresses were sufficiently high to cause particle breakage. These were found to correspond to the boundary regions on the rotating surfaces. To ensure a reasonable match of flow stresses in the pilot centrifuge with those in the rotating disc device, the condition that the thickness of the boundary over the maximum stresses occurring in the pilot machine had to be at least $200\ \mu\text{m}$ thus matching that in the rotating disc device, was imposed.

3.2.2. Centrifugation

The characterisation of the performances of the laboratory and pilot centrifuges used in this study has been described fully by Boychyn *et al.* (2000a) using the Sigma concept of equivalent settling areas. Details of centrifuge operation are provided in the experimental section and equations used to calculate equivalent settling areas are explained in section 2.2.2.1.

3.3. MATERIALS AND METHODS

3.3.1. Chemicals

All chemicals, unless specified otherwise, were obtained from Sigma Chemical Co. Ltd. (Dorset, UK) and were of analytical grade.

3.3.2. Preparation of precipitate suspension

A standard protocol, described in section 2.3, was used to prepare the precipitate suspension. Clarified homogenate, derived from packed Bakers' yeast (DCL, UK) re-suspended to 280 g packed cells L⁻¹ in 0.1 M KH₂PO₄ (pH 6.5) at 4°C was brought rapidly to 40% saturation with saturated (NH₄)₂SO₄ (3.93 M, buffered with 0.1 M KH₂PO₄, pH 6.5), and agitated at a mean velocity gradient of $\bar{G} = 200 \text{ s}^{-1}$ for 0.63 h ($\bar{G}t = 10^5$) in a batch stirred-tank reactor (described in Table 2.1).

3.3.3. Separation of suspension

At the laboratory scale, 15 mL (V_{lab}) samples of suspension were clarified in 20 mL graduated (bottom 30 mm of tube graduated in 1 mm or 0.05 mL increments, representing $\pm 0.1\%$ as a fraction of the total volume), clear polyvinyl chloride tubes placed in a Beckman J2-MI laboratory centrifuge with JS-13.1 swing-out rotor (Beckman Instruments Ltd., High Wycombe, UK; $R_1 = 0.070 \text{ m}$, $R_2 = 0.130 \text{ m}$, $N = 130 \text{ r s}^{-1}$, $RCF_{mean} = 6550$, $t_{lab} = 0.072 \text{ to } 1.5 \text{ h}$, $\Sigma_{lab} = 1.7 \text{ m}^2$, $C_{lab} = 1.0$). Most experiments were conducted under conditions ($t_{lab} = 0.35 \text{ h}$, $V_{lab}/t_{lab}C_{lab}\Sigma_{lab} = 6.3 \times 10^{-9} \text{ m s}^{-1}$) to mimic settling in the pilot centrifuge. At the pilot scale, suspension was fed, via a peristaltic pump, to a Westfalia KDD 605 multichamber-bowl centrifuge (Westfalia Separator AG, Oelde, Germany), usually operated in the continuous mode ($N = 167 \text{ r s}^{-1}$, $RCF_{mean} = 6550$, $Q_{mc} = 22 \text{ L h}^{-1}$, $\Sigma_{mc} = 1110 \text{ m}^2$, $C_{mc} = 0.88$, $Q_{mc}/C_{mc}\Sigma_{mc} = 6.3 \times 10^{-9} \text{ m s}^{-1}$;

Boychyn, *et al.*, 2000a) with a fully flooded feed zone. Flooding of the entrance region was ensured using a back-pressure valve (1.5 barg) on the supernatant line until liquid began to over-flow the centrifuge bowl. The multichamber-bowl was also run under non-flooded conditions (valve on supernatant line completely open) and in the batch mode in which the bowl was filled and spun for a set time ($V_{mc} = 1.4$ L, $\Sigma_{mc} = 187$ m², $t_{mc} = 0.38$ h, $V_{mc}/t_{mc}C_{mc}\Sigma_{mc} = 6.3 \times 10^{-9}$ m s⁻¹).

3.3.4. High-speed laboratory rotational device

The original design of the rotating-disc device is described elsewhere (Levy *et al.*, 1998). For the purpose of the work described here, the basic design was modified to take different rotating elements including a disc and cylinders of a range of aspect ratios. Briefly, the device consisted of Perspex chamber of diameter 40 mm. The rotating elements were fabricated from a smooth aluminum alloy (Durell, Smith Ltd., UK), coated with a thin layer of PTFE, mounted on a stainless steel shaft. The Perspex chamber was constructed of four interchangeable sections that could be arranged to give different heights from 10 to 40 mm. Two rotating elements were used both having diameters of 30 mm and depths of 1 mm (disc) and 31 mm (cylinder), operated with the smallest and largest chamber configurations, respectively. The shaft of the elements was extended through the top cover via a relatively airtight (clearance of 0.1 mm) PTFE bearing and was connected to a high-speed DC motor (Groupher Speed 500 BB RACE, UK). The motor was powered by a set of trickle batteries, which, via a transformer, was capable of delivering a set of fixed voltages, between 2 and 12 V, thus providing six fixed speeds of rotation. The speed was measured and displayed digitally using an optical probe (model 31/9448-03, RDP Electronics Ltd., UK). Battery operation was used instead of mains because of the rapid acceleration that could be achieved with the former. Despite this,

upon application of higher voltages approximately 1-2 s were required for the attainment of maximum speed.

The top and bottom Perspex chambers contained entrance and exit holes, respectively, of 1.5 mm diameter. They were fitted with flexible tubing to remove any air trapped in the suspension whilst filling, and then sealed prior to operation of the device. The whole assembly was mounted on a heavy metal base to reduce vibration during the experiments.

3.3.5. Analysis

3.3.5.1. *Physical properties of the suspension*

The density of the protein precipitate suspension was 1115 kg m^{-3} , measured with a specific gravity bottle. The viscosity of the suspension (0.0030 Pa s at shear rates above 10^3 s^{-1}) was measured with a concentric cylinder Contraves Rheomat 115 viscometer (Contraves Industrial Products, Ruislip, U.K.).

3.3.5.2. *Assay for particle damage*

The two techniques used to assay for particle damage were particle size analysis of the sheared suspension and the clarity of the supernatant after centrifugation. In both cases, a non-sheared sample was used as a control and all samples were assayed within one hour after processing. The stability of sheared precipitates was tested by leaving these samples for set times prior to centrifugation. No re-agglomeration of particles was observed for resting periods of at least 1 h.

3.3.5.3. *Particle size measurements*

The particle size distribution was measured using an electrical sensing zone and a laser light scattering method in order to cover the full range of particle sizes. In the former case, an Elzone 280 PC particle sizer (Particle Data U.K. Ltd., Hereford, UK)

equipped with an 12 μm orifice tube calibrated with standard latex particles of sizes 1.09 μm , 2.02 μm and 5.00 μm was used to give a measurement range of approximately 0.55 to 8.9 μm (accurate range of 0.6 to 6 μm) divided into 128 channels. Prior to size analysis, the precipitate suspension was diluted 200 fold in 40% $(\text{NH}_4)_2\text{SO}_4$ saturated buffer (0.2 μm filtered using Sartobran filter capsules; Sartorius AG, Gottingen, Germany) and then analysed for 20 s at constant vacuum pressure of 160 mbarg. The counting procedure was repeated twice and an average taken. To eliminate coincidence effects the counting rate was never more than approximately 1000 counts s^{-1} . Particle size data were corrected for electrolyte background noise. Owing to the small density difference between the particles and the electrolyte, particle sedimentation during analysis was negligible. The high surface resistance of the precipitate particles allowed the use of a high aperture current and a low-resistance suspension buffer to maximise the sensitivity of the measurements.

Samples were also sized by dynamic light scattering using a Zetasizer 3000 (Malvern Instruments Ltd., Malvern, UK). Size measurements were carried out at a 90° angle (fixed setting) and analysed using the Automatic analysis mode software supplied by the manufacturer. The light scattering cumulant mean size or “Z Average” was automatically calculated using the “moments” method by the Malvern data analysis software and represents the hydrodynamic diameter. Samples were diluted 100 fold in 40% $(\text{NH}_4)_2\text{SO}_4$ saturated buffer. Every measurement was carried out in five serial measurements with a counting time of 60 s each and at a set temperature of 25°C . Samples were analysed in duplicate.

3.3.5.4. Clarification

Clarification as a function of $V_{lab}/t_{lab}C_{lab}\Sigma_{lab}$ was calculated by the following expression:

$$\%Clarification = \left(\frac{OD_{feed} - OD_{supernatant}}{OD_{feed} - OD_{reference}} \right) \times 100 \quad (3.7)$$

where OD is the optical density at 670 nm of a sample (measured with a Beckman DU 650 spectrophotometer). Samples were diluted from 1–10 fold in 40% $(NH_4)_2SO_4$ saturated buffer (to prevent precipitates becoming soluble) to ensure readings were in the linear range of the spectrophotometer (0.05 to 1.0). Reference samples were spun in the reference centrifuge, i.e. Microfuge ($V_{ref}/t_{ref}C_{ref}\Sigma_{ref} = 0.65 \times 10^9 \text{ m s}^{-1}$).

To gain an appreciation for the amount of damage that precipitate aggregates had undergone during shearing in the rotating-disc device, results are often presented in terms of relative clarification for the same $V_{lab}/t_{lab}C_{lab}\Sigma_{lab}$:

$$\% \text{ Relative Clarification} = \left(\frac{Clarification_{sheared}}{Clarification_{non-sheared}} \right)_{V_{lab}/t_{lab}C_{lab}\Sigma_{lab}} \times 100 \quad (3.8)$$

The relative clarification of a multichamber-bowl centrifuge run was defined as the percentage ratio of the pilot clarification value to that of the non-sheared, laboratory sample.

3.3.6. Experimental design

Figure 3.2 is a schematic flow chart of the experimental design showing how the high-speed rotating device was used in combination with the laboratory centrifuge in order to identify how the separation performance of the pilot centrifuge may best be mimicked. In a typical experiment, the precipitation process was carried out under a fixed

set of conditions in a mechanically agitated vessel (Boychyn *et al.*, 2000a). Use of a peristaltic pump excluded the possibility of precipitate damage due to pumping as Hoare *et al.* (1982) demonstrated that this device was very low-shear and showed no disruptive effect even on larger casein precipitates ($>10 \mu\text{m}$).

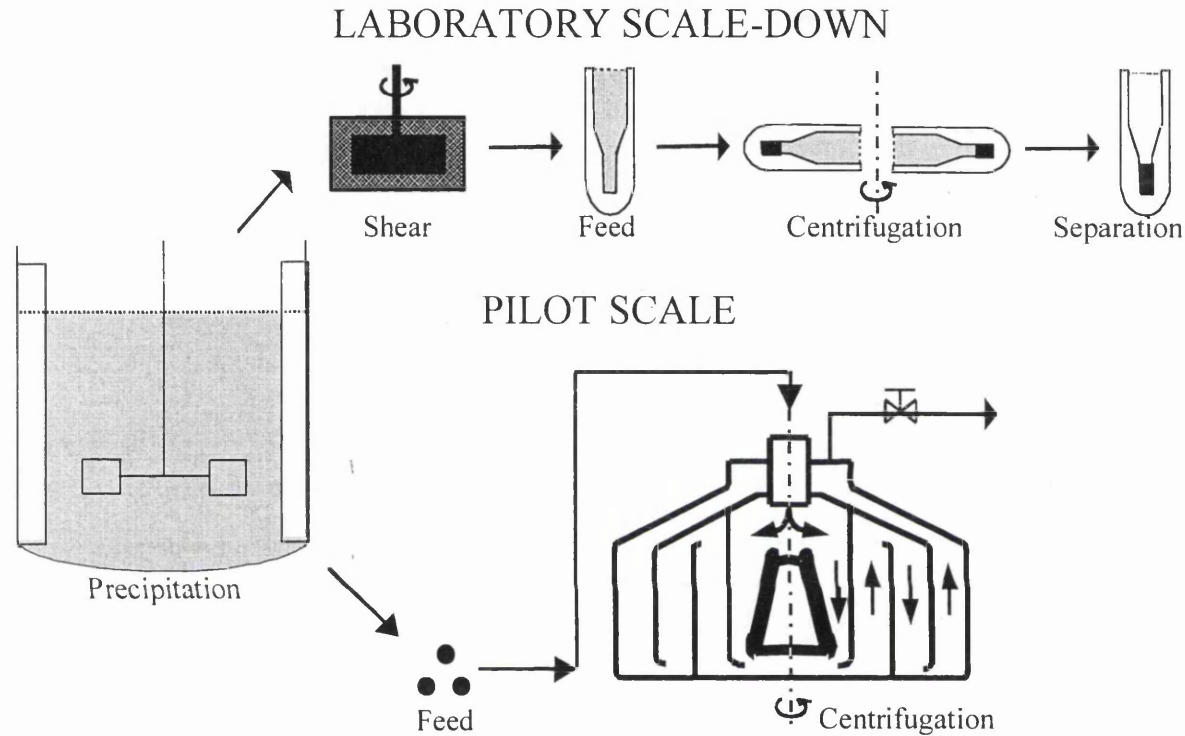


Figure 3.2. Laboratory scale-down of large-scale precipitation and centrifugal recovery achieved with the novel utilisation of a shear device. Precipitation conditions are listed in section 2.3.4: $V = 50 \text{ L}$ and $\bar{G} = 200 \text{ s}^{-1}$. Centrifugation conditions are determined based on equivalent settling area, Σ , through Q or V/t , and a correction factor C to allow for deviations from ideal flow. Theoretically equivalent sedimentation occurs when

$$\frac{Q_{mc}}{C_{mc} \Sigma_{mc}} = \frac{V_{lab}/t_{lab}}{C_{lab} \Sigma_{lab}} \quad (C_{mc} = 0.88 \text{ and } C_{lab} = 1.0).$$

All centrifugation dimensions and conditions are given in section 3.3.3.

3.4. RESULTS AND DISCUSSION

3.4.1. Particle size

Figure 3.3 shows the size distribution of the precipitated particles representing the feed material (no shear). Data are also plotted showing the change in the distribution resulting from shearing the sample in the small shear device (for 20 s) using the rotating cylinder at its maximum tip speed of 31 m s^{-1} (333 r s^{-1}) and the disc at its maximum of 44 m s^{-1} (462 r s^{-1}). The shift in the size distribution towards smaller particles shown in Figure 3.2 is indicative of particle breakage, which is expected to reduce clarification.

3.4.2. Dependence of clarification on time of centrifugation

Figure 3.4 compares the recovery of unsheared and sheared suspensions (using the cylinder and disc at maximum speeds) as a function of a range of centrifugation conditions. Using the unsheared sample at $V_{lab}/t_{lab}C_{lab}\Sigma_{lab} = 6.3 \times 10^{-9} \text{ m s}^{-1}$ as a reference point, the changes in the size distribution with Figure 3.3 were used to predict the effect of shearing and of different centrifugation conditions. Reasonable agreement is observed between predicted and experimental curves. The size distribution measurements do not take into account changes in morphology or density – it is expected that shearing will lead to more spherical and more compact particles and hence better clarification is observed in Figure 3.4. The shallower experimental line compared to predicted curves (calculated using a modified grade efficiency function) of clarification with centrifugation conditions are likely due to errors in extrapolation of size distribution to the fine end.

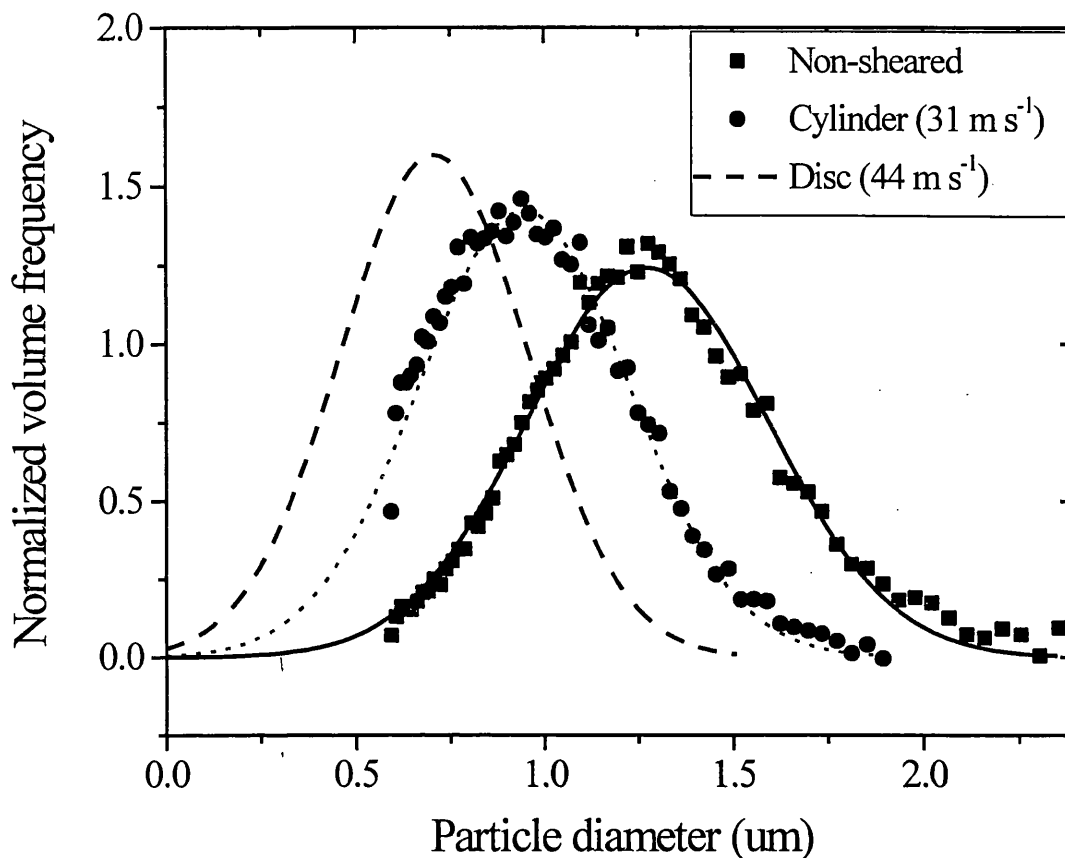


Figure 3.3. Particle size distributions of precipitate suspension exposed to the rotating-element device; (■) non-sheared; (●) cylinder-sheared, 31 m s^{-1} ; and disc-sheared, 44 m s^{-1} (- - -). The normalised volume frequency is defined as the mean particle size divided by the product of channel width and total volume of the distribution. Data points shown are as obtained in the Elzone for feed and cylinder-sheared samples. Laser light scattering showed the same trend in mean size for these two samples and further decrease in size for the disc-sheared sample. All curves shown are Gaussian distributions. For the feed and cylinder-sheared samples, the best fit to the data is shown; a similar fit is used for the disc-sheared sample. The mean and standard variation of the curves are 1.29 ± 0.32 , 0.95 ± 0.28 and $0.71 \pm 0.24 \text{ }\mu\text{m}$ for non-sheared, cylinder-sheared and disc-sheared samples, respectively.

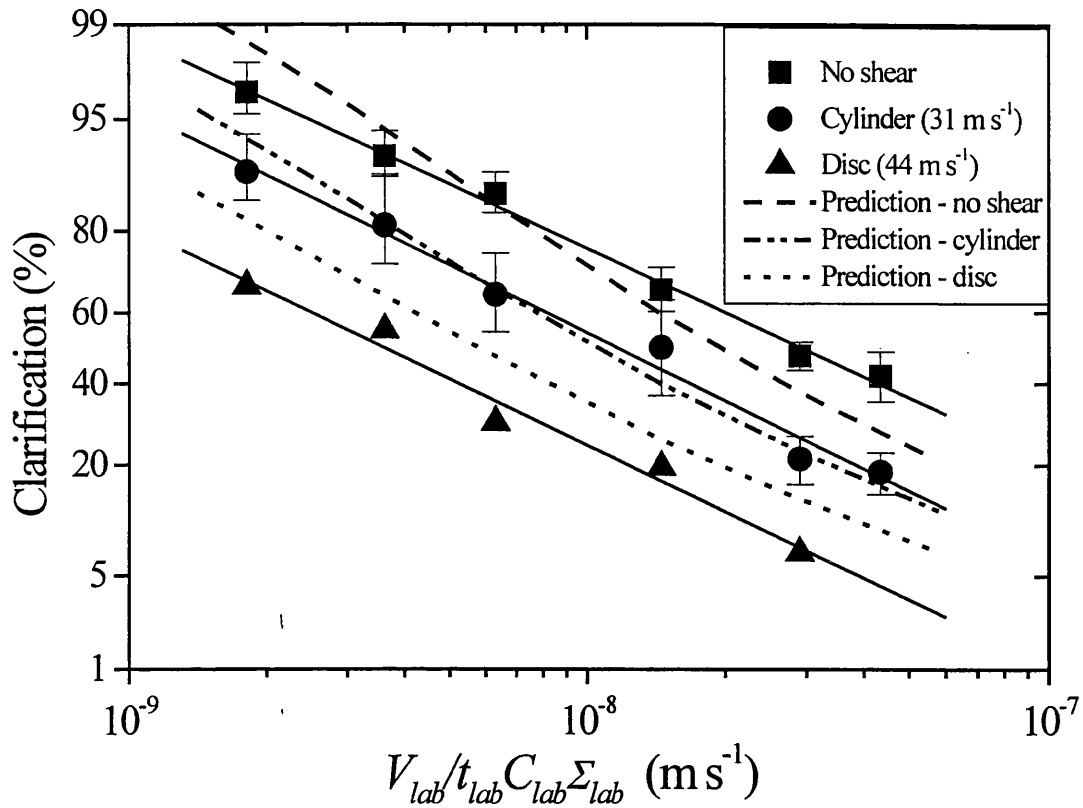


Figure 3.4. Relationship between clarification and ratio of equivalent flow rate to centrifuge separation area plotted on probability-logarithmic axes. Precipitate suspension exposed to the following shear conditions in the rotational device: (■) non-sheared; (●) cylinder, 31 m s⁻¹; and (▲) disc, 44 m s⁻¹. All samples were sheared for 20 s. Data points indicate mean values with errors defining the 95% confidence interval for duplicate runs. Solid lines represent the line of best for each data set; intermittent lines are predictions from grade-efficiency calculations.

3.4.3. Dependence of clarification on tip speed and residence time

The data in Figure 3.5 show that the degree of clarification is a strong function of tip speed, but is practically unaffected by the residence time of the precipitates in the device except at lower rotational velocities. All further samples were sheared for 20 s to avoid errors due to significant acceleration and deceleration times of the disc. The time dependency becomes negligible above a tip speed of 20 m s^{-1} , suggesting that the breakage of precipitate particles may be assumed to be independent of time of exposure. Experiments in which the breakage of protein precipitates was found to have time dependent properties at much lower energy dissipation levels, such as those found in a mechanically agitated vessel, were previously described (Ayazi Shamlou *et al.*, 1994). The time dependency trends in Figure 3.5 are consistent with previous observations of stable size distributions being reached more rapidly at higher imposed flow stresses for protein precipitates (Ayazi Shamlou *et al.*, 1996b), and aggregates of latex (Gierczycki and Ayazi Shamlou, 1996) and chalk (Ayazi Shamlou *et al.*, 1996a) particles.

3.4.4. Laboratory compared to pilot-scale centrifugation

Table 3.1 shows the clarification obtained from samples subjected to the pilot centrifuge with the non-sheared, laboratory-centrifuged sample as the reference (88 %). Results are shown for three different conditions of operation. In all of the cases shown in Table 3.1, the pilot centrifuge was operated at a fixed speed of 167 r s^{-1} ($RCF_{mean} = 6550$). The data indicate that the degree of clarification is strongly affected by the mode of operation with little loss of clarification capacity when pilot centrifugation is carried out in batch mode compared to the modes of continuous operation. Some loss of clarification for batch operation is probably due to some re-entrainment of solids during siphoning of supernatant out of the bowl. The observations suggest loss of clarification due to

disruption in the centrifuge feed zone. The extent of disruption is further increased when centrifugation is carried out with a non-flooded feed zone. This result and other reported work (Hoare *et al.*, 1982; Ayazi Shamlou *et al.*, 1996) suggest that the extent of disruption is determined by the distribution of the energy dissipation rate in the centrifuge feed zone.

Table 3.1. Dependence of clarification achieved in the laboratory and pilot centrifuges operated at $V_{lab}/t_{lab}C_{lab}\Sigma_{lab} = V_{mc}/t_{mc}C_{mc}\Sigma_{mc} = Q_{mc}/C_{mc}\Sigma_{mc} = 6.3 \times 10^{-9} \text{ m s}^{-1}$. Results are the mean values of multiple samples (reproducibility of $\pm 1\%$); where multiple runs ($n=9$ for the laboratory and $n=3$ for the continuous, flooded feed zone centrifuge) were carried out, data are presented in terms of the 95% confidence interval.

Centrifuge	Laboratory (non-sheared)	Pilot		
		Batch	Continuous – flooded feed zone	Continuous – non-flooded feed zone
Clarification (%)	88 ± 2	79 ± 1	39 ± 5	26 ± 1

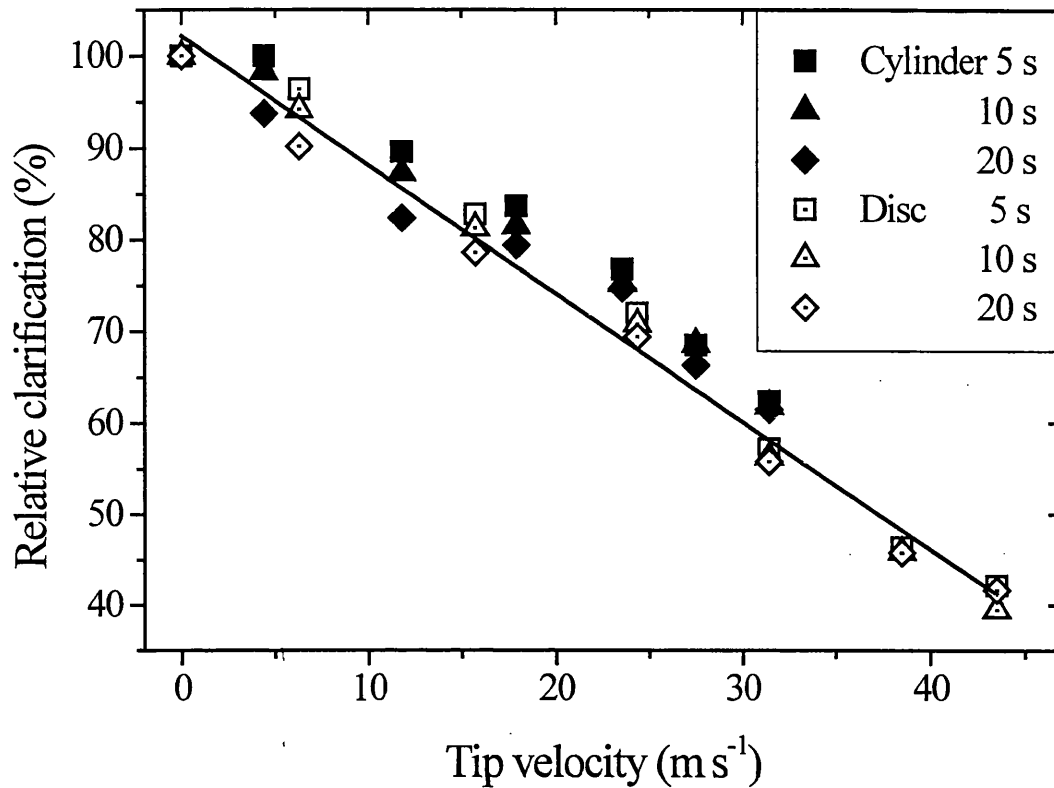


Figure 3.5. Dependence of the relative clarification on tip velocity for times of shearing in the laboratory, rotational device. Precipitate suspension sheared in the cylinder (solid symbols) and disc (open symbols) devices for (■) 5 s, (▲) 10 s and (◆) 20 s. Samples were spun in the laboratory centrifuge at $V_{lab}/t_{lab}C_{lab}\Sigma_{lab} = 6.3 \times 10^{-9} \text{ m s}^{-1}$.

3.4.5. Process intensification

Process intensification is the study of how a process may be rendered more efficient. This may involve eliminating superfluous steps; replacing a series of unit operations with a single better performing one or integrating them together; replacing several smaller units with a large one; and/or operating at higher concentrations to reduce processing times. The last option was investigated briefly in this study. In the standard process, precipitates are derived from well-clarified homogenate originally at 280 g L^{-1} packed yeast. With the aim of minimising the time of homogenisation, others were prepared using clarified homogenate initially at 560 g L^{-1} but then diluted by a factor of two to ensure the same protein concentration. As displayed in Figure 3.6, the aggregates originating from the more concentrated starting material clearly exhibit greater breakage with power dissipation. Shearing with the cylinder at maximum speed resulted in average clarifications of $41 \pm 3 \%$ and $60 \pm 4 \%$ for suspension prepared by homogenisation at double and normal yeast concentrations, respectively.

It was originally hypothesised that this large discrepancy was a result of a higher debris content during precipitation due to the poorer separation of the more concentrated homogenate (85% compared to the normal 97%) as a result of more hindered settling. Therefore, an experiment was devised in which precipitations were carried out using starting pools of protein homogenate (prepared at 280 g L^{-1}) clarified and or diluted to give different concentrations. Aggregates prepared from the raw homogenate homogenate proved to be the most resistant to shear, exhibiting only a slight decline in the % solids sedimented. Break-up becomes more prominent and reaches a maximum with the *completely clarified* sample as shown in Table 3.2. This is not surprising given

the shear-insensitive nature of cell debris, which can serve as nucleation sites thus giving aggregates a denser and stronger core.

Table 3.2. Dependence of shear-sensitivity of precipitates on cell debris concentration. Samples were exposed to the rotating disc operating at 38 m s^{-1} for 20 s and centrifuged at $V_{lab}/t_{lab}C_{lab}\Sigma_{lab} = 6.3 \times 10^{-9} \text{ m s}^{-1}$.

Cell debris concentration of starting material (g L^{-1})	Percent increase in clarification
35	30 ± 2
70	33 ± 2

Another possible explanation for the difference in precipitates a physico-chemical one. The pH of the suspension decreased markedly upon homogenisation, from 6.5 to 5.0, due to the double yeast concentration and lack of buffering capacity; the pH normally drops only to 6.0. In all experiments, the pH was adjusted to 6.5 just prior to precipitation meaning that the debris suspension was at this lower pH for at least two hours. This significant shift that may cause protein denaturation, interaction between proteins and debris, etc., the combination of effects leading to weaker precipitate particles.

3.4.6. CFD of pilot-continuous centrifuge

Figures 3.7 and 3.8 are CFD simulations, derived by numerical solution of Equations B.5-B.8, of flow in the pilot centrifuge running continuously with the feed zone under flooded and non-flooded conditions respectively. The volume fraction plots, Figures 3.7a and 3.8a, show the volume fraction occupied by the liquid in blue and that occupied by gas (air) in yellow, the other colours indicate a two phase gas-liquid mixture. Clearly, the feed zone in Figure 3.7a is almost completely filled with liquid (approximately 99%), while in Figure 3.8a gas and gas-liquid zones are prevalent resulting in only 70% flooding. Suspension enters from the top of the centrifuge, strikes

the rapidly rotating feed distributor, and is then thrown radially outwards and atomised into droplets, as indicated by the gas-liquid zone outside of the distributor. The initial feed will strike the inner bowl wall where it accumulates (due to a partial back-pressure) forming a pool of liquid, as shown by the blue zone in Figure 3.8a.

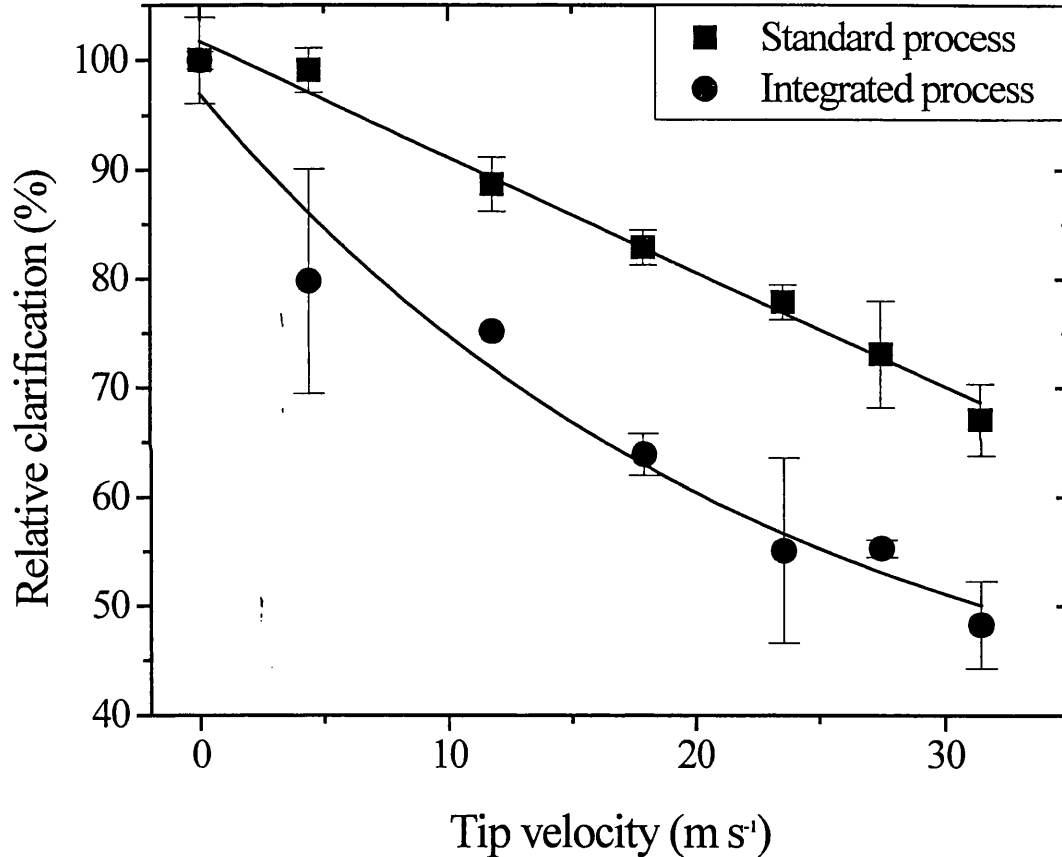


Figure 3.6. Influence of process integration on shear-sensitivity of particles. (■) Standard process: yeast suspended to 280 g L^{-1} , homogenised, well clarified (97%) and proteins precipitated with ammonium sulphate. (●) Integrated process: yeast suspended to 560 g L^{-1} , homogenised, clarified (85%) and then diluted two-fold prior to salting-out. All results were obtained with a residence time of 20 s in the rotational cylinder device. Errors bar indicate 95% confidence interval for multiple (at least duplicate) runs.

Figures 3.7b and 3.8b show the corresponding energy dissipation rates where the zones of maximum energy dissipation rates are shown in red. The greatest energy

dissipation rates are concentrated around the disc region of the feed distributor and along the base and exit of the inner chamber. For purposes of comparison, Figures 3.7b and 3.8b have the same scale, with the variation in energy dissipation rates lying between 0.86×10^5 and $6.0 \times 10^5 \text{ W kg}^{-1}$. The maximum for the flooded conditions is $6.0 \times 10^5 \text{ W kg}^{-1}$ and $12 \times 10^5 \text{ W kg}^{-1}$ for the non-flooded case. From the plots in Figures 3.7b and 3.8b, it is noticeable that when the feed zone is under non-flooded conditions the CFD simulations indicate larger critical zones due to higher values of maximum energy dissipation. In gas-liquid regions indicated in the volume fraction plot, more than 99% of the energy per unit mass is dissipated into the liquid phase due to its much higher density (approximately 1000-fold that of the gas). Put together, the flooded and non-flooded results indicate that the observed differences in the clarification data obtained when the pilot centrifuge is operated under different modes is due to differences in the degree of shear damage experienced by the precipitates.

3.4.7. CFD of rotating disc device

Figure 3.9 displays the laboratory disc device rotating at the appropriate speed to generate the same maximum energy dissipation rate occurring in the pilot centrifuge's feed zone. For the fully flooded case ($6.0 \times 10^5 \text{ W kg}^{-1}$), the disc must rotate at 415 r s^{-1} , as displayed in Figure 3.9a. This prediction is validated by scale-down and pilot experimental results shown in Figure 3.10. Simulation of a disc speed of 545 r s^{-1} in Figure 3.9b shows that the maximum energy dissipation rate ($12 \times 10^5 \text{ W kg}^{-1}$) for the non-flooded case is attained.

3.4.8. Experimental verification of CFD prediction

In Figure 3.10, clarification data is plotted as a function of the energy dissipation rate. The energy dissipation data for the rotating disc and cylinder were obtained from

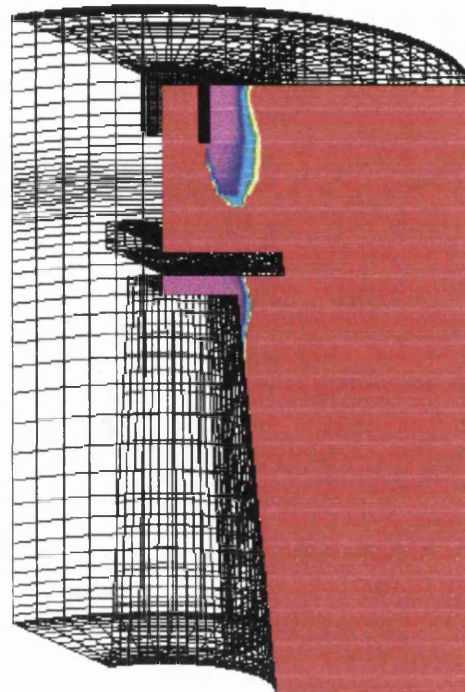
CFD simulations (results not shown). The CFD simulations of energy dissipation rates for the rotating disc were reported by Levy *et al.* (1999). The maximum energy dissipation rate was found to occur in the boundary layer over the rotating disc, which was confirmed by analytically solving Equations 3.1 to 3.6. The data in Figure 3.10 indicate that the maximum energy dissipation rate is a good unifying parameter for correlating the clarification data obtained from the different runs. The decrease in clarification exhibits a consistent exponential decay. The samples sheared with the cylinder resulted in a similar but consistently slightly greater clarification than disc-sheared samples; this may be attributed to incomplete mixing and hence less damage occurring in the cylinder system. The maximum speed (333 r s^{-1}) of the cylinder was insufficient to mimic the extent breakage experienced in the pilot-continuous centrifuge, and consequently, effort was focussed on the rotating disc which could achieve considerably higher speeds (maximum of 462 r s^{-1}). It has been shown that the rotating disc operating at a speed of 415 r s^{-1} produces an energy dissipation rate that practically matches that of the centrifuge operating continuously under fully flooded conditions; the scale-down prediction of the relative clarification of 45% agrees extremely well with the actual value of 44%. Similarly, to mimic the flow conditions in the centrifuge running continuously under non-flooded conditions requires the small disc to be operated at a speed of approximately 545 r s^{-1} giving a clarification of 27% (extrapolated value), which is in good agreement with the pilot value of 30%. Reasonable clarification agreement was obtained between the pilot-batch (90%) and laboratory centrifuge (100%), the pilot value being lower due to solids re-entrainment. Negligible shear occurs in the latter two cases because the suspension was accelerated very gradually (from 0 to 167 r s^{-1} over 200 s) and the liquid is moving at the same speed as the bowl. The overriding conclusion

from the plots in Figure 3.10 is the confirmation of the applicability of the proposed engineering framework for the assessment of the impact of flow stresses on the separation performance of centrifuges.

VOLUME FRACTION



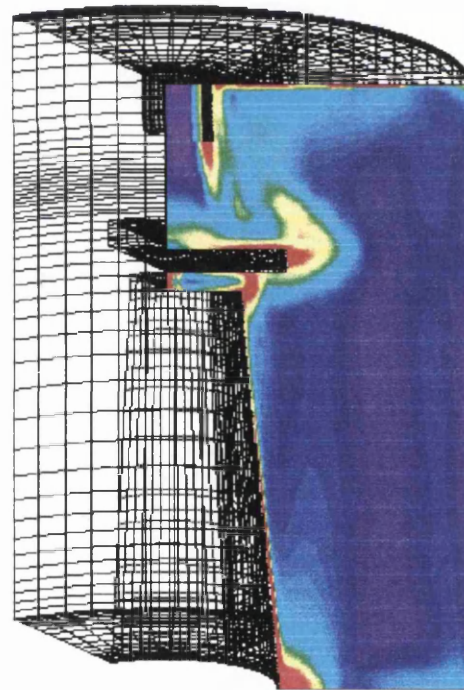
0.86 - 1.00
0.71 - 0.86
0.57 - 0.71
0.43 - 0.57
0.29 - 0.43
0.14 - 0.29
0 - 0.14



(a)

ENERGY DISSIPATION RATE
(W kg⁻¹)

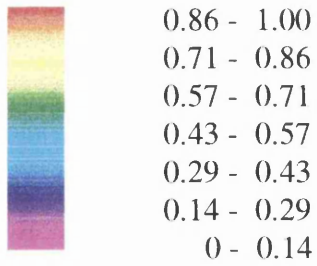
5.14×10^5 - 6.00×10^5
4.29×10^5 - 5.14×10^5
3.43×10^5 - 4.29×10^5
2.57×10^5 - 3.43×10^5
1.71×10^5 - 2.57×10^5
8.57×10^4 - 1.71×10^5
0 - 8.57×10^4



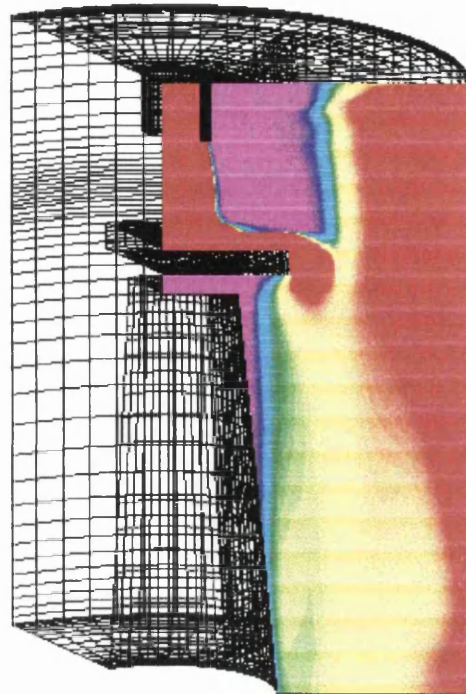
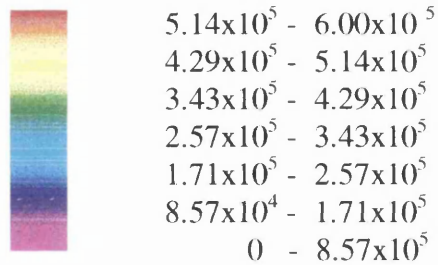
(b)

Figure 3.7. Computational fluid dynamic (CFD) simulation of the pilot multichamber-bowl centrifuge operated at $Q_{mc} = 22 \text{ L h}^{-1}$ and $N = 167 \text{ r s}^{-1}$ with a fully flooded feed zone. **(a)** is a volume fraction plot displaying regions of liquid in blue, gas in red and gas-liquid ones in other colors. **(b)** shows the variation in energy dissipation rates (W kg^{-1}), from the lowest (blue) to the highest (red; a maximum of $6.0 \times 10^5 \text{ W kg}^{-1}$).

VOLUME FRACTION



(a)

ENERGY DISSIPATION RATE
(W kg^{-1})
(maximum 12×10^5)

(b)

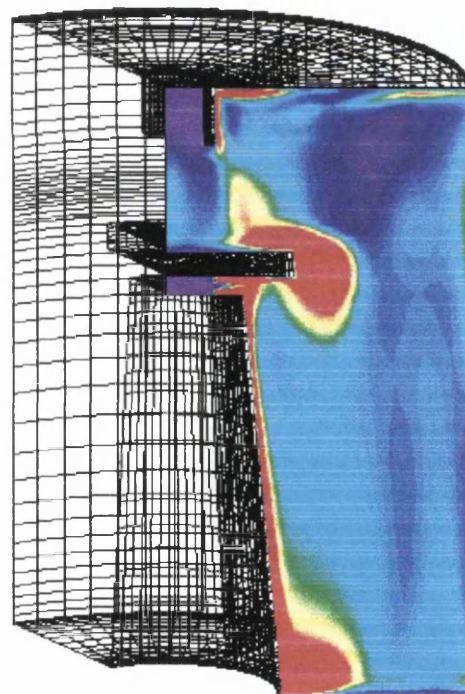
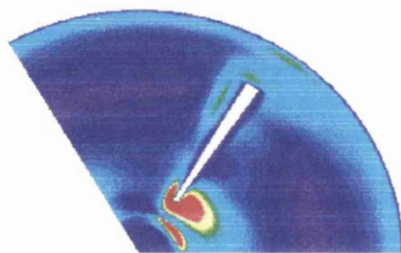
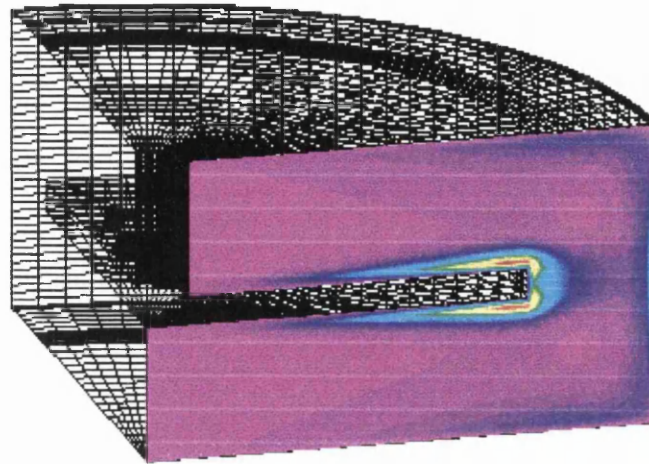
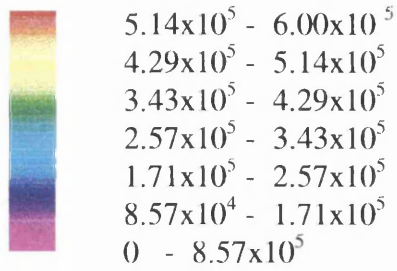


Figure 3.8. CFD simulation of the pilot multichamber-bowl centrifuge operated under non-flooded conditions ($Q_{mc} = 22 \text{ L h}^{-1}$ and $N = 167 \text{ r s}^{-1}$). (a) refers to volume fraction and (b) is energy dissipation rate (a maximum of $12 \times 10^5 \text{ W kg}^{-1}$). The smaller diagram (120 degree arc) adjacent to the power plot is a top view of the feed zone, showing a red region at the inner tip of the blade of the feed distributor (see Figure 3.1).

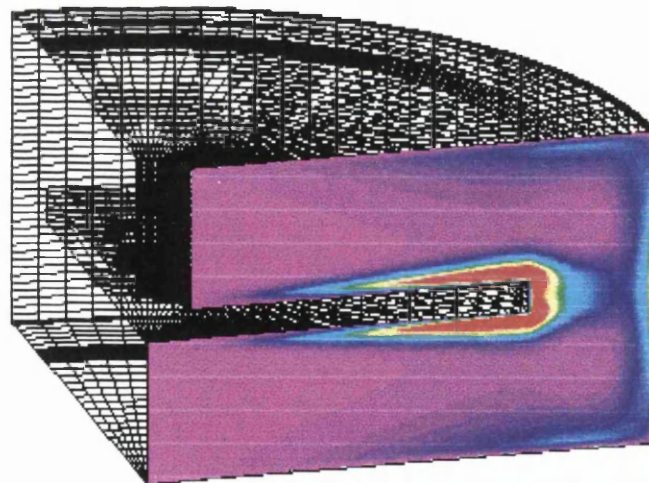
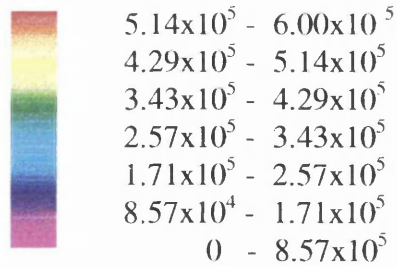
ENERGY DISSIPATION RATE
(W kg⁻¹)



Rotational speed: 415 r s⁻¹

(a)

ENERGY DISSIPATION RATE
(W kg⁻¹)
(maximum 12 x 10⁵)



Rotational speed: 545 r s⁻¹

(b)

Figure 3.9. CFD simulation of the laboratory disc device (fully flooded) rotating at (a) 415 r s⁻¹ and (b) 545 r s⁻¹ to match the maximum energy dissipation rates occurring the pilot centrifuge feed zone when operated under fully flooded (6.0 x 10⁵ W kg⁻¹) and non-flooded conditions (12 x 10⁵ W kg⁻¹), respectively.

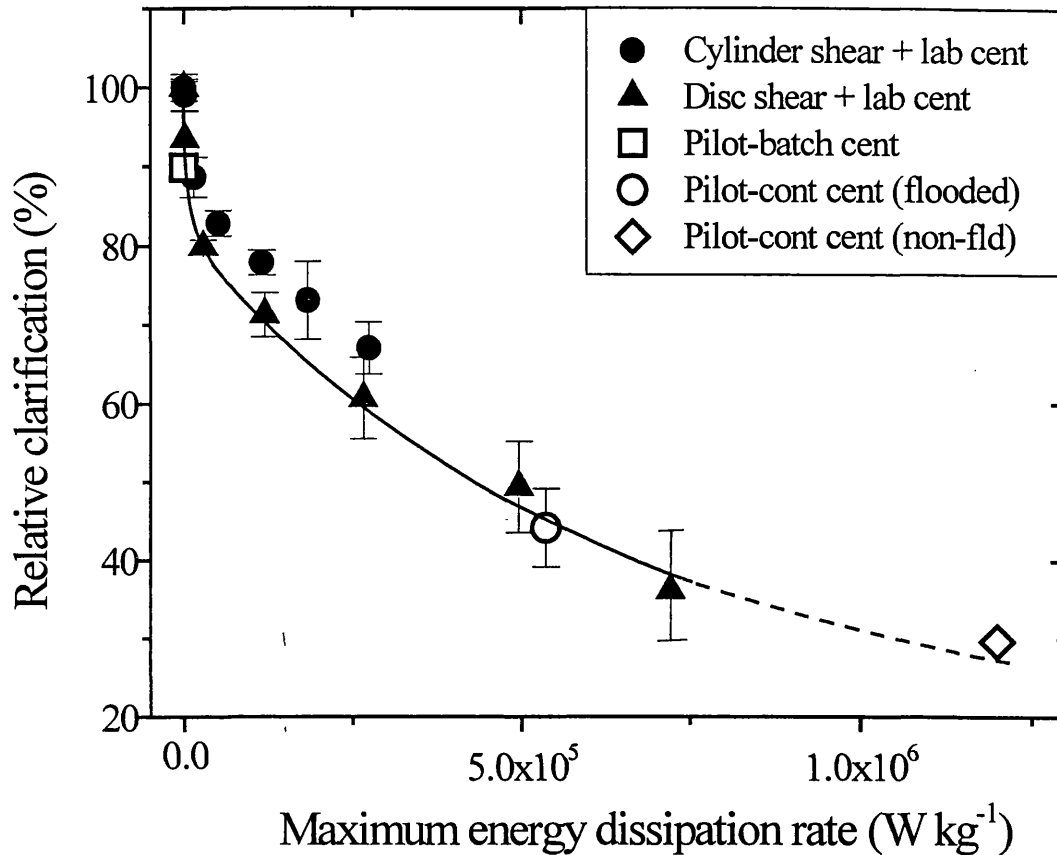


Figure 3.10. Dependence of the relative clarification on maximum energy dissipation rate. Solid points represent laboratory samples sheared for 20 s in the rotating (●) cylinder or (▲) disc device, and centrifuged. Open symbols refer to pilot centrifuge operating under the following conditions: (□) batch mode; (○) continuous mode, flooded feed zone; and (◇) continuous mode, non-flooded feed zone. All samples were centrifuged at $V_{lab}/t_{lab}C_{lab}\Sigma_{lab} = Q_{mc}/C_{mc}\Sigma_{mc} = 6.3 \times 10^{-9} \text{ m s}^{-1}$. Only laboratory-disc results were used to obtain the curve of best fit; the disc device could only achieve $7.3 \times 10^5 \text{ W kg}^{-1}$, so the fit was extrapolated (- -) to $1.25 \times 10^6 \text{ W kg}^{-1}$ to encompass the pilot-continuous centrifuge with non-flooded feed zone. Data points indicate mean values and error bars show the 95% confidence interval for multiple (at least triplicate) runs.

3.5. CONCLUSIONS

A theoretical analysis of the flow field in a pilot centrifuge was carried out using CFD techniques. A small rotating-disc device was used to mimic the CFD-predicted flow stresses in the critical zones (those displaying maximum energy dissipation rates) of the centrifuge entrance region. A suspension of protein precipitates, prepared under a fixed set of conditions was sheared in the disc device operating under flow conditions that mimicked those in the critical region of the centrifuge. The sheared material was subsequently clarified in a laboratory centrifuge. The results were used to predict the performance of a multichamber-bowl centrifuge running under different modes of operation. The technique developed in this work is generic and has important applications in the design of new centrifuges and in cases where large quantities of test materials are not available.

4. **CHAPTER 4: PREDICTION OF THE PERFORMANCE OF INDUSTRIAL CENTRIFUGES USING SCALE-DOWN MODELS**

ABSTRACT

Boychyn *et al.* (2000b) used CFD (computational fluid dynamics) to model the high flow forces found in the feed zone of a multichamber-bowl centrifuge and reproduced these in a small, high-speed rotating disc device. Linking the device to scale-down centrifugation, permitted accurate prediction of the performance of the continuous centrifuge for shear-sensitive protein precipitates. However, CFD can be laborious and time consuming. Consequently, this research investigated the validity of scaling based on constant tip velocity of the critical structure (defined as the first region of contact between the feed stream and the centrifuge) and compared this to the CFD method for the prediction of clarification in a pilot disc stack, CARR, multichamber-bowl and production multichamber-bowl centrifuge. The tip velocity technique was a good predictor ($\pm 15\%$) of large-scale clarifications, but CFD was required to obtain greater accuracy, particularly for non-flooded feed zones. Under standard operating conditions, the following centrifuges generate greater flow forces and hence more particle break-up in ascending order: pilot disc stack, multichamber-bowl, CARR and production multichamber-bowl; nevertheless, the CARR can attain very low flow rates (due to effective cooling of the bowl), which result in greater separation. Critically, the scale-down centrifugation process proved to be a much more accurate predictor of production multichamber-bowl performance than the pilot centrifuge.

4.1. INTRODUCTION

4.1.1. Previous work

Centrifugation has been successfully scaled from laboratory through to pilot scale for species that are structurally unsusceptible to high-flow fields (Ambler, 1959; Maybury *et al.*, 1999). However, shear sensitive particles, such as protein precipitates, are readily damaged in the feed zone of continuous centrifuges. Boychyn *et al.* (2000b) modelled the high flow forces found in the feed zone of a multichamber-bowl centrifuge and reproduced these in a small, high-speed rotating disc device. This break-up of particles in the entrance region of the continuous centrifuge resulted in great discrepancies between laboratory scale-down predictions of clarification and actual pilot values (Boychyn *et al.*, 2000a). Processing material in the disc device prior to scale-down centrifugation, represented a good mimic of the larger machine's performance. The challenge remains to extend this predictive technology to other continuous-flow centrifuges in order to verify its general utility.

4.1.2. Modelling using computational fluid dynamics (CFD)

Fluid flow in equipment with a complex geometry is not amenable to standard theoretical analysis, but is possible using computational fluid dynamics. In Chapter 3, the CFD package was validated by correlation to boundary layer theory analysis of flow over a rotating disc (Schlichting, 1979). CFD involves inputting a detailed drawing of the centrifuge's entrance region into a CFD package and then simulating the flow to locate the regions of highest power dissipation.

4.1.3. Modelling using tip velocity

The other predictive method is based on maintaining a constant tip velocity between the rotating disc device and the *critical structure* in the feed zone of the continuous

centrifuge. The latter is the area of *initial contact and acceleration* of the process stream. Figure 4.1 displays the feed zone and critical structure of several types of continuous centrifuges. In a disc stack machine (Figure 4.1a), the lock nut represents the initial point of contact for the feed suspension; the flow-distributor (Figure 4.1b) and contact-disc (Figure 4.1c) are critical in multichamber-bowl and CARR centrifuges, respectively.

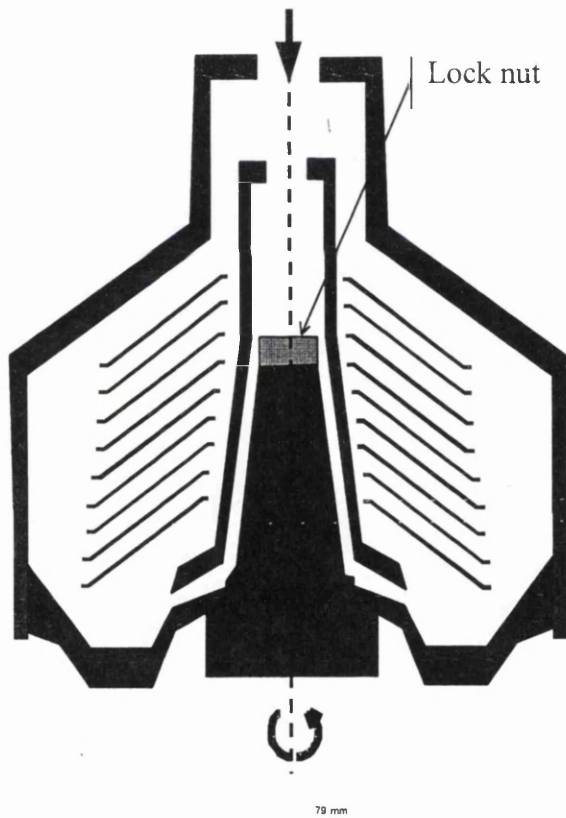
Once the structure has been identified, the critical radius must be selected. For the lock nut, this is the maximum radius at its top, and similarly so for the disc in the CARR. However, the geometry of the multichamber-bowl is rather more complex: material first contacts a disc but is then thrown radially outwards, passing the top of the blades or fans of the distributor before reaching the bowl wall. Thus, the critical diameter is the top outer radius of the distributor (i.e. distance between the centre of rotation and the top outer edge of the distributor blade). For the relevant centrifuge, tip velocity can be converted into maximum power dissipation (see section 3.2.1.2), and the performance of the industrial centrifuge predicted from a plot of relative clarification versus energy dissipation rate (obtained with laboratory data).

4.1.4. Description of centrifuges

The disc stack centrifuge is widely used in the biotechnology industry for the recovery of cells, cell debris, inclusion bodies and precipitates, etc., and hence, has been described by numerous authors. Its key features are a central stack of conical discs, in which the great majority of separation occurs, and its ability to perform intermittent solids discharge. It usually achieves good clarification but relatively poor dewatering compared to solid-bowl centrifuges such as the tubular bowl or multichamber-bowl.

The multichamber-bowl has been described extensively in Chapter 2. With the many chambers, long liquid residence times exist, resulting in good clarification, dewatering and a superior solids-handling capacity than the tubular-bowl design.

The CARR Powerfuge™ is a high-speed industrial centrifuge similar to a tubular-bowl design, but the former has baffles that serve to reinforce its structural integrity and assist in solids retention. Like the tubular-bowl, the high relative centrifugal force of the CARR provides good clarification and solids compaction, however, it is also able to perform automated solids discharge. A vibrating knife that scrapes away sediment from the bowl wall while it rotates at low speed accomplishes this. Thus the CARR combines the advantages of tubular-bowl and disc stack centrifuges.



(a)

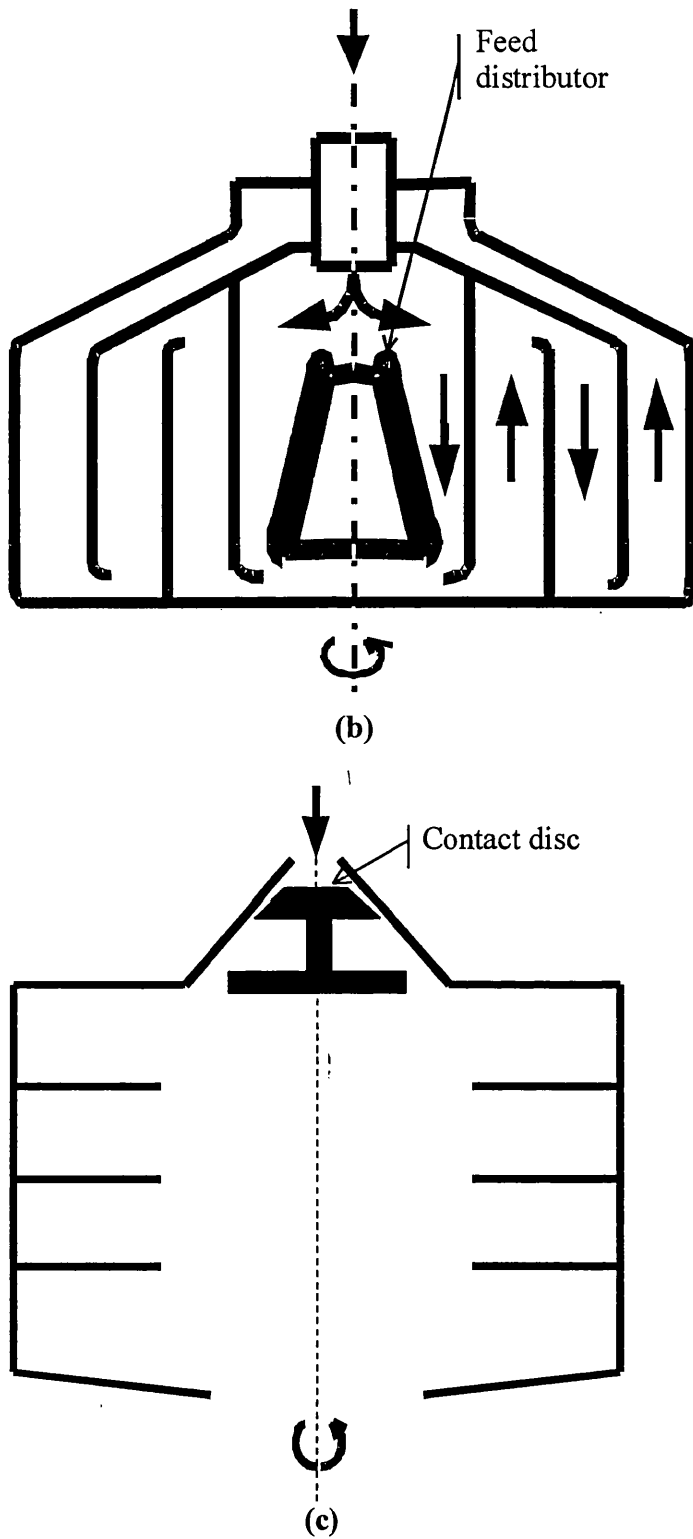


Figure 4.1. Schematics of continuous-flow centrifuges: **(a)** pilot disc stack centrifuge, with central lock nut ($r_{cr} = 0.015$ m; $N_c = 166$ r s⁻¹) in feed zone; **(b)** pilot multichamber-bowl centrifuge, with feed distributor ($r_{cr} = 0.0375$ m; $N_c = 165$ r s⁻¹); and **(c)** pilot CARR centrifuge, with feed contact disc ($r_{cr} = 0.029$ m; $N_c = 255$ r s⁻¹).

4.2. THEORETICAL CONSIDERATIONS

4.2.1. Scaling on tip velocity

The magnitude of the forces occurring in the feed zone of a continuous centrifuge may be estimated by determining the tip velocity v_{cr} , of the critical structure:

$$v_{cr} = r_{cr} \omega_C = 2\pi N_C r_{cr} \quad (4.1)$$

where r_{cr} is the critical radius of the structure and N_C is the rotational speed of the continuous centrifuge. The critical velocity is then maintained in the laboratory rotating disc device of radius r_{rd} , its rotational speed N_{rd} , determined by:

$$N_{rd} = \frac{r_{cr} N_C}{r_{rd}} \quad (4.2)$$

From this, an associated maximum energy dissipation rate can be calculated.

4.2.2. Maximum energy dissipation rate

The flow over a disc of radius R , rotating at an angular speed of ω , has been theoretically described by Schlichting (1979) and discussed in Chapter 3. The maximum energy dissipation rate per unit mass, ε_{max} , is given by Equation 3.5. The theoretical values correlate very well with ones calculated by CFD analysis (Levy *et al.*, 1999). CFD theory is discussed in Chapter 3 and Appendix B.

4.2.3. Recovery curves

A recovery curve is a plot of the percentage clarification against the ratio centrifuge flow rate (Q) to equivalent separation area (Σ) on probability-logarithmic axes (Ambler, 1959); usually, linearity is observed. Therefore, a NORMSINV function (found in Origin 5.0, Microcal Software, Inc., Northampton, USA), which returns the inverse of the standard normal cumulative distribution (a mean of zero and a standard deviation of 1), is required to convert the clarification (i.e. a probability) into the corresponding $Q/C\Sigma$:

$$\text{NORMSINV}\left(\frac{100 - \text{Clar}}{100}\right) = -A - B \log\left(\frac{Q}{C\Sigma}\right) \quad (4.3)$$

where *Clar* is the percentage clarification, *A* and *B* are the respective ordinate intercept and slope of the recovery line, and *C* is a correction factor (see Chapter 2).

4.2.4. Centrifugation

Sigma (Σ) expressions for the laboratory batch, tubular-bowl and multichamber-bowl centrifuges are detailed in section 2.2. The CARR is considered to be a tubular-bowl centrifuge for purposes of calculating Σ . For a disc stack centrifuge,

$$\Sigma_{ds} = \frac{2\pi n \omega^2 (r_2^3 - r_1^3)}{3g \tan \theta} F_L \quad (4.4)$$

where *n* is the number of discs, θ is the half disc angle, r_1 and r_2 are the respective inner and outer radii of the discs, and F_L is a correction factor to account for the spacing between discs.

$$F_L = 1 - \left(\frac{3Z_L B_L}{4\pi r_2} \right) \left(\frac{1 - (r_1/r_2)^2}{1 - (r_1/r_2)^3} \right) \quad (4.5)$$

where Z_L is the number of caulks on a disc and B_L is the caulk width.

4.3. MATERIALS AND METHODS

4.3.1. Chemicals

All chemicals, unless specified otherwise, were obtained from Sigma Chemical Co. Ltd. (Dorset, UK) and were of analytical grade.

4.3.2. Description of equipment

Laboratory and pilot-scale equipment used in preparing the yeast-protein precipitate suspension is detailed in Chapter 2. Well-clarified homogenate (derived from packed Bakers' yeast re-suspended to 280 wet g L⁻¹ in 0.1 M KH₂PO₄, pH 6.5, 4°C) was brought rapidly to 40% saturation with saturated (NH₄)₂SO₄ (519 g L⁻¹, buffered with 0.1 M KH₂PO₄, pH 6.5), and agitated so that $\bar{G} = 200 \text{ s}^{-1}$ for 0.63 h ($\bar{G}t = 10^5$).

The other system investigated was Fraction IV suspension (F:IV; 3% w/v protein, 40% w/v ethanol, pH 5.85, -5°C) of the Kistler-Nitschmann cold-ethanol plasma fractionation process (a modified Cohn method 6) for the purification of human serum albumin (More and Harvey, 1991). A sample (1 L) of Fraction IV suspension was taken from the Production Department of Bio Products Laboratory (Elstree, UK), placed in a glycol-cooled baffled vessel (2 L) and agitated at 5 r s⁻¹.

All centrifuges and their relevant operating conditions are listed in Table 4.1. Prior to laboratory centrifugation, most precipitate samples were processed in a high-speed rotating disc device described in Chapter 3. A residence time of 20 s in the disc reactor was selected to ensure full mixing, however breakage kinetics were shown to be extremely rapid at higher speeds for the yeast-protein system. Due to the heat labile F:IV precipitates, the suspension were only sheared for 5 s.

Table 4.1. Name, type and operating conditions (flow rate or spin time, speed and Σ value) of the studied centrifuges. Centrifuge correction factors were found in Svarovsky (1990) or calculated using experimental data or ** data provided by Westfalia. All symbols are explained in section 4.2.

Centrifuge	N_c ($r\ s^{-1}$)	Σ (m^2)	C	V (L)	t (h)	$V/tC\Sigma$ ($10^{-9}\ m\ s^{-1}$)	$Clar$ (%)
Yeast-protein system (Laboratory and pilot centrifuges)							
Beckman J2-M1 Laboratory batch centrifuge with JS-13.1 swing-out rotor (Beckman Instruments Ltd., High Wycombe, UK; $R_1 = 0.070\ m$, $R_2 = 0.130\ m$)	50	0.29	1.0	0.015	0.26	56	34
	100	1.12			0.31	12	72
	130	1.70			0.35	6.3	88 ± 2
					Q ($L\ h^{-1}$)	$Q/C\Sigma$	
Westfalia SAOOH Disc Stack (non-flooded feed zone; $r_1 = 0.021\ m$, $r_2 = 0.053$, $Z = 6$, $B = 0.005\ m$);	165	1500	0.4	1.0	13	6.3	56
Westfalia KDD 605 Multichamber-bowl (Westfalia Separator AG, Oelde, Germany; see Figure 2.1 for dimensions)	167	1110	0.88*	1.5	21	6.3	39 ± 5 26
Non-flooded							
CARR Powerfuge P6 (CARR, USA; $r_i = 0.0508\ m$, $r_o = 0.0762\ m$, $L = 0.127\ m$)	83.3	112	0.9	1.0	20	56	7.1
	167	446			20	12	14
	255	1040			20	6.3	24
Plasma system (Laboratory and production centrifuges)							
					t (h)	$V/tC\Sigma$ ($10^{-9}\ m\ s^{-1}$)	
Sorvall RC-5B Refrigerated Superspeed Laboratory batch centrifuge (DuPont Instruments, USA) with HS-4 swing-out rotor and 00480 inserts ($R_1 = 0.071\ m$, $R_2 = 0.158\ m$)	113	1.50	1.0	0.020	0.25	15	76 ± 4
					Q ($L\ h^{-1}$)	$Q/C\Sigma$	
Westfalia BKA45 Multichamber-bowl ($r_{1i} = 0.075\ m$, $r_{1o} = 0.20\ m$, $L_1 = 0.25\ m$, $r_{2i} = 0.20\ m$, $r_{2o} = 0.25\ m$, $L_2 = 0.29\ m$)	90.8	5080	0.80**	45	200	14	44 ± 5

4.3.3. Analyses

4.3.3.1. *Physical properties*

The densities of the yeast-protein and plasma precipitate suspensions were 1115 and 970 kg m⁻³, respectively, measured with a specific gravity bottle. The dynamic viscosity of the yeast-protein precipitate suspensions was determined to approach 3.0 mPa s (at shear rates greater than 10³ s⁻¹) using a Contraves Rheomat 115 viscometer with concentric cylinders (Contraves Industrial Products, Ruislip, UK); the plasma suspension had a viscosity of 9.0 mPa s measured with a Bohlin CS 10 Rheometer in the parallel plate configuration (Bohlin Instruments Limited, Gloucestershire, UK).

4.3.3.2. *Assay for particle damage*

Samples were spun down in 20 mL graduated tubes in the laboratory centrifuge for $V_{lab}/t_{lab}C_{lab}\Sigma_{lab} = Q_c/C_c\Sigma_c$ (values listed in Table 4.1). As a control, a non-sheared sample was centrifuged commensurately with the sheared samples to ensure the same processing conditions.

4.3.3.3. *Clarification*

For the yeast-protein system, clarity was assessed by the OD at 670 nm with the spectrophotometer by diluting samples in a solution of 40% (NH₄)₂SO₄. A Digital Direct-Reading Turbidity Meter (Orbeco-Hellige, Europe) was used to determine the turbidity of plasma samples.

4.4. RESULTS AND DISCUSSION

4.4.1. Estimating maximum energy dissipation rates using tip velocity

The maximum energy dissipation rate in the feed zone of a continuous centrifuge can be estimated by CFD or tip velocity of the critical structure. Table 4.2 provides the commensurate rotational speeds and maximum power dissipations of the laboratory disc device for each centrifuge. Despite the higher rotational speeds of the pilot centrifuges, particularly the CARR, the much larger critical radius of the production multichamber-bowl (geometrically similar to the pilot one) necessitates the greatest disc speed of 696 r s^{-1} , which is approximately 1.4-fold greater than the CARR and 4-fold greater than the pilot disc stack. Larger speeds entail increasing energy dissipation rates.

4.4.2. Dependence of relative of clarification on maximum energy dissipation rate

Figure 4.2 displays the dependence of relative clarification on maximum energy dissipation rate for yeast-protein precipitate (a) and plasma precipitate (b) suspensions. Each laboratory sample was exposed to the rotating disc at different speeds for a set time and centrifuged. Yeast-protein precipitates show an exponential-decay relationship (same laboratory data points as in Figure 3.10), while linearity is exhibited in Figure 4.2b. Moreover, the plasma precipitates appear to be less susceptible to flow forces as the relative clarification in Figure 4.2 decreases much more gradually (with increasing power dissipation) than that in 4.2. The superior shear-resistance of plasma precipitates may be attributed to their smaller size (it was not possible to verify this with particle sizing instruments) and density, which contribute to strength. Due to higher viscosity, laminar flow predominates around the disc in the plasma system ($Re < 10^5$) unlike in the yeast-protein one, where turbulence may appear as the maximum Reynolds number (2.4×10^5)

approaches that for the transition region (3.0×10^5). Lower maximum shear rates are also experienced in the more viscous plasma suspension.

Table 4.2. Comparison of predicted and experimental clarifications. Maximum energy dissipation rates calculated using tip velocity (of the critical structure in the feed zone of the continuous centrifuge; $r_{rd} = 0.015$ m) or CFD. Predicted clarifications (by tip velocity or CFD method) were calculated using Equation 4.3 with the respective $Q/C\Sigma$ value, slope (-1.6 and -3.1 for yeast-protein and plasma systems, respectively) and an ordinate intercept determined from Figure 4.4. All symbols are explained in section 4.2.

Centrifuge	N_c ($r\ s^{-1}$)	r_{cr} (m)	N_{rd} ($r\ s^{-1}$)	ε_{max} ($10^5\ W\ kg^{-1}$)		Clar (%)		
				Tip velocity	CFD	Tip velocity	CFD	Exp.
Yeast-protein system								
Disc stack	165	0.015	165	0.333	2.0	70	58	75 [*]
Pilot multichamber- bowl - Flooded	167	0.0375	417	5.36	6.0	40	40	39 \pm 5
- Non-flooded						40	24	25
CARR	83.3	0.029	160	0.304	0.50	16	15	7.1
	167		320	2.43	2.5	38	37	14
	255		490	8.70	14	30	21	24
Plasma system								
Production multichamber-bowl	90.8	0.115	696	25.0	---	38	---	45 \pm 4

Based on normalised data extracted from Maybury (1999) for similar yeast-protein precipitates: $Clar_{lab} = 65\%$, $Clar_{ds} = 56\%$, $Rel\ Clar_{ds} = 86\%$ at $Q/C\Sigma = 6.3 \times 10^{-9}\ m\ s^{-1}$. Assuming that the precipitate particles have approximately the same shear-sensitivity as those in this study, the relative clarification will remain constant. Then, $(Clar_{lab})_{present\ study} = (Rel\ Clar_{ds})(Clar_{lab}) = 75\%$.

4.4.3. Recovery curves

Increasing the speed of disc rotation results in more particle break-up. As seen in Figure 4.3a, this shifts the recovery line down, such that lower $V/tC\Sigma$ values are needed to achieve the same clarification, e.g. an 80% clarification is obtained at $V/tC\Sigma = 10^{-8}\ m\ s^{-1}$ with non-sheared material, and at $V/tC\Sigma = 10^{-9}\ m\ s^{-1}$ with suspension sheared in the disc device at $44\ m\ s^{-1}$. All curves in this Figure 4.3a have very similar slopes, indicating little change in the width of the size distribution.

Figure 4.3b shows the clarification of the plasma precipitates centrifuged for different times – the steeper slope indicates a tighter particle size distribution. Given the results of the yeast-protein system, it is assumed that sheared plasma precipitates would similarly exhibit a linear and approximately parallel dependence of clarification on centrifugation conditions.

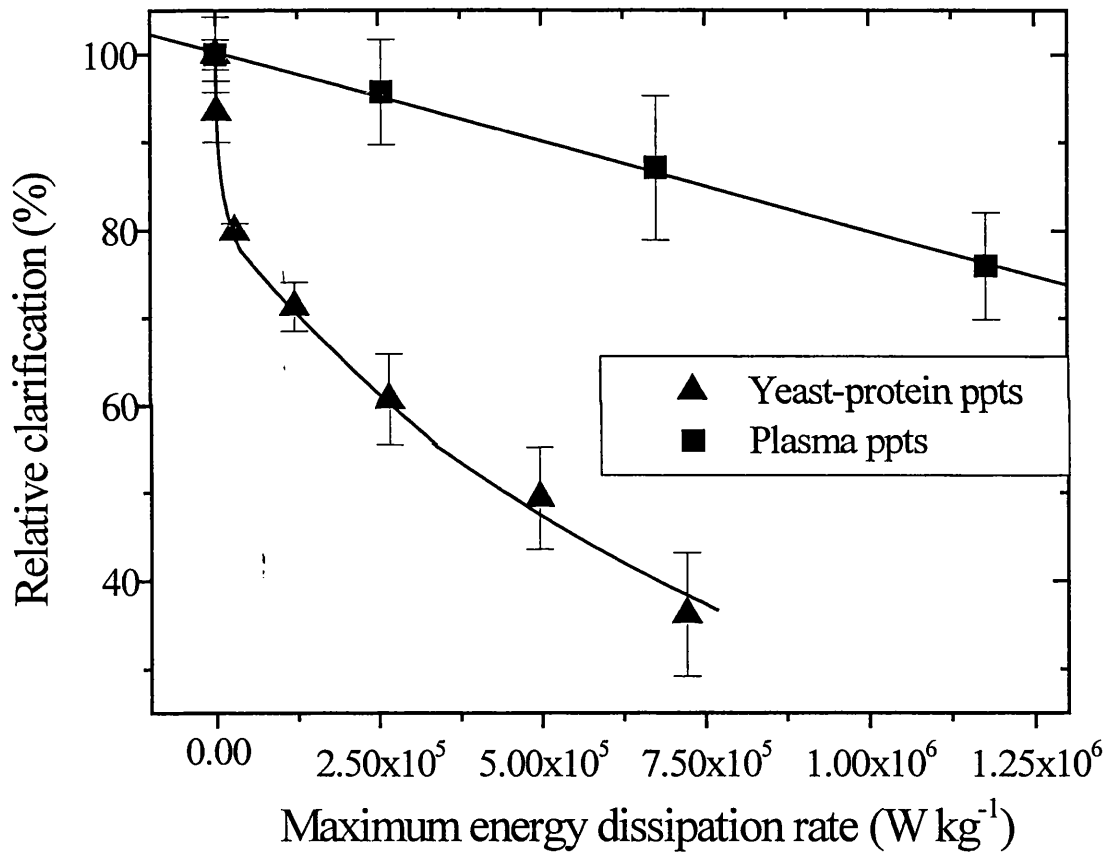
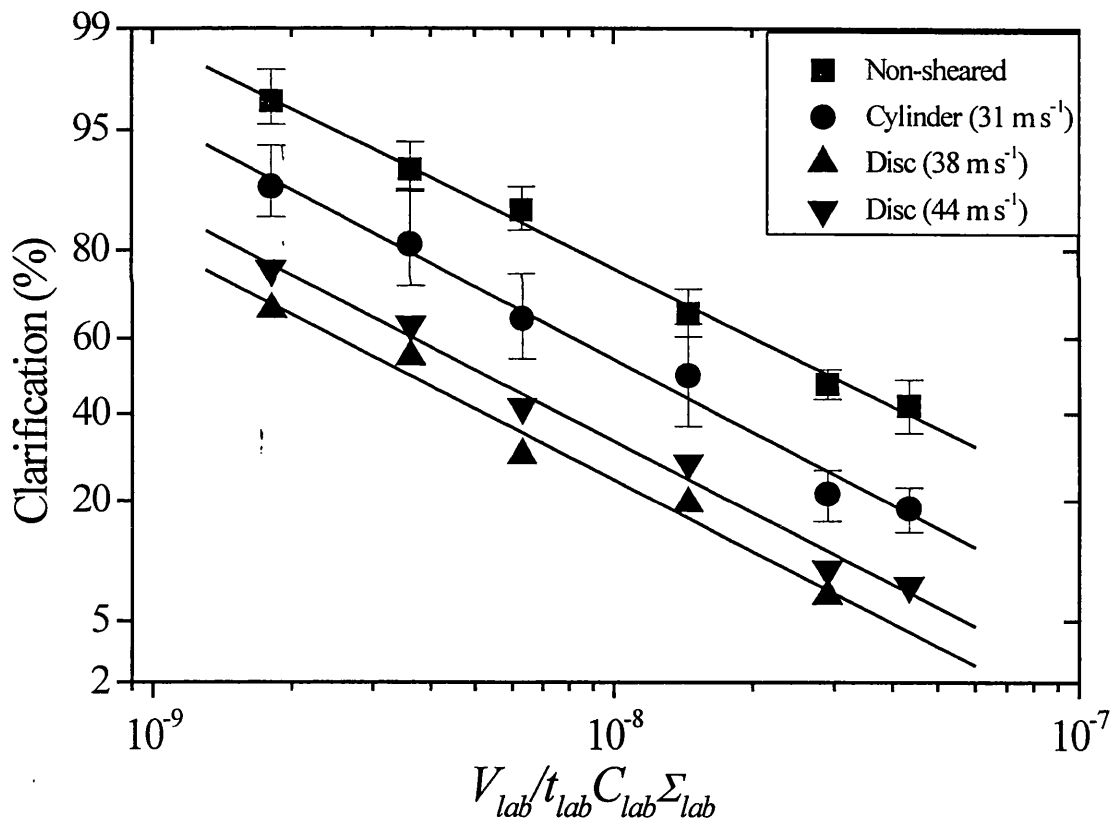


Figure 4.2. Dependence of the relative clarification on maximum energy dissipation rate for precipitates processed through the laboratory rotating disc device and centrifuge. The yeast-protein precipitate suspension (▲) was centrifuged at $V_{lab}/t_{lab}C_{lab}\Sigma_{lab} = 6.3 \times 10^{-9} \text{ m s}^{-1}$ and the plasma precipitates (■) at $V_{lab}/t_{lab}C_{lab}\Sigma_{lab} = 14 \times 10^{-9} \text{ m s}^{-1}$, in order to mimic settling conditions in the pilot and production multichamber-bowl centrifuges, respectively. Relative clarification is defined as the ratio of the clarification for sheared to non-sheared material.

Since the slope remains constant regardless of the magnitude of the applied shear, the shift in the recovery curve can be quantified by plotting the ordinate (i.e. Y-axis) intercept of the lines in Figure 4.3 against maximum power dissipation. This was done for yeast-protein precipitates (Figure 4.4a) which display an exponential decaying relationship, and for plasma precipitates (Figure 4.4b) which show a linear relationship. The more pronounced drop in the intercept value is evidence of the greater shear sensitivity of yeast-protein precipitates.



(a)

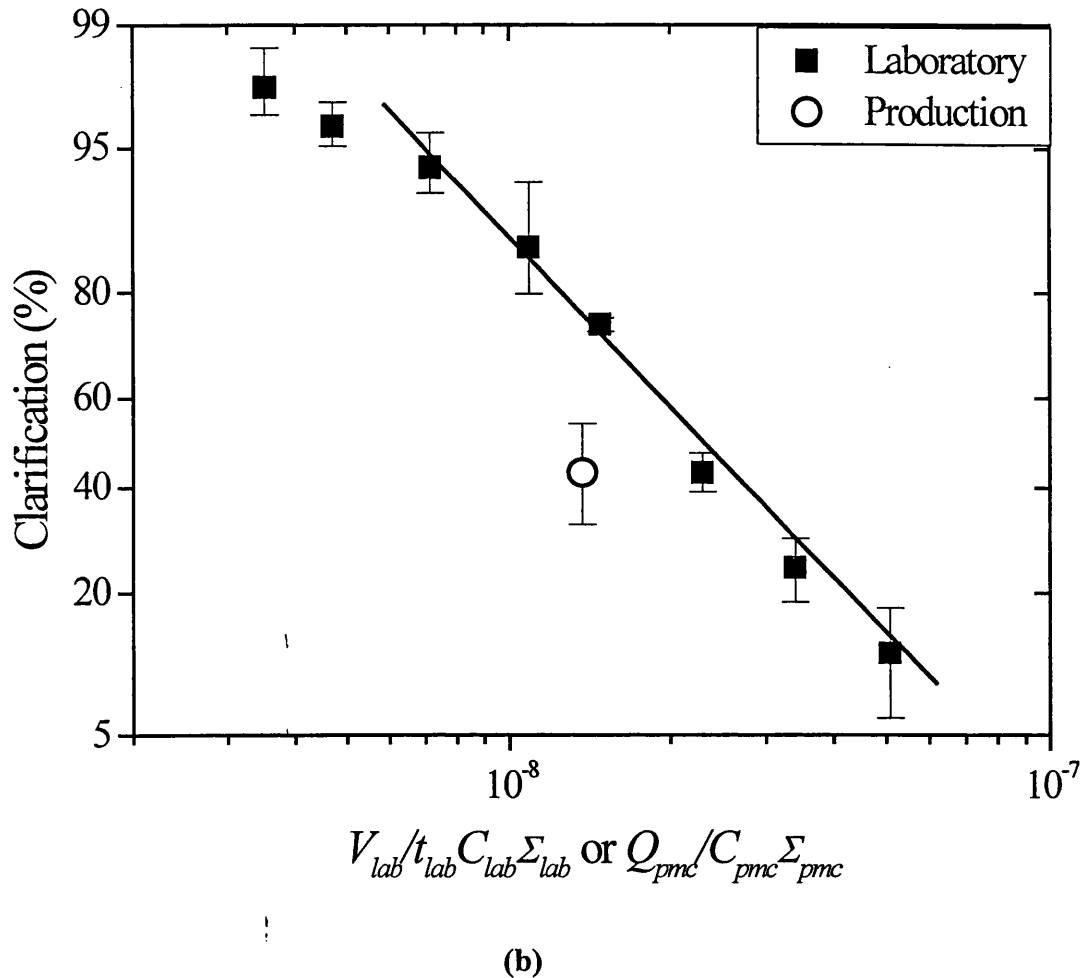
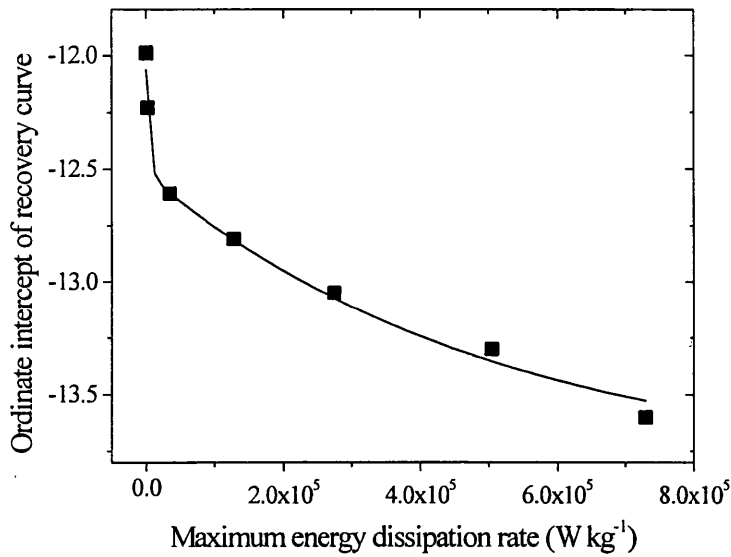


Figure 4.3. Recovery curve (dependence of clarification on ratio of equivalent flow rate to centrifuge separation area plotted on probability-logarithmic axes) for yeast-protein and plasma precipitate suspensions.

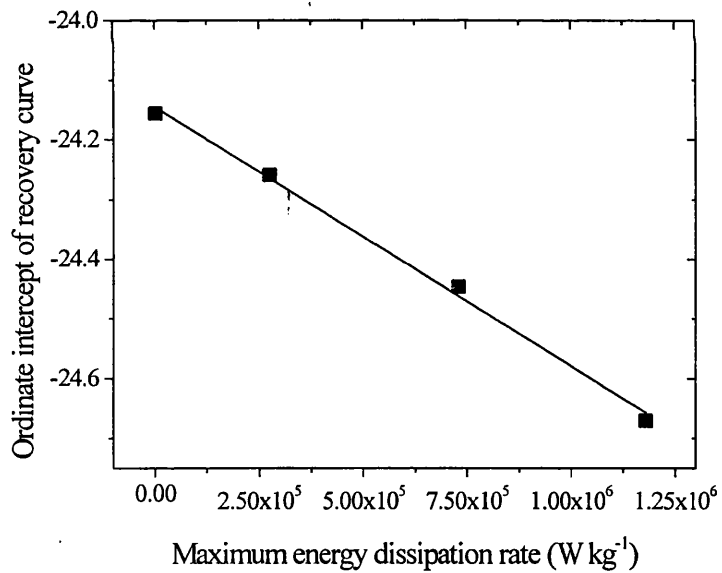
(a) Yeast-protein system. Suspension was exposed to the following tip velocities in the rotational device prior to laboratory centrifugation: (■) non-sheared; (●) cylinder, 31 m s^{-1} ; (▼) disc, 38 m s^{-1} ; and (▲) disc, 44 m s^{-1} (some data previously presented in Figure 3.4). All lines have an approximate slope of -1.6 .

(b) Plasma system. Suspension was *not* sheared in the disc device prior to laboratory (■) or production (○) centrifugation. The laboratory line has a slope of -3.1 .

Data points indicate mean values with errors defining the 95% confidence interval for multiple runs.



(a)



(b)

Figure 4.4. Dependence of the ordinate intercept of the recovery curve (Figure 4.3) on maximum power dissipation of the rotating-disc device for (a) yeast-protein and (b) plasma precipitates. Ordinate intercepts of the operating lines passing through each laboratory clarification point (i.e. at each disc speed) in Figure 4.2 were calculated using Equation 4.3 with a constant slope (-1.6 for yeast-protein and -3.1 for plasma).

4.4.4. Scaling on tip velocity

The relative clarifications of the yeast-protein precipitate suspension obtained in various continuous centrifuges are plotted in Figure 4.5a, and measured clarification values are listed in Table 4.2. These indicate that the order of centrifuges (operating normally) in terms of increasing maximum energy dissipation rate is the pilot disc stack, pilot multichamber-bowl and CARR (255 r s^{-1}) and finally the production multichamber-bowl. Good agreement exists between laboratory-predicted and actual pilot-scale values for flooded entrance regions; however, experimental values were significantly lower in the case of the non-flooded multichamber-bowl and CARR (especially when operating at 167 r s^{-1}) centrifuges, but higher for the disc stack. The slight over-prediction of flow intensity, and hence under-prediction of clarification (80% predicted compared to 86% actual), occurring in the disc stack may be due to the precipitate particles in the previous study (Maybury, 1999) being stronger, which could be the result of more debris carry-over (see Table 3.2) and a higher mean velocity gradient in the precipitation reactor (approximately 600 s^{-1} versus 200 s^{-1}).

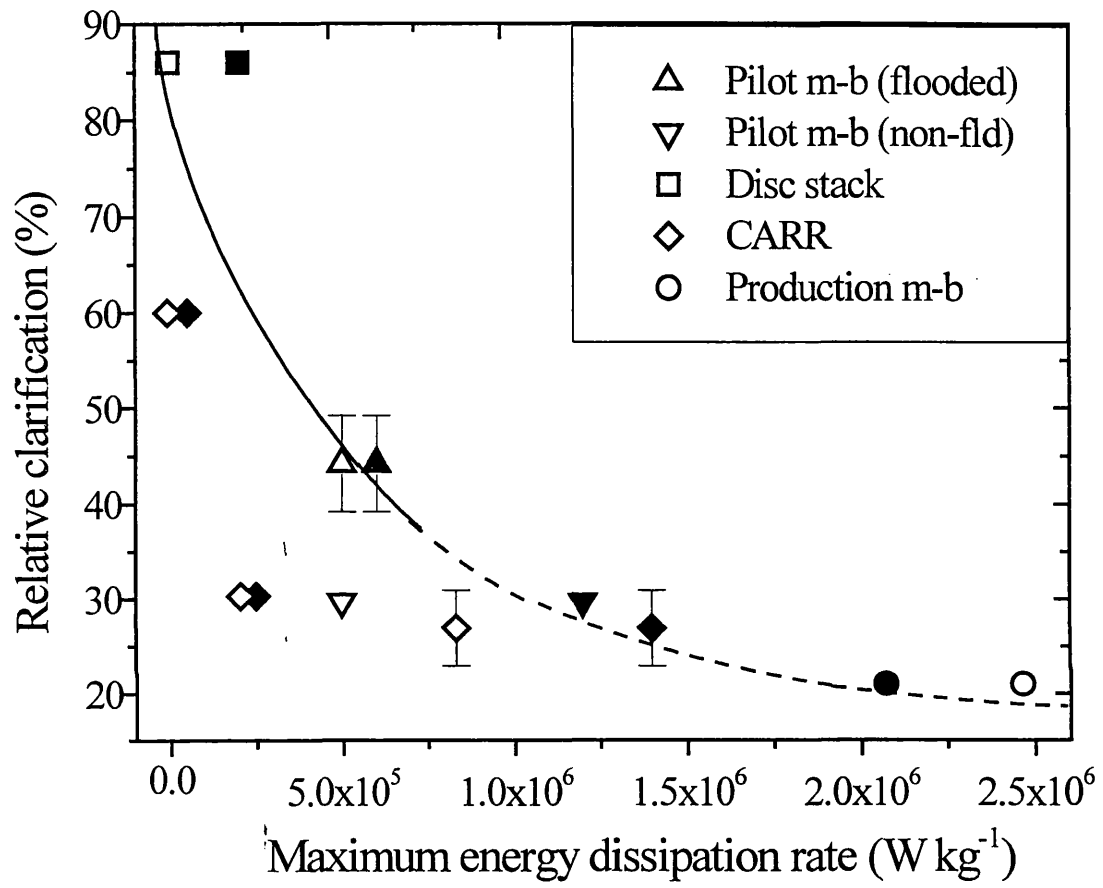
As discussed in Chapter 3, the presence of gas-liquid interfaces generates even greater power dissipations, as confirmed by CFD. The CARR does not have a flooded feed zone but operates under vacuum. When operated at its standard (i.e. maximum) speed of 255 r s^{-1} , the clarification obtained in the CARR lies closer to the laboratory line, but at lower speeds it deviates considerably. The disc stack and lowest-speed (83.3 r s^{-1}) CARR result occur at virtually the same predicted power dissipation but their clarifications differ by about 25%, indicating that the CARR generates much more shear. The above results suggests that tip velocity is generally a good *approximate* ($\pm 15\%$ relative) predictor of particle breakage but more rigorous analyses such as CFD, are needed to acquire an accurate determination of flow intensity.

The above rationale was then extended to manufacturing scale using the plasma suspension. In Figure 4.5b, the relative clarification in the production multichamber-bowl centrifuge was $58 \pm 5 \%$ compared to $87 \pm 8 \%$ in the laboratory disc device operated at its *original* maximum of 462 r s^{-1} (44 m s^{-1}), but constant tip velocity dictates that the disc rotate at approximately 696 r s^{-1} (66 m s^{-1}). Consequently, the device was modified to achieve higher speeds by attaching the disc to a dentist's drill powered by compressed air. Nonetheless, only 542 r s^{-1} (51 m s^{-1}) could be attained (at 12 barg – input compressed air), resulting in a decrease in relative clarification to $76 \pm 9 \%$. Extrapolating the operating line for plasma yields a predicted relative clarification for the production multichamber-bowl of 50%, compared to 58% measured.

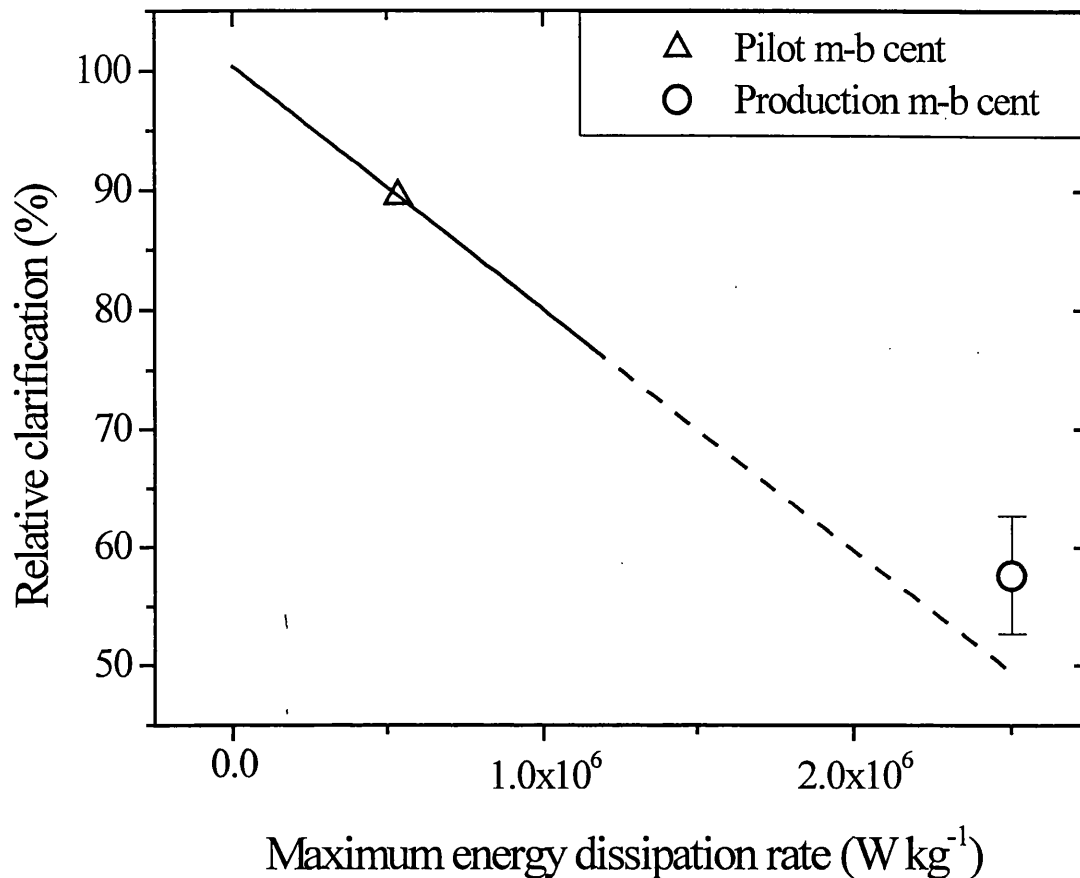
Applying the maximum power dissipation (tip velocity) for the flooded production multichamber-bowl centrifuge to Figure 4.5a, the relative clarification of yeast-protein precipitates is predicted to be only 21%.

4.4.5. Scale-down versus pilot plant trials

Using the maximum power dissipation calculated by tip velocity for the flooded *pilot* multichamber-bowl centrifuge, the relative clarification of the plasma suspension would be 90% compared to only 58% for the production-scale counterpart, as displayed in Figure 4.5b. In other words, using the pilot centrifuge to predict production performance leads to a relative 50% over-estimate, whereas the scale-down process (disc device plus laboratory centrifugation) gives only a 14% under-prediction. This is a critical result because it demonstrates the tremendous value of scale-down experimentation, which can obviate the need for pilot plant trials by generating a more accurate prediction of the performance of a production process.



(a)



(b)

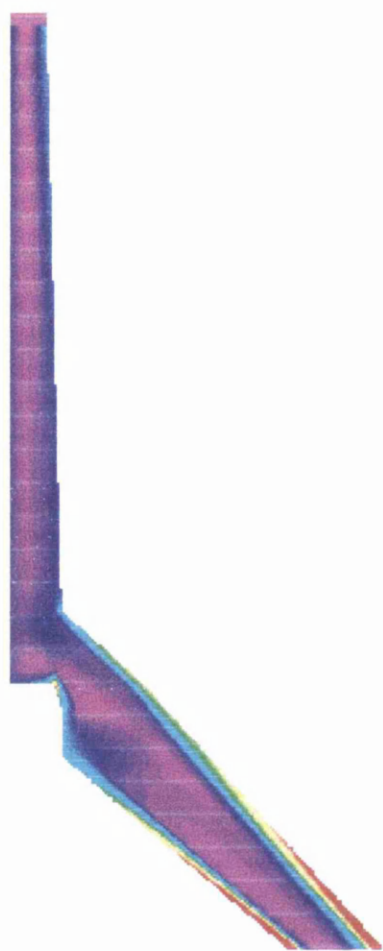
Figure 4.5. Dependence of the relative clarification on maximum energy dissipation rate for (a) yeast-protein precipitates ($V_{lab}/t_{lab}C_{lab}\Sigma_{lab} = 6.3 \times 10^{-9} \text{ m s}^{-1}$) and (b) plasma precipitates ($V_{lab}/t_{lab}C_{lab}\Sigma_{lab} = 14 \times 10^{-9} \text{ m s}^{-1}$). The maximum power dissipation was determined by the tip velocity method (open points) or CFD (solid points). The solid curve represents the fit to laboratory data in Figure 4.2 (disc shear + laboratory centrifuge), its extrapolation indicated by the dashed section. The following continuous centrifuges were investigated: disc stack (■), pilot multichamber-bowl (▲, flooded; ▼, non-flooded), CARR (◆) and production multichamber-bowl (●; maximum energy dissipation rate for closed point was calculated from experimental values in Figure 4.5b, the result is listed in Table 4.2).

4.4.6. CFD versus tip velocity

Figure 4.6 is a CFD image of the entrance regions of a pilot disc stack (a) and CARR (b) centrifuge. The energy dissipation rate is mapped from the lowest values (in blue) to the greatest ones (red). In all cases, the zones of greatest power dissipation are located around the critical structure, i.e. where the feed first contacts the rotating part of the centrifuge. These CFD images confirm that much greater power dissipations occur in the CARR's feed zone ($14 \times 10^5 \text{ W kg}^{-1}$ at $N_c = 255 \text{ r s}^{-1}$) than the disc stack's ($2.0 \times 10^5 \text{ W kg}^{-1}$ at $N_c = 165 \text{ r s}^{-1}$), as also predicted by the tip velocity method. However, the CFD maximum energy dissipation rate in the disc stack centrifuge is approximately an order of magnitude greater than that estimated by the tip velocity method, the latter prediction being the more accurate to the actual value.

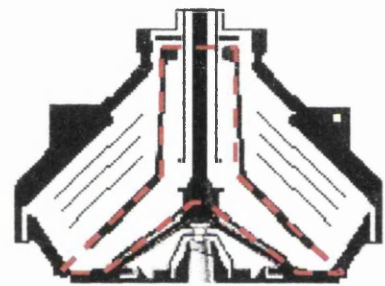
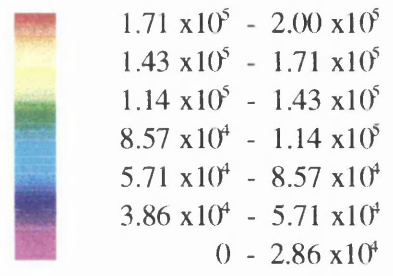
As discussed in Chapter 3, the presence of air-liquid interfaces, due to a failure or an inability to regulate properly the back-pressure on the supernatant line results in a non-flooded feed zone and causes higher energy dissipation rates. From Table 4.2, for the pilot multichamber-bowl running non-flooded, the maximum power dissipation is $12 \times 10^5 \text{ W kg}^{-1}$ (Figure 3.7) compared to $6.0 \times 10^5 \text{ W kg}^{-1}$ (Figure 3.8) for the flooded case. Compared to the CFD values, the tip velocity method also significantly underestimates energy dissipation rates in the CARR.

Referring again to Figure 4.5a, the relative clarifications of continuous centrifuges lie much closer to the scale-down (disc shear + laboratory centrifuge) line when the maximum power dissipation is determined using CFD as opposed to tip velocity, notably for the non-flooded, pilot multichamber-bowl centrifuge. This is due to consideration of two-phase flow in the CFD analysis, which is not the case when using only tip velocity. For reasons discussed in section 4.4.4, the power dissipation estimated by tip velocity agreed better with the experimental value than CFD.

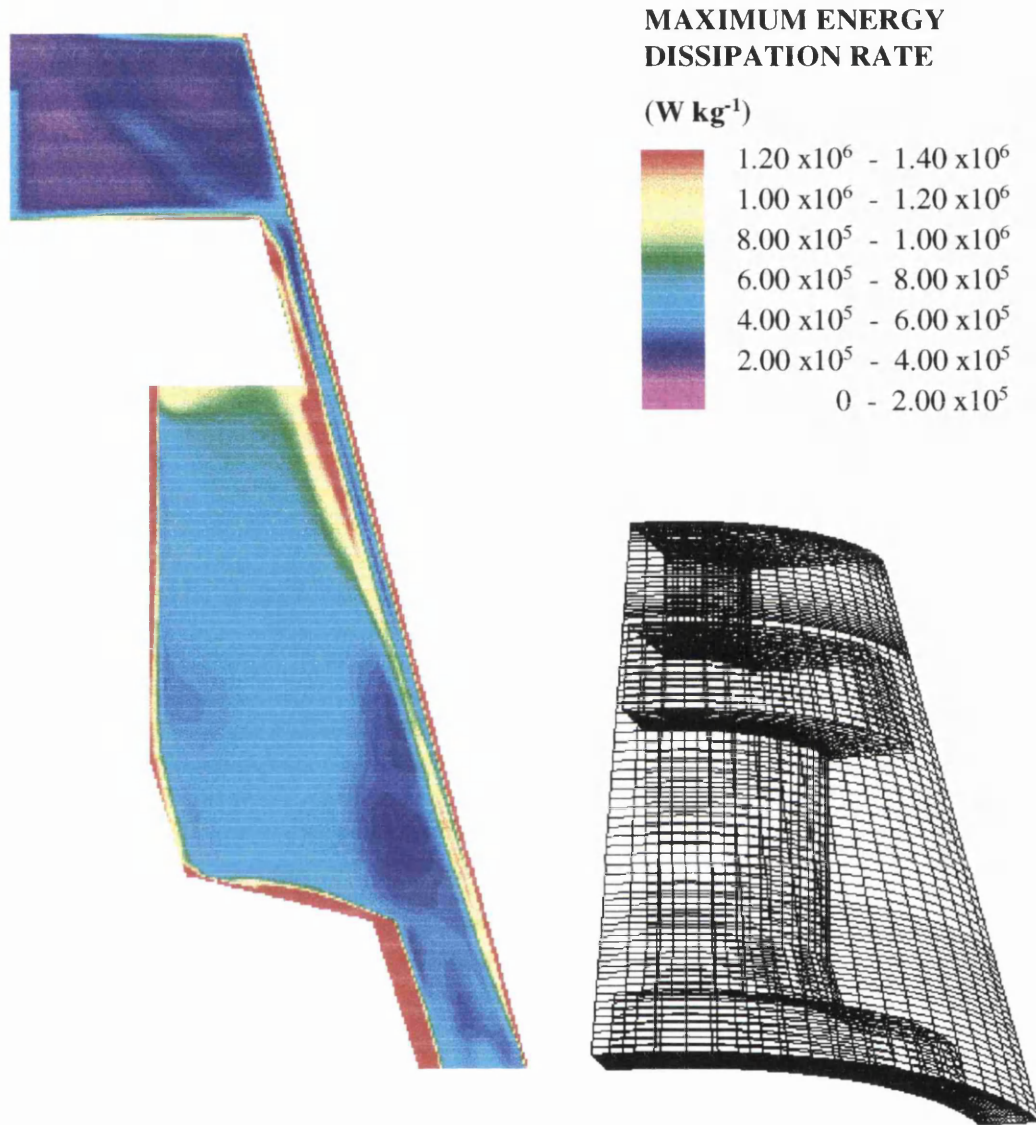


**MAXIMUM ENERGY
DISSIPATION RATE**

(W kg⁻¹)



(a)



(b)

Figure 4.6. CFD analysis of the feed zone of a: (a) pilot disc stack centrifuge, $N_c = 165 \text{ r s}^{-1}$ and $Q = 13 \text{ L h}^{-1}$; and (b) pilot CARR centrifuge, $N_c = 255 \text{ r s}^{-1}$ and $Q = 20 \text{ L h}^{-1}$. Greatest energy dissipation rates are indicated in red, while the lowest ones are in purple. Both centrifuges have non-flooded feed zones.

4.4.7. Maximum centrifugation performance

From a cursory examination of Figure 4.5a, it would appear that the CARR centrifuge has the second poorest performance since it results in very low relative clarifications and thus substantial particle breakage. However, all centrifuges have a *practical* minimum flow rate (or maximum spin time) mainly due to flooding (the feed zone) or cooling requirements. The latter certainly exist in plasma fractionation to prevent product denaturation and re-dissolution of precipitates, hence the minimum flow rate of 200 L h^{-1} through the production multichamber-bowl; 20 L h^{-1} is required through the pilot counterpart to achieve flooded conditions. If solids are over-compacted or get too overheated in a disc stack centrifuge, they can become difficult to discharge. The minimum throughput is a constraint on $Q/C\Sigma$, which can be represented by a vertical line on a graph of clarification against $Q/C\Sigma$ (Figure 4.7). With precipitate break-up, the operating line shifts down and the slope remains constant (Figure 4.3) due to the size distribution maintaining an approximately constant relative width. The point of intersection between the minimum $Q/C\Sigma$ line and the recovery curve defines a maximum clarification possible in the centrifuge.

Figure 4.8 displays the predicted maximum clarifications (based on ε_{max} determined empirically) achievable in each of the centrifuges; operating conditions and clarification values are listed in Table 4.3. Clearly, the laboratory centrifuge has the best performance since it does not shear material. The greater shear-induced particle break-up and higher minimum $Q/C\Sigma$ values serve to reduce the maximum clarification attainable in the continuous centrifuges. The vertical distance between the points and the laboratory line represents the extent of precipitate breakage. Despite its relatively high level of shear, the lowest flow rate through the CARR (255 r s^{-1}) of 2 L h^{-1} allows it to achieve a greater clarification (83%) than that possible in the other large-scale machines.

Nonetheless, it is predicted that the disc stack can attain a very similar maximum clarification (81%) but at a 5-fold greater throughput. The remaining centrifuges in order of maximum clarification performance are the pilot (42%) and the production multichamber-bowl (7.4%).

Table 4.3. Predicted maximum clarification obtainable in the continuous-flow centrifuges based on their minimum throughput, for yeast-protein precipitates. Clarifications were calculated using Equation 4.3 with the $Q_{min}/C\Sigma$ value, a slope of -1.6 and an ordinate intercept determined from Figure 4.4a. Symbols are as per Tables 4.1 and 4.2.

Centrifuge	Q_{min} (L h ⁻¹)	$Q_{min}/C\Sigma$ (10 ⁻⁹ m s ⁻¹)	$Clar_{max}$ (%) using ϵ_{max} from:		
			Tip velocity	CFD	Exp.
Disc stack	10	4.64	77	66	81
Pilot multichamber- bowl - Flooded	20	5.70	43	40	42
	- Non-flooded	10	2.85	62	44
CARR	2	5.54	73	72	56
	2	1.38	88	88	66
	2	5.91	87	81	83
Production multichamber-bowl	200	13.7	6.9	---	7.4

4.4.8. Procedure to predict clarification in a continuous centrifuge

The following procedure is used to predict the clarification (of yeast-protein and plasma precipitates) obtained in a certain continuous centrifuge:

1. Identify critical structure and measure r_{cr} of the continuous centrifuge.
2. Calculate N_{rd} from Equation 4.2.
3. Calculate ϵ_{max-c} using Equation 3.5 and by CFD.
4. From Figure 4.4 and ϵ_{max-c} , determine the ordinate intercept of the recovery.
5. Calculate the predicted clarification at the desired $Q_c/C_c\Sigma_c$ (i.e. the value at which the actual clarification is measured) using Equation 4.3.

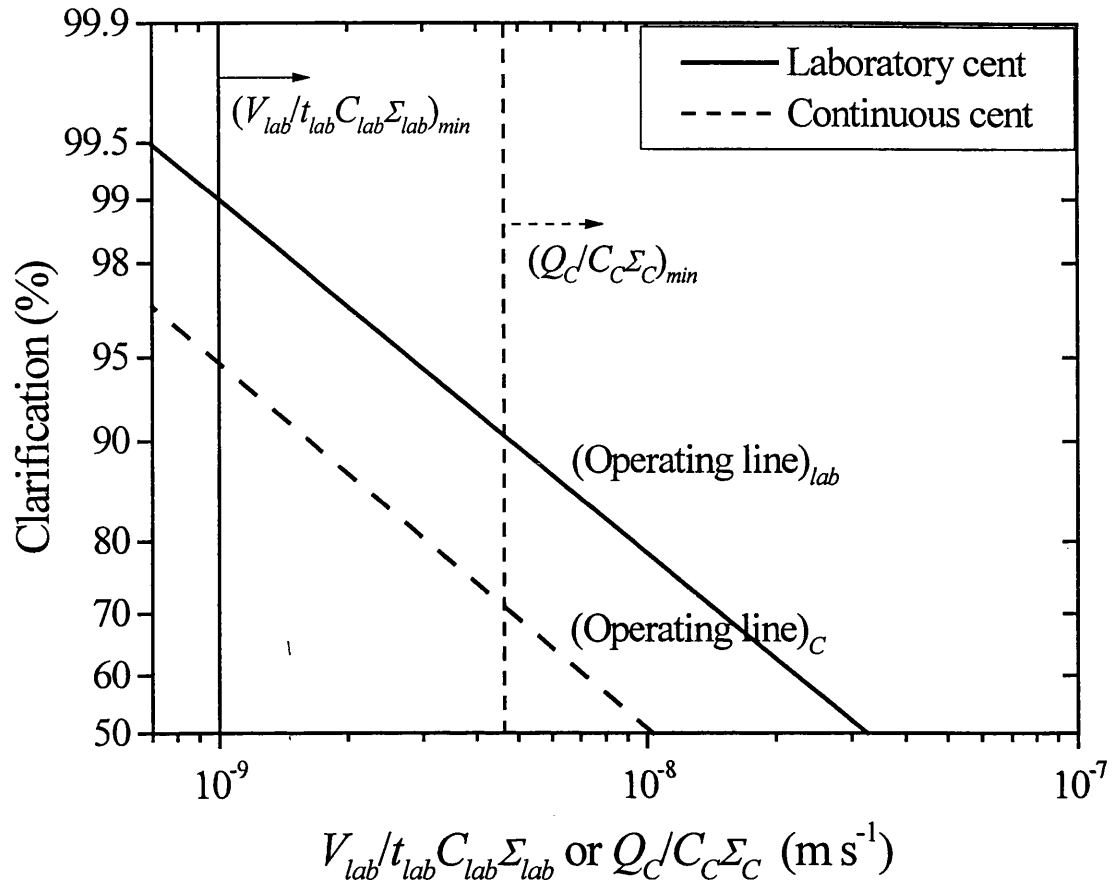


Figure 4.7. Effect of particle break-up and operating conditions on the centrifuge recovery curve. The laboratory operating line (solid, diagonal; non-sheared material) lies above that of the continuous centrifuge (dashed) because of particle break-up in the entrance zone of the latter machine. Furthermore, the continuous centrifuge has a higher minimum $Q_C/C_C \Sigma_C$ (dashed vertical line) than the laboratory centrifuge (solid vertical line), leading to a superior maximum clarification for the latter machine.

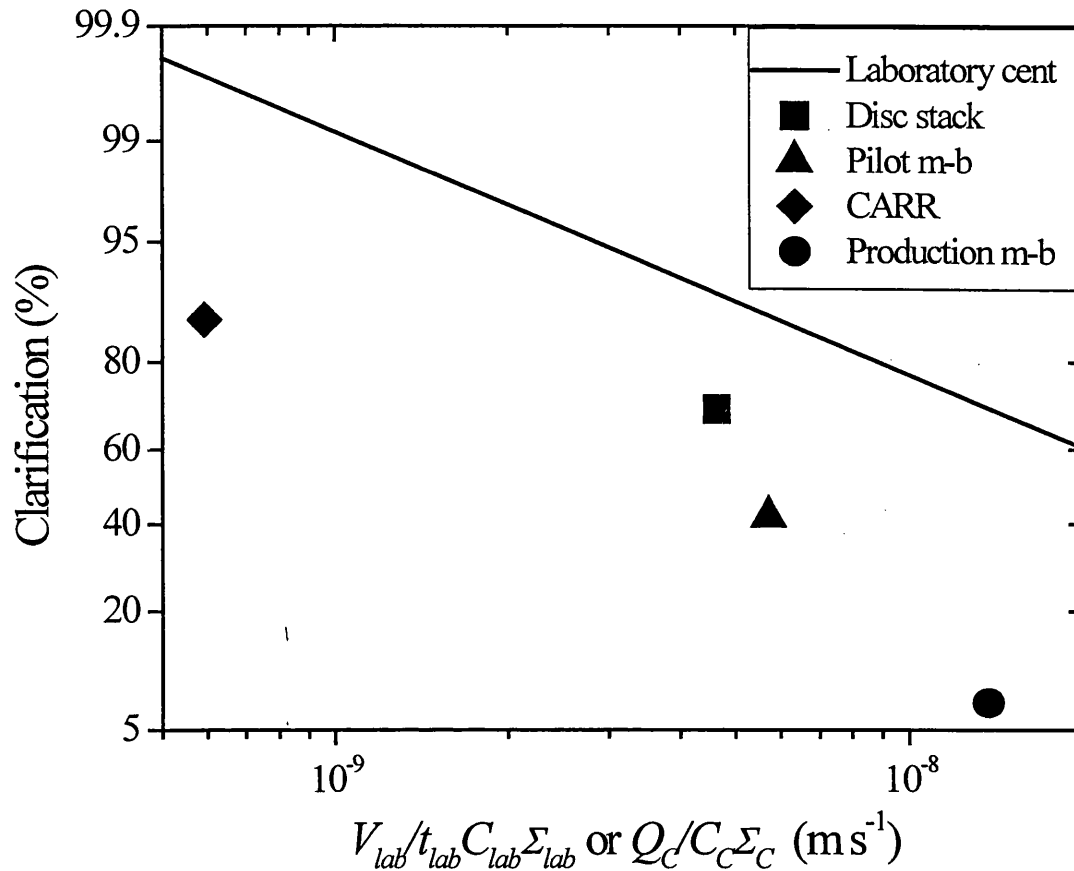


Figure 4.8. The predicted maximum clarification of yeast-protein precipitates achievable in the continuous centrifuges. Symbols are as per Figure 4.5. Maximum clarifications were calculated according the procedure in section 4.4.7, using minimum flow rates listed in Table 4.3 and maximum energy dissipation rates determined experimentally with Figure 4.5. The vertical distance between a point and the laboratory line represents the amount of precipitate break-up occurring in the continuous centrifuge. The very low minimum throughput of the CARR ($2 L h^{-1}$) permits it to achieve superior clarifications to the other continuous centrifuges.

4.5. CONCLUSIONS

Constant tip velocity between the laboratory rotating-disc device and the critical structure in the large-scale centrifuge proved to be a good ($\pm 15\%$) scaling parameter, but CFD is needed for greater accuracy. More disruption was observed in non-flooded entrance regions due to the higher dissipations in the presence of air-liquid interfaces, as confirmed by CFD. The plasma precipitates exhibit considerably less breakage than their yeast-protein counterparts at similar power dissipations. Under standard operating conditions, the following centrifuges generate greater flow forces and hence more particle break-up in ascending order: pilot disc stack, pilot multichamber-bowl, pilot CARR and production multichamber-bowl. Importantly, the performance of the production multichamber-bowl centrifuge was predicted more accurately by the scale-down process than the pilot one.

5. CHAPTER 5: SCALE-DOWN OF CONTINUOUS FILTRATION: **PERFORMANCE ANALYSIS AND COMPARISON TO CENTRIFUGATION**

ABSTRACT

This chapter reports the research into a laboratory mimic of a production-scale rotating vertical pressure-leaf filter (RVLF) by implementing modifications (insert, connection to a diaphragm pump, horizontal placement and rotation) to a laboratory-batch, Nutsche filter. Constant- and step-pressure tests were carried out with the laboratory filter to determine the average specific cake resistance and its dependence on pressure. The compressibility factor was then used to calculate the pressure increase over time required to maintain constant flux, the theoretical curve having an ever-increasing slope. At the same constant pressure, a lower specific cake resistance was observed in the scale-down RVLF than the batch filter. This may be attributed to several reasons: proper mixing in the feed tank, gradual delivery of suspension to the filter and its rotation, all contributed to the formation of a *homogeneous* cake however, the cake was rounded due to impingement of solids, which could be prevented by lower feed flow rates. When operating the continuous filter with a fixed pumping rate, an unexpected flux profile was obtained; the pressure initially built up slowly and increased as predicted, but then levelled off with a concomitant decrease in the flux rate. Filtration performance was found to be superior to the equivalent manufacturing-scale centrifuge in terms of clarity of processed material and dryness of sediment.

5.1. INTRODUCTION

5.1.1. General

Filtration equipment has been developed from practical experience with limited attention paid to theory (Wolthuis and Dichiarla, 1997). This is in part due to the limitations of filtration theory due to complex interactions between the different process parameters; these vary during the filtration process itself on account of the evolving mechanical properties of the cake. Furthermore, the unique nature of many slurries, such as the variability of precipitate properties attributed to fluctuating process or scaling parameters, implies that filtration should be conducted on the actual material if possible.

5.1.2. Scale-Up and Down

The scaling of filtration is traditionally based on the same geometry, applied pressure profile, pore size, and ratio of filtrate volume to surface area. Batch laboratory tests are first performed on a filter of simple geometry to narrow the myriad process options (filter cloth, type of filter aid, precoat, body feed, etc.) using a single pressure. Next, the average flux and the cake resistance are determined as functions of pressure so that the type and size of large-scale filter can be selected. The laboratory data are then used to calculate the pressure profile required for *continuous, constant-rate* operation of the industrial filter. This marks the major difference between laboratory and manufacturing-scale filter; the former is a batch device usually with compressed air as the driving force, whereas material is constantly fed to the latter via a pump. To surmount potential discrepancies between laboratory predictions and industrial performance, it will be necessary to examine at a small scale, features such as cake growth and stability, as well as flux, transmission and dewatering. Results of the scale-down filter will be compared to standard filtration runs and centrifugation.

5.1.3. Filtration performance

As with all other solid/liquid separation operations, filtration performance is assessed by: the mass fraction of the solids recovered, often referred to as the separation efficiency or degree of clarification; and the moisture content in the recovered solids, which is a measure of the liquid separation. Several steps in the entire filtration process contribute to its performance, these being the application of precoat, actual filtration of the slurry, washing, cake dewatering, removal, and cleaning. Clarity of the filtrate is mostly a function of the precoat type, particle size distribution, porosity and thickness. Washing is concerned with removing the soluble material from the liquid remaining in the cake and is conducted in two ways: on the filter itself or re-slurry washing where the cake is re-suspended with clean wash liquor and re-filtered, the latter method being considerably more expensive. Deliquoring or dewatering refers to purging the major proportion of the liquid from the cake pores by blowing large volumes of air at high pressure; very long periods of blowing after breakthrough may result in the removal of entrapped liquid by a drying mechanism. Effective cake dewatering and washing are essential to avoid low yields in processes involving multiple separation stages such as plasma fractionation (Pineiro and Cabral, 1993).

At the production scale a very important parameter is the rate of filtration (i.e. the volume of filtrate collected per unit time) since this impacts on processing time and costs. But an emphasis upon a high initial rate of filtration may prove detrimental to performance if the sludge is non-homogeneous. If the starting pressure is high, this will force colloidal particles into interstices of the granular portions of the filter cloth, essentially plugging it and decreasing the rate of filtration. Even if the feed contains only large crystalline solids, these will be compacted into a tight mass that fills the surface pores of the cloth, thus narrowing flow channels. It is advisable to slowly ramp up the

pressure so that the filter cake can develop a more open structure. This results in a higher overall filtration rate and easier removal of the cake from the filter medium. However, in filters with large cross-sectional areas it is more difficult to obtain a perfectly uniform cake structure due to regional pressure fluctuations caused by an uneven flow distribution (i.e. turbulent eddies). Therefore, when scaling-down it may be necessary to increase the pressure more rapidly than normal in order to mimic the poorer performance of the large-scale filtration device.

5.1.4. Types of filters

Types of filters used in the isolation of protein precipitates are the Nutsche, candle, plate and frame, tubular, leaf filters and microfiltration systems; this paper focuses only on conventional ones. A Nutsche (Figure 5.1) is a simple batch filter composed of a vessel with a false bottom, perforated, which may support a filter medium or acts as filter medium. The slurry is fed into the tank and then the solid-liquid separation takes place as a result of gravitational forces, pressure, vacuum or a combination of these forces (Rushton *et al.*, 1996). Operation is generally at constant pressure such that the flux decreases with time due to cake build-up.

Leaf filters are constructed with horizontal or vertical leaves in a vertical or horizontal vessel. Horizontal leaves are used in intermittent operations as a polishing filter where solids loading is low since solids can only accumulate on the upper leaf faces (used when cake adherence to the filter cloth is poor). Vertical leaves are designed for ease of cake removal and when solids fraction is higher since particles may accumulate on two surfaces. Pressure-leaf filters are generally considered to be cleaner and more reliable than other pressure filters, however, careful attention must be paid to filter cake properties (Rushton *et al.*, 1996). In the case of a vertical leaf displayed in Figure 5.2, the stability of the cake on the filter element is crucial because a loss of pressure during the

filter cycle could result in some of the cake falling away from the element. Furthermore, competition occurs between gravitational and stabilising forces caused by fluid flow and friction, and any change in fluid velocity through the cake may create local areas of instability. To promote fluid flow and thus uniform cake formation, most circular leaf units with vertical elements are rotated slowly (3 rpm). Bridging between leaves must be avoided by considering plate spacing relative to the volume of cake filtered per batch. Bridging can lead to mechanical damage to the end leaves due to excessive pressure.

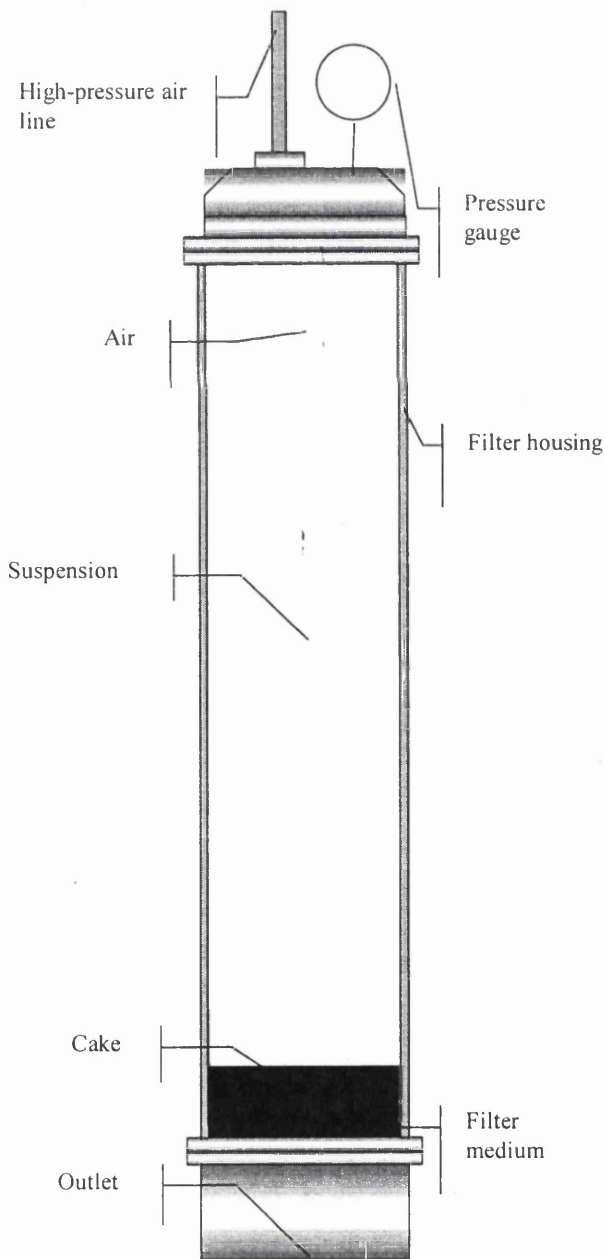


Figure 5.1. A standard laboratory, batch Nutsche filter driven by pressure.

5.1.5. Filtration in plasma fractionation

Filtration has recently gained a more active role in solid-liquid separations during human plasma fractionation (More and Harvey, 1991). The basic process involves a series of cold-ethanol precipitations (each one followed by a separation step) to exploit differences in solubility of the various blood proteins, mainly albumin, immunoglobulins and clotting factors. Hao (1985) carried out a pilot plant scale preparation of human serum albumin (HSA) and concluded that depth filtration was superior to centrifugation in terms of time and labour savings, though a small percentage of albumin was not recoverable due to entrapment in the filter bed. This problem is exacerbated by filter-aids despite their ability to significantly improve rates of filtration. Friedli *et al.* (1976) claimed that the adsorptive capacity of diatomaceous earth caused unacceptably low recoveries in purer fractions, but others suggested that in-situ washing sufficiently alleviates this problem (More and Harvey, 1991). De Jonge *et al.* (1995) concluded that filtration has the following advantages over centrifugation: relative ease of recovery of mother liquor from the solid; faster rate of separation and thus a high capacity per unit of floor space; improved compliance with current GMP requirements (e.g. clean-in-place); easy maintenance; less noise disturbance; and reduced energy costs.

Suspensions with a more uniform particle size display improved filtration characteristics. De Jonge *et al.* (1995) investigated ways of tightening precipitate distributions by avoiding localised supersaturated areas of reagent, which favour the formation of large numbers of nuclei instead of orthokinetic growth, and avoiding excessively vigorous mixing leading to shear break-up of particles. They were successful in reducing the amount of filter aid required for most fractions by decreasing the rate of ethanol addition, adding the precipitant in the fluid just above the tip of the mixer and generating only a mildly turbulent flow regime. Filtration properties of Fraction IV

could not be bettered by the above methods, most probably due to the fine particle size. Darcy's law (see Equation 5.1) was found to be valid for suspension containing more than 1% v/v filter aid.

Some work has also focused on cross-flow systems for solid-liquid separations. Grandgeorge *et al.* (1989) developed a full-scale automated MF system with an area of 72 m² capable of handling 32 000 L of precipitate mixtures per day, thus replacing nine centrifuges. This method has not yet been adopted by the plasma fractionation industry due to concerns about the more limited solids-handling capacity than conventional methods (More and Harvey, 1991).

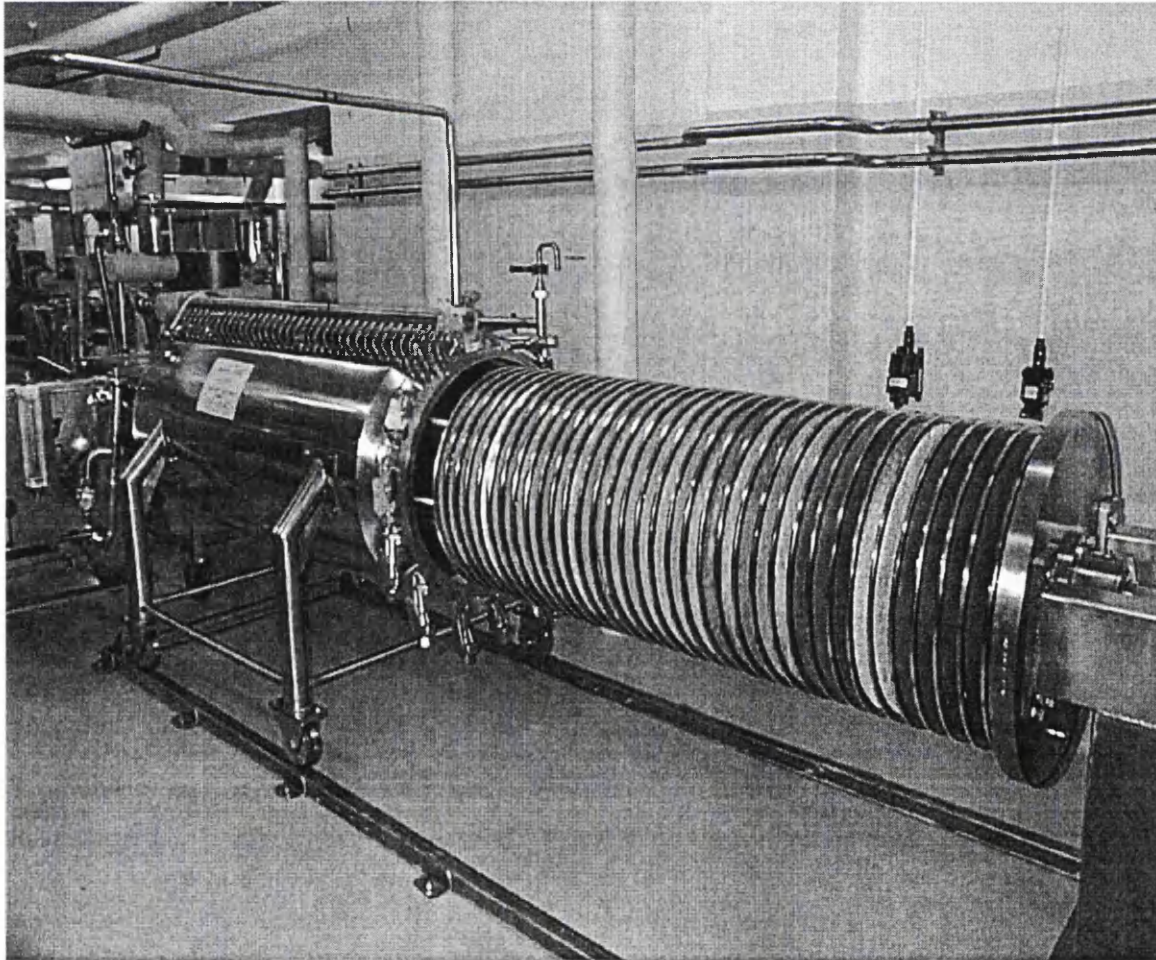


Figure 5.2. Photograph of an LFC Rotojet rotating vertical leaf filter (LFC Lochem, The Netherlands; filtration area of 24 m²).

5.2. THEORETICAL CONSIDERATIONS

5.2.1. Permeability

Darcy discovered that the pressure loss ΔP , of a fluid passing through a porous bed of solid spheres, is directly proportional to the flow rate dV/dt :

$$\frac{\Delta P}{L} = \frac{\mu}{kA} \frac{dV}{dt} \quad (5.1)$$

where L is the depth of the bed of solids, μ is the liquid viscosity, k is the bed permeability, V is the volume of fluid flowing in time t . Darcy's law assumes that the pressure loss is only due to friction between the solid and liquid (i.e. skin friction or form drag) under streamline flow conditions (Rushton *et al.*, 1996).

Filtration is basically an empirical exercise due to the inability to calculate accurately cake permeability, particularly for complex mixtures. Kozeny derived the best known equation for permeability:

$$k = \frac{\varepsilon^3}{K(1-\varepsilon)^2 S_v^2} \quad (5.2)$$

where ε is the porosity of the bed of solid particles, S_v is the surface area per unit volume of the particles and K is the Kozeny constant. Substituting Equation 5.2 into Darcy's law gives the Kozeny-Carman equation:

$$\frac{\Delta P}{L} = \frac{\mu}{A} \left(\frac{K(1-\varepsilon)^2 S_v^2}{\varepsilon^3} \right) \frac{dV}{dt} \quad (5.3)$$

The Kozeny-Carman expression is used extensively, but is only valid for rigid particles in a fixed geometry and in point contact with each other; only liquid drag and pressure (predominant forces for particles larger than 10 μm) are considered. The equation is a function of porosity, particle size, shape, distribution and packing, rate of cake formation,

concentration of the slurry, etc. (Rushton *et al.*, 1996). With all of these variables, it is easier to deduce an empirical permeability from laboratory tests.

5.2.2. Constant-pressure filtration

Filtration can be operated in three different modes: constant-pressure filtration; constant-rate filtration; and variable-pressure, variable-rate filtration. For constant-pressure filtration, the linearised parabolic rate law is often used:

$$\frac{t}{V} = \frac{\mu c \alpha_{av}}{2A^2 \Delta P} V + \frac{\mu R_m}{A \Delta P} \quad (5.4)$$

where t is the time, V is the volume of filtrate collected, A is the filter area, c is the mass of dry solids deposited per unit volume of filtrate, α_{av} is the average specific cake resistance, and R_m is the medium resistance. The total pressure differential is defined as that over the cake (ΔP_c) and the medium (ΔP_m). A *specific* resistance is used because the cake resistance R_c , will rise with cake depth L_c , because $R_c = L_c/k_c$. The mass of dry solids is determined from the following equation:

$$c = \frac{s\rho}{1-sm} \quad (5.5)$$

where s is the mass fraction of solids in the feed, ρ is the liquid density and m is the ratio of wet cake to dry. Assuming m to be unity often results in considerable error (Holdich *et al.*, 1993).

Some modifications are made to Equation 5.4 when using a filter aid for difficult clarifications: R_m becomes the resistance of both the medium and the precoat; α_{av} is the combined specific resistance of the filter aid body feed and solids intrinsic to the suspension; c includes not only the dry solids mass of the original suspension, but also the body feed dosage. In practice, it is the mass of filtrate M , which is recorded so that M/ρ

replaces V . The medium resistance is usually negligible compared to that of the cake, so Equation 5.4 becomes:

$$\frac{t}{M} = \frac{\mu c \alpha_{av}}{2A^2 \Delta P} M \quad (5.6)$$

Plotting t/M against M theoretically yields a straight line; the cake resistance can be determined from the slope ($\mu c \alpha_{av}/2A^2 \Delta P$); in practice however, deviations from linearity occur. When filtering a *uniform* suspension under constant pressure, a filter cake of approximately *constant concentration* results; hence, the concept of specific resistance. Nevertheless, the filtration of mixtures containing particles of considerably different properties (e.g. filter aid consists of large, porous particles unlike the much smaller precipitates) means the larger ones will settle radically faster than the smaller ones. The slurry concentration can be maintained uniform if adequate mixing is provided, but this is not usually the case in laboratory, batch filtration vessels such as the Nutsche; the feed slurry is mixed with filter aid, decanted into the chamber, the latter is sealed and pressured applied. This leads to the formation of a cake whose composition varies from bottom to top, as observed by a changing (usually increasing) resistance during the filtration, i.e. a non-linear plot of t/M vs. M . Therefore, an *average* cake concentration and specific resistance is defined (Rushton *et al.*, 1996).

Several forms of the parabolic rate equation (5.4) exist. Plotting instantaneous rate of filtration against volume also produces a line, but this requires graphical differentiation (i.e. taking tangents) of the filtration volume-time curve, which is difficult to perform accurately. Another form of the law involves plotting $(t-t_1)/(M-M_1)$ against M , where t_1 and M_1 are some arbitrary datum values; this is especially useful when analysing filtration data in which step changes in pressure were introduced (Rushton *et al.*, 1996).

Constant pressure filtration is generally applied in the case of compressible cakes at laboratory scale to determine the dependence of specific resistance on pressure over the cake. The usual empirical relation between these two variables is:

$$\alpha_{av} = \alpha_o (1 - n) (\Delta P)^n \quad (5.7)$$

where α_o is a constant determined largely by the size and morphology of the particles in the cake, and n is the cake compressibility coefficient. Plotting α_{av} vs. ΔP on logarithmic axes linearises the above equation, the compressibility is given by the slope.

5.2.3. Constant-rate filtration

As opposed to laboratory experiments normally conducted at constant pressure, constant rate filtration is utilised for large-scale processes. Knowledge of the compressibility allows calculation of the pressure increase over time needed to maintain flow:

$$\Delta P = \mu c \alpha_{av} (1 - n) \Delta P_c^n \left(\frac{Q}{A} \right)^2 t + \mu R_m \left(\frac{Q}{A} \right) \quad (5.8)$$

The expression is simplified in the case of an incompressible (i.e. $n = 0$) cake. R_m can be subject to substantial variation and is often negligible compared to the cake resistance so that Equation 5.8 reduces to:

$$\Delta P = \left(\mu c \alpha_{av} (1 - n) \left(\frac{Q}{A} \right)^2 t \right)^{1/(1-n)} \quad (5.9)$$

In reality, it is extremely difficult to maintain the flux entirely constant; there is always some delay between sensors detecting a decrease in flow rate and delivery pressure by the feed pump (usually a centrifugal or diaphragm pump). This occurs as a consequence of increasing total resistance to filtration due to the increase in cake depth. The instantaneous flow rate can be substituted into Darcy's law to give:

$$\frac{\Delta P}{q} = \left(\frac{\mu w}{A^2} \right) V + \left(\frac{\mu R_m}{A} \right) \quad (5.10)$$

where both the pressure and flow rate are independent variables, and w is the instantaneous mass of cake deposited per unit area. Oja and Nystrom (1995) developed a method for the evaluation of filtration tests during which the pressure is gradually increased. To calculate accurately the specific resistance at each pressure, the instantaneous flow rate and pressure must be known, from which the total resistance (left hand term of above equation) and mass of cake deposited can be determined. This rests upon the ability to collect the filtrate without a time delay, otherwise the uncertainty of synchronous measurement of the filtrate volume and pressure disturbs the calculation of the compressibility coefficient. The mass of cake deposited per unit area can be expressed as:

$$w = \frac{cV}{A} + sV_o v_s t \quad (5.11)$$

where V_o is the volume of the original suspension and v_s is the settling velocity of the feed slurry. The latter is difficult to measure accurately, as a wide distribution of particles within a suspension generally exists.

A true description of the filtration process involving a compressible cake requires a mathematical investigation reflecting the mechanical properties of the filter cake, but this is beyond the scope of this work.

5.3. MATERIAL AND METHODS

5.3.1. Chemicals

All chemicals, unless specified otherwise, were obtained from Sigma Chemical Co. Ltd. (Dorset, UK) and were of analytical grade.

5.3.2. Description of equipment

Separation of the feed suspension was achieved in two ways. One method, centrifugation, involved use of a Sorvall RC-5B Refrigerated Superspeed centrifuge with HS-4 swing-out rotor and 00480 inserts (Dupont Instruments, USA) at the laboratory scale and a Westfalia BKB 45 Multichamber-bowl (Westfalia Separator AG, Oelde, Germany). Dimensions and operating conditions of centrifuges are provided in Table 4.2. The other involved filtration with a stainless steel Fundabac Nutsche (Dr Muller AG, Switzerland) of 35.5 mm internal diameter (i.e. active area of 10^{-3} m^2) with Celpure 1000 filter aid (Advanced Mineral Corporation, CA, USA) supported on a GF/B glass microfibre filter cloth (Whatman International Ltd, Maidston, UK). The filter was operated in batch mode with compressed air as the driving force, or in the continuous mode by means of a NF1.30KNDCG Micro-Diaphragm Liquid Pump (KNF Neuberger, Inc., Switzerland). The filtrate was collected in a beaker (with funnel to prevent evaporation of ethanol) placed on a balance connected to a computer with the software program recording the filtrate mass every 5 s.

5.3.3. Preparation of feed suspension

The feed suspension was Fraction IV (F:IV; 3-5% w/v protein, 40% v/v ethanol, pH 5.85, -5°C) of the Cohn fractionation process; this suspension was selected due to its small particle size (mean diameter of approximately $1 \mu\text{m}$), which presents a substantial separation challenge. 1 L of F:IV was obtained from Bio Products Laboratory's (BPL)

Production Department from standard manufacturing batches (~ 5000 L at the F:IV stage), placed in a cooled (-5°C) stirred-tank and agitated at 5 r s^{-1} .

5.3.4. Filtration

The Nutsche filter was operated in two modes. First, it was used as a standard, laboratory batch filter in which flow is driven by compressed air. The second involved modifying it into a continuous, scaled-down RVLFF, as described below.

5.3.4.1. Laboratory batch

Celpure 1000 (0.5 g) was suspended in 100 mL of RO water, mixed vigorously and poured into the filter housing to give a precoat of 0.5 kg m^{-2} which was formed under 1.0 barg of pressure. The pressure was maintained for 30 s after the entire buffer had been filtered. For body feed, Celpure (1.5 g) was then added to 98.5 g of F:IV (concentration of 15 g L^{-1}), well mixed and dispensed on top of the precoat. Both constant and ramping pressure experiments were performed to determine the cake resistance over the range of 0.5-4.0 barg, as described by Holdich *et al.* (1993). In the ramping mode, the pressure was incremented by a set amount after every 20 mL of filtrate to give the following profiles: 0.5-1.0-2.0-4.0, 0.5-1.5-2.5-3.5 and 1.0-2.0-3.0-4.0 barg. The filtrate was collected in a flask (no cooling) placed on a balance. In all experiments, the final pressure was maintained until the same mass was observed three times consecutively.

5.3.4.2. Scale-down (continuous) RVLFF

The goal was to create a laboratory mimic of the production-scale RVLFF shown in Figure 5.2. A major difference between it and a laboratory filter is that the latter is a batch device, whereas the RVLFF is fed with suspension via a pump. A plunger insert permitted the continuous flow of suspension into the Nutsche when connected to the diaphragm pump, yielding the scale-down RVLFF as shown in Figure 5.3. The entire assembly is displayed in Figure 5.4. The concentric shape and double O-ring

configuration prevents any leakage of liquid (seal is maintained up to 4.0 barg) between it and inside of the filter housing. Since the spacing between leaves on the RVLFF is 30 mm, the insert should be set at a height of 15 mm inside the Nutsche. The industrial filter is a *vertical* leaf type meaning that the Nutsche should be turned on its side to a horizontal position (i.e. the filter surface is then in a vertical position). The scale-down filter must also be rotated to mimic the motion of the RVLFF. This was accomplished by mounting the Nutsche on a bearing and connecting it to motor, rotation made possible with the use of quick-connect couplings. The pressure head exerted by the pump was monitored with a P200 XH Manometer (Digitron, UK) and the pumping rate controlled by a GPR-3060D Laboratory DC Power Supply (0 to 24 V; Good Will Instrument Co., Ltd., Malaysia). For all runs with the scale-down RVLFF, the pre-coat was applied at a pump setting of 3.5 V (approximately 0.5 r s^{-1}). The time, mass of filtrate and pressure were recorded manually for all scale-down RVLFF runs.

The filtration unit was operated in two ways. In the first method, the pumping rate was maintained constant, and the rise in pressure and decrease in volumetric flow rate monitored. In the other mode, the pumping rate was decreased accordingly to maintain constant pressure.

5.3.5. Centrifugation

Dimensions of the centrifuges used in this study are detailed in Table 4.2.

5.3.5.1. Laboratory

Precipitate suspension, 20 mL, was placed in 20 mL graduated, clear tubes (described in section 3.3.3). The tubes were centrifuged under specific conditions for purposes of reference ($N_{lab} = 113 \text{ r s}^{-1}$, $t_{lab} = 2 \text{ h}$, $\Sigma_{lab} = 1.59 \text{ m}^2$, $V_{lab}/t_{lab}C_{lab}\Sigma_{lab} = 1.7 \times 10^{-9} \text{ m s}^{-1}$) and scale-down ($t_{lab} = 0.25 \text{ h}$, $V_{lab}/t_{lab}C_{lab}\Sigma_{lab} = 15 \times 10^{-9} \text{ m s}^{-1}$), after which the

supernatant was removed slowly using a 5 mL pipette down to the sediment-liquid boundary.

5.3.5.2. Production

At production scale, the suspension was fed continuously to the multichamber ($Q_{mc} = 200 \text{ L h}^{-1}$, $N = 90.8 \text{ r s}^{-1}$, $\Sigma_{mc} = 5080 \text{ m}^2$, $C_{mc} = 0.80$, $Q_{mc}/C_{mc}\Sigma_{mc} = 14 \times 10^{-9} \text{ m s}^{-1}$) for a period of approximately 8 h.

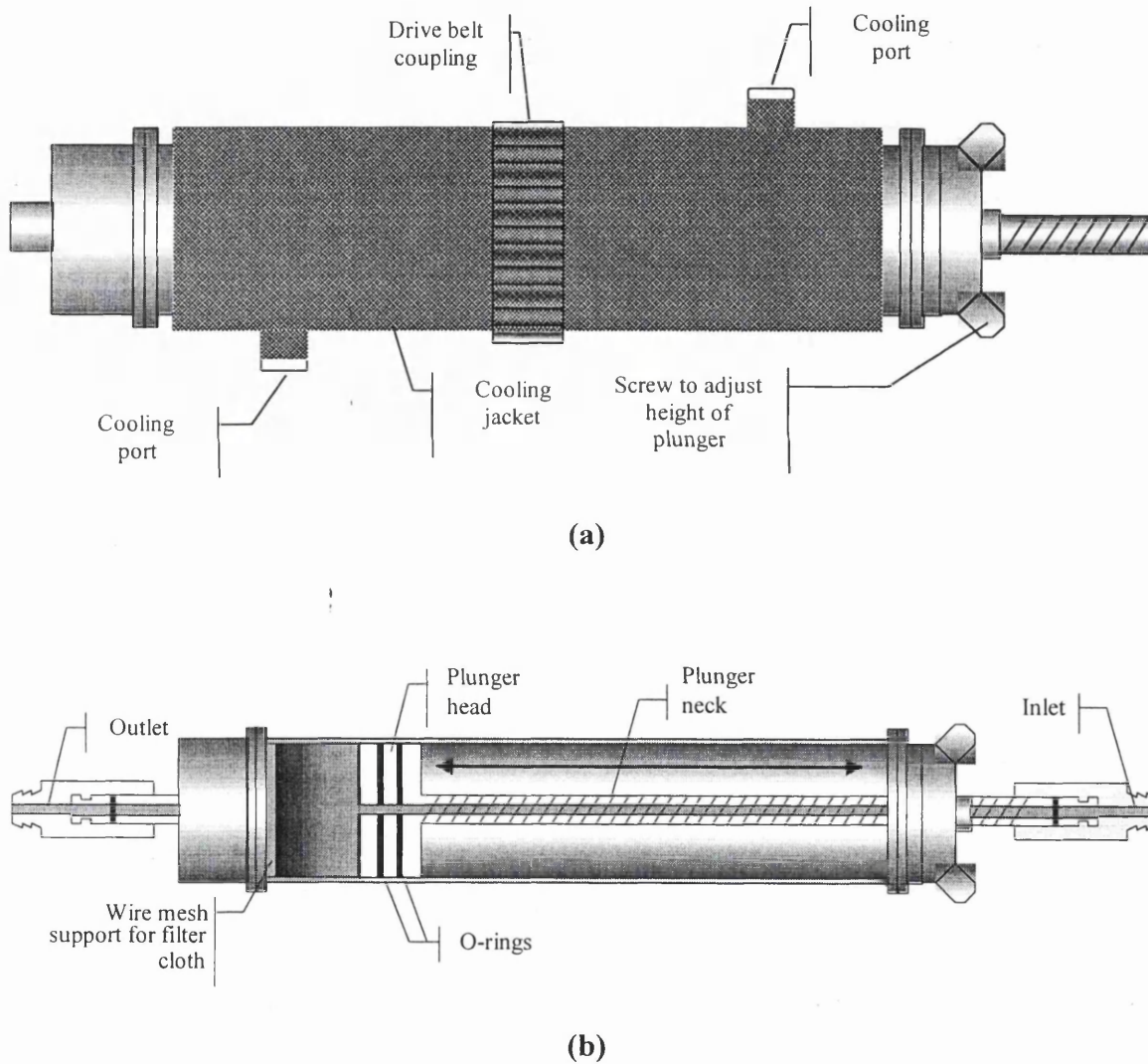


Figure 5.3. Schematic of the scaled-down rotating vertical leaf filter: (a) view of filter's outside and (b) its cross section. The scale-down RVLf (rotating vertical leaf filter) consists of a laboratory Nutsche placed horizontally, with a piston insert so as to adjust chamber volume (i.e. distance between the filter cloth and the chamber inlet).

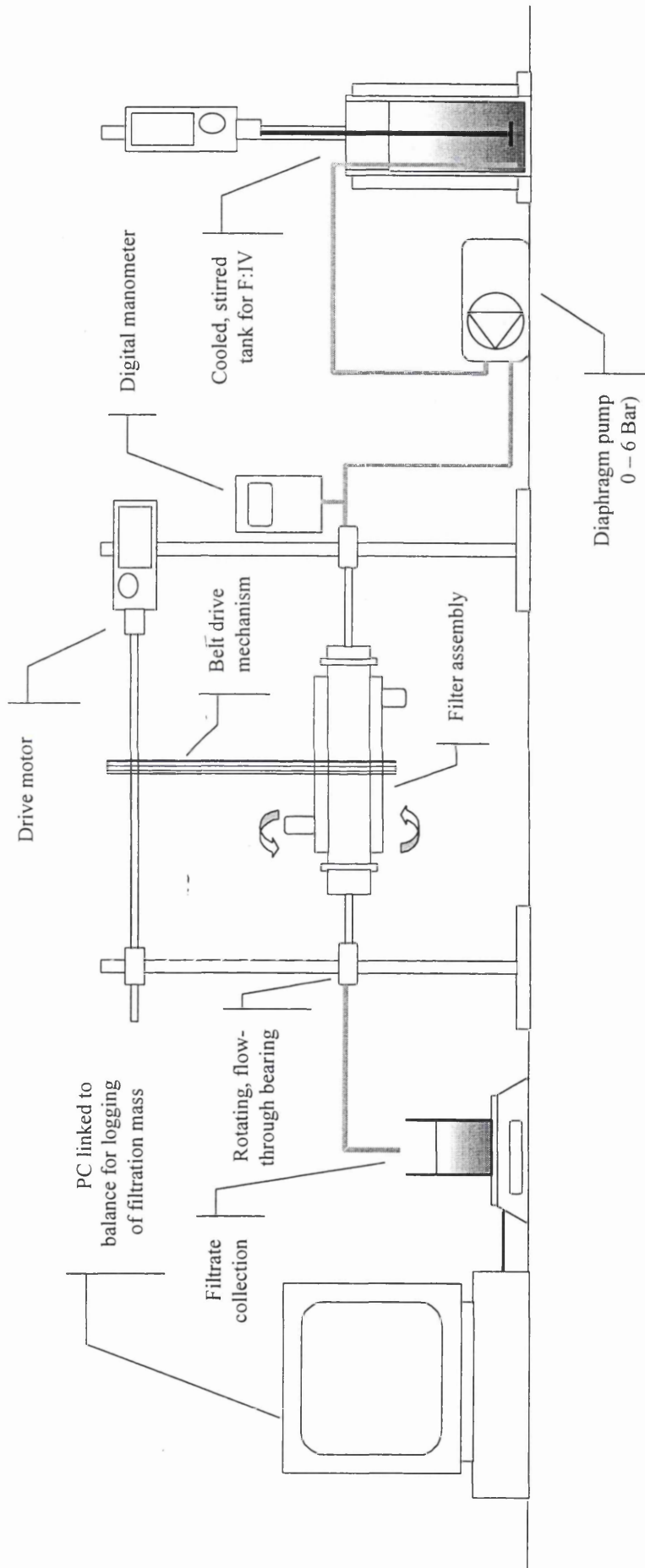


Figure 5.4. Illustration of the scale-down RVLf experimental apparatus. The filter assembly is rotated by means of a belt-drive mechanism and motor, and a universal coupling attached to the inlet and outlet of the housing. Suspension is fed to the filter via a diaphragm pump.

5.3.6. Analyses

5.3.6.1. Turbidity

The turbidity of each stream was measured in a Digital Direct-Reading Turbidity Meter (Orbeco-Hellige, UK).

5.3.6.2. Moisture content

The dryness of filter cakes was measured with a HG53 Halogen Moisture Analyser (Mettler Toledo, Switzerland) set to 175°C and a sensitivity level of 3 until a constant mass was achieved. The percent moisture of centrifuge sediments was determined by weighing the tubes before and after drying in an oven at 106°C for 24 h.

5.3.6.3. Physical properties

The dynamic viscosity of the liquid was estimated to be 6.5 mPa s (Weast, 1978) and the density was measured as 967 kg m⁻³ with a specific gravity bottle.

5.4. RESULTS AND DISCUSSION

5.4.1. Vacuum filtration

One of the initial things to consider when clarifying a suspension is the design of the filtration equipment. Perhaps the most common laboratory filter is the vacuum-leaf filter; it consists of a filter placed in a horizontal support, which rests upon a sealed collection flask connected to an air pump to create suction. Despite its widespread use for many solid-liquid separations, vacuum filtration is generally not used with organic solvents such as ethanol due to their volatility and high flammability. An attempt was made to vacuum-filter F:IV suspension, which is 40% ethanol, but the filtrate measurements were erroneous due to considerable evaporation. Therefore, all future experiments were conducted with the pressure-Nutsche filter, designated henceforth as the laboratory filter.

5.4.2. Effect of precoat

Another consideration when specifying filtration conditions is the filter medium. Initial filtration runs were conducted at 1.0 barg with no filter aid (precoat or body feed) resulting in an average approximate clarification of 96% but a high specific cake resistance of $1.9 \times 10^{13} \text{ m kg}^{-1}$. An even higher resistance ($6.6 \times 10^{13} \text{ m kg}^{-1}$) was observed at 4.0 barg, the higher pressure most likely driving finer particles into the filter thus increasing its resistance. For purposes of clarification, a precoat of 0.5 kg m^{-2} (Celpure 1000) on top of the filter cloth was then used; the clarification improved to at least 99% and the resistance decreased to $1.2 \times 10^{13} \text{ m kg}^{-1}$. The most important fact in each of the above experiments was that the filtration did not completely finish such that most of the liquid (>70%) was still trapped above the filter even after 1 h. Therefore, the addition of filter aid to the suspension was then investigated.

5.4.3. Effect of body feed

The precoat mainly determines the quality of the filtrate, whereas the body feed concentration affects the rate of filtration. Experiments were carried out with different body feed concentrations at 1.0 barg. The ideal concentration must satisfy a couple criteria. First, the minimum average flux is $140 \text{ kg m}^{-2} \text{ h}^{-1}$ (discussed later in Section 5.4.6). Second, the solids capacity of the RVLf (360 L) must not be exceeded. A body feed concentration of 15 g L^{-1} was selected because it satisfied these criteria; lower concentrations resulted in unacceptably low fluxes while higher ones would have caused bridging. Once a fraction has been collected from manufacturing, it is best to ascertain data on the material within a limited time because its properties may not remain stable for extended periods. Figure 5.5 shows a linear relationship between average flux and the range of pressures investigated. A low relative error ($\pm 6\%$) between filtration runs for identical conditions (i.e. same batch and filtration conditions) indicates good reproducibility; however, some batch-to-batch variability was observed as evidenced by the large 95% confidence interval for the fluxes at 2.5 and 3.0 barg. It was also observed that the cake height varied from 7.5 mm when using 0.5 barg, down to 6.0 mm at 4.0 barg, a 20% decrease in cake volume. This has serious implications for the solids capacity of the RVLf. The latter parameter is critical to efficiency since it is desirable to feed as much suspension as possible to the filter so as to attain its maximum solids loading. Obviously significant gains in filter capacity can be realised by using higher pressures, but extreme care must be taken not to exceed the capacity as this can lead to bridging of the cake across leaves, which can cause structural damage to the end leaves of the filter.

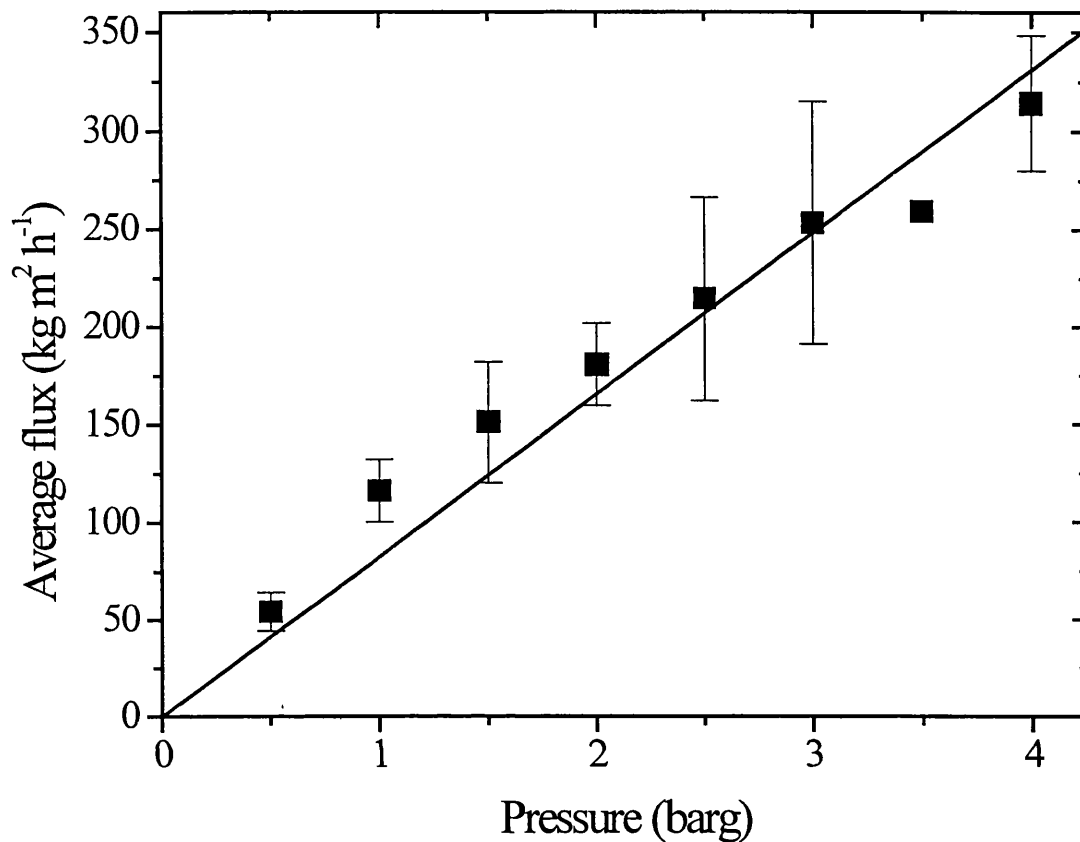


Figure 5.5. The dependence of average flux on pressure in the batch filter for F:IV, plasma precipitate suspension (precoat of 0.5 kg m^{-2} and body feed of 1.5 kg m^{-3} using Celpure 1000, pH 5.8, -5°C). Runs were conducted at constant pressure, which was applied until three consecutive and identical filtrate readings were recorded. The line of best fit was determined using linear regression with the origin as a fixed point. Error bars indicate 95% confidence interval for multiple runs (≥ 3). The average flux for step-pressure experiments of 0.5-1.0-2.0-4.0 barg was $166 \pm 13 \text{ kg m}^{-2} \text{ h}^{-1}$.

5.4.4. Constant pressure batch filtration

Figure 5.6 shows the relationship between the mass of filtrate and time; initially the filtrate mass increases rapidly but then gradually slows and reaches a plateau. It was assumed that filtration was complete once three consecutively and identical readings had been observed. The general shape of Figure 5.6 (1.0 barg) is valid for all pressures, the plateau occurring sooner at higher pressures.

Figures 5.7 and 5.8 are typical linearised plots for constant-pressure and step-pressure tests, respectively. Some deviations from linearity are present in both. For the constant-pressure curve, the slope is constant save at the beginning and end of filtration. These regions were omitted from linear regression analysis of all curves to give a squared correlation coefficient (i.e. R^2) greater than 0.99. In Figure 5.8, the initial data points following a step change in the pressure are erroneous due to the time to effect the pressure rise and for the system to settle. At 1.0 barg, the average specific cake resistances for the constant- and step-pressure experiments were 3.8×10^{11} and 3.5×10^{11} m kg⁻¹ respectively; these being approximately two orders of magnitude lower than the results obtained without body feed (10^{13} m kg⁻¹).

5.4.5. Compressibility

Figure 5.9 is a compressibility curve and summary of cake resistance for all batches. Good agreement exists between the constant-pressure and step-pressure data, giving slopes of 0.48 and 0.55, respectively, resulting in an average of 0.51. Linearity was obtained for both sets of experiments save for the 4.0 barg result in the step-pressure trials. This deviation is probably due to even greater cake compression compared to that for all other filtration conditions.

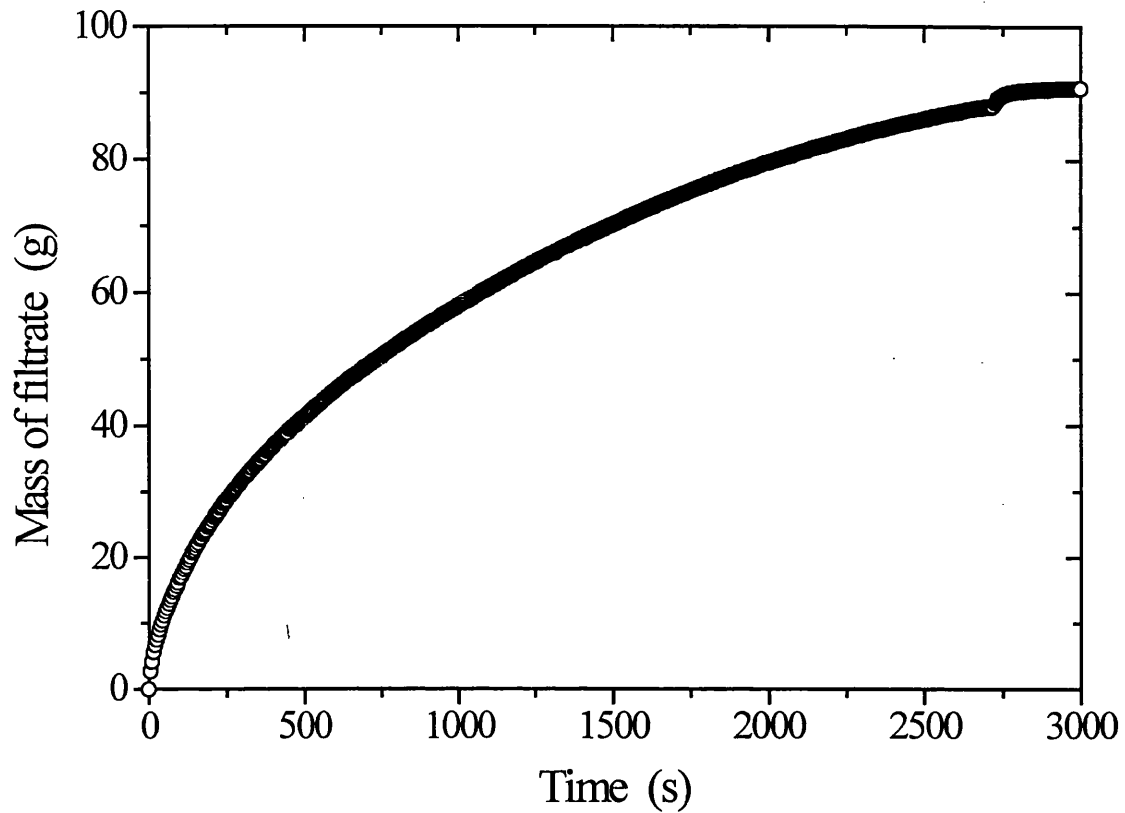


Figure 5.6. Filtration curve: dependence of the mass of filtrate on time for a constant pressure of 1.0 barg in the laboratory batch filtration of F:IV (see legend of Figure 5.5). The mass of filtrate increases sharply initially and then more gradually until a plateau is reached (at 90 g approximately).

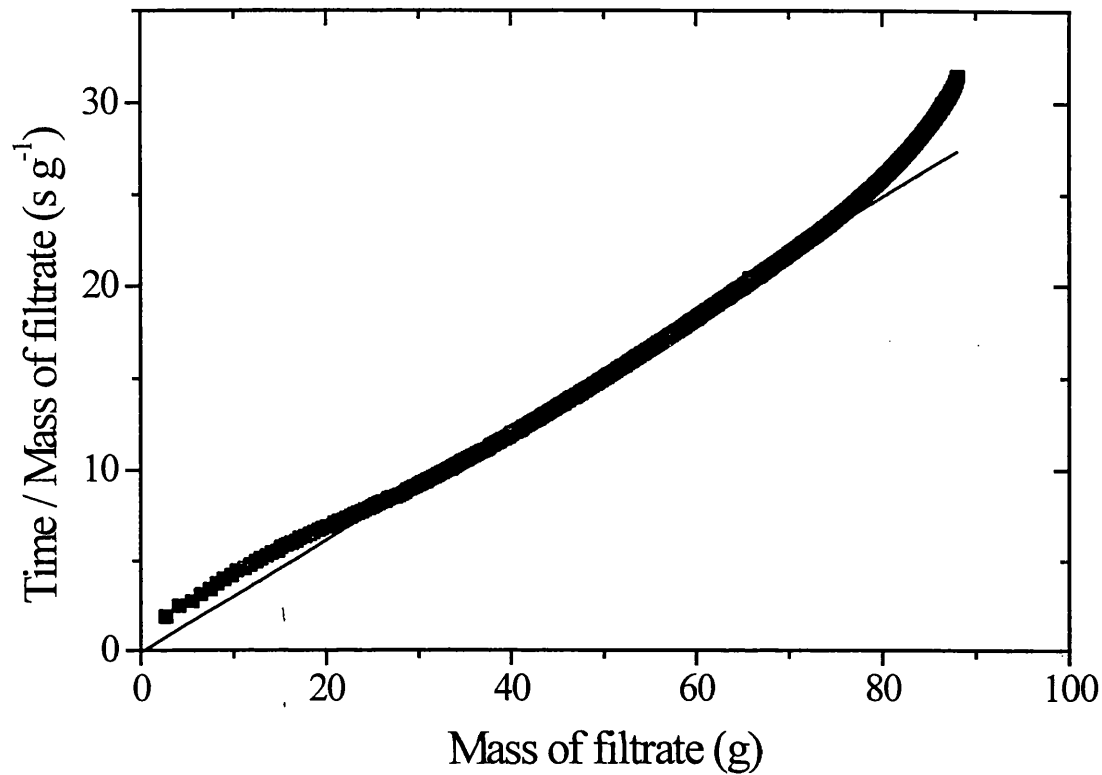


Figure 5.7. The dependence of the ratio of time to mass of filtrate on mass of filtrate. Conditions are as per Figure 5.6. The curve exhibits a slight concave-up shape, which becomes much more pronounced towards the end of filtration. Therefore, the line of best fit (slope = 0.31 s g^{-2}) was determined over the data range from 20 to 80 g, using linear regression. The average specific cake resistance was calculated to be $4.0 \times 10^{11} \text{ m kg}^{-1}$ using Equation 5.6.

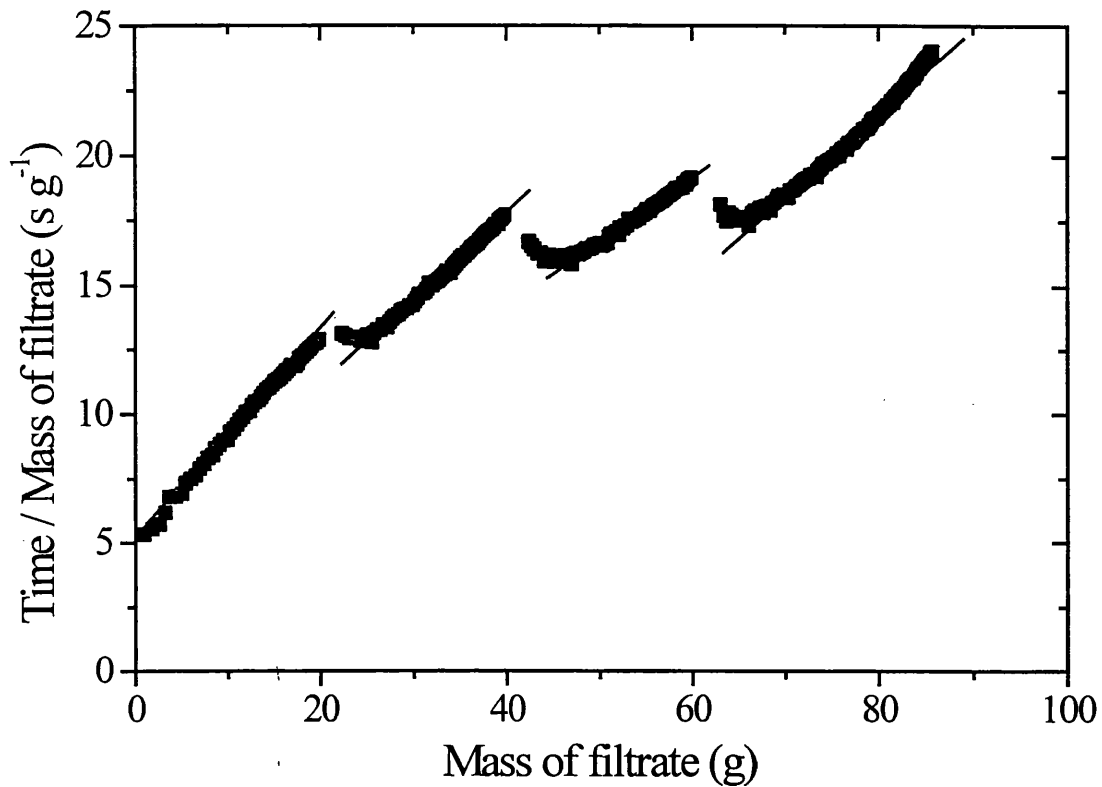


Figure 5.8. The dependence of the ratio of time to mass of filtrate on mass of filtrate for step-pressure increases (0.5-1.0-2.0-4.0 barg). The curve exhibits linearity for each constant-pressure region except at the beginning of each region signalling that some time is required for the system to settle after a step change in pressure. Slopes were determined to be 0.40, 0.33, 0.24 and 0.32 s g^{-2} at pressures of 0.5, 1.0, 2.0 and 4.0 barg, respectively, using linear regression (first few data points of each region ignored); the respective average specific cake resistances were 2.7, 4.5, 6.4 and $18 \times 10^{11} \text{ m kg}^{-1}$.

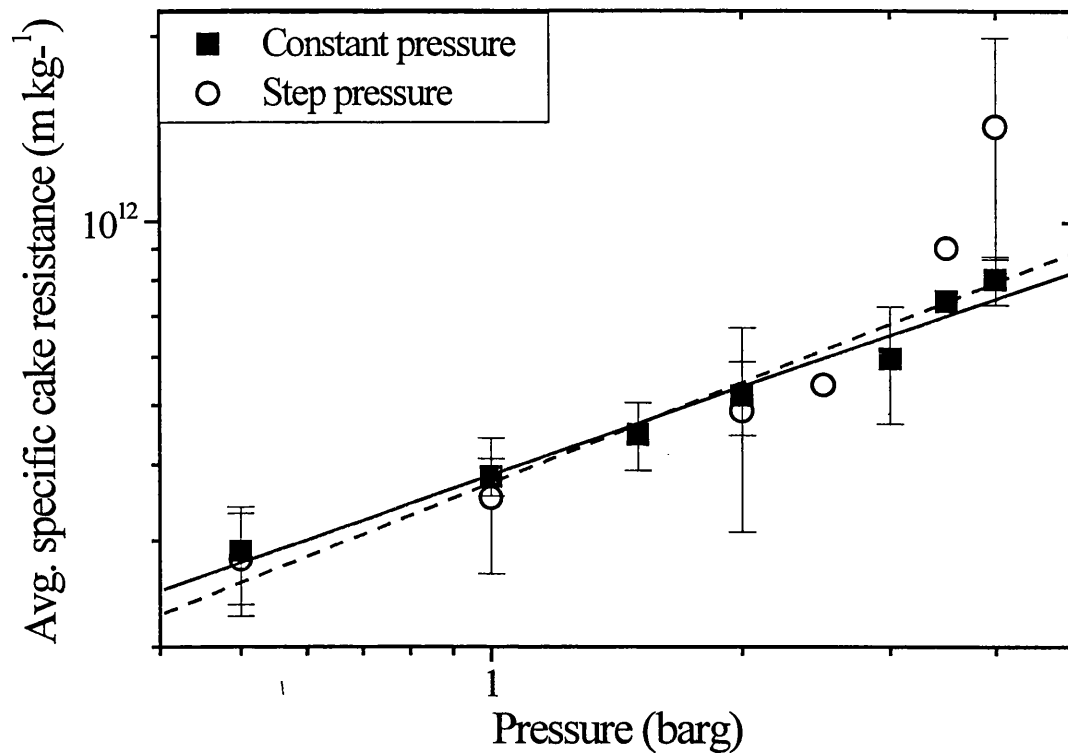
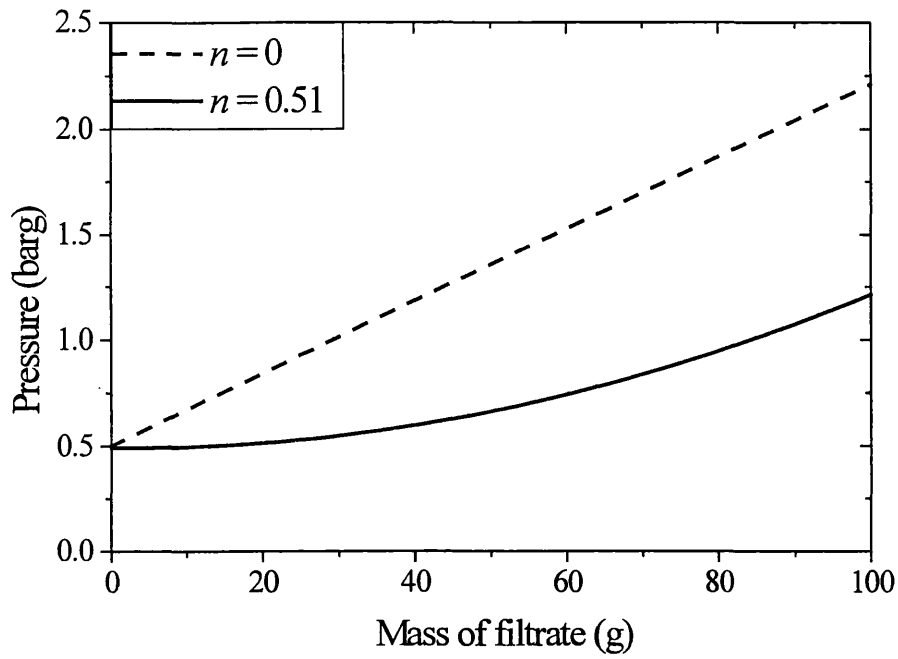


Figure 5.9. The average specific cake resistance plotted against pressure on logarithmic axes. The slopes of the lines for constant-pressure (■) and step-pressure (○) data were calculated to be 0.48 ± 0.03 and 0.55 ± 0.1 , respectively, and are equal to the compressibility coefficient, n , in Equation 5.7. Error bars indicate 95% confidence interval for multiple runs (≥ 3).

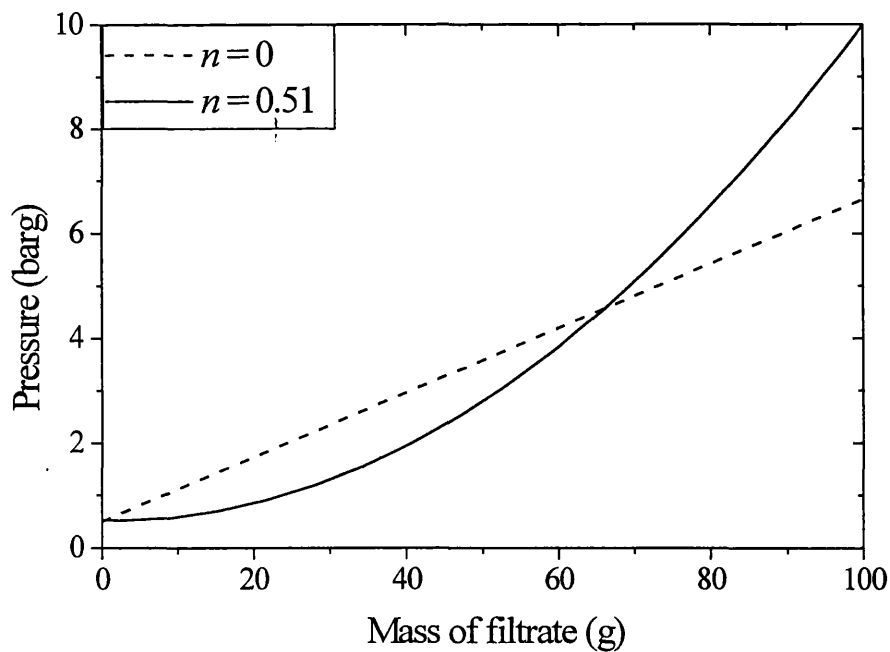
5.4.6. Predicted performance of scale-down RVLf

Due to the inability to conduct tests with the industrial filter at the time of this study, it is assumed that its small-scale counterpart gives very similar performance in terms of filtrate clarity (previously shown to depend only on the precoat) and pressure increase profile to maintain constant flux. For this work, a total separation cycle can last no longer than 5 h at production scale. Application of the precoat consumes 0.5 h. A standard batch of F:IV is 5 000 L and should be processed in 1.5 h through the 24m² RVLf, representing a minimum flux rate of 140 kg m⁻² h⁻¹. This is because the standard downtime required for cake removal, clean-in-place (CIP) and sterilise-in-place (SIP) is approximately 2 h, and typical air drying conditions are 1 000 N m³ m⁻² h⁻¹ for 0.5 h, leaving another 0.5 h for cake washing.

The projected required pressure increase (calculated with Equation 5.9) is shown in Figure 5.10a for the minimum flux (140 kg m⁻² h⁻¹) and compressibilities of 0 and 0.51. In the case of an incompressible cake ($n = 0$), it is predicted that the pressure would have to be increased steadily from 0.5 to 2.2 barg. Considering the compressible nature of the suspension under study, it can be seen that the pressure ramping profile is somewhat parabolic. This translates into a very gradual but ever more rapid rise in pressure, however the maximum attained was only 1.2 barg and the steepest gradient of the curve (both of which occur at $M = 100$ g) was less than the line for the rigid cake. Neglecting compressibility leads to increased pressures. Figure 5.10b is the same as 5.10a except that the flux has been increased to 500 kg m⁻² h⁻¹. It can be seen that, unlike for the lower flux, the compressible cake necessitates higher pressures towards the end of filtration than the non-compressible case, thus demonstrating the significant dependence of the pressure profile on flow rate, i.e. the pressure is proportional to the square of the flow rate.



(a)



(b)

Figure 5.10. Theoretical pressure-ramping profiles required for constant-flux rate filtration. Pressures were calculated using Equation 5.9 with compressibilities, $n = 0$ and 0.51 (experimental average) at flux rates of (a) 140 and (b) 500 kg m⁻² h⁻¹.

5.4.7. Actual performance of scale-down RVLf

Figure 5.11 displays filtrate mass against time for the scale-down RVLf operated at constant pressure of 1.5 barg, which was accomplished by decreasing the pumping rate accordingly. A linear relationship was obtained, resulting in an average specific cake resistance of $1.9 \times 10^{11} \text{ m kg}^{-1}$, which is less than the result of $4.7 \times 10^{11} \text{ m kg}^{-1}$ for the batch. The lower value may be attributed to the more even build-up of a cake of uniform composition in the case of continuous filtration. Proper mixing in the feed tank and low flow rates ensured that a homogenous suspension was delivered to the filter, and hence accumulation of a more uniform cake. In laboratory tests, filter aid was added to the precipitates, the resultant suspension shaken and then poured on to the precoat prior to application of air-pressure. Cake formation was very non-uniform due to the much greater settling velocity of the diatomaceous earth particles than those of the precipitates and poorer mixing. Once the filter aid had settled, the finer precipitates accumulated on top, creating a compressible layer of low permeability. Despite the non-uniform composition of the batch-filter cake, it had a very level surface compared to that of the continuous filter, which was slightly rounded. This may have been the result of solids impinging against the filtrate plane due to the flow rate, which despite being the lowest possible was still too high to prevent impingement. This could be corrected by increasing the distance between the inlet to the filter chamber (i.e. by adjusting the position of the plunger) and the cloth, but this would increase the chamber volume and hence not permit determination of the filter's feed capacity. A more even cake surface could also be achieved by rotating the filter more slowly, thus allowing more time for solids to settle and prevent them from directly (i.e. following the main axis) impacting the cake surface.

Figure 5.12 is similar to 5.11 except that the pumping rate was maintained constant, and the concomitant rise in pressure and fall in flux recorded. The pressure initially

increases and then sharply at the 20 g filtrate mark from about 0.2 to 2 barg where it plateaus around the 80 g point. This pattern was observed repeatedly and it is not clear why but it is believed to be due to a leak in the filtration apparatus at higher pressures and not a loss in efficiency of the pump as this is rated to a maximum of 6.0 barg. The flux is approximately constant at $500 \text{ kg m}^{-2} \text{ h}^{-1}$ between 0 and 60 g, with the pressure rising by 2 barg as predicted by the profile in Figure 5.10b. After the 60 g mark, the pressure levels off and the flux decreases (i.e. the inverse flux decreases).

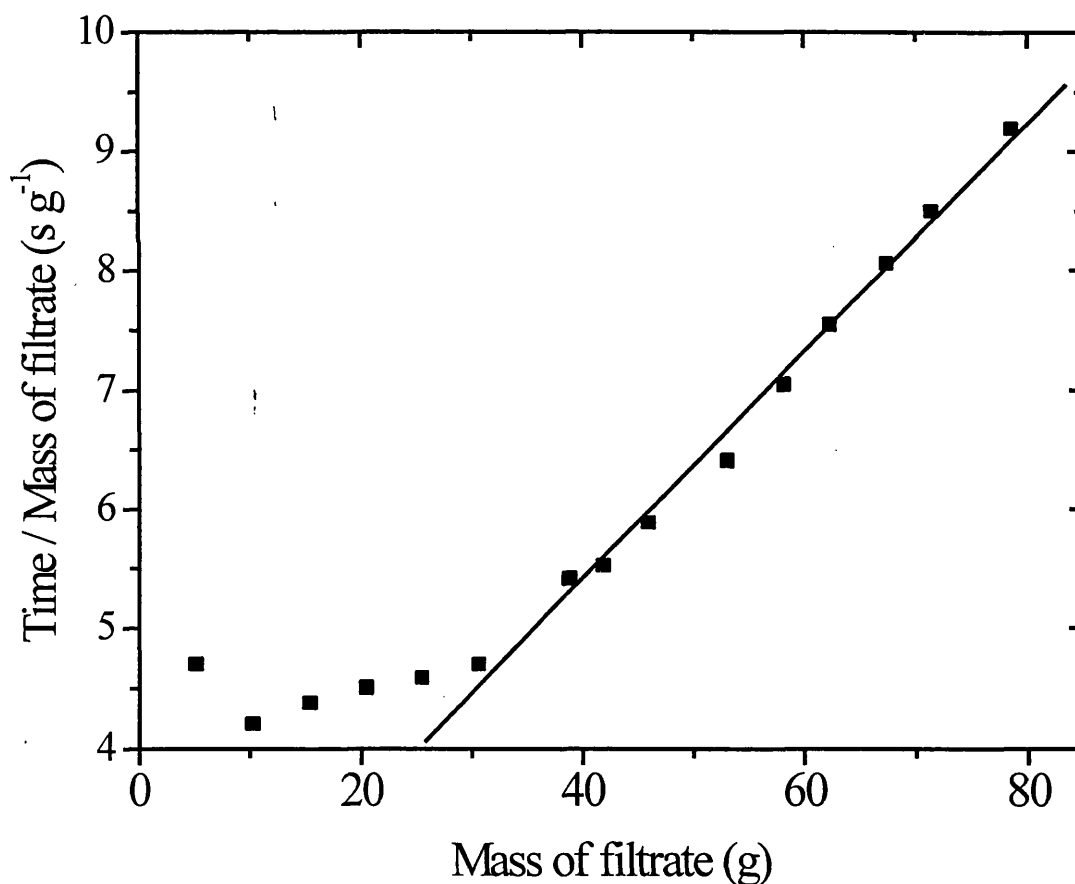


Figure 5.11. Linear relationship between ratio of time to mass of filtrate and mass for the scale-down rotating vertical leaf filter. The pumping rate was adjusted to maintain the pressure constant at 1.5 barg. The slope of the line was 0.095 s g^{-2} determined by linear regression (from 30 to 80 g), giving an average specific cake resistance of $1.9 \times 10^{11} \text{ m kg}^{-1}$.

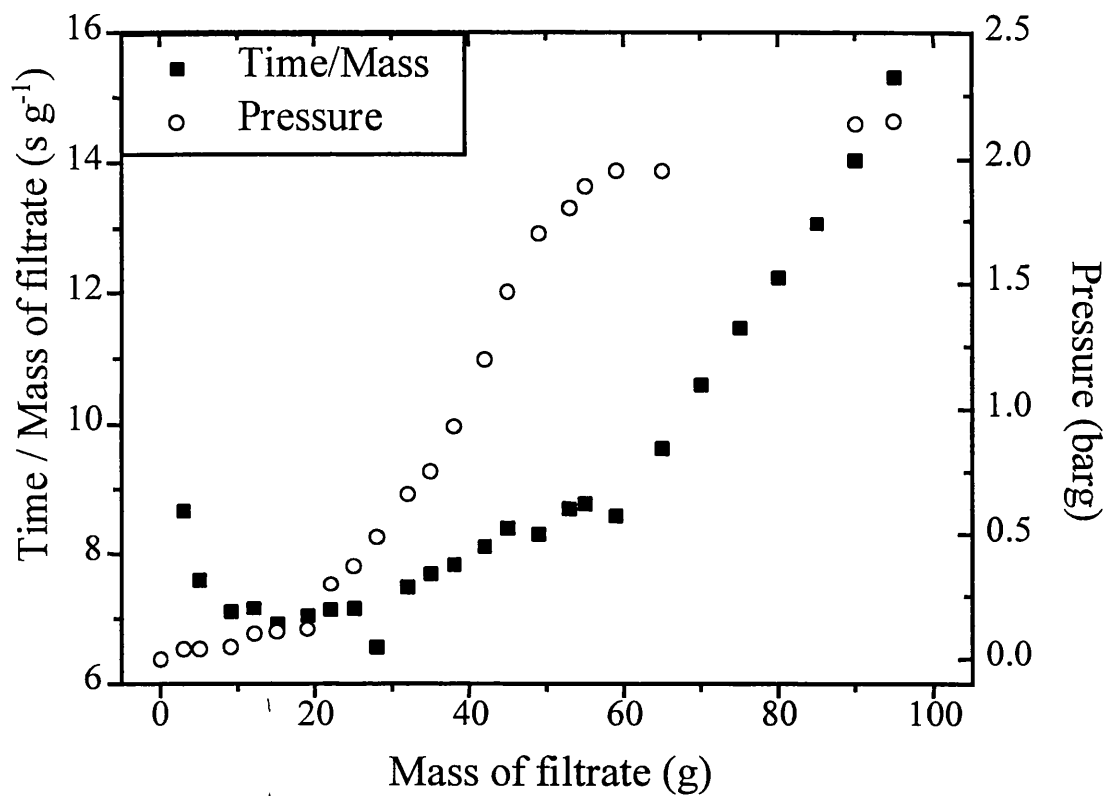


Figure 5.12. Dependence of the ratio of time to mass of filtrate and mass for the scale-down rotating vertical leaf filter. The pump rate was maintained constant at 4.7 V (1 r s^{-1}), but the volumetric flow rate and pressure did vary with time.

5.4.8. Comparison of filtration and centrifugation performance

Table 5.1 provides a comparison between centrifugation and filtration performance in terms of clarification and sediment dewatering. The industrial multichamber-bowl gives a poor clarification (46% at $Q_{mc}/C_{mc}\Sigma_{mc} = 14 \times 10^{-9} \text{ m s}^{-1}$) compared to that of the mimic (77% at $V_{lab}/t_{lab}C_{lab}\Sigma_{lab} = 15 \times 10^{-9} \text{ m s}^{-1}$); the difference being principally due to the shear break-up of precipitates in the feed zone of continuous centrifuges (Boychyn *et al.*, 2000a). Only the reference centrifuge could achieve a similar clarification (99% at $V_{lab}/t_{lab}C_{lab}\Sigma_{lab} = 1.7 \times 10^{-9} \text{ m s}^{-1}$) to that of the filter (99%). The quality of filtrate does not depend on pressure as evidenced by very similar clarification values for virtually all filtration runs. Sediment dewatering in the scale-down centrifuge ($RCF_{max} = 8010$, $t = 0.25 \text{ h}$) was quite similar to that in the production machine ($RCF_{max} = 8140$, $t = 8 \text{ h}$), despite the latter being spun for a 30-fold longer time. Surprisingly, the reference centrifuge ($RCF_{max} = 8010$, $t = 2 \text{ h}$) gave the lowest sediment dryness (35%) even though it was spun much longer than the scale-down samples. This higher moisture content may be due to settling of the finer particles (as a result of a lower $V_{lab}/t_{lab}C_{lab}\Sigma_{lab}$), which have a lower settling velocity and thus dewatering potential. Furthermore, reference samples had solids fractions approximately twice that of scale-down ones (4% compared to 2%) because of greater clarification and potentially, the formation of additional precipitates attributable to more effective cooling in the laboratory centrifuge than the precipitation reactor.

Only filter cakes formed at the lowest pressure of 0.5 barg were similar in dryness to the best centrifuge sediments (45% compared with 44%). As expected, dewatering of the cake increased with pressure from 45% at 0.5 barg to 60% at 4.0 barg and to 61% with the step-pressure runs. The negligible difference in moisture content between the

Table 5.1. The average sediment dryness and clarification as a function of centrifugation and batch filtration operating conditions. Uncertainty (\pm) represents the 95% confidence interval for at least duplicate runs.

Pressure (barg)	Sediment dryness (%)	Clarification (%)
0.5	44.6 \pm 1.5	97.3 \pm 2.1
1.0	47.9 \pm 1.5	99.0 \pm 0.5
1.5	50.0 \pm 2.0	99.5 \pm 0.2
2.0	51.4 \pm 1.8	99.2 \pm 0.2
2.5	54.8	99.0
3.0	52.4 \pm 1.3	98.8 \pm 0.1
3.5	57.4	99.0
4.0	60.2 \pm 5.9	98.9 \pm 0.2
0.5-1.5-2.5-3.5	61.1 \pm 0.5	99.1 \pm 0.5
0.5-1.0-2.0-4.0	61.3 \pm 2.5	98.9 \pm 1.3
Reference centrifuge ($RCF_{max} = 8010$, $t = 0.25$ h; $V_{lab}/t_{lab}C_{lab}\Sigma_{lab} = 1.7 \times 10^{-9}$ m s $^{-1}$)	35.0 \pm 2.7	99.1 \pm 0.2
Scale-down centrifuge ($RCF_{max} = 8010$, $t = 0.25$ h; $V_{lab}/t_{lab}C_{lab}\Sigma_{lab} = 15 \times 10^{-9}$ m s $^{-1}$)	44.1 \pm 1.1	76.5 \pm 3.4
Production centrifuge ($RCF_{max} = 8140$, $t = 8$ h; $Q_{mc}/C_{mc}\Sigma_{mc} = 14 \times 10^{-9}$ m s $^{-1}$)	40.6 \pm 2.4	45.6 \pm 2.6

constant- and step-pressure runs suggests that cake dewatering is independent of the ramping profile for the suspension under study. The much drier filter cakes indicate that overall separation efficiency of the filter is considerably higher than that of the centrifuge. This may be due to the fact that the sediment in a centrifuge always has a head of liquid; solids can settle into a fairly tight packing arrangement, with the fluid being somewhat further displaced by compression of the actual precipitate aggregates. However, in pressure filtration, the liquid is pushed through a bed of solids and in order for air to penetrate the cake completely, much of the interstitial fluid must be displaced; higher pressures lead to significant bed compression and hence dewatering.

5.5. CONCLUSIONS

The filter cake was compressible; a consistently logarithmic relationship was exhibited between the applied pressure and specific cake resistance. The compressibility coefficients calculated using step pressure data was within 10% of that determined by constant pressure experiments. At the same pressure, a lower specific cake resistance was observed in the scale-down RVLFF than the batch, pressure-Nutsche filter due to the former having a continuous delivery of a well-mixed suspension leading to a cake of homogeneous composition. An unexpected profile was obtained when operating the continuous filter with a fixed pumping rate; the pressure initially built up slowly and increased as predicted, but then levelled off with a concomitant decrease in the flux rate. The batch filter gave better clarification and sediment dewatering of the plasma precipitate suspension than the production-scale centrifuge.

6. CHAPTER 6: IMPACT OF PRIMARY SEPARATION ON CHROMATOGRAPHY

ABSTRACT

This research focused on how the extent and type of primary solid-liquid separation (i.e. centrifugation or precoat filtration) of a yeast homogenate influenced guard filtration and the purification of ADH using hydrophobic interaction chromatography (HIC). The increasing resistance of the guard filter correlated well with decreasing clarification of the suspension. Column dynamic capacity decreased somewhat with more turbid supernatants, but primary filtrates gave considerably inferior chromatographic performance, which was not predicted by the response of the guard filter.

6.1. INTRODUCTION

Cartridge filters and pretreatments (e.g. precipitation and flocculation) have been used to protect more expensive unit operations such as ultrafiltration and chromatography, by removing fine solids which may foul them. Use of guard filtration often results in lower pressure drops and higher fluxes for downstream membranes (Rushton *et al.*, 1996; Kwon *et al.*, 1997), but little quantitative data has been reported on sensitivity of pre-filters to the turbidity of feed material (Meltzer and Jornitz, 1998), as well as the influence of foulants on dynamic column capacity and purity (Soriano, 1995). Consequently, this chapter briefly examines how the extent and method of primary solid-liquid separation impact on the performance of guard filtration and chromatography, and whether the response of the filter can be used to predict that of the purification column. This work is not a detailed examination of fouling species or mechanisms (e.g. no physical analysis of filters or chromatographic resins by SEM, particle sizing, etc.), as these are varied, complex and generally require an in-depth knowledge of protein,

colloidal and surface chemistry (Maa and Hsu, 1999; Maa and Hsu, 1996; Meagher *et al.*, 1996; Guell *et al.*, 1999; Yiantsios and Karabelas, 1998; Guell and Davis, 1996; Herrero *et al.*, 1997).

Centrifugation, conventional and micro-filtration are the main competing technologies in the clarification of suspensions with substantial fractional solids volumes. Tangential-flow membranes were not considered in this study, but several authors have investigated the fouling of these membranes (Gan *et al.*, 1997; Song, 1998; Yiantsios and Karabelas, 1998; Herrero *et al.*, 1997).

Several types of foulants have been identified: particles (cells, cell debris, precipitates), proteins, nucleic acids, lipids, pluronics (anti-foam and other surfactants), fermentation additives, and certain polysaccharides, minerals and metal complexes. Fouling components may be soluble, colloidal or insoluble. Here, particulate fouling is of central concern, but the relative contributions of DNA and lipids are also estimated. This is possibly due to the different separation mechanisms. Significant adsorption of very large macromolecules (like DNA) may occur during permeation of a liquid through a tortuous bed of diatomaceous earth (Singhvi *et al.*, 1996). Centrifugal forces cause many lipids to float to the surface of a suspension and coalesce in large (100-2000 μm), defined masses, allowing their easy retention when passed through virtually any filter medium.

Cartridge filters have been used by many industries to clarify a wide variety of liquids. The two most important measures of their performance are filtration efficiency (i.e. rating) and retention capacity (Jourdan and Peuchot, 1994). These obviously depend on properties of the feed stream (volume, particle size, density and concentration distribution, viscosity, pH, etc.) and the removal technology (filter type, composition, charge, hydrophobicity, size, geometry, priming, flow rate, washing, etc.) (Hellot, 1993). When particle density is similar to that of the suspending fluid, as is the case for many

biological materials such as cell debris and precipitates, the dominant capture mechanisms are direct interception and straining, with some diffusion and hydrodynamic interactions (Rushton *et al.*, 1996). As the filter collects solids, it becomes clogged and usually retains finer particulates such that its rating improves with time and use. However, an increasing pressure is required to maintain flow and this becomes excessive at some point, signaling the need for a change of filter. Failure to do so can result in structural failure if the feed pump has spare capacity. Maximum differential pressures allowed with cartridge filters are typically less than 2.0 bar. Higher pressure drops improve throughput but reduce the capture efficiency associated with adsorptive sequestration (Meltzer and Jornitz, 1998). Depth filters are often placed prior to 0.45 or 0.2 μm membranes, which frequently guard chromatographic columns from any remaining significant particles and contamination. The presence of such a final filter, even one which is rarely challenged, adds minimal capital and running costs, but has protected extremely valuable processes in many instances (Rushton *et al.*, 1996).

Chromatography is the most widely used and accepted method for achieving high-resolution product purification. Only scant attention has been paid to the fouling of chromatographic matrices (Pettersson, 1989; Johansson and Ellstrom, 1985) and how pre-treatment methods can improve purification performance (Murphy *et al.*, 1999). This work researches how the extent and type of primary solid-liquid separation influences the purification of ADH using hydrophobic interaction chromatography.

6.2. MATERIAL AND METHODS

6.2.1. Chemicals

All chemicals, unless specified otherwise, were obtained from Sigma Chemical Co. Ltd. (Dorset, UK) and were of analytical grade.

6.2.2. Description of equipment

The equipment used in laboratory experiments is listed below. Homogenisation was carried out using the Lab 40, as described in sections 2.3.2 and 2.3.4. Primary separation of the homogenate was achieved in two major ways: processing it in a Beckman J2-M1 laboratory centrifuge with JA 20 fixed-angle rotor (Beckman Instruments Ltd., High Wycombe, UK; $C_{lab} = 1.0$) or through a stainless steel filter housing of 36 mm internal diameter (i.e. active area of 10^{-3} m^2) with filter aid.

The above material (supernatant or filtrate) was then processed in parallel. Half of the material was clarified through a guard depth filter and the other half loaded on to a HIC (hydrophobic interaction chromatography) column (Pharmacia LKB Biotechnology, Uppsala, Sweden) controlled with a BioCAD (Perseptive Biosystems, Framingham, USA).

6.2.3. Preparation of feed suspension

Baker's yeast was suspended to 8% packed wet weight per volume in 0.1 M KH_2PO_4 buffer (pH 6.5). This was then homogenised at 500 barg for five discrete passes. 160 mL of homogenate were placed into a baffled stirred-tank reactor, to which 40 mL of a saturated solution of $(\text{NH}_4)_2\text{SO}_4$ (3.93 M, buffered with 0.1 M KH_2PO_4 , pH 6.5) were added rapidly in one batch (at the surface and near the impeller) resulting in a 20% saturated (0.78 M) suspension. This was agitated at a mean velocity gradient, $\bar{G} = 200 \text{ s}^{-1}$ for $t = 0.63 \text{ h}$ (Camp number, $\bar{G}t = 10^5$).

6.2.4. Centrifugation

30 mL (V_{lab}) aliquots of suspension were transferred to 50 mL polycarbonate tubes and centrifuged ($R_1 = 0.060$ m, $R_2 = 0.090$ m, $C_{lab} = 1.0$) under the conditions, listed in Table 6.1, to give a range of clarifications. The lipid layer formed at the top of the liquid surface in the tube was removed by decanting the supernatant on to a single sheet of lint-free filter paper (Kimberly-Clark, Kent, UK).

Table 6.1. Operating conditions of the laboratory centrifuge.

N_{lab} ($r\ s^{-1}$)	t_{lab} (h)	Σ_{lab} (m^2)	$V_{lab}/t_{lab}C_{lab}\Sigma_{lab}$ ($10^{-9}\ m\ s^{-1}$)
250	0.67	20.2	0.62
250	0.31	19.3	1.4
250	0.16	18.3	2.9
100	0.17	3.13	16

6.2.5. Filtration

6.2.5.1. Primary

Operation of batch-mode filtration is described in Chapter 5. The precoat of $1.0\ kg\ m^{-2}$ Celpure 1000 filter aid (Advanced Mineral Corporation, CA, USA), supported on a GF/B glass microfibre filter cloth (Whatman International Ltd, Maidston, UK), was applied in 20% $(NH_4)_2SO_4$ saturated aqueous buffer at 1.0 barg for approximately 30 s. The body feed concentration was $3.0\ kg\ m^{-3}$ in 100 mL of suspension (2 batches required). The initial pressure (supplied by a cylinder of compressed nitrogen) of 0.5 barg was maintained for the first 50 mL and then incremented by 0.5 barg until a maximum of 1.5 barg was attained.

6.2.5.2. Guard

Zeta Plus 90LA Grade depth filters (Cuno Incorporated, Parkway, USA) were chosen because of their low nominal rating ($0.2\ \mu m$) and suitability for cell debris removal. A 47 mm disc was wetted in salt buffer prior to placement in a Cuno disc

holder. 100 mL of the supernatant or primary filtrate were then placed into a pressure vessel, 0.5 barg applied and the flux decline monitored manually.

6.2.5.3. Membrane

Sartolab P20 Plus 0.2 μm cellulose acetate 20 cm^2 disposable membranes (Sartorius AG, Goettingen, Germany) were used to clarify filtrates further for reference purposes. The membranes are hydrophilic (i.e. low protein binding) and robust. 100 mL of guard filtrate was processed through a membrane at 0.5 barg.

6.2.6. Chromatography

ADH purification (Smith, 1997) was performed by Shane Storey (Department of Biochemical Engineering, University College London) using the BioCAD with a fresh 1 mL Phenyl Sepharose column (Pharmacia 17-1411-02), equilibrated for 0.5 h at a flow rate of 18 mL h^{-1} with HIC running buffer (0.78 M $(\text{NH}_4)_2\text{SO}_4$; 20 mM KH_2PO_4 , pH 7.0).

After running buffer equilibration, yeast homogenate streams were fed downwards through the column at a constant flow rate of 18 mL h^{-1} . Once feeding steady state was achieved (pH 7.0, conductivity of 100 mS), the tube leading from the bottom of the column was detached to allow continuous sampling of the effluent. The passage from the column to the analytical equipment is long, and as the experiment sought to enforce a strict breakthrough criterion, it was thought better to detach and sample directly ex-column, and avoid the unnecessarily large hold-up volume in the apparatus. The upstream plumbing was unaffected, so the column supply pressure could still be monitored.

Samples drawn during the loading period were immediately assayed for ADH, and once the breakthrough concentration had reached 15% of the previously determined feed concentration, the column was immediately detached from the BioCAD apparatus. The

feed line was then flushed with HIC running buffer, so that when the column was reconnected, no additional feed would be introduced. Washing was performed at 54 mL h⁻¹, using the HIC running buffer. Feed application used a lower flow rate because the feed streams would contain particulates and other foulants and there was the chance the column would be damaged if higher flow rates were used. In all cases, once feed application was complete, washing at the higher flow rate caused no compression problems. The wash volume was sampled and assayed for ADH until the concentration had fallen to less than 1% of the original feed.

ADH elution was achieved by a step reduction in ionic strength, feeding a 20 mM KH₂PO₄ solution (pH 7.0) at 12 mL h⁻¹, seeking to elute the captured ADH into the smallest possible volume. Column eluate samples were collected continuously, again ex-column, and stored frozen at -20°C until it was convenient to assay for both ADH and protein concentration. Once both sets of assays were complete, specific activities were calculated, and fractions with greater than 100 U mg⁻¹ were pooled, giving the final ADH yield.

6.2.7. Analyses

6.2.7.1. General

Clarification was measured by the protocol in section 3.3.5.4. Some samples were diluted 10-fold in 20% saturated (NH₄)₂SO₄ solution to keep readings between 0.05 and 1; this buffer was also used as the blank. Protein and ADH assays were conducted according to the methods in sections 2.3.6.2 and 2.3.6.3, respectively.

6.2.7.2. Guard filter fouling

The degree of fouling can be assessed by determining the slope of a plot of t/M against M (Equation 5.7), which is a linearised form of the reciprocal rate filtration

equation (Equation 5.4). A higher slope indicates greater resistance and thus fouling.

Results are presented in terms of a fouling index, F , which is a normalised slope:

$$F = \frac{\text{Slope}_{\text{sample}}}{\text{Slope}_{\text{ref}}} \quad (6.1)$$

where the subscript *ref* indicates the reference sample.

6.2.7.3. Chromatographic breakthrough time

The chromatography loading flow rate was 18 mL h⁻¹, meaning that effluent flow was drop-wise. Only 25 μL of sample is required per ADH assay. One drop samples were collected in Eppendorf tubes and immediately assayed for ADH, allowing the real-time construction of a time series breakthrough curve. The bulk feed was diluted 20-fold and then assayed in triplicate for ADH, so that the concentration corresponding to 15% breakthrough could be calculated. Once this condition was reached, the time was noted and feeding ceased. Results were processed to yield a normalised breakthrough time, τ_N :

$$\tau_N = \frac{\tau_{\text{sample}}}{\tau_{\text{ref}}} \quad (6.2)$$

6.2.7.4. Dynamic capacity and process yields

The data was plotted as chromatograms in Microcal Origin 5.0. The mathematical functions built into the software package allowed the chromatograms to be integrated numerically with respect to time, thus calculating the amount of ADH and protein present in the pooled samples. The ADH concentration profile over the complete elution time course produced the dynamic capacity results, which also provided the gross process yield. Narrowing the limits of integration to consider only the pooled fractions (> 100 U mg protein⁻¹) defined the net process yield. Results were expressed in the form of a normalised dynamic capacity Γ_N :

$$\Gamma_N = \frac{\Gamma_{sample}}{\Gamma_{ref}} \quad (6.3)$$

6.2.8. Experimental design

The performance of guard filtration and chromatography was assessed with the streams listed in Table 6.2. Stream 1 is the reference to which all other streams are normalised.

Table 6.2. Description of process streams.

Stream	Unit operations prior to guard filtration or HIC
1 (reference)	Centrifugation ($V_{lab}/t_{lab}C_{lab}\Sigma_{lab} = 0.73 \times 10^{-9} \text{ m s}^{-1}$), guard filtration, membrane (0.2 μm)filtration (overall clarification considered to be 100%)
2	Centrifugation ($V_{lab}/t_{lab}C_{lab}\Sigma_{lab} = 0.73 \times 10^{-9} \text{ m s}^{-1}$)
3	Centrifugation ($V_{lab}/t_{lab}C_{lab}\Sigma_{lab} = 1.40 \times 10^{-9} \text{ m s}^{-1}$)
4	Centrifugation ($V_{lab}/t_{lab}C_{lab}\Sigma_{lab} = 2.96 \times 10^{-9} \text{ m s}^{-1}$)
5	Centrifugation ($V_{lab}/t_{lab}C_{lab}\Sigma_{lab} = 16.4 \times 10^{-9} \text{ m s}^{-1}$)
6	Primary filtration, guard filtration, membrane filtration
7	Primary filtration

6.3. RESULTS AND DISCUSSION

6.3.1. Selection of starting material

The chosen suspension should be difficult to clarify and one in which small changes in separation efficiency greatly impact downstream operations. Homogenates represent such a system. Bakers' yeast was selected due to ease of availability, good knowledge base from numerous research studies on the organism and low cost. Under standard conditions, its homogenate has a small mean particle diameter of approximately $1.5 \mu\text{m}$ concomitant with a broad distribution ($0.01\text{-}3 \mu\text{m}$). A concentration of $80 \text{ g packed yeast L}^{-1}$ was selected to give an ADH activity of approximately 100 U mL^{-1} , so that breakthrough would occur within 20 column volumes of material (total capacity of an HIC column is approximately 2000 U).

Furthermore, it was desired that any influences on chromatography be attributed only to the method and extent of solid-liquid separation, and not pre-treatments such as precipitation. Significant precipitation of protein and cell debris occurs when the concentration of ammonium sulphate surpasses 30% saturation (as done in previous chapters); the suspension was brought to only 20% salt saturation as dictated by ADH-HIC binding conditions.

6.3.2. Filter fouling

Figure 6.1 is a typical plot of the mass of guard filtrate against time; as with Figure 5.4, the mass increases rapidly initially and then slows. A true plateau, i.e. an extremely low flux, would be exhibited if more suspension were processed, thus testing the solids capacity of the guard filter. Figure 6.2 represents the data in the form of Equation 5.6; except for the first few points, linearity is displayed over the entire range of data. Table 6.3 gives the clarity of the suspension loaded on to the guard filter for each stream (listed

in Table 6.2), and the commensurate fouling index and post-filter clarification. Stream 1, the reference, is considered to achieve a clarification of 100% due to processing through the 0.2 μm membrane. As expected, it gave the lowest slope of the linear filtration curve and hence a fouling index value of 1.0. The clarification after guard filtration remained unchanged at 100%. Stream 2 had a lower clarification and a higher slope. Interestingly, Streams 3 and 4, which have lower clarifications than Stream 2 due to the inferior centrifugation conditions, gave lower slopes than the cleaner Stream 2. These results may be attributed slight differences in viscosity due to lack of temperature control during filtration. Stream 5 had the lowest clarification and produced the greatest fouling response of 6.5. Stream 7 was clarified to 95% with precoat filtration and exhibited a slope greater than stream 2, but much less than Stream 5. Figure 6.3 displays a fair correlation between clarity of the feed stream to the guard filter and fouling index, the line of best fit having a squared correlation coefficient (R^2) of 0.86.

Table 6.3. The degree to which the suspension (yeast homogenate, prepared with 80 g packed cells L^{-1} , taken to 0.78 M $(\text{NH}_4)_2\text{SO}_4$ at pH 7.0, 4°C; $\text{OD} = 7.8 \pm 0.4$) was clarified, the fouling index of the stream loaded on to the guard filter and the clarification effected by this filter, are provided for each stream listed in Table 6.2. The reference is Stream 1, which has a clarification of 100% ($\text{OD} = 0.37 \pm 0.04$) and a fouling index (the slope of its linearised filtration curve was 0.017 s g^{-2}) of 1.0.

Stream	Clarification of suspension (%)	Fouling index	Clarification of guard filtrate (%)
1	100	1.0	100
2	97.9	2.7	99.36
3	95.0	2.1	98.23
4	93.1	2.3	98.25
5	81.0	6.5	94.87
6	100	(not measured)	100
7	95.8	3.2	98.48
Average			97.8 ± 1.5

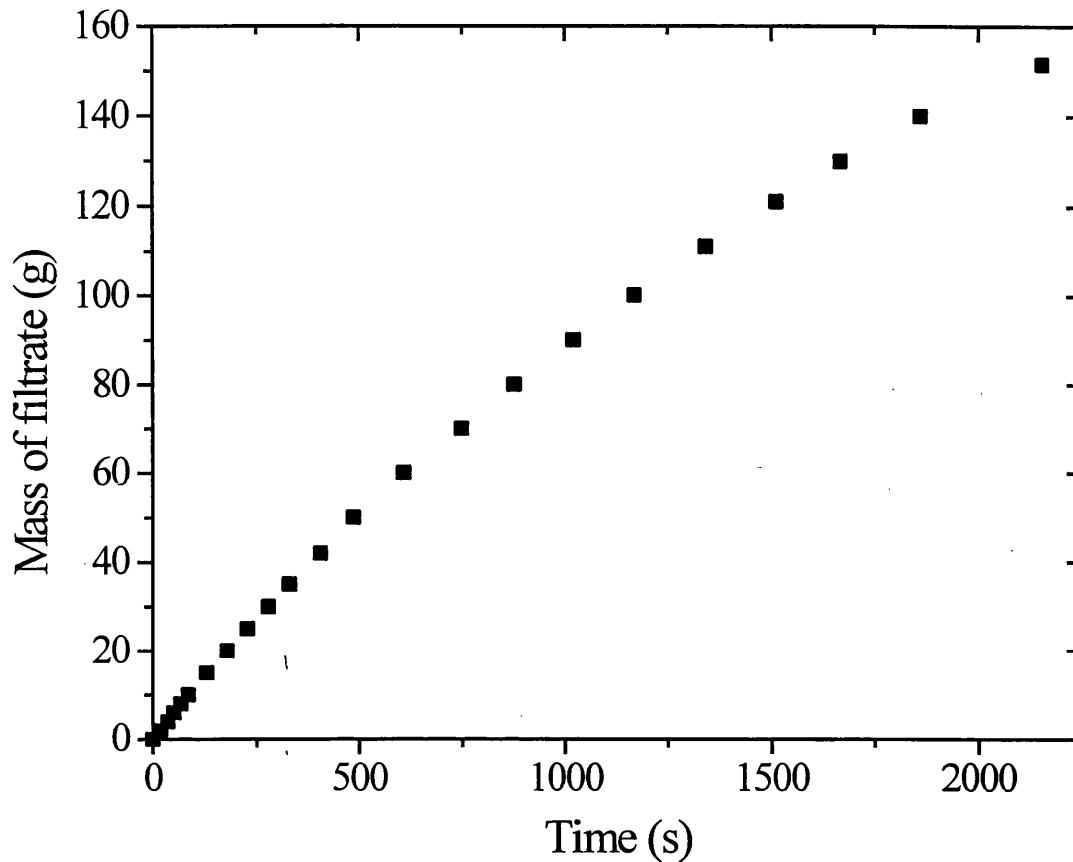


Figure 6.1. Filtration curve: dependence of the mass of filtrate on time at a constant pressure of 0.5 barg in the guard filter. The mass of filtrate increases sharply initially and then more gradually due to fouling. The feed was Stream 3 (see Table 6.2), the original suspension (yeast homogenate, prepared with 80 g packed cells L^{-1} , taken to 0.78 M $(NH_4)_2SO_4$ at pH 7.0, 4°C) clarified to 95%.

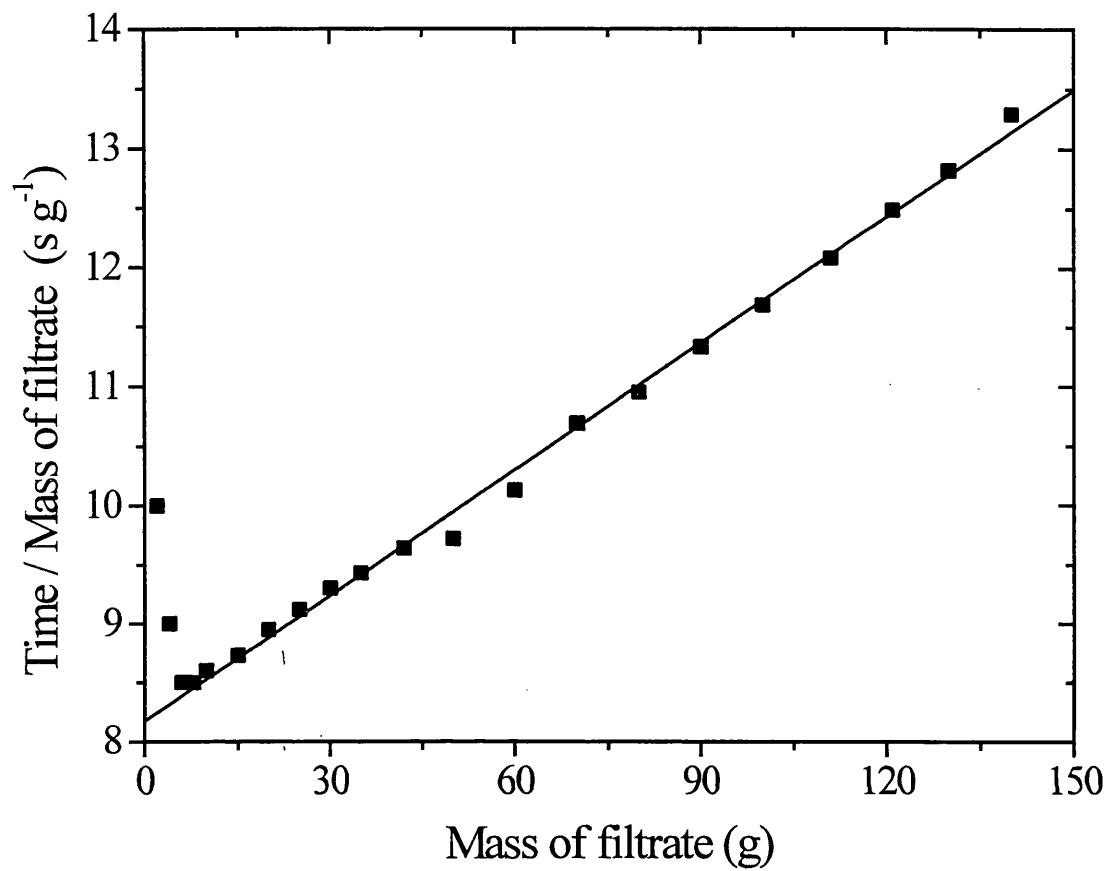


Figure 6.2. Dependence of the ratio of time to mass of filtrate on mass of filtrate. Conditions are as per Figure 6.1. The line of best fit (slope = 0.035 s g^{-2}) was determined over the entire data range (excluding first three points) using linear regression (squared correlation coefficient, $R^2 = 0.99$).

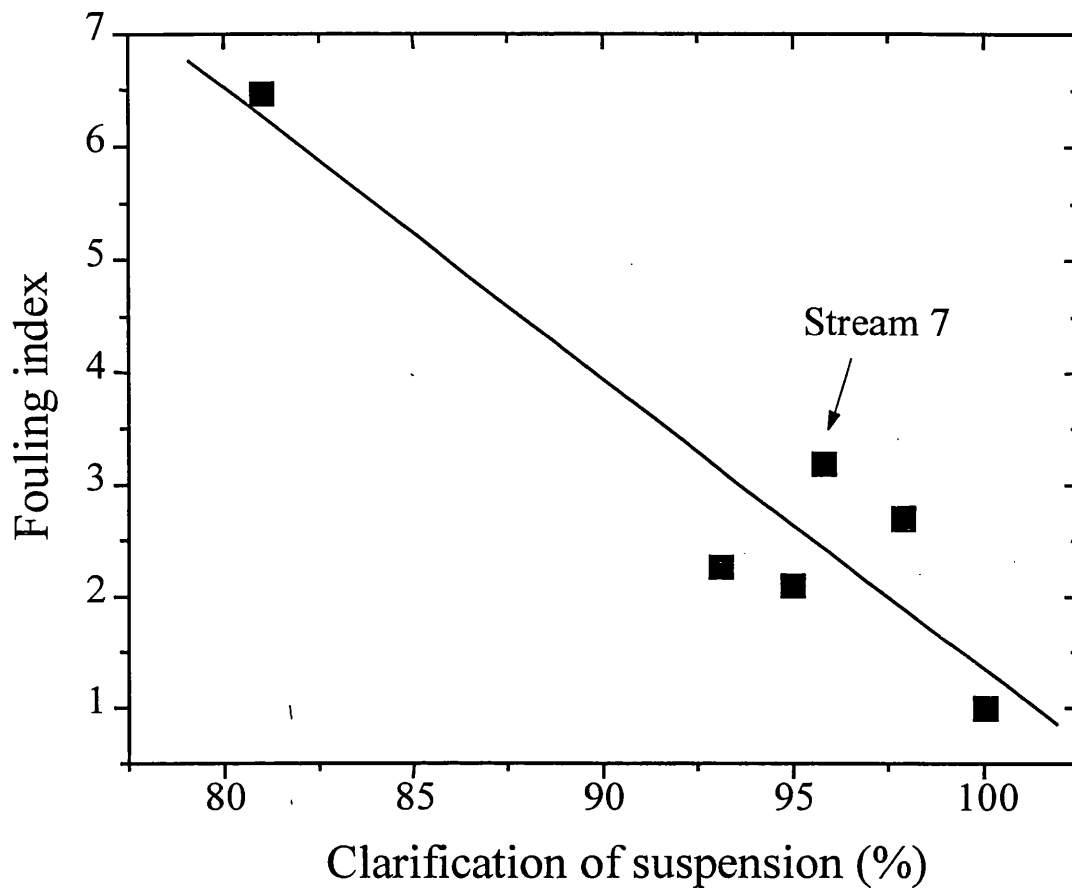


Figure 6.3. Dependence of the filtration index (normalised slope of the linearised filtration curve) on clarification for Streams 1-5 and 7 (see Table 6.2). The data point for stream 7 is indicated, as this is the only one that has been primary filtered; all other streams were centrifuged. Linear regression was used to determine the line of best fit, yielding $R^2 = 0.86$. *Reference:* Stream 1 had the maximum clarification of 100% and the minimum fouling index of 1.0 (see Table 6.3).

6.3.3. Quality of filtrate

From a brief examination of Table 6.3, it would appear that, except for Stream 5, the clarity of the guard filtrate was virtually the same for all streams, with a mean value of 98.6 ± 0.5 %. However, plotting the clarification achieved after the guard filter against that of the suspension (i.e. feed to the filter), as shown in Figure 6.4, gives an excellent correlation of 0.99. This indicates that the quality of the material fed to the guard filter affects not only its flux (as evidenced by Figure 6.3) but also its separation performance. The latter is not expected to occur with a membrane, which has an absolute rating due to a tight size distribution of surface pores that retain solids by a sieving mechanism. A filter, such as the guard filters used in this study, relies on a series of progressively finer pores with increasing depth to capture solids by adsorption or inertial interception. If a more turbid feed stream is introduced, the probability of solids retention initially remains the same, so that more debris penetrates the filter, resulting in a less clear filtrate. As pores become filled with solids, finer and finer particles will be captured, thus improving the filter's rating with time. Nevertheless, for small ratios of feed volume to filter area, the quality of the pooled filtrate is dependent on that of the feed, which explains the relationship exhibited in Figure 6.4.

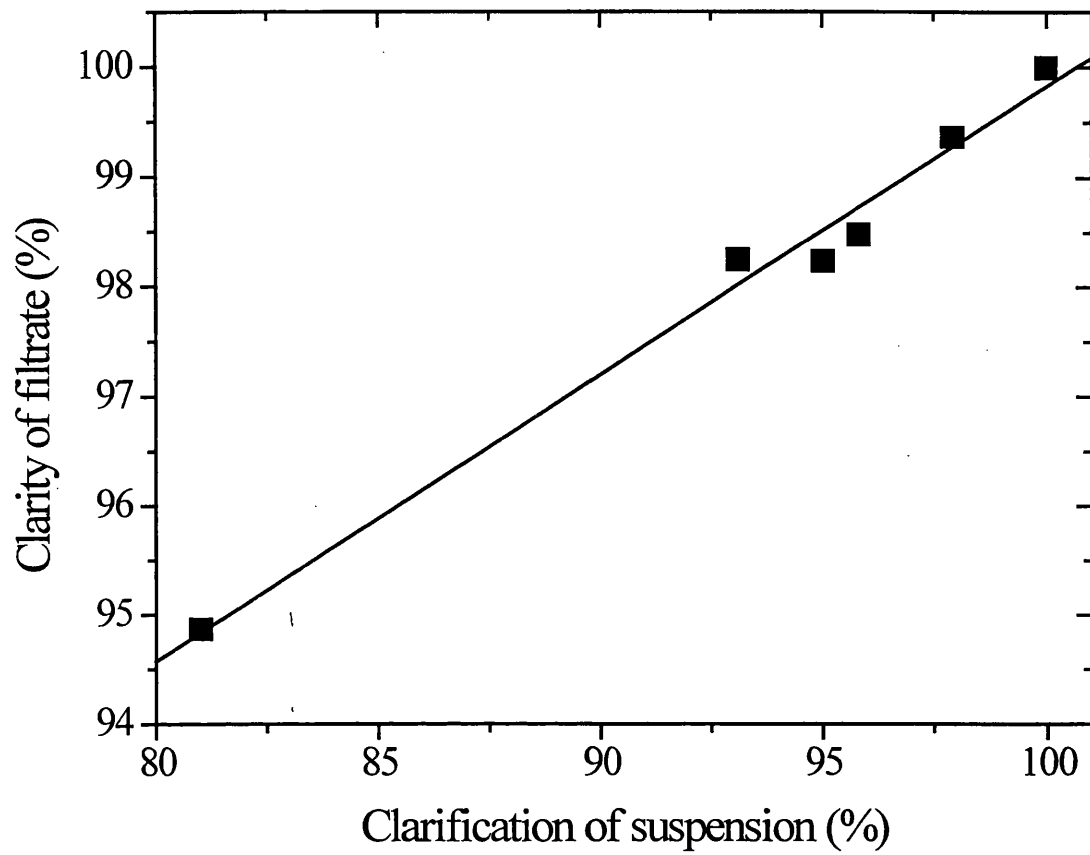


Figure 6.4. Dependence of the clarity of the guard filtrate on the clarification of the original suspension. Conditions are as per Figure 6.3. The line of best fit has $R^2 = 0.99$.

6.3.4. Chromatographic performance

Figure 6.5 show the breakthrough curves of the various streams, the normalised times listed in Table 6.4. Streams 6, is the first to breakthrough followed closely by Streams 5 and 6. Better clarified centrifugation streams (i.e. Streams 1-3) breakthrough later than the more turbid ones (Streams 4 and 5). Interestingly, Stream 1 had an earlier breakthrough time than Streams 2 and 3 despite the former being membrane-filtered. It is obvious that the streams involving primary filtrates (Streams 6 and 7) are grouped to the left-hand side of the graph despite their high clarifications (> 95%).

Table 6.4. The clarification of the suspension, normalised breakthrough times and dynamic capacities (Storey *et al.*, 2000a; Storey *et al.*, 2000b). The streams are as per Table 6.3. The reference dynamic capacity (Stream 1) was 2360 U. Stream 2 was considered to be the reference for breakthrough since this sample had the largest time of 1.97 h (35.6 column volumes).

Stream	Clarification of suspension (%)	Normalised breakthrough time	Normalised dynamic capacity
1	100	0.90	1.0
2	97.9	1.0	0.98
3	95.0	0.96	0.93
4	93.1	0.78	0.87
5	81.0	0.69	0.85
6	100	0.62	0.75
7	95.8	0.70	0.56

Figure 6.6 displays the ADH elution peaks for a few streams. Despite having very different clarifications (95 and 81%), the two centrifugation streams (3 and 5) elute in a very similar manner. It is striking that Stream 7 yields a much lower and broader peak than the other two streams, signalling significantly poorer chromatographic performance.

Integration of the elution curve gives the dynamic capacity, the normalised values detailed in Table 6.4 and displayed in Figure 6.7. Despite higher clarifications, the two filtrate streams (6 and 7) have lower normalised dynamic capacities than the

centrifugation samples, particularly so for Stream 7 with a value of only 0.56. The correlation between capacity and clarification for the entire data range displayed in Figure 6.7 is extremely poor ($R^2 = 0.04$); this attests to the inability to predict chromatographic performance based solely on the clarity of the feed material and hence, fouling index. However, for centrifugation samples only, the degradation in capacity correlates fairly well with supernatant clarity ($R^2 = 0.75$).

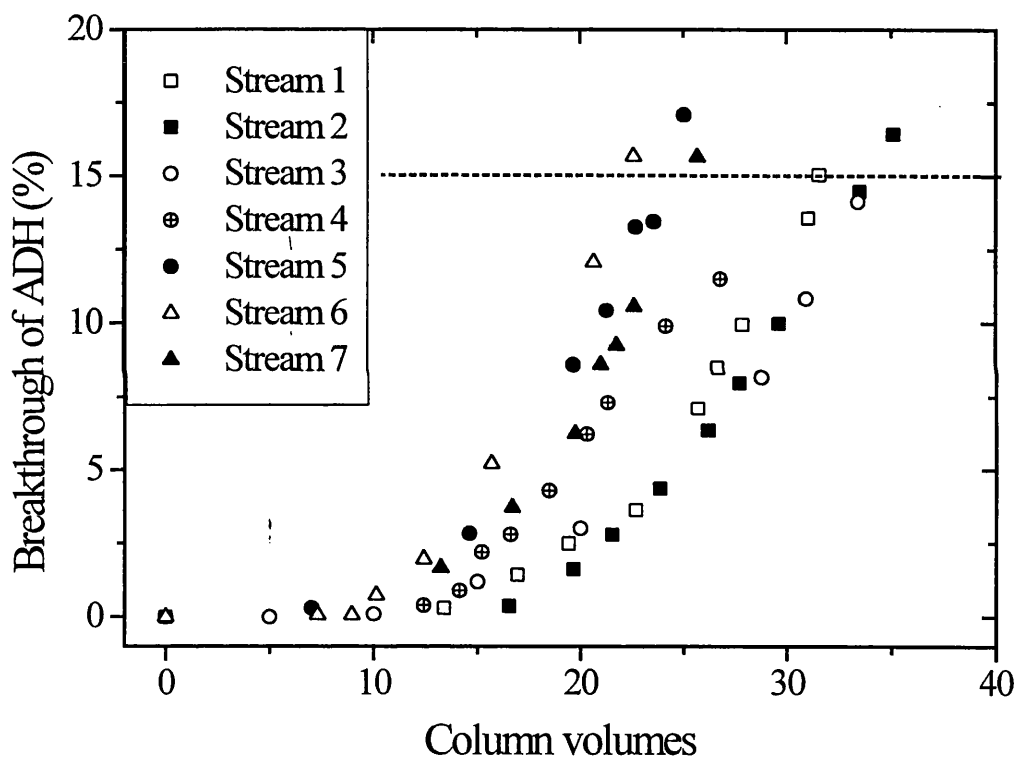


Figure 6.5. Solute breakthrough curves: dependence of the % breakthrough of ADH on the number of column volumes for Streams 1-7 (see Table 6.2). 1 mL Phenyl Sepharose columns were fed 100 U mL^{-1} ADH at 18 mL h^{-1} . Normalised times determined at 15% breakthrough (dashed line) are given in Table 6.4.

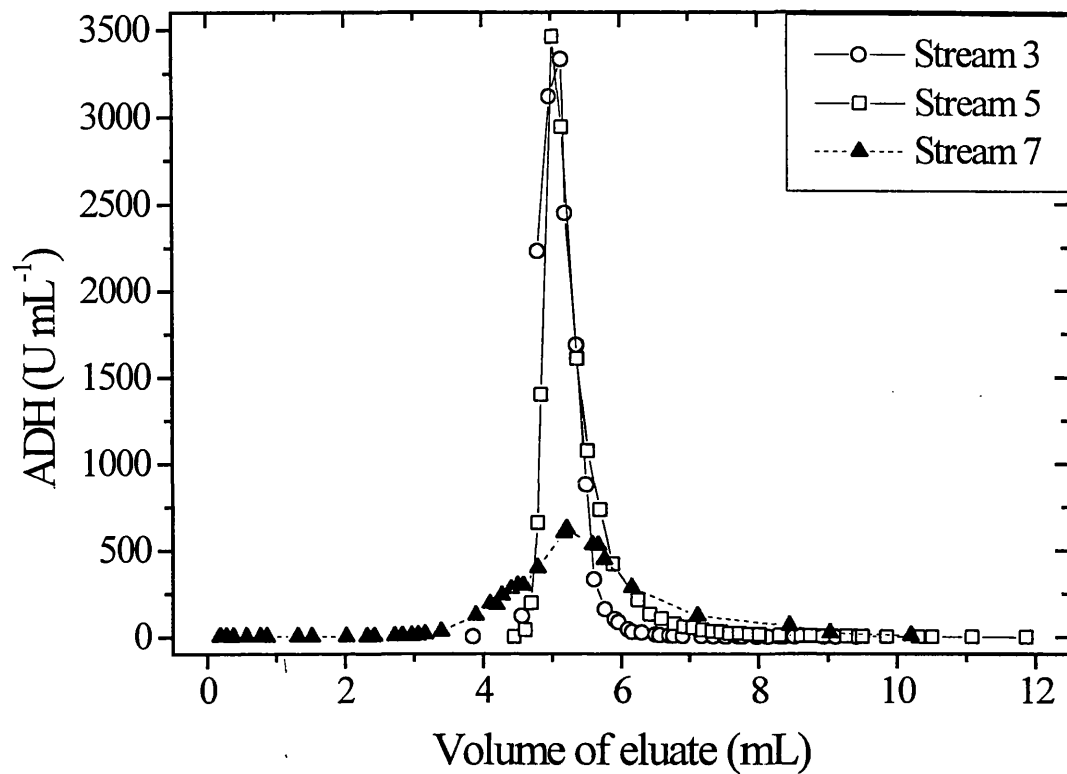


Figure 6.6. Elution peaks for HIC purification of ADH: dependence of activity on volume for Streams 3, 5 and 7 (see Table 6.2). 1 mL Phenyl Sepharose columns were eluted with phosphate buffer (20 mM KH_2PO_4 , pH 7.0) at 12 mL h^{-1} .

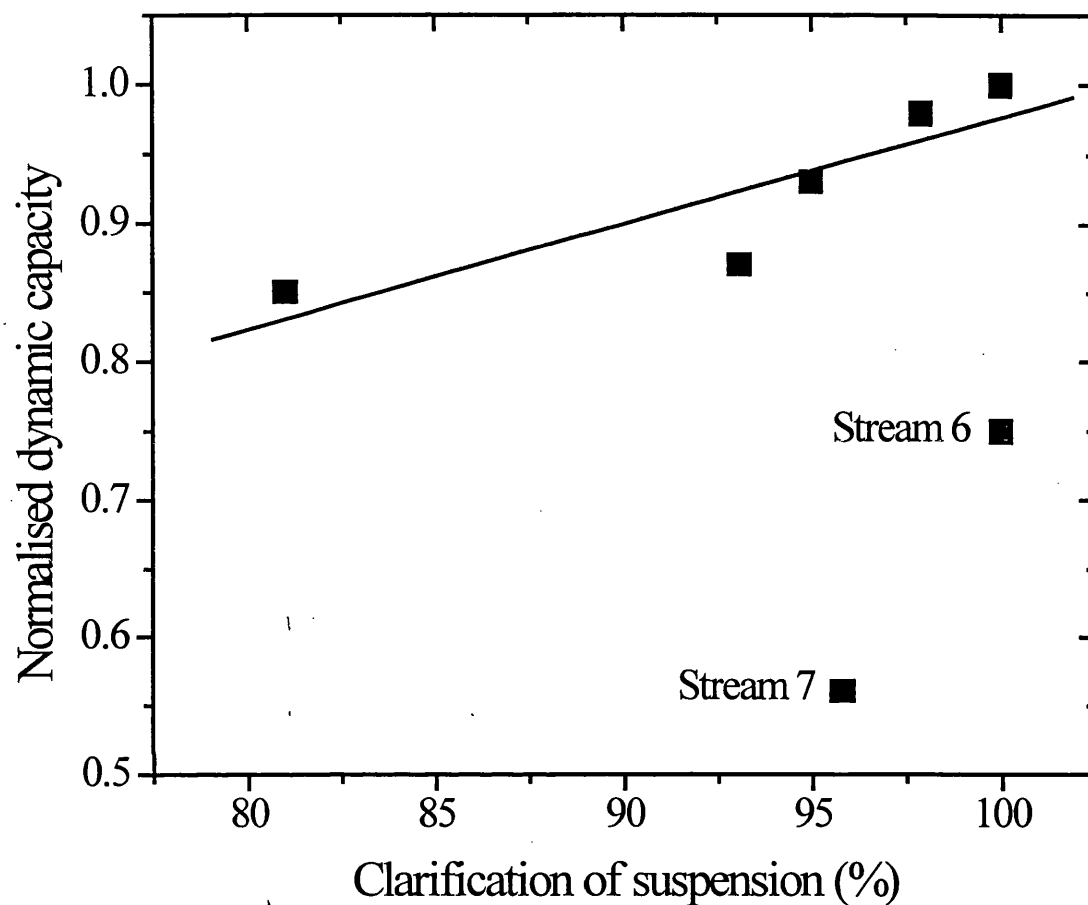


Figure 6.7. Dependence of the normalised dynamic capacity on clarification of the suspension for Streams 1-7 (see Table 6.2). The line of best fit was determined with linear regression using only centrifugation samples (excluding Streams 6 and 7) with $R^2 = 0.75$; for the entire data range, $R^2 = 0.04$. Results are tabulated in Table 6.4 with reference values.

Figure 6.8 shows that the yield of ADH decreases concomitantly with lower clarification and that the filtrate samples have considerably lower yields, with Stream 7 having the lowest. Interestingly, passing Stream 7 through the guard and membrane filters (i.e. Stream 6) improves the yield by 50%, the specific activity by 100% and the capacity by 30%, but results in an earlier breakthrough. In fact, despite a greatly reduced dynamic capacity, the product from Stream 6 has a greater specific activity that is 50% more than that of the reference. There is obviously some component in the primary filtrate which is reduced by the membrane.

The above results also indicate that there is some foulant present in considerably greater concentrations in the filtrate streams than the centrifugation ones. The probable foulant that is more abundant in filtrates than supernatants is lipids. Exertion of a centrifugal force causes many lipids to float and some to sink with the solids. It was observed that centrifuged homogenates had a thin layer at the top surface, what is believed to be coalesced lipids. To remove this lipid layer, supernatants were decanted and passed through the filter paper. During filtration, lipids remain in their colloidal form and many are not captured due to their small size; however, some are retained by the guard filter and membrane as evidenced by the superior capacity of Stream 6. Filtrate streams having lower dynamic capacities than centrifuged samples (even the most poorly clarified), indicates that lipids are more “fouling” than cell debris, at least in the case of the HIC purification of ADH from yeast homogenate. In other words, soluble or colloidal species can have a more pronounced effect on chromatography than insoluble ones.

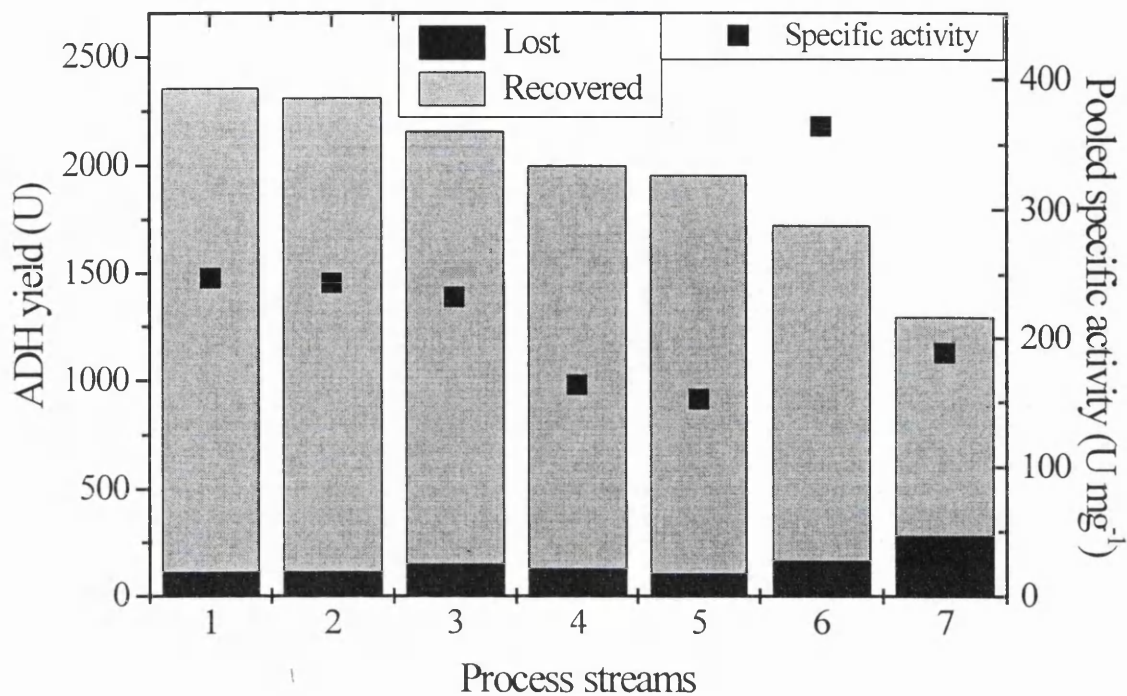


Figure 6.8. Process yields and purity results for HIC purification of ADH for Streams 1-7 (see Table 6.2). Grey-shaded bars represent pooled elution samples containing more than 100 U mg protein⁻¹; black-shaded region represents ADH lost. Total yield of ADH is defined as the dynamic capacity of the column at 15% solute breakthrough.

6.4. CONCLUSIONS

The resistance of the guard filter increased linearly with a decrease in clarification of the homogenate suspension. Centrifuged samples gave significantly better column dynamic capacities than filtered ones, despite a consistent drop in capacity with supernatant clarity. The results demonstrate that chromatographic performance depends not only on the efficiency of, but mainly on the type of solid-liquid separation.

7. CONCLUSIONS

The ability to predict the performance of large-scale processes is central to the rapid development of successful operations at the pilot and industrial scale. Precipitate material prepared at the same mean velocity gradient and ageing time in the laboratory and pilot plant resulted in particles with similar characteristics, as evidenced by approximately equivalent clarifications in the laboratory scale-down centrifuge. Good agreement was achieved between the scale-down and pilot multichamber-bowl centrifuges in terms of solids dewatering and also for precipitate recovery in the batch-operated, pilot machine. Operation of the pilot machine in the batch mode confirmed that the great difference in clarification between the scale-down and continuous-flow centrifuges was due to precipitate break-up in the feed zone of the latter.

CFD analysis was used to quantify the magnitude of the flow forces occurring in the entrance region of the pilot centrifuge. Shearing the suspension of protein precipitates in a small rotating-disc device at the maximum energy dissipation rates occurring in the multichamber-bowl, followed by scale-down centrifugation permitted accurate mimicking of pilot-scale clarification for different modes of operation. More disruption was observed in non-flooded entrance regions due to the higher power dissipations in the presence of air-liquid interfaces, as confirmed by CFD.

Constant tip velocity between the laboratory rotating-disc device and the critical structure in a continuous-flow centrifuge was also a good ($\pm 15\%$) scaling parameter, but CFD is needed for greater accuracy. The plasma precipitates exhibit considerably less breakage than their yeast-protein counterparts at similar power dissipations. Under standard operating conditions, the following centrifuges generate greater flow forces and hence more particle break-up in ascending order: pilot disc stack, pilot multichamber-bowl, pilot CARR and production multichamber-bowl. Importantly, it was shown that

the recovery obtained in the production centrifuge is predicted more accurately by the scale-down process than the pilot multichamber-bowl.

Turning to precoat and body feed filtration as an alternative type of separation to centrifugation, the specific cake resistance of the plasma suspension exhibited a consistently logarithmic dependence on the applied pressure for both constant and step pressure tests. Cake dryness, unlike clarification that was relatively constant, increased with pressure. At the same pressure, a lower specific cake resistance was observed in the scale-down vertical leaf filter than the batch filter due to the former having a cake of relatively homogeneous composition. Operation of the RVLFF at a fixed pump rate resulted in the pressure initially building up slowly and increasing as predicted, but then levelled off, signalling a decrease in the flux rate. Filtration performance was found to be superior to the equivalent manufacturing-scale centrifuge in terms of clarity of the processed material and sediment dewatering.

Finally, it was demonstrated that HIC-based purification of ADH depends not only on the efficiency of, but mainly on the type of solid-liquid separation. Column dynamic capacity decreased somewhat with more turbid supernatants, but dramatically (up to 55%) with primary filtrates. The drop in chromatographic performance was not predicted by the response of the guard filter, the resistance of which increased linearly with a decrease in clarification of the homogenate suspension.

The above results emphasise the need to assess the impact of a unit operation on downstream steps and not treat it in isolation. Only consideration of the whole bioprocess, from product formation to high-resolution purification, will lead to the optimal design, its development made more efficient by scale-down.

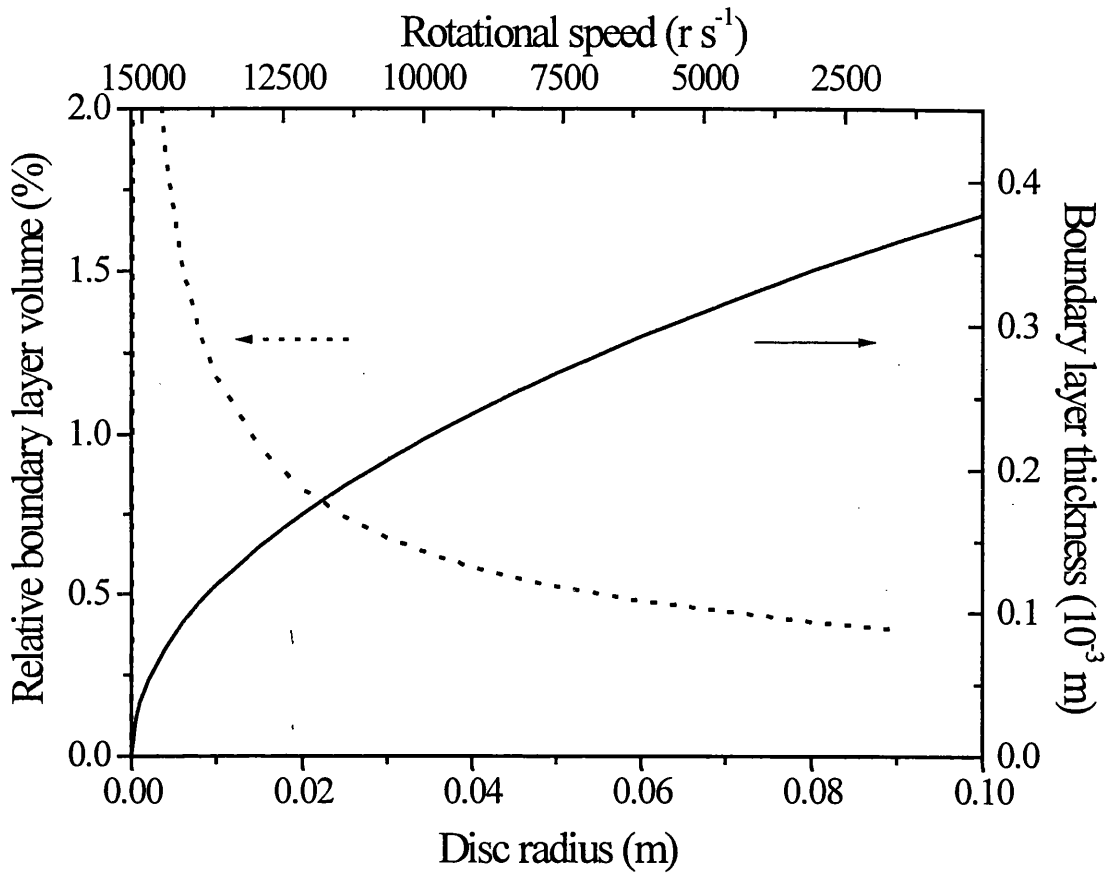
8. FUTURE WORK

8.1. HIGH-VELOCITY FLOW FIELDS

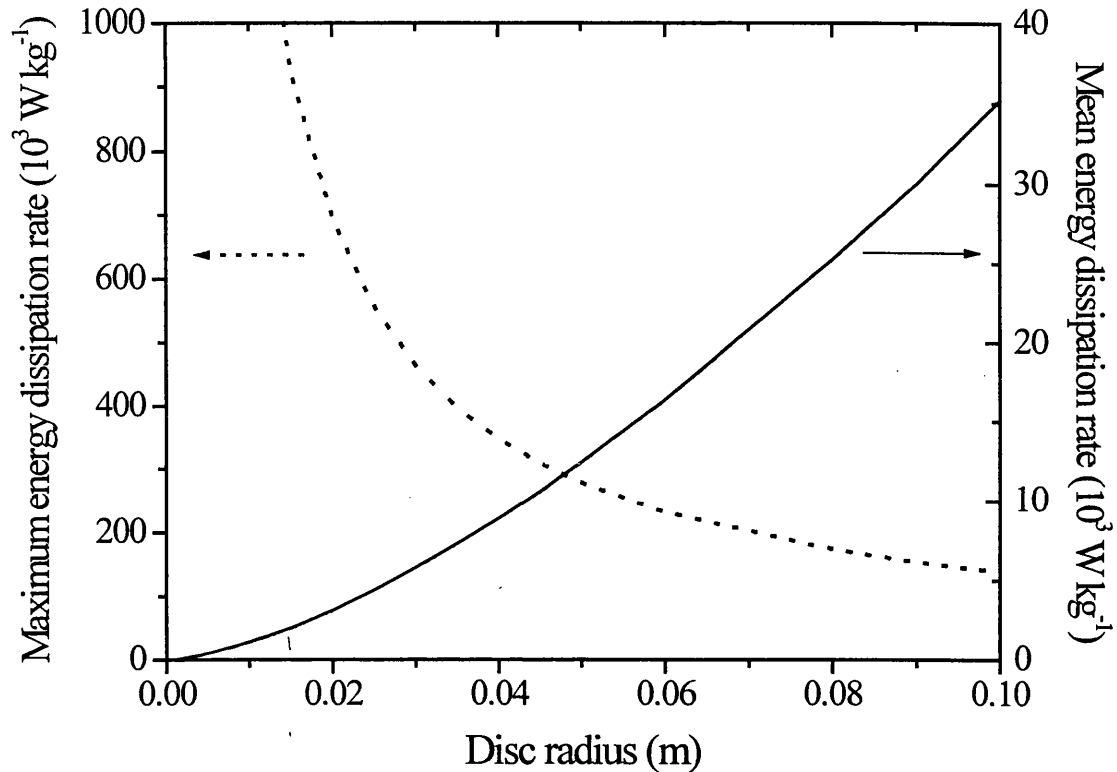
8.1.1. Scaling on tip velocity

As a general rule, scaling on tip velocity with a laboratory disc device should only be used for a continuous centrifuge with a flooded feed zone and a critical radius less than an order of magnitude that of the disc. From the results in Chapter 4, the tip speed method yields good predictions, but greater accuracy necessitates computational fluid dynamics (CFD).

While in many circumstances perfectly good scale-down is achieved by maintaining constant tip velocity of the centrifuge's feed distributor, care should be taken when estimating the maximum power dissipation by this method since the magnitude of the predicted value depends on the *size* of the laboratory disc being used. Even when tip speed is maintained constant, several parameters *vary* with disc size. Figure 8.1a displays the relative volume of the boundary layer (ratio of boundary layer volume to chamber volume) and its thickness as a function of disc radius, all at constant tip velocity. The thickness increases with disc size, but the relative boundary layer volume decreases rapidly and then progressively more gradually. This indicates that proper mixing (so that all precipitates are exposed to the boundary layer) can become more challenging as the scale increases. Figure 8.1b reveals that the mean power dissipation increases exponentially with radius, however, the maximum energy dissipation rate is inversely proportional to the boundary layer to disc size. As the maximum power dissipation depends directly on the size of the scale-down disc, care should be taken when scaling on tip velocity.



(a)



(b)

Figure 8.1 Variation in fluid dynamic parameters with disc size at a constant tip speed of 47.1 m s^{-1} . Results were calculated using equations 3.1 to 3.6.

- (a) Dependence of relative volume and thickness of the boundary layer on disc radius. The relative volume of the boundary layer is the ratio of the boundary layer volume to chamber volume. All chamber volumes were calculated by maintaining exact geometrical proportionality to the standard disc ($r_{rd} = 0.015 \text{ m}$, $r_{chamber} = 0.02 \text{ m}$, $h_{rd} = 0.0015 \text{ m}$, $h_{chamber} = 0.015 \text{ m}$), i.e. same aspect ratio, ratio of disc to chamber radius, ratio of disc to chamber height.
- (b) Dependence of the mean and maximum energy dissipation rates on disc radius. Means values were calculated using the volume of the chamber, while maximum power dissipations considered only the volume of the boundary layer.

8.1.2. Incorporation of shear into scale-down

The extent, kinetics and mechanism of disruption are system specific; these will depend on the balance between the mechanical properties of the biological material, its concentration, the type, magnitude and the time of exposure to the flow.

It would be advantageous to incorporate the study of flow effects (i.e. Chapter 3) into the strategy of laboratory scale-down given minimal sample volumes and process development times. By analysing the amount of damage (break-up of aggregates in the case of precipitation) at various velocities in a laboratory device, a characteristic *shear / shear damage* relationship can be obtained, e.g. Figure 3.3, 3.5 or 3.10. A main design challenge is to choose a small scale apparatus (capillary, rotating disc, cylinder, impeller, or propeller, etc.) and operate it in a manner (speed, batch or continuous, residence time) which most closely approximates the engineering flow field occurring in the piece of processing equipment under investigation. Selection of the appropriate device configuration and operation, would permit prediction of the probable amount of damage and hence, performance (for example, clarification) when linked to other scale-down equipment.

8.1.3. Incorporation of shear into bioprocess synthesis

Ultimately and more simply, a variety of biological materials could be tested at various speeds and times¹ in a standardised bench-top device, leading to the compilation of a “shear-sensitivity index”. The scaling parameter would be maximum energy dissipation rate, because this is the only parameter that is *independent* of suspension density and viscosity since the changes in mean power and boundary layer volume negate each other. Unlike maximum shear stress and shear rate, maximum power dissipation depends only on the geometry of the disc and its rotational speed.

The assays designed to determine the response of (i.e. damage to) the material would be case specific, including clarification, particle size, cell viability, release of intracellular or periplasmic proteins from a cell, enzyme activity, degree of supercoiling (DNA), antibody specificity, etc.

It is here proposed that the small rotating disc apparatus with fixed dimensions (volume of about 11 mL) should be used to generate a standard shear-sensitivity index for several biological materials including precipitates, flocs, cells, proteins, enzymes, antibodies and antibody fragments, viruses, plasmids, liposomes and their complexes, DNA, RNA, etc. Once sufficient data has been amassed on each of major type of material, then an index of a new system can be estimated and verified experimentally with relative ease since the appropriate range of speeds and times to be investigated is known. With a concerted effort, sufficient data could be compiled relatively quickly.

Concurrent with the production of a shear index database, all major types of bioprocess equipment (baffled-stirred tanks aerated and non-aerated, pumps, homogenisers, centrifuges, tangential-flow filters, syringes, etc.) operating under typical conditions should be analysed by CFD to identify the regions of highest flow and hence, energy dissipation. The fraction of feed material exposed to these zones must also be determined. CFD analysis is laborious, and demands expert knowledge and substantial computing power, meaning that the proposed project could easily take some time.

Combining the shear-compilation of bioprocess equipment with knowledge of the critical maximum energy dissipation rate at which the material of interest begins to degrade unacceptably, permits one to identify feasible unit operations. Thus, the shear indices of material and equipment would facilitate bioprocess synthesis and design.

8.2. FILTRATION

More design features must be added to the Nutsche filter in order to convert it into a proper scale-down model of a rotating vertical leaf filter (RVLF). First, a flat cake surface must be produced. For all experiments in Chapter 5, the plunger head was fixed at a distance of 15 mm, which is the maximum allowable height of cake in the RVLF. However, this generated a rounded cake that was higher in the centre due to particles

impacting the surface directly because they did not have sufficient time to spread radially towards the wall of the filter vessel. Upon exit from the plunger, the feed stream may be directed in quite a narrow stream to the cake, with regions (radially) outside of this path being relatively stagnant. This could be overcome by several methods. Lower flow rates could be used, which would only require replacing the pump. The plunger head could be positioned further from the cake, but this would not permit determination of the amount of suspension that can be fed to RVLFF since the mimic would have a different solids capacity. Last, the rotational speed of the scale-down filter should be slowed to that of its industrial counterpart, which would require a better grip system and a more powerful motor. This author proposes implementing the first and last option, as this would maintain geometrical similarity with the industrial RVLFF.

Furthermore, it would be advantageous to have electronic recording not only of the filtrate mass and time, but also pressure and pump rate. An algorithm should also be written to control the pump rate automatically based on the flux during constant rate filtration, which is the most common type at pilot or production scale. An on-line turbidity meter to monitor filtrate quality continuously would also provide valuable data.

8.3. IMPACT OF PRIMARY SEPARATION ON CHROMATOGRAPHY

In Chapter 6, it was shown that mainly the type and not the extent of solid-liquid separation influenced the dynamic capacity of the HIC column, used for the purification of ADH from yeast homogenate. Since the response of the guard filter correlated well with clarity of the feed suspension, filter fouling was not a good indication of chromatographic performance. Degradation of the latter is believed to be due to lipid colloids that are removed during centrifugation but not filtration. This supposition should be verified by performing a mass balance on lipids and other major components including protein and nucleic acids. Elucidation of the chromatographic fouling mechanism would

also be useful, probably requiring particle size analysis of feed and elution streams, and scanning electron microscopy (SEM) of the resin for structural analysis.

The above experiments should be translated to other biological systems in order to ascertain the relative propensity of feed components to foul a chromatographic column for different loading conditions and types of matrix. Identification of the most fouling species would guide one to investigate their removal by techniques such as precipitation or the addition of a lipase or nuclease. The decision to implement proposed pre-treatments would probably be governed by process economics, namely whether the gain in chromatographic capacity more than offsets the total cost (capital, operating, yield loss, validation) of the additional step(s) (Storey and Dunnill, 2000).

8.4. SCALE DOWN OF THE ENTIRE UNIT OPERATION

To date much effort in academic institutions has been focused on scaling-down the *core* of a unit operation, i.e. the elements that determine the composition of feed and outlet *process streams*, such as clarification and dewatering in centrifugation. However, little effort has been devoted to mimicking the *entire* operation including CIP which impacts considerably on turnaround time. For example, the CIP of a membrane could be conducted on a geometrically scale-down model. However, it is impossible to mimic the self-cleaning mechanism of a disc stack centrifuge with a laboratory one; in effect a small disc stack machine would have to be constructed. For convenient scheduling, manufacturing often has holding/freezing stages that may influence product quality, but which are generally not included in the scaled-down process. More rapid processing at the small scale may fail to detect the effects of pH, ionic strength, temperature or proteases and other agents on product stability over prolonged times. The transfer of process material from one unit operation to another must also be considered, e.g. the

shear from some types of pumps. Where practical, the above production details should be incorporated into a scale-down process.

8.5. SCALE-DOWN FOR ACCELERATED BIOPROCESS DEVELOPMENT

Due to the research in this thesis and that of several others, it will soon be possible to scale down the process performance of most pieces of equipment. Nevertheless, standardisation of industrial equipment (i.e. adopting only one supplier each major unit operation) would make the development of small-scale mimics easier since fewer types of equipment would need to be scaled. The scale-down and large-scale unit operations could be tested easily in a systematic manner. This method is very advantageous for companies focussing on a certain type of product (e.g. monoclonal antibodies), but may hinder the inclusion of (new) equipment with superior performance for a different biological system.

Scaling down an existing production process is beneficial, but the key driver of a pharmaceutical business is the discovery and development of novel compounds since the highest profits can be extracted from new products. High-throughput genomic screening is generating thousands of new biological targets and compounds. And for each new product, several manufacturing processes can be hypothesised (i.e. flow-sheeting), thus leading to an overwhelming burden on development teams.

One way of dealing with this onslaught is the miniaturisation of unit operations, since it is not feasible to investigate the myriad of potential bioprocesses at even the tens of millilitre scale. Everything from fermentation (surface aeration should be sufficient) to chromatography (flash columns require less than 1 mL of material) would take place on microwell (< 0.5 mL) plates. Some laboratory centrifuge rotors are designed to hold microlitre plates. The speed of screening compounds will increase with automation;

programmable machines capable of pipetting down to phase boundaries and transferring the liquid onto other operations are now available.

The challenge remains to modify these miniaturised laboratory processes into scale-down ones. But is it worth injecting this sort of engineering design into such a small-scale process? Experimental error increases at such a scale as any inaccurate measurement, particularly in liquid transfers (e.g. due to adsorption to the outside of a pipette tip), would have a tremendous influence on the result. It is most likely not worthwhile to perform an entire microlitre process when screening several cell strains exist. But when screening for a suitable precipitant, it could prove useful to have an estimate (however approximate) of an aggregate's susceptibility to shear if this can be done quickly. Obviously, a coherent synthesis strategy should exist to guide development of the bioprocess by dictating how to implement the following efficiently and synergistically: flow-sheet formulation based on material and equipment indices (estimated or measured); mathematical modelling; and scale-down experiments.

It will be necessary to demonstrate the advantages of taking into account engineering issues at such an early stage in development; familiarising scientists with manufacturing realities should prevent effort being expended on processes that will obviously not be practical at production scale, and improve overall development efficiency. As laboratory mimics are refined, scale-down will play an increasingly important and productive role despite discussion surrounding its positioning within the research and development cycle.

REFERENCES

Alsaffar, L., Newsome, P., Titchener-Hooker, N.J. (1993). Purification of alcohol dehydrogenase (ADH) from baker's yeast – process interactions during fractional precipitation. *ICHEME Res. Event*, **1**, 132-134.

Ambler, C.M. (1959). The Theory of Scaling up Laboratory Data for the Sedimentation Type Centrifuge. *J. of Biochem. and Microbio. Tech. and Eng.*, **1**, 185-205.

Anicetti, V., Hancock, W.W. (1994). Analytical Considerations in the Development of Protein Purification Processes, In *Protein Purification Process Engineering* (Ed., Harrison, R.G.). Marcel Dekker, Inc., New York, 11-35.

Ashton, C. (1999). Reinventing drug development. *Chem. & Ind.*, **7 June**, 422-425.

Atkinson, B., Mavituna, F. (1991). Scale-Up of Processes, In *Biochemical Engineering and Biotechnology Handbook*. Macmillan, Basingstoke, 1116-1220.

Ayazi Shamlou, P., Gierczycki, A.T., Titchener-Hooker, N.J. (1996a). Breakage of flocs in liquid suspension agitated by vibrating and rotating mixers. *Chem. Eng. J.*, **62**, 23-34.

Ayazi Shamlou, P., Stavrinides, S., Titchener-Hooker, N., Hoare, M. (1994). Growth-independent breakage frequency of protein precipitates in turbulently agitated bioreactors. *Chem. Eng. Sci.*, **49**, 2647-2656.

Ayazi Shamlou, P., Stavrinides, S., Titchener-Hooker, N., Hoare, M. (1996b). Turbulent breakage of protein precipitates in mechanically stirred bioreactors. *Bioprocess Eng.*, **14**, 237-243.

Bell, D.J., Brunner, K.-H. (1983). A method for the evaluation of the floc break-up in centrifuges. *Filtration and Separation*, **20**, 274-286.

Bell, D.J., Dunnill, P. (1982). Shear disruption of soya protein precipitate particles and the effect of ageing in a stirred tank. *Biotech. Bioeng.*, **24**, 1271-1285.

Bell, D.J., Hoare, M., Dunnill, P. (1983). The formation of protein precipitates and their centrifugal recovery. In *Advances in Biochemical Engineering/Biotechnology* (ed. Fiechter, A.). Springer-Verlag, Berlin, **26**, 1-57.

Bergmeyer, H.U. (1983). *Method of enzymatic analysis* (3rd Ed.). Verlag Chemie, Weinheim.

Bird, R.B., Stewart, W.E., Lightfoot, E.N. (1960). *Transport Phenomena*. Wiley, New York.

Bloomberg. (15 November, 1999). Aviron Sees Delay in Introduction of FluMist Vaccine. *Bloomberg.com*.

Bobrowicz, G. (1999). The Compliance Costs of Hasty Process Development. *BioPharm*, **August**, 35-38.

Boychyn, M., Bulmer, M., More, J., Hoare, M. (2000a). The laboratory scale-down of processes involving fractional precipitation and centrifugal recovery. *Biotech. Bioeng.*, in press.

Boychyn, M., Yim, S.S.S., Ayazi Shamlou, P., Bulmer, M., More, J., Hoare, M. (2000b). Characterisation of flow intensity in continuous centrifuges for the development of laboratory mimics. Submitted to *Chem. Eng. Sci.*

Bradford, M. M. (1976). A rapid and sensitive method for the quantification of microgram quantities of protein utilising the principle of protein-dye binding. *Analytical Biochemistry*, **72**, 248-254.

Brose, D., Dosmar, M., Cates, S., Hutchinson, F. (1995). Studies on the Scale-Up of Crossflow Filtration Devices. *PDA Journal of Pharmaceutical Science & Technology*, **50**, 252-260.

Bulmer, M. (1992) Selective flocculation for the improved recovery of intracellular proteins from bacterial homogenates. *Ph.D. thesis*, University of London.

Bylund, F., Guillard, F., Enfors, S.-O., Larsson, G. (1999). Scale down of recombinant protein production: a comparative study of scaling performance. *Bioprocess Eng.*, **20**, 377-389.

Carr, G. (21 Feb 1998). Survey: The Alchemists. *The Economist*.

Clarkson, A.I., Lefevre, P., Tichener-Hooker, N.J. (1993). A study of process interactions between cell disruption and debris clarification stages in the recover of yeast intracellular products. *Biotech. Prog.*, **9**, 462-467.

De Jonge, E., van Leeuwen, M.A.W., Radema, H., Linssen, P.H.J.M., Over, J. (1993). Filtration processes in the Cohn fractionation. In *Biotechnology of Blood Proteins* (Eds. Rivat, C., Stoltz, J.F.), Colloque INSERM, **227**, 49-54.

Dunnill, P., Lilly, M. (1972). Continuous enzyme isolation. *Biotech. Bioeng. Symp.*, **3**, 97-113.

Enfors, S.-O., Jahic, M., Rozkov, A., *et al.* (1998). Bioprocess scale-up strategy based on integration of fluid dynamics and microbial physiology. *2nd European Symp. on Biochem. Eng. Sci.*, **Sep**, 7-12.

Englard, S., Seifter, S. (1990). Precipitation techniques, In *Methods in Enzymology*. **182**, 285-306.

Fisher, R.R., Glatz, C.E. (1988). Polyelectrolyte precipitation of proteins: I. The effects of reactor conditions. *Biotech. Bioeng.*, **32**: 777-785.

Fisher, R.R., Glatz, C.E., Murphy, P.A. (1986). Effects of mixing during acid addition on fractionally precipitated protein. *Biotech. Bioeng.*, **28**, 1053-1063.

Foo, F., Karri, S., Davies, E., Titchener-Hooker, N.J., Dunnill, P. (2000). Biopharmaceutical process development. Submitted to *Biopharm. Europe*.

Foster, P.R. (1994). Blood Plasma Fractionation. In *Kirk-Othmer Encyclopedia of Chemical Technology* (4th ed.). John Wiley & Sons, London, **11**, 990-1021.

Foster, P.R., Dunnill, P., Lilly, M.D. (1976). The kinetics of protein salting-out: precipitation of yeast enzymes by ammonium sulphate. *Biotech. Bioeng.*, **18**, 545-580.

Freitag, R., Horvath, C. (1995). Chromatography in the Downstream Processing of Biotechnological Products. In *Advances in Biochemical Engineering/Biotechnology* (ed. Fiechter, A.). Springer-Verlag, Berlin, **53**, 17-59.

Friedli, H., Mauerhofer, M., Faes, A., Kistler, P. (1976). Studies on new process procedures in plasma fractionation at an industrial scale, III. *Vox Sang*, **33**, 93-96.

Gan, Q., Riedl, R.W., Bird, M.R., England, R., Howell, J.A., McKechnie, M.T., Oshaughnessy, C.L. (1997). Beer clarification by cross-flow microfiltration: Fouling mechanisms and flux enhancement. *Chem. Eng. Res. Design*, **75** (A1), 3-8.

Gierczycki, A.T., Shamlou, P.A. (1994). Aggregation of monosized particles in turbulently agitated suspensions - A simplified approach. *Chem. and Biochem. Eng. Quart.*, **10**, 125-128.

Glatz, C.E., Hoare, M., Landa-Vertiz, J. (1986). The formation and growth of protein precipitates in a continuous stirred-tank reactor. *AIChE J.*, **32**, 1196-1204.

Gosman, A.D. (1998) Development in industrial computation fluid dynamics. *Trans. IChemE.*, **76 A**, 153-161.

Grandgeorge, M., Vernon, J.L., Cueille, G. (1989). Separation d'un precipite proteique par microfiltration tangentielle au cours de la purification de l'Albumine Humaine. In *Biotechnology of Plasma Proteins* (Eds. Stoltz, J.F., Rivat, C.), Colloque INSERM, **175**, 25-32.

Guell, C., Czekaj, P., Davis, R.H. (1999). Microfiltration of protein mixtures and the effects of yeast on membrane fouling. *J. Membrane Sci.*, **155**, 113-122.

Guell, C., Davis, R.H. (1996). Membrane fouling during microfiltration of protein mixtures. *J. Membrane Sci.*, **119**, 269-284.

Hao, Y.-L. (1985). Pilot plant scale preparation of human serum albumin. *Vox Sang*, **49**, 1-8.

Harris, C.K., Roekaerts, D., Rosendal, F.J.J., Buitendijk, F.G.J., Daskopoulos, Ph., Vreenegoor, A.J.N., Wang, H. (1996). Computational fluid dynamics for chemical reactor engineering. *Chem. Eng. Sci.*, **51**, 1569-1594.

Harrison, R.G. (Ed.) (1994). *Protein Process Engineering*. Marcel Dekker Inc., New York.

Hellot, C. (1993). Filtration technology. *Revue Francaise de Transfusion et d'Hemobiologie*, **36**, 223-242.

Hermia, J, Brocheton, S. (1994). Comparison of beer filters. Proceedings of *New developments in filtration and separation in the beverage industry*, F.E.G.C., Vienna, **March**, 9-20.

Herrero, C., Pradanos, P., Calvo, J.I., Tejerina, F., Hernandez, A. (1997). Flux decline in protein microfiltration: influence of operative parameters. *J. of Colloid and Interface Sci.*, **187**, 344-351.

Hetherington, P.J., Follows, M., Dunnill, P., Lilly, M.D. (1971). Release of protein from bakers' yeast (*Saccharomyces cerevisiae*) by disruption in an industrial homogeniser. *Trans. Instn. Chem. Engrs.*, **49**, 142-148.

Hoare, M. (1982). Growth of protein precipitates during hindered settling or exposure to shear. *Trans. Instn. Chem. Eng.*, **60**, 157-163.

Hoare, M., Narendranathan, T.J., Flint, J.R., Heywood-Waddington, D., Bell, D.J., Dunnill, P. (1982). Disruption of protein precipitates during shear in Couette flow and in pumps. *Ind. Eng. Chem. Fundam.*, **21**, 402-406.

Holdich, R.G., Tarleton, E.S., Shaw, F.J. (Oct. 1993). A new experimental technique for the analysis of cake filtration. *Filtech 93 Conference*, Karlsruhe.

Humphrey, A. (1998). Shake flask to fermentor: what have we learned? *Biotech. Prog.*, **14**, 3-7.

International Conference on Harmonization. (Dec. 1995). Viral safety evaluation of biotechnology products derived from cell lines of human or animal origin. *ICH Viral Safety Document: Step 2*, ICH Secretariat, Geneva.

Iyer, H.V., Przybycien, T.M. (1994). Protein precipitation: effects of mixing on protein solubility. *AIChE J.*, **40**, 349-359.

Iyer, H.V., Przybycien, T.M. (1995). Metal affinity precipitation: effects of mixing, protein concentration, and modifiers on protein fractionation. *Biotech. Bioeng.*, **48**, 324-332.

Johansson, B. -L., Ellstrom, C. (1985). Column lifetime of a new agarose medium for HPLC gel filtration chromatography at basic pH. *J. Chrom.*, **330**, 360-364.

Jones, W. P., Launder, B. E. (1972). The prediction of laminarisation with a two-equation model of turbulence. *Int. J. Heat Mass Transfer*, **15**, 301-314.

Jourdan, M.F., Peuchot, C. (1994). New test method for evaluation of water cartridge filters. *Filt. & Sep.*, **31**, 427 et seq.

Kaltenbrunner, O., Jungbauer, A., Yamamoto, S. (1997). Prediction of the preparative chromatography performance with a very small column. *J. Chrom.*, **760**, 41-53.

Kennedy, C.M., Sofer, G., McEntire, J., Akers, J. (1995). Biotechnology Product Validation, Part 10: Managing Equipment and Procedural Change Control. *BioPharm*, April, 34-37.

Kennedy, J.F., White, C.A., Rivera, Z. (1988). *International Industrial Biotechnology*, 8, 15.

Kossen, N.W.F. (1992). Scale-Up in Biotechnology, In *Recent Advances in Biotechnology* (Eds. Vardar-Sukan, F., Suha Sukan, S.). Kluwer Academic Publishers, London: 147-182.

Kwon, D.Y., Vigneswaran, S., Ngo, H.H., Shin, H.S. (1997). An enhancement of critical flux in cross-flow microfiltration with a pretreatment of floating medium flocculator/prefilter. *Water Sci. & Tech.*, 36, 267-274.

Lauder, B.E., & Spalding, D.B. (1974). The Numerical Computational of Turbulent Flows. *Comput. Methods Appl. Mech. Eng.*, 3, 269-289.

Lesins, V., Ruckenstein, E. (1988). Protein coated adsorbents for use in potential barrier chromatography-fouling chromatography. *Biotech. Prog.*, 4, 12-24.

Leser, E.W., Asenjo, J.A. (1992). Rational Design of Purification Processes for Recombinant Proteins. *Biomedical Applications*, 584, 43-57.

Leser, E.W., Lienqueo, M.E., Asenjo, J.A. (1997). Implementation in an Expert System of a Selection Rationale for Purification Processes for Recombinant Proteins. *Annals New York Academy of Sciences*, 782, 441-455.

Levy, M.S., Ciccolini, L.A.S., I.J., Yim, S.S., Tsai, J.T., Titchener-Hooker, N.J., Ayazi Shamlou, P., Dunnill, P. (1999). The effects of material properties and fluid flow intensity on plasmid DNA recovery during cell lysis. *Chem. Eng. Sci.*, 54, 3171-3178.

Levy, M.S., Collins, I.J., Yim, S.S., Ward, J.M., Keshavarz-Moore, E., Titchener-Hooker, N.J., Ayazi Shamlou, P., & Dunnill, P. (1998). Effect of shear on plasmid DNA in solution. *Bioprocess Eng.*, **20**, 7-13.

Lien, K., Suzuki, G., Westerberg, A. (1987). The role of expert systems technology in design. *Chem. Eng. Sci.*, **42**, 1049-1071.

Lienqueo, M.E., Leser, E.W. Asenjo, J.A. (1996). An Expert System for the Selection and Synthesis of Multistep Protein Separation Processes. *Computers Chem. Eng.*, **20**, s189-s194.

Maa, Y.F., Hsu, C.C. (1999). Investigation on fouling mechanisms for recombinant human growth hormone sterile filtration. *J. Pharm. Sci.*, **87**, 808-812.

Maa, Y.F., Hsu, C.C. (1996). Membrane fouling in sterile filtration of recombinant human growth hormone. *Biotech. Bioeng.*, **50**, 319-328.

Mackler, B.F., Landa, M.M., Gamerman, G.E. (1996). FDA Primer: I. the drug and biologic approval process. *Biotechnol. Appl. Biochem.*, **23**, 191-196.

Mannweiler, K., Titchener-Hooker, N.J., Hoare, M. (1989). Biochemical engineering improvements in the centrifugal recovery of biological particles. *IChemE.-Symp. on Adv. in Biochem. Eng.*, **1**, 105-117.

Mannweiler, K., Hoare, M. (1992). The scale-down of an industrial disc stack centrifuge. *Bioproc. Eng.*, **8**, 19-25.

Maybury, J.P. (1999). Scale-down of a bioprocess for the recovery and purification of an intracellular protein. *Ph.D. thesis*, University of London.

Maybury, J.P., Mannweiler, K., Titchener-Hooker, N.J., Hoare, M., Dunnill, P. (1998). Performance of scaled down industrial disc stack centrifuge with a reduced feed material requirement. *Bioproc. Eng.*, **18**, 191-199.

Maybury, J.P., Hoare, M., Dunnill, P. (2000). The use of laboratory centrifugation studies to predict performance of industrial machines: Studies of shear-sensitive and shear-insensitive materials. *Biotech. Bioeng.*, **43**, 32-34.

Meagher, L., Klauber, C., Pashley, R.M. (1996). The influence of surface forces on the fouling of polypropylene microfiltration membranes. *Colloids and Surfaces A-Physicochem. and Eng. Aspects*, **106**, 63-81.

Meltzer, T.H., Jornitz, M.W. (Eds.) (1998). *Filtration in the Biopharmaceutical Industry*. Marcel Dekker, New York.

More, J.E., Harvey, M.J. (1991). Purification technologies for human plasma albumin. in *Blood Separation and Plasma Fractionation* (Ed. Harris, J.R.), Wiley-Liss, Inc., London, 261-306.

Murphy, J.C., Wibbenmeyer, J.A., Fox, G.E., Willson, R.C. (1999). Purification of plasmid DNA using selective precipitation by compaction agents – A scaleable method for the liquid-phase separation of plasmid DNA from RNA, *Nature Biotech.*, **17**, 822-823.

Murrell, N. (1997). An engineering study of the recovery of shear-sensitive biological materials by high-speed disc stack centrifugation. *PhD thesis*, University of London.

Nagy, E., Mayr, B., Moser, A. (1993). Bioprocess Scale-Up Using a Structured Mixing Model. *Computers Chem. Eng.*, **18**, s663-s667.

Oja, M., Nystrom, L. (Oct. 1995). Evaluation of filtration tests with gradual pressure increase and sedimentation. *Filtech Europa 95 Conference*, Karlsruhe.

Oldshue, J.Y. (1983). *Fluid mixing technology*. McGraw-Hill, New York.

Oosterhuis, N.M.G., Kossen, N.W.F., Olivier, A.P.C., Schenk, E.S. (1985). Scale-down and optimization studies of the gluconic acid fermentation by *Gluconobacter oxydans*. *Biotech. Bioeng.*, **27**, 711-720.

Paul, E.L., Rosas, C.B. (1990) Challenges for chemical engineers in the pharmaceutical industry. *Chem. Eng. Prog.*, **86**, 17-25.

Petterson, T. (1989). Optimisation in chromatography: column maintenance. *University College Summer Course*, University of London.

Pinheiro, H., Cabral, J.M.S. (1993). *Filtration in Recovery processes for Biological Materials*. John Wiley & Sons Ltd, New York, 67-95.

Pisano, G.P. (1997). *The Development Factory*. Harvard Business School Press, Boston.

Reisman, H.B. (1993). Problems in Scale-Up of Biotechnology Production Processes. *Critical Reviews in Biotechnology*, **13**, 195-253.

Richardson, P., Hoare, M., Dunnill, P. (1990). A new biochemical engineering approach to the fractional precipitation of proteins. *Biotech. Bioeng.*, **36**, 354-366.

Rothstein, F. (1994). Differential precipitation of proteins: Science and Technology, *Protein Process Engineering* (Ed. Harrison, R.G.). Marcel Dekker Inc., New York, 115-208.

Rushton, J.H., Costich, E.W., Everett, H.J. (1950). Power characteristics of mixing impellers, Part 2. *Chem. Eng. Prog.*, **46**, 467-476.

Rushton, A., Ward, A.S., Holdich, R.G. (1996). *Solid-Liquid Filtration and Separation Technology*. VCH, Cambridge, UK.

Schlichting, H. (1979). *Boundary Layer Theory* (7th Ed.). Pergamon Press, London.

Shih, T. M. (1984). *Numerical Heat Transfer*. Hemisphere, Washington.

Siddiqi, S.F., Titchener-Hooker, N.J., Shamlou, P.A. (1997). High pressure disruption of yeast cells: The use of scale down operations for the prediction of protein release and cell debris size distribution. *Biotech. Bioeng.*, **55**, 642-649.

- Siirola, J.J. (1996). Strategic process synthesis: Advances in the hierarchical approach. *Computers Chem. Eng.*, **20**, s1637-s1643.
- Singhvi, R., Schorr, C., O'Hara, C., Xie, L., Wang, D.I.C. (1996). Clarification of animal cell culture process fluids using depth microfiltration. *BioPharm*, **9**, 35-41.
- Smith, M.P. (1997). An evaluation of expanded bed adsorption for the recovery of proteins from crude feed stocks. *Ph.D. thesis*, University of London.
- Smith III, F. G. (1997). A model of transient mixing in a stirred tank. *Chem. Eng. Sci.*, **52**, 1459-1478.
- Sofer, G., Hagel, L. (1997). *Handbook of process chromatography*. Academic Press Limited, London.
- Song, L.F. (1998). Flux decline in crossflow microfiltration and ultrafiltration: mechanisms and modeling of membrane fouling. *J. Memb. Sci.*, **139**, 183-200.
- Soriano, G. (1995). An engineering study of compression and fouling of chromatographic matrices. *Ph.D. Thesis*, University of London.
- Stavrinides, S., Ayazi Shamlou, P., Hoare, M. (1993). Effects of engineering parameters on the precipitation recovery and purification of proteins, In *Processing of Solid-Liquid Suspensions* (Ed. Ayazi Shamlou, P.). Butterworth Heinmann, London, 118-158.
- Storey, S.A., Dunnill, P. (2000). Physical properties for bioprocess synthesis: addressing bioprocess development in the product discovery laboratory. In preparation for *Biotech. Bioeng.*
- Storey, S.A., Boychyn, M., Titchener-Hooker, N.J., Hoare, M., Dunnill, P. (2000a). Fouling properties of centrifuged yeast homogenate: correlations between HIC process performance and adsorption parameters measured in a separate, distinct chromatographic system. In preparation for *Biotech. Bioeng.*

- Storey, S.A., Boychyn, M., Titchener-Hooker, N.J., Hoare, M., Dunnill, P. (2000b). A comparison of process alternatives based on chromatographic fouling measurements using frontal analysis. In preparation for *Biotech. Bioeng.*
- Struck, M.M. (1994). Biopharmaceutical R&D Success Rates and Development Times. *Bio/Tech.*, **12**, 674-677.
- Svarovsky, L. (1990). Separation by centrifugal sedimentation, In *Solid-Liquid Separation* (Ed. Svarovsky, L.). Butterworth & Co. Ltd., London, 251-278.
- Thomas, C.R., Zhang, Z. (1998). The effects of hydrodynamics on biological materials, *Advances in Bioprocess Engineering II* (Eds. Galindo, E., Ramirez, O.T.). Kluwer Academic Publishers, Netherlands, 137-170.
- van Reis, R., Goodrich, E.M., Yson, C.L., Frautschy, L.N., Dzengeleski, S., Lutz, H. (1997). Linear scale ultrafiltration. *Biotech. Bioeng.*, **55**, 737-746.
- Varga, E.G., Titchener-Hooker, N.J., Dunnill, P. (1998). Use of scale-down methods to rapidly apply natural yeast homogenisation models to a recombinant strain. *Bioprocess Eng.*, **19**, 373-380.
- Versele, M., Dewaela, C. (1985). Preparative High Performance Chromatography: A Practical Guideline. RSL/Alltech, Eke.
- Ward, P.N., Hoare, M. (1990). The dewatering of biological suspensions industrial centrifuges, *Sep. in Biotech.*, **2**, 93-101.
- Weast, R.C. (Ed.) (1978). *Handbook of Chemistry and Physics* (58th ed.). CRC Press, Inc., Florida, D193.
- Wheelwright, S.M. (1987). Designing downstream processes for large-scale protein-purification. *Bio-Tech.*, **5**, 789 et seq.

- Wheelwright, S.M. (1991). *Protein Purification: Design and Scale up of Downstream Processing*. Carl Hanser Verlag, New York.
- Wolthuis, R., Dichiarla, V.C. (1997). Conventional Filtration, In *Handbook of Downstream Processing*. Hackie Academic & Professional, London, 20-47.
- Woodley, J.M., Titchener-Hooker, N.J. (1996). The Use of Windows of Operation as a Bioprocess Design Tool. *Bioprocess Eng.*, **14**, 263-268.
- Yao, S.-H., Murase, R., Iritani, E., Suzuki, T., Nakanomori, S., Shirato, M. (1993). Filtration with different diatomaceous precoating. *International Chem. Eng.*, **32**, 172-180.
- Yiantsios, S.G., Karabelas, A.J. (1998). The effect of colloid stability on membrane fouling. *Desalination*, **118**, 143-152.
- Young, R.E., Campbell, J.A., Morgan, J.A. (1984). Physical simulation: The use of scaled down fully functional components to analyse and design automated production systems. *Comput. & Indus. Eng.*, **8**, 73-85.
- Zhou, Y.H., Titchener-Hooker, N.J. (1999). Visualizing integrated bioprocess designs through “windows of operation”. *Biotech. Bioeng.*, **65**, 550-557.

APPENDIX A

Table A.1. Experimental mass balance data for protein ($1270 \pm 50 \text{ mg mL}^{-1}$) and ADH ($17300 \pm 1000 \text{ U mL}^{-1}$).

LABORATORY DATA											
Q_{eq} (L h ⁻¹)		Feed	Ideal centrifuge					Process centrifuge			
			Soluble	Solid	Ppt (%)	Sum	Diff (%)	Sup	Sed	Sum	% Diff
Ideal	Prot (mg)	1258	854	430	34.2	1283	2.1	857	436	1292	2.8
	ADH (U)	16017	15037	1428	8.9	16465	2.8	15417	1392	16809	4.9
10	Prot (mg)	1287	874	411	32.0	1285	-0.1	899	357	1256	-2.4
	ADH (U)	18096	17725	1350	7.5	19075	5.4	18170	1428	19598	8.3
	Prot (mg)	1350	940	393	29.1	1333	-1.3	988	372	1361	0.8
	ADH (U)	18907	18298	1191	6.3	19489	3.1	18422	1321	19743	4.4
	Prot (mg)	1307	917	421	32.2	1338	2.4	875	347	1222	-6.5
	ADH (U)	18745	16544	1170	6.2	17714	-5.5	17936	1344	19280	2.9
20	Prot (mg)	1181	809	341	28.9	1150	-2.6	893	318	1211	2.6
	ADH (U)	15774	14524	826	5.2	15350	-2.7	14469	1201	15670	-0.7
	Prot (mg)	1265	844	377	29.8	1221	-3.5	874	339	1212	-4.1
	ADH (U)	16611	15393	885	5.3	16278	-2.0	15887	1200	17087	2.9
	Prot (mg)	1251	859	368	29.4	1227	-1.9	928	361	1289	3.0
	ADH (U)	16368	15994	1120	6.8	17114	4.6	15776	1355	17131	4.7
	Prot (mg)	1249	868	367	29.4	1235	-1.1	948	332	1279	2.4
	ADH (U)	15423	14360	1625	10.5	15985	3.6	14254	1157	15411	-0.1
	Prot (mg)	1215	917	347	28.6	1264	4.1	955	305	1261	3.8
	ADH (U)	17745	17433	1963	11.1	19395	9.3	17160	1314	18474	4.1
	Prot (mg)	1320	832	467	35.4	1300	-1.5	866	408	1274	-3.5
	ADH (U)	16611	15393	885	5.3	16278	-2.0	15696	1375	17071	2.8
40	Prot (mg)	1181	809	341	28.9	1150	-2.6	919	305	1224	3.7
	ADH (U)	15774	14524	826	5.2	15350	-2.7	14068	1230	15298	-3.0
	Prot (mg)	1265	831	364	28.8	1195	-5.5	992	306	1297	2.6
	ADH (U)	16611	15393	885	5.3	16278	-2.0	15796	1263	17059	2.7
	Prot (mg)	1251	859	368	29.4	1227	-1.9	975	348	1323	5.8
	ADH (U)	16368	15994	1120	6.8	17114	4.6	16167	1396	17563	7.3

80	Prot (mg)	1181	809	341	28.9	1150	-2.6	974	239	1212	2.7
	ADH (U)	15774	14524	826	5.2	15350	-2.7	14090	1246	15336	-2.8
	Prot (mg)	1265	811	385	30.4	1195	-5.5	961	238	1199	-5.2
	ADH (U)	16611	14770	845	5.1	15614	-6.0	14123	1425	15548	-6.4
	Prot (mg)	1251	859	368	29.4	1227	-1.9	1066	214	1281	2.4
	ADH (U)	16368	16615	1162	7.1	17776	8.6	15025	1290	16315	-0.3
	Prot (mg)	1298	857	430	33.1	1287	-0.9	1120	260	1380	6.3
	ADH (U)	15423	13627	1625	10.5	15252	-1.1	13750	1540	15290	-0.9
120	Prot (mg)	1287	842	379	29.5	1221	-5.1	1049	224	1273	-1.1
	ADH (U)	18096	17725	1350	7.5	19075	5.4	17573	1772	19345	6.9
	Prot (mg)	1350	980	353	26.2	1333	-1.3	1185	184	1369	1.5
	ADH (U)	18907	18298	1191	6.3	19489	3.1	17936	1501	19437	2.8
	Prot (mg)	1307	917	421	32.2	1338	2.4	1074	200	1274	-2.5
	ADH (U)	18745	16544	1170	6.2	17714	-5.5	16903	1464	18367	-2.0
PILOT-SCALE DATA											
20	Prot (mg)	1249	843.25	342.2	27.4	1185	-5.1	1121.3	86.3	1208	-3.3
	ADH (U)	15423	14360	1625	10.5	15985	3.6	15110	190	15300	-0.8
	Prot (mg)	1100.9	796.1	367.6	33.4	1164	5.7	979.9	91.2	1071	-2.7
	ADH (U)	15314	14332	1701	11.1	16033	4.7	14759	326	15085	-1.5
	Prot (mg)	1244.9	862.2	418.2	33.6	1280	2.9	1067.9	131.3	1199	-3.7
	ADH (U)	16044	15155	1549	9.7	16704	4.1	14867	376	15243	-5.0
	Prot (mg)	1215	917	347.1	28.6	1264	4.1	883.5	382	1265	4.2
	ADH (U)	17745	17433	1963	11.1	19395	9.3	16744	2492	19236	8.4

APPENDIX B

COMPUTATIONAL FLUID DYNAMICS (CFD)

Mapping of the flow field

The time-dependent flow field in the multichamber-bowl centrifuge was computed from the continuity equation:

$$\frac{\partial \rho}{\partial t} + \frac{1}{r} \frac{\partial(\rho r u)}{\partial r} + \frac{\partial(\rho v)}{\partial z} = 0 \quad (\text{B.1})$$

and the momentum equations,

$$\frac{\partial(\rho u)}{\partial t} + \frac{1}{r} \frac{\partial(\rho r u u)}{\partial r} - \frac{w^2}{r} + \frac{\partial(\rho u v)}{\partial z} = -\frac{\partial p}{\partial r} - \left(\frac{1}{r} \frac{\partial(r \tau_{rr})}{\partial r} - \frac{\tau_{\theta\theta}}{r} + \frac{\partial r \tau_{zr}}{\partial z} \right) \quad (\text{B.2})$$

$$\frac{\partial(\rho v)}{\partial t} + \frac{1}{r} \frac{\partial(\rho r u v)}{\partial r} + \frac{\partial(\rho v v)}{\partial z} = -\frac{\partial p}{\partial r} - \left(\frac{1}{r} \frac{\partial(r \tau_{rz})}{\partial r} + \frac{\partial \tau_{zz}}{\partial z} \right) + \rho g \quad (\text{B.3})$$

$$\frac{\partial(\rho w)}{\partial t} + \frac{1}{r} \frac{\partial(\rho r u w)}{\partial r} + \frac{\rho u w}{r} + \frac{\partial(\rho w v)}{\partial z} = -\frac{1}{r} \frac{\partial(r \tau_{r\theta})}{\partial r} - \frac{\tau_{r\theta}}{r} - \frac{\partial \tau_{z\theta}}{\partial z} \quad (\text{B.4})$$

In these equations, u , v and w are the fluid velocities, τ_{ij} are the components of the stress tensor, ρ is the fluid density and p the pressure. The velocities and pressures are time-averaged quantities and the stress tensor components are the sums of viscous shear stresses and turbulent Reynolds stresses (Bird *et al.*, 1960). The process fluid was assumed to have Newtonian properties and as a first approximation, particle concentration was assumed to have a negligible effect on the fluid flow field. This assumption is reasonable considering the low density and the relatively small size of most biological particles, particularly yeast-protein precipitates.

In solving Equations B.1-B.4, the usual assumption was made that turbulent stresses could be modelled by the introduction of the turbulent viscosity coefficient μ_t . This allowed the dynamic viscosity term in the fluid stress tensors of the Navier Stokes

equations to be replaced by the sum of the molecular and turbulent components (Smith III, 1997). The coefficient of turbulent eddy viscosity was computed from the turbulent kinetic energy (k) and the energy dissipation rate (ε), thus:

$$\mu_t = \rho \frac{c_\mu k^2}{\varepsilon} \quad (\text{B.5})$$

where c_μ is the constant of proportionality, which was taken to be equal to 0.09 as recommended by Jones and Launder (1972). k and ε were obtained from the two-dimensional conservation versions of Equations B.1-B.4 in cylindrical co-ordinates (Shih, 1984). Thus:

$$\frac{\partial(\rho k)}{\partial t} + \frac{1}{r} \frac{\partial(\rho r u k)}{\partial r} + \frac{\partial(\rho v k)}{\partial z} = \frac{1}{r} \frac{\partial}{\partial r} \left(\frac{\mu}{\sigma_k} r \frac{\partial k}{\partial r} \right) + \frac{\partial}{\partial z} \left(\frac{\mu}{\sigma_k} \frac{\partial k}{\partial z} \right) + G - \rho \varepsilon \quad (\text{B.6})$$

and

$$\frac{\partial(\rho \varepsilon)}{\partial t} + \frac{1}{r} \frac{\partial(\rho r u \varepsilon)}{\partial r} + \frac{\partial(\rho v \varepsilon)}{\partial z} = \frac{1}{r} \frac{\partial}{\partial r} \left(\frac{\mu}{\sigma_\varepsilon} r \frac{\partial \varepsilon}{\partial r} \right) + \frac{\partial}{\partial z} \left(\frac{\mu}{\sigma_\varepsilon} \frac{\partial \varepsilon}{\partial z} \right) + c_1 \frac{\varepsilon}{k} G - c_2 \rho \frac{\varepsilon^2}{k} \quad (\text{B.7})$$

where G is the term which represents the production of turbulent kinetic energy and was computed using the following equation recommended by Smith III (1997):

$$G = \frac{\mu_t}{\mu^2} \left\{ \frac{1}{2} [\tau_{rr}^2 + \tau_{\theta\theta}^2 + \tau_{zz}^2] + \tau_{rz}^2 + \tau_{r\theta}^2 + \tau_{z\theta}^2 \right\} \quad (\text{B.8})$$

In employing the standard k - ε model, the following values for the coefficients were used in Eqs. B.6 and B.7 as recommended by Launder and Spalding (1974):

$$c_1 = 1.44, \quad c_2 = 1.92, \quad \sigma_k = 1.0 \quad \text{and} \quad \sigma_\varepsilon = 1.33.$$

The entrance region of the centrifuge, forming the computational domain for the solution of Equations B.5-B.8 was “body fitted” for grid generation and solved using the finite volume method (CFX 4.2, AEA Technology, Oxfordshire, UK). The equations were solved with appropriate initial and boundary conditions using a personal computer (Hewlett Packard, Vectra, Pentium II 400 MHz). Grid independent solutions were

obtained by using a mesh design consisting of 90,000 grids. The grids were refined to allow the details of flow to be examined in regions where rapid changes in flow occurred.